Uncertainty and robustness analysis of biochemical reaction networks via convex optimisation and robust control theory

Von der Fakultät Konstruktions-, Produktions-, und Fahrzeugtechnik und dem Stuttgart Research Centre for Simulation Technology der Universität Stuttgart zur Erlangung der Würde eines Doktors der Ingenieurwissenschaften (Dr.–Ing.) genehmigte Abhandlung

Vorgelegt von

Steffen Waldherr

aus Friedrichshafen

Hauptberichter:	Prof. Dr.-Ing. Frank Allgöwer
Mitberichter:	Prof. Pablo A. Iglesias, PhD
	Prof. Dr.-Ing. Elling W. Jacobsen

Tag der mündlichen Prüfung: 30. September 2009

Institut für Systemtheorie und Regelungstechnik

Universität Stuttgart

2009

Acknowledgments

The results presented in this thesis are based on my work as a research assistant at the Institute for Systems Theory and Automatic Control (IST) of the University of Stuttgart from 2005 to 2009. During that time, I was also a PhD student in the Graduate School Simulation Technology of the University of Stuttgart, and a visiting researcher at the Automatic Control laboratory of the Swedish Royal Institute of Technology.

I want to thank Prof. Frank Allgöwer for motivating me to work in the field of systems biology, and for his supervision during my doctoral studies. His great enthusiasm has certainly been one of the driving forces in this work. I am also grateful to Prof. Elling Jacobsen for inviting me to spend some time doing research in his group, on which some of the results in this thesis are based, and want to thank him and Prof. Pablo Iglesias for being on my thesis committee.

The interactions with many colleagues sharing related interests was crucial to my work. First, I want to mention Thomas Eißing, Madalena Chaves, Prof. Rolf Findeisen, and Prof. Peter Scheurich for guiding me into the field of systems biology, each with their own unique approach. I also want to thank other members of the IST systems biology group, namely Christian Breindl, Marcello Farina, Jan Hasenauer, Prof. Jung-Su Kim, Solvey Maldonado, and Monica Schliemann for very helpful discussions about the work presented here and related topics throughout the major part of my doctoral studies. Also, my research benefited greatly from interactions with other groups. In particular, I want to mention Malgorzata Doszczak from the experimental side, and Stefan Streif and Prof. Fabian Theis for their collaboration in applications of my results. In addition to those already mentioned, I want to thank Prof. Christian Ebenbauer, Ulrich Münz, Prof. Nicole Radde, Marcus Reble, Markus Rehberg, Daniella Schittler, Simone Schuler, and Gerd Schmidt for helpful comments on this thesis.

I also want to thank all my former and current colleagues at the IST for creating a very enjoyable and stimulating working atmosphere. It was always a pleasure doing both academic and non-academic activities in this group. Last but not least, I want to thank Annie and my parents for their love and support in all these years.

Stuttgart, October 2009 Steffen Waldherr

If a man will begin with certainties, he shall end in doubts; but if he will be content to begin with doubts, he shall end in certainties.

Francis Bacon
Proficience and Advancement of Learning

Contents

Index of notation

Acronyms

Acronym	Description
GMA	generalised mass action
MAPK	mitogen activated protein kinase
ODE	ordinary differential equation
SDP	semi-definite program
TNF	tumor necrosis factor

Notation

Symbol	Description
$\operatorname{in} A$	inertia of square matrix A
$\operatorname{diag} x \in \mathbb{R}^{n\times n}$	diagonal matrix with entries of $x \in \mathbb{R}^n$ on the diagonal
$\mathbb{R}_+$	non-negative real numbers
$\mathbb{R}[x]$	ring of polynomials in the vector variable x over $\mathbb{R}$
$\mathcal{S}^k$	space of real symmetric $k \times k$ matrices
$M \geq 0$	matrix or vector M is elementwise non-negative
$P \succ (\succeq) 0$	matrix P is positive (semi-)definite
$\mathcal{A} \subset \mathcal{B}$	the set $\mathcal{A}$ is a subset of the set $\mathcal{B}$ (not necessarily proper)
$A \setminus B$	relative complement of the set B in the set A
I_n	identity matrix in $\mathbb{R}^{n\times n}$

Model and uncertainty description

Symbol	Description
$\alpha_{ij} \in \mathbb{R}$	exponent for i–th species in j–th reaction for GMA networks
$A \in \mathbb{R}^{n\times n}$	system's Jacobian $A = \frac{\partial F}{\partial x} = SV$
$\chi \in \mathbb{R}^{n+q}$	state–parameter pair
$F : \mathbb{R}^n \times \mathbb{R}^q \to \mathbb{R}^n$	ODE right hand side $F = Sv$
$k_j \in \mathbb{R}_+$	reaction rate constant for j–th reaction
$M_j \in \mathbb{R}_+$	Michaelis-Menten saturation parameter for j–th reaction
$p \in \mathbb{R}^q$	vector of reaction rate parameters
$\tilde{p} \in \mathbb{R}^q$	perturbed parameter vector
$\varphi \in \mathbb{R}$	adjustable parameter
$\mathcal{P} \subset \mathbb{R}^q$	set of parameter vectors
$S \in \mathbb{R}^{n\times m}$	stoichiometric matrix

$v(x,p) \in \mathbb{R}^m$	vector of reaction rates
$\tilde{v}(x,p) \in \mathbb{R}^m$	perturbed reaction rate vector
$V(x,p) \in \mathbb{R}^{m\times n}$	reaction rate Jacobian $V = \frac{\partial v}{\partial x}$
$x \in \mathbb{R}^n$	vector of state variables
$\mathcal{X} \subset \mathbb{R}^n$	set of state vectors

Model analysis

Symbol	Description
(A_o, B_o, C_o)	state space representation of linearised open loop system
$\beta \in \mathbb{N}$	number of critical frequencies (elements of $\mathcal{R}$)
$\bar{\Delta},\ \Delta \in \mathbb{R}^{m\times n}$	unscaled, scaled kinetic perturbation
$f(x,u,p) \in \mathbb{R}^n$	vector field for open loop system
$g(\chi, j\omega_c^i(\chi)) \in \mathbb{R}$	transfer function value at i–th branch of critical frequencies
$G(\chi,s) \in \mathbb{C}$	transfer function of input–output system
$h(x) \in \mathbb{R}$	output function for open loop system
$K \in \mathbb{R}^{(2k-2)\times k}$	matrix for the representation of affine state and parameter constraints
$\mathcal{M} \subset \mathbb{R}^{n+q}$	q–dimensional manifold of steady state–parameter pairs
$\psi \in \mathbb{R}$	robustness radius for qualitative dynamical behaviour
$\Phi : \mathbb{R}^{n+q} \to \mathbb{R}^n$	functional representation of manifold $\mathcal{M}$
$Q(\cdot), R(\cdot) \in \mathbb{C}$	transfer function decomposition $G = QR^{-1}$
$\mathcal{R} \subset \mathbb{R}$	realness locus of a transfer function
$\varrho \in \mathbb{R}$	robustness radius for steady state values
$s \in \mathbb{C}$	complex frequency variable
$\bar{\sigma} \in \mathbb{R}^n$	change in local sensitivity with respect to φ
$\bar{\Sigma},\ \Sigma \in \mathbb{R}^{n\times q}$	unscaled, scaled local sensitivity of steady state
$T \in \mathbb{R}[\chi]$	multiplier polynomial for Handelman representation
$u,\ y \in \mathbb{R}$	input, output for open loop system
$U \in \mathcal{S}^k$	matrix for the sum of squares representation of ODE right hand side
$W \in \mathcal{S}^k$	matrix derived from the dyadic product $\xi\xi^{\mathrm{T}}$
$\omega \in \mathbb{R}$	frequency variable
$x_s(p) \in \mathbb{R}^n$	steady state in dependence of parameters
$\xi \in \mathbb{R}^k$	vector of monomials
$\Xi(p) \subset \mathbb{R}^{n+q}$	set of steady state–parameter pairs for parameter p
$Y \in \mathbb{R}[\chi]$	polynomial for equality constraints
$Z \in \mathbb{R}[\chi]$	polynomial for inequality constraints

Abstract

In the area of systems biology, dynamical models of biochemical reaction networks are used to derive model-based predictions about the related biological processes. This thesis provides new methods to study how parametric uncertainty affects such predictions. The focus of this study is on predictions about the steady states and the type of dynamical behaviour, such as bistability or oscillations.

Concerning steady states, the problem of uncertainty analysis is investigated. For a given extent of parametric uncertainty, the objective is to compute bounds on the variations in the steady states. In view of an underlying feasibility problem, a method based on semidefinite programming is developed to solve this problem. The approach is also applied to compute a measure for the robustness of the location of steady states in the presence of parametric uncertainty.

Regarding the effect of parametric uncertainty on the type of dynamical behaviour, the robustness problem is considered. A robustness measure is defined by the extent of parametric uncertainty for which no local bifurcations occur. An approach to solve the robustness problem with frequency domain methods is investigated. The proposed feedback loop breaking method allows to characterise parametric uncertainties for which the type of dynamical behaviour is robust. On the one hand, a lower bound on the corresponding robustness measure is computed by providing Positivstellensatz infeasibility certificates for the underlying equations. On the other hand, the feedback loop breaking concept is adopted for the design of a bifurcation search algorithm in a high-dimensional parameter space. The results of the search algorithm thereby provide an upper bound on the robustness measure.

In addition, the novel concept of kinetic perturbations is introduced. This is a class of specific parametric uncertainties which are particularly useful for the analysis of biochemical reaction networks. It is shown that a robustness analysis is performed efficiently for kinetic perturbations by use of the structured singular value. As a side result, the direct relation between kinetic perturbations and changes to the sensitivity of steady states in a biochemical reaction network is demonstrated.

To complement the methodological results, a novel model for a specific biochemical signal transduction system within the TNF induced signalling network is constructed. The model is analysed with methods developed in this thesis. In addition to an illustrative application of the new methods, the findings of this analysis also provide new biological insight into TNF signal transduction.

Deutsche Kurzfassung

Forschungsfrage dieser Arbeit

Viele Vorgänge in lebenden Organismen basieren auf biochemischen Reaktionsnetzwerken. Für Aussagen über das Verhalten solcher Netzwerke werden meist dynamische Modelle, beispielsweise in der Form von gewöhnlichen Differentialgleichungen, benötigt. In diesen Modellen werden Modellparameter verwendet, deren Werte allerdings oft einer großen Unsicherheit unterliegen.

Parameterunsicherheiten beeinträchtigen die Möglichkeit, mittels des Modells Aussagen über das betrachtete biochemische Reaktionsnetzwerk zu treffen. Das Thema dieser Arbeit ist die Analyse solcher Auswirkungen von Parameterunsicherheiten in Modellen biochemischer Reaktionsnetzwerke. Dabei werden besonders Aussagen über die Ruhelagen sowie den Typ des dynamischen Verhaltens, beispielsweise Oszillationen und Bistabilität, betrachtet.

Für die Analyse werden zwei komplementäre Wege betrachtet: die Unsicherheitsanalyse und die Robustheitsanalyse. Bei einer Unsicherheitsanalyse geht man davon aus, dass bestimmte Schranken bekannt sind, innerhalb derer die Parameterwerte unsicher sind. Das Ziel ist dann, einen Bereich für das mögliche Modellverhalten, beispielsweise die Position der Ruhelagen, zu bestimmen. In einer Robustheitsanalyse wird der umgekehrte Ansatz verfolgt. Dabei wird ein bestimmtes gewünschtes Modellverhalten vorgegeben, beispielsweise aufgrund einer Beobachtung am realen Prozess. Zu diesem Modellverhalten wird ein Parameterbereich bestimmt, innerhalb dessen jede mögliche Wahl der Parameter zum gewünschten Modellverhalten führt. Hieraus erhält man Grenzen für die Parameterunsicherheiten, welche keinen Einfluss auf eine entsprechende Aussage zum Modellverhalten haben. Beispielsweise lassen sich mit den in dieser Arbeit entwickelten Verfahren Parameterbereiche bestimmen, innerhalb derer das Auftreten von Oszillationen sichergestellt werden kann.

Einführung in das Thema der Arbeit

Mathematische Modellierung biochemischer Reaktionsnetzwerke

Zentrale Prozesse auf zellulärer Ebene, wie etwa der Stoffwechsel, biochemische Signalübertragung und Genregulation, lassen sich in abstrakter Form als (bio-)chemische Reaktionsnetzwerke beschreiben. Die Struktur eines solchen Reaktionsnetzwerkes wird über eine Liste von chemischen Reaktionen definiert. Jede Reaktion beschreibt dabei ein Umwandlungsgesetz, durch das eine Menge chemischer Moleküle (die Reaktanden) in eine andere solche Menge (die Produkte) umgewandelt wird. Die Reaktionsliste legt jedoch

nur die Struktur des Netzwerkes fest, die Dynamik ist dabei nicht berücksichtigt. Ohne Betrachtung der Dynamik können jedoch nur sehr beschränkte Aussagen über den Prozess gemacht werden, dem das Reaktionsnetzwerk zugrunde liegt. Nur mittels der Dynamik kann jeweils die Anzahl oder Konzentration der im System vorhandenen Moleküle und deren zeitliche Entwicklung beschrieben werden. Die Konzentrationen sind jedoch entscheidend für die Funktion des jeweiligen Prozesses. Beispielsweise hängt die Wachstumsrate von Organismen von der Menge der erzeugten Stoffwechselprodukte ab, und die Aktivität einzelner Gene wird entscheidend von der Konzentration der für diese Gene spezifischen Transkriptionsfaktoren im Zellkern beeinflusst.

Für die dynamische Modellierung ist die Festlegung von Reaktionsraten erforderlich. Diese beschreiben, wie oft jedes Reaktionsgesetz pro Zeiteinheit zur Ausführung kommt. Die Reaktionsraten hängen typischerweise von der Konzentration der jeweiligen Reaktanden ab. Aus der Struktur des Netzwerkes und den Reaktionsraten kann dann mittels Massenbilanzierung eine Differentialgleichung aufgestellt werden, welche die Entwicklung der Molekülmengen oder -konzentrationen über der Zeit beschreibt. Eine solche Differentialgleichung ist ein vollständiges Modell für die Dynamik des betrachteten Netzwerkes.

Dynamische Modelle in der Form von Differentialgleichungen beinhalten meist mehrere Parameter, d.h. Systemgrößen, deren Werte sich nicht aus dem Modell ergeben, sondern extrinsisch vorgegeben werden müssen. In biochemischen Reaktionsnetzwerken übliche Parameter sind beispielsweise Reaktionskonstanten, die für den Zusammenhang zwischen den Reaktionsraten und der Konzentration der Reaktanden erforderlich sind. Reaktionskonstanten hängen unter anderem von physikalischen Eigenschaften der Reaktanden ab, die bei der hier beschriebenen Modellierung nicht eigens berücksichtigt werden, und müssen daher als Parameter in das Modell integriert werden. Weitere Parameter, die etwa bei Stoffwechselnetzwerken verwendet werden, sind die Konzentrationen von Enzymen. Diese katalysieren zwar Reaktionen, werden dabei aber nicht verbraucht oder neu gebildet.

Analyse von Unsicherheiten in dynamischen Modellen

In vielen Fällen wird ein mathematisches Modell verwendet, um Aussagen über einen realen Prozess zu machen. Dabei tritt das Problem auf, dass ein Modell nie exakt die realen Zusammenhänge beschreibt, sondern immer Unsicherheiten auftreten. In biochemischen Reaktionsnetzwerken kann bereits die Struktur des Netzwerkes unsicher sein. Dies betrifft sowohl das Vorhandensein einzelner Reaktionen im Netzwerk wie auch die Beteiligung einzelner Moleküle an den Reaktionen. Zusätzlich besteht eine Unsicherheit in der Form des Reaktionsratengesetzes, d.h. des mathematischen Zusammenhangs zwischen Reaktionskonstanten, Konzentration der Reaktanden und Reaktionsrate. Unsicherheiten solcher Art werden als strukturelle Unsicherheiten bezeichnet.

Weiterhin treten oft sogenannte Parameterunsicherheiten auf, bei denen statt genauer Parameterwerte nur Bereiche bekannt sind, in denen Parameterwerte liegen können. Für biochemische Prozesse auf zellulärer Ebene sind Parameterunsicherheiten im Vergleich zu physikalischen oder technischen Systemen oft besonders ausgeprägt. Hierfür gibt es mehrere Gründe. Einige Parameter können zwar direkt experimentell gemessen werden, jedoch sind Messungen auf zellulärer Ebene oft mit großen Messfehlern behaftet. Falls Parameter nicht direkt gemessen werden können, müssen sie indirekt aus potenziell fehlerhaften

Messungen anderer Systemgrößen ermittelt werden. Oft beinhalten Parameterwerte auch Umgebungsgrößen, etwa die Temperatur, von deren Wert die Dynamik des Reaktionsnetzwerkes abhängt. Häufig ist allerdings die Umgebung, in welcher der modellierte Prozess abläuft, nicht genau bekannt, wodurch zusätzliche Unsicherheiten generiert werden.

Ein elementarer Teil der Modellanalyse besteht darin, die Auswirkungen der Unsicherheiten auf die modellbasierten Aussagen über den betrachteten Prozess abzuschätzen. Wichtige modellbasierte Aussagen betreffen beispielsweise mögliche Ruhelagen, d.h. stationäre Zustände, die sich bei konstanter äußerer Einwirkung nach einiger Zeit einstellen. Die Auswirkung von kleinen Parameterunsicherheiten auf die Ruhelagen kann mittels einer (lokalen) Sensitivitätsanalyse berechnet werden. Für große Parameterunsicherheiten, wie sie in biologischen Systemen oft bestehen, gibt es jedoch keine etablierten deterministischen Methoden für eine entsprechende Untersuchung. Es werden daher oft nichtdeterministische Ansätze verwendet, bei denen die Variation der Ruhelagen nur probabilistisch bestimmt wird. Allerdings können bei diesen Ansätzen keine sicheren Schranken für die Variation berechnet werden.

Eine weitere für biologische Systeme relevante modellbasierte Aussage betrifft komplexes dynamisches Verhalten in einem biochemischen Reaktionsnetzwerk. Damit bezeichnet man die Eigenschaft, dass der Zustand des Systems nicht zu einer eindeutigen Ruhelage strebt, sondern beispielsweise Bistabilität oder Oszillationen aufweist. Unter Bistabilität versteht man die Eigenschaft, dass ein System in Abhängigkeit vom Anfangszustand und äußeren Einflüssen unterschiedliche Ruhelagen erreichen kann. Im Hinblick auf Parameterunsicherheiten ist für das dynamische Verhalten vor allem das Problem der Robustheit interessant. Die Fragestellung ist dabei, wie groß eine Parameterunsicherheit sein kann, ohne dass sie sich auf den Typ des dynamischen Verhaltens auswirkt. Falls nur wenige (üblicherweise maximal zwei) Parameter unsicher sind, wird das Robustheitsproblem durch eine Bifurkationsanalyse teilweise gelöst. Dabei werden Kurven im Parameterraum berechnet, auf denen sich der Typ des dynamischen Verhaltens verändert. Solche Kurven bilden Grenzen für Bereiche, in denen sich das dynamische Verhalten nicht ändert. Meist kann allerdings nicht ausgeschlossen werden, dass es abseits der berechneten Kurven noch weitere Parameterwerte gibt, für die eine Änderung des dynamischen Verhaltens auftritt.

Forschungsbeiträge und Gliederung der Arbeit

In dieser Arbeit werden Methoden zur Unsicherheits- und Robustheitsanalyse für biochemische Reaktionsnetzwerke mit Parameterunsicherheiten entwickelt. Die entwickelten Methoden betreffen die Analyse möglicher Ruhelagen sowie die Robustheit des dynamischen Verhaltens bei unsicheren Parametern.

Für die Untersuchung der Ruhelagen wird in erster Linie eine Unsicherheitsanalyse vorgeschlagen. Dabei werden für einen gegebenen Parameterbereich Schranken für die Variation der Ruhelagen ermittelt. Aufgrund des zugrundeliegenden Erreichbarkeitsproblems eignen sich für dieses Problem Ansätze der konvexen Optimierung, speziell der semidefiniten Programmierung. Dieselben Ansätze lassen sich auch zur Untersuchung der Robustheit von Ruhelagen gegenüber unsicheren Parametern verwenden.

Für die Auswirkungen von Parameterunsicherheiten auf den Typ des dynamischen Verhaltens wird das Robustheitsproblem betrachtet. Eine wesentliche Rolle für das komple-

xe dynamische Verhalten spielt die Rückkopplungsstruktur des Netzwerkes. Da sich die Regelungstheorie auf abstrakter Ebene ausführlich mit den Eigenschaften dynamischer Rückkopplungen befasst, wird in dieser Arbeit zur Lösung des Robustheitsproblems für das dynamische Verhalten ein Ansatz entwickelt, der auf etablierten Konzepten der robusten Regelungstheorie beruht. Ein entscheidender Schritt bei der Verwendung dieser Konzepte ist die Transformation des Problems in den Frequenzbereich. Die Frequenzbereichs-Transformation wird dabei mit dem neu vorgeschlagenen Verfahren des Aufschneidens einer Rückkopplung erreicht, durch welches das biochemische Netzwerk regelungstechnischen Ansätzen zugänglich wird.

Kapitel 2 – Dynamische Modellierung biochemischer Reaktionsnetzwerke In diesem Kapitel wird die dieser Arbeit zugrundeliegende Modellklasse zur Beschreibung biochemischer Reaktionsnetzwerke eingeführt. Zusätzlich werden Differentialgleichungsmodelle für zwei in der Literatur intensiv behandelte Netzwerke vorgestellt, die in den folgenden Kapiteln mit den neu entwickelten Methoden beispielhaft untersucht werden.

Kapitel 3 – Unsicherheits- und Robustheitsanalyse stationärer Zustände Dieses Kapitel behandelt die Auswirkungen von Parameterunsicherheiten auf die Ruhelagen des Netzwerkes. Es werden Methoden zur Lösung des Unsicherheits- und des Robustheitsproblems für diese Fragestellung entwickelt. Mittels sogenannter Nichterreichbarkeitszertifikate werden zur Lösung des Unsicherheitsproblems Schranken bestimmt, innerhalb derer alle möglichen Ruhelagen für eine vorgegebene Parameterunsicherheit liegen. In ähnlicher Weise wird zur Lösung des Robustheitsproblems ein Parameterbereich bestimmt, für den garantiert werden kann, dass eine vorgegebene Variation in den Ruhelagen nicht überschritten wird.

Kapitel 4 – Robustheitsanalyse des dynamischen Verhaltens In diesem Kapitel werden Methoden zur Quantifizierung der Robustheit des dynamischen Verhaltens gegenüber Parameterunsicherheiten entwickelt. Da die Ruhelagen selbst das dynamische Verhalten wesentlich beeinflussen, basieren diese Methoden teilweise auf den Ergebnissen des vorigen Kapitels. Zur Untersuchung komplexen dynamischen Verhaltens wird ein Ansatz vorgeschlagen, der durch ein Aufschneiden der Rückkopplung einfach zu treffende Aussagen über Änderungen des dynamischen Verhaltens zulässt. Mit diesem Ansatz ist es möglich, für bestimmte Parameterbereiche zu garantieren, dass in diesen Bereichen keine Änderung des dynamischen Verhaltens auftritt. Somit kann eine untere Grenze für die Parameterunsicherheit berechnet werden, bis zu der Robustheit des dynamischen Verhaltens sichergestellt ist.

Kapitel 5 – Bifurkationssuche in hochdimensionalen Parameterräumen Der im vorigen Kapitel entwickelte Ansatz mit einem Aufschneiden der Rückkopplung wird hier verwendet, um in hochdimensionalen Parameterräumen Punkte zu finden, an denen sich der Typ des dynamischen Verhaltens ändert. Da solche Punkte eine obere Grenze für die Robustheit des betrachteten Systems ergeben, ist diese Methode komplementär zu dem im vorigen Kapitel entwickelten Ansatz. Zusätzlich lässt sich mit dieser Methode ermitteln, welche Parameter besonders relevant für Änderungen im dynamischen Verhalten des

Netzwerkes sind.

Kapitel 6 – Robustheitsanalyse und Veränderung der Sensitivität mit kinetischen Perturbationen In diesem Kapitel werden kinetische Perturbationen als neuer, für biochemische Netzwerke relevanter Unsicherheitstyp eingeführt. Kinetische Perturbationen nehmen eine Mittelstellung zwischen strukturellen und parametrischen Unsicherheiten ein. Es wird gezeigt, dass sich kinetische Perturbationen effizient zur Robustheitsanalyse des dynamischen Verhaltens nutzen lassen. Hierfür kann der in der Regelungstechnik etablierte Ansatz der strukturierten Singulärwerte verwendet werden. Zusätzlich wird ein Zusammenhang zwischen kinetischen Perturbationen und einer Änderung der Sensitivität von Ruhelagen hergestellt.

Kapitel 7 – Erstellung und Analyse eines Modells für die TNF Signalübertragung Es wird ein neues Modell zur Beschreibung eines TNF induzierten Signalweges vorgestellt, wobei im Gegensatz zu früheren Modellen besonders die Interaktionen zwischen zwei unterschiedlichen Rezeptortypen berücksichtigt werden. Das Modell dient als Fallbeispiel für die Anwendung der in dieser Arbeit entwickelten Methoden. Die Ergebnisse der verwendeten Analysemethoden erlauben dabei von biologischer Seite neue Erkenntnisse über das untersuchte System.

Chapter 1

Introduction

1.1 Research motivation

Many processes in living organisms are based on biochemical reaction networks. On the cellular level, biochemical reaction networks describe central elements like metabolism, biochemical signal transduction or gene regulation in an abstract way. Most predictions about the behaviour of such networks require the use of dynamical models. A common framework for the dynamical modelling of biochemical reaction networks is the use of ordinary differential equations, which describe the temporary evolution of the amount of the chemical species considered in the network.

Differential equations describing biochemical reaction networks usually include model parameters. However, the parameter values corresponding best to the features of the real network are typically not exactly known. This effect is denoted by the term *parametric uncertainty*. Often, the uncertainty stems from insufficient biological knowledge about the modelled network. Another source of uncertainty are the experimental difficulties involved in measuring model parameters *in vivo*. Despite the uncertainty, a dynamical model may be used to make predictions about the behaviour of the real network. However, in such a situation, model-based predictions need to be complemented by an additional analysis to assess their reliability. One option for such an assessment is to compute the range of possible model behaviours for a given uncertainty directly. We refer to this approach as uncertainty analysis. Another option, commonly called robustness analysis, is to estimate up to which level of uncertainty a specific model behaviour is not affected by the uncertainty. A robustness analysis thereby yields bounds on the magnitude of uncertainty for which predictions remain reliable.

In the following, we will argue that current methods to deal with parametric uncertainty in models of biochemical reaction network are insufficient in many cases. This insufficiency opens a methodological gap which is addressed in this work. To fill this gap, this thesis provides computational methods for evaluating the effect of parametric uncertainty on the dynamics of biochemical reaction networks. The focus is on two network properties which play major roles in the analysis of a dynamical model: the locations of steady states and the emergence of complex dynamical behaviour, such as sustained oscillations.

1.2 Research topic overview

1.2.1 History of modelling biochemical reaction networks

Mathematical modelling of biochemical reaction networks has accompanied general research in intracellular biological chemistry for decades, but has received varying appreciation from experimental biologists over time. An early landmark paper in this respect is A. M. Turing's (1952) paper on basic mechanisms in development, one of the first papers where a dynamical model for an intracellular signalling process based on chemical reactions was constructed. Also, gene regulation mechanisms have been modelled and analysed mathematically shortly after the discovery of the underlying molecular mechanisms (Griffith, 1968a,b). However, most of the early studies were concerned with networks of biochemical reactions in metabolism. Researchers in the 1960s and 70s worked on mathematical models of metabolic pathways (Savageau, 1976), using basic mathematical formulations for chemical reaction rates, such as the law of mass action or the Michaelis-Menten mechanism (Michaelis and Menten, 1913). An important impulse for these efforts was the discovery of the allosteric regulation of enzyme activity (Monod *et al.*, 1965), which set the basis for the construction of metabolic networks with complex regulatory interactions. Mathematical modelling permitted to realise that such regulatory interactions may induce a loss of stability, which has led to the study of stability conditions for metabolic pathways (Dibrov *et al.*, 1982). In this context, also the chemical reaction network theory should be mentioned, which provides a thorough treatment of steady states and their stability in certain classes of reaction networks (Feinberg, 1988, 1987). Due to an increase in mechanistic biological knowledge, mathematical modelling of the dynamics of biochemical signal transduction started to flourish in the 1990s, forming the basis for systems biology as a new research field. This is for example marked by important papers like the Goldbeter (1991) model of the mitotic oscillator, describing a process at the core of the eukaryotic cell cycle, or the presentation of the first dynamical model for the MAPK (mitogen activated protein kinase) cascade by Huang and Ferrell (1996). In the last decade, increasingly complex dynamical models for complete pathways have been constructed, as exemplified by a model for the EGF (epidermal growth factor) induced MAPK cascade proposed by Schoeberl *et al.* (2002). Yet, small models remain useful in order to understand various dynamical phenomena in biological signal transduction, like bistability in the lac operon (Ozbudak *et al.*, 2004). In recent years, the benefits of using dynamical models to understand biochemical processes are increasingly recognised also by experimental biologists (Eungdamrong and Iyengar, 2004).

1.2.2 Analysis tools for models of biochemical reaction networks

Let us next give an overview of established mathematical analysis tools for models of biochemical reaction networks, also pointing out problems in relation to parametric uncertainty analysis. Given the availability of very efficient numerical solvers for ordinary differential equations, the most straightforward tool for model analysis is the numerical simulation. To account for different environmental or internal conditions the system may face, simulations are often performed for a wide range of corresponding parameter values. The collection of all simulation results indicates the range of possible model behaviour.

However, in most cases it will not be known whether this range is well represented by the simulations. It is for instance possible that parameter values for which no simulation has been performed would put the model behaviour beyond the estimated range.

Apart from numerical simulation, many analysis techniques are concerned with steady states of the dynamical model. This is not only because steady states are more accessible mathematically, but also due to the significant relevance of steady states for the biological interpretation of the model. However, steady states can often only be computed numerically, and the computation of steady states for nominal parameter values is already challenging in many cases.

Given a specific steady state, a frequent question in relation to parametric uncertainty is how the steady state changes under variations of parameter values. The basic tool to answer this question is local sensitivity analysis, which uses the implicit function theorem to evaluate steady state changes in a neighbourhood of the nominal state (Rabitz *et al.*, 1983; Streif *et al.*, 2009; Varma *et al.*, 1999). For the analysis of metabolic networks, this basic approach has opened up a whole field of research, which is commonly referred to by the term *metabolic control analysis*. The origins of this field date back to 1973 (reprinted in Kacser *et al.*, 1995), when the basic principles of this approach were first introduced. In the following decades, various generalisations and extensions have been proposed (Heinrich and Schuster, 1996; Kahn and Westerhoff, 1991; Klipp *et al.*, 2005; Reder, 1988). In practice, the methods based on local sensitivity analysis have found widespread application in the field of metabolic engineering. They are commonly used to suggest genetic modifications of microorganisms which may improve a metabolic process with respect to a specific biotechnical objective (Stephanopoulos, 1999).

With respect to parametric uncertainty, local sensitivity analysis is a valuable tool, providing basic information about how a steady state is affected by small parameter variations. Thus, it allows to obtain a first estimate for the effect of parametric uncertainty on the variation in steady state values. Large uncertainties, which are frequently present in models of biochemical reaction networks, can however not be handled by local sensitivity analysis (Streif *et al.*, 2009).

In addition to the steady state location and local sensitivity, the dynamical properties of the network are of interest for many systems ranging from metabolism to signal transduction. This involves local stability of steady states (Dibrov *et al.*, 1982; Prill *et al.*, 2005), but also different types of instability related for example to switch-like, excitable or oscillatory behaviour (Tyson *et al.*, 2003). With respect to variations in model parameters, bifurcation analysis is the major tool to evaluate how dynamical properties of a steady state in the model depend on parameter values (Angeli *et al.*, 2004; Breindl *et al.*, 2009; Conradi *et al.*, 2007a; Eissing *et al.*, 2007b; Müller *et al.*, 2009; Tyson *et al.*, 2002). Stability of steady states and bifurcations are directly related to complex dynamical behaviour in biochemical reaction networks, such as bi- or multistability, i.e. the existence of two or several stable steady states, limit cycle oscillations, and non-periodic oscillations. There are many examples in which it is possible to relate complex dynamical behaviour in a biochemical reaction network to a biological function. Some examples from the specific area of biochemical signal transduction within living cells are the bistability in the MAPK pathway to induce developmental processes (Ferrell and Xiong, 2001), rapid activation of caspases upon an over-threshold stimulus in programmed cell death (Eissing *et al.*, 2004), and sustained oscillations in circadian clocks (Leloup and Goldbeter, 2003).

For a model in which one or two parameters are uncertain, a characterisation of the dynamical behaviour of the system within the relevant parameter range may be achieved by bifurcation analysis. However, bifurcation analysis can often only give a first estimate for possible dynamical properties, because more than two parameters are uncertain in most models, and simultaneous variations in all uncertain parameters need to be considered for a thorough analysis (Kim *et al.*, 2006; Stelling *et al.*, 2004).

1.2.3 Robustness of biochemical reaction networks

As indicated in Section 1.1, the effects of parametric uncertainty may also be evaluated by a robustness analysis. Generally, the aim of robustness analysis is to quantify the perturbations which a system can tolerate before losing a specific function (Kitano, 2004). Robustness analysis thereby allows to evaluate up to which level of uncertainty the function is maintained. A robustness analysis for a given system requires a specification of the function to be maintained as well as the type of perturbations which are taken into account. Due to the observation that the function of biological systems is inherently robust to many, possibly large, perturbations (Kitano, 2007; Stelling *et al.*, 2004), robustness issues are of particular relevance for such systems. On a biochemical level, robustness with respect to parametric uncertainty was first noticed in the adaptation of chemotactic receptors to different stimulus strengths (Barkai and Leibler, 1997). Robustness of complex dynamical behaviour has e.g. been suggested for the circadian clock, where oscillations need to be maintained to ensure biological function (Trané and Jacobsen, 2007), or in programmed cell death, where robust bistability ensures a reliable execution of programmed cell death (Eissing *et al.*, 2005). Robustness analysis is therefore a valuable tool for model validation: if a biochemical network is robust, but the corresponding model is not, then the model is not an adequate representation of the real network (Cimatoribus *et al.*, 2005; Morohashi *et al.*, 2002). In addition, robustness analysis may yield insights into the role of cellular regulation mechanisms, thereby improving our understanding of biological systems (Trané and Jacobsen, 2007).

However, biological systems are also fragile to certain perturbations, as pointed out by Carlson and Doyle (2002) with their concept of *highly optimised tolerance*. Robustness analysis is useful in this respect, because it allows to detect fragilities, i.e. perturbations for which the function of the system breaks down (Chaves *et al.*, 2005; Shoemaker and Doyle III, 2008). Knowledge of fragilities may help to find targets for pharmaceutical intervention, either by attacking malicious systems at weak points, or by protecting the weak points of beneficial systems which are perturbed in a disease.

With the growing industrial usage of engineered biosystems, the relevance of robustness analysis will further increase in the future. From an analysis perspective, it will be important to know the level of uncertainty, e.g. in the cellular environment, for which the system maintains the function it has been designed for. In addition, robustness issues will also directly be incorporated into the design strategies (Purnick and Weiss, 2009), with similar goals as in today's robust controller design methods.

Quantification of the robustness for a given system, function, and class of perturbations requires the definition of an appropriate robustness measure. If a suitable norm for the considered perturbations is available, a straightforward definition of a robustness measure is the norm of the smallest perturbation leading to a loss of function. Such a definition

is for example used by Ma and Iglesias (2002), where the function is defined by the qualitative dynamical behaviour, the considered perturbations are variations in a single parameter, and the perturbation norm is the factor by which the parameter value is varied. In this case, it is possible to perform the robustness analysis by numerical bifurcation analysis. Extending the same concept to variations in several parameters turned out to be quite difficult. Using the structured singular value approach from robust control theory (Zhou *et al.*, 1996), only partly conclusive results could be obtained (Kim *et al.*, 2006; Ma and Iglesias, 2002). Yet, a robustness analysis with the structured singular value can be used efficiently for structural perturbations, although it remains difficult to relate the considered perturbation class to physically justified variations in the biochemical network (Jacobsen and Cedersund, 2008; Trané and Jacobsen, 2008).

1.2.4 Methodological challenges

In general, methods from control engineering seem to provide efficient means to address the outlined problems of parametric uncertainty. However, the parametric uncertainty and robustness analysis of biochemical reaction networks generally faces three challenges, the combination of which is typically not dealt with adequately in control engineering methods. First, dynamical models for biochemical reaction networks are mostly nonlinear. Second, as mentioned above, one needs to consider simultaneous uncertainty of several parameters. Third, uncertainty in parameter values almost always implies an uncertainty in the steady states of the model. An additional point concerns the type of dynamical behaviour being considered. Robustness analysis methods in control theory almost exclusively focus on stability. However, for many biological systems, complex dynamical behaviour like multistability or oscillations is of high relevance. Therefore, methods for the analysis of these cases clearly have to go beyond the robustness of stability usually sought for in control engineering. These observations can be seen as main reasons, why the transfer of uncertainty and robustness analysis methods from control engineering to systems biology is more challenging than the apparent similarity of the considered problems may suggest.

1.3 Contribution of the thesis

To address the outlined problems of parametric uncertainty in models of biochemical reaction networks, we develop methods for uncertainty and robustness analysis of these models. The methods proposed in this thesis are essentially based on two concepts stemming from the field of control engineering: set-based uncertainty descriptions and analysis of feedback systems in the frequency domain. The developed methods aim at the analysis of steady states and the qualitative dynamical behaviour. All methods developed in this thesis are illustrated by examples, where the methods are applied to models from the literature.

The first part of the thesis builds on set-based uncertainty descriptions. Concerning the uncertainty of steady states, we propose the use of infeasibility certificates for the underlying feasibility problem. Infeasibility certificates are well suited in this context, because they can be obtained from the solution of a semidefinite program, for which

efficient numerical algorithms are available. For the steady state uncertainty analysis, we develop an algorithm to compute bounds on the steady state variability for a given parametric uncertainty, making use of the proposed infeasibility certificates. In a similar manner, we provide a robustness analysis method, for computing bounds on the parametric uncertainty which guarantee that a given limit on the steady state variability is not exceeded. In contrast to previous approaches, the proposed methods for the analysis of steady states directly consider uncertainty sets and do not rely on extrapolation from the local sensitivity. Thus, they offer an advantage for the analysis of large parametric uncertainties compared to sensitivity based methods.

For the qualitative dynamical behaviour, we focus on the robustness problem. To approach this problem, a robustness measure in parameter space is proposed, yielding bounds on a multi-dimensional parametric uncertainty which does not affect the qualitative dynamical behaviour. In the specific case of robust stability, we show how classical, Lyapunov based robustness tests can be applied to approximate the proposed robustness measure. In particular, this requires to make use of the previously described method for quantifying the steady state uncertainty. Otherwise, classical Lyapunov based methods could not cope with the problem of steady state variability under parametric uncertainty.

Concerning the robustness of instability, a feedback loop breaking approach is developed, building on frequency domain methods and concepts from robust control theory which form the core of the second part of the thesis. In particular, the feedback loop breaking approach allows to characterise parametric uncertainties for which the dynamical behaviour is robust. For typical models of biochemical reaction networks, the resulting equations are polynomial. This motivates the development of a method where the Positivstellensatz is combined with linear programming to obtain robustness certificates for the dynamical behaviour. Our method thus enables the robustness analysis of complex dynamical behaviour such as sustained oscillations or bistability. Based on the feedback loop breaking approach, we also develop an algorithm to search for bifurcations in a high-dimensional parameter space via a gradient-directed continuation method. This complements the methods for robustness analysis of the dynamical behaviour by providing upper bounds on the corresponding robustness measure.

Furthermore, the concept of kinetic perturbations is introduced as a new uncertainty class for biochemical reaction networks. It is shown how this concept allows a stringent robustness analysis. Thereby we use classical tools from robust control theory, in particular the structured singular value. A further application of kinetic perturbations is the computation of small variations in the system which shape the steady state behaviour with respect to an adjustable parameter in a specified way.

Beyond the methodological contributions, a novel model for a specific biochemical signal transduction pathway is developed, involving the tumor necrosis factor (TNF) receptors and the pro-inflammatory NF-κB[1] pathway. The application of the proposed analysis methods to this model gives new insights into oscillatory modes of the NF-κB pathway, as well as into mechanisms governing the network's response in the adaptor protein TRAF2[2] to a stimulation with the TNF ligand. In addition, the TNF signalling model serves as a comprehensive and realistic case study for part of the methods.

[1] NF-κB – nuclear factor κ-light-chain-enhancer of activated B cells (a mammalian transcription factor)
[2] TRAF2 – TNF receptor associated factor 2

Above, we have argued that a direct application of classical control engineering analysis methods to the problem of parametric uncertainty in biochemical reaction networks is often not possible. The results of this thesis show that, after overcoming the aforementioned challenges, taking a control engineering perspective is nevertheless an efficient way to approach the outlined problems. However, this requires that the concepts used in control are brought into a framework which is compatible with the special features of biochemical reaction networks.

1.4 Outline of the thesis

Chapter 2 contains fundamental concepts which are referred to from the remainder of the thesis. First, the modelling framework used throughout the thesis is presented, and some preliminaries concerning the model analysis, such as removal of conservation relations and local sensitivity analysis, are introduced. Second, two classical dynamical models describing specific biochemical signal transduction pathways are discussed. These models serve as application examples for the analysis methods developed in later chapters of the thesis.

In **Chapter 3**, a novel approach to the analysis of steady state location with respect to uncertain parameters is developed. This includes the computation of guaranteed bounds on the steady states for a given region where parameters may vary, and the computation of parameter sets for which it can be guaranteed that the corresponding steady states are located in a specified region.

Chapter 4 deals with the robustness of dynamical properties with respect to parametric uncertainty. In the first part of the chapter, we are considering specifically the robustness of stability. Based on the results of Chapter 3, a method for computing robust parameter sets is suggested. In the second part, the focus is turned towards the robustness of instability, which is related to complex dynamical behaviour like oscillations or bistability in biochemical reaction networks. Based on a newly introduced feedback loop breaking approach, a robustness analysis method in the frequency domain is developed, using the Positivstellensatz and linear programming to evaluate the robustness of stability or instability in a biochemical reaction network.

The methods suggested in Chapter 4 provide lower bounds on the size of the parametric uncertainty up to which the dynamical behaviour of the network remains robust. In **Chapter 5**, we consider the problem of finding an upper bound, which is solved by explicitly searching a bifurcation close to the nominal parameter values. Using again the feedback loop breaking approach presented in Chapter 4, we suggest a gradient-directed continuation method which is able to find nearby bifurcations from some nominal parameters.

In **Chapter 6**, a new uncertainty class called kinetic perturbations is introduced. Thereby we denote parametric or structural perturbations not affecting the nominal steady state of the system. Such perturbations may however still affect the dynamical properties and stationary stimulus–response characteristics of the system. We discuss the robustness of dynamical properties of a steady state with respect to kinetic perturbations in terms of the structured singular value. In addition, an approach to change the system's local sensitivity at the nominal point via kinetic perturbations is developed.

Chapter 7 provides an exemplary application for methods developed in earlier chapters. First, a novel model for a part of the tumor necrosis factor (TNF) signalling network is constructed. Then, methods developed in this thesis are used to analyse oscillatory behaviour and sensitivity of the system with respect to a TNF stimulus. In this way, the chapter provides a case study which combines new biological insight and an illustrative application of methods developed in this thesis.

Chapter 2

Dynamical models for biochemical reaction networks

This chapter provides some background material concerning the dynamical modelling of biochemical reaction networks. Section 2.1 describes the derivation of ODE models, and how to eliminate conservation relations, which may otherwise complicate the analysis of dynamical properties, from the model. Section 2.2 contains a short summary of local sensitivity analysis as the most basic technique to study the effect of parameter variations on a model. Finally, in Section 2.3, we describe some established models of biochemical signalling pathways, which will be used in examples throughout this thesis.

2.1 Basic modelling techniques

2.1.1 Construction of dynamical models

Biochemical reaction networks are composed of two main elements: Chemical species, each of which represents an ensemble of chemically identical molecules in a specific compartment of the cell, and chemical reactions, which are processes transforming one group of species into another one.

The structure of a biochemical reaction network is characterised completely by the list of involved species, denoted as $X_1, X_2 \ldots, X_n$, and the list of reactions, denoted as

$$\sum_{i=1}^{n} S_{ij}^{(r)} X_i \to \sum_{i=1}^{n} S_{ij}^{(p)} X_i, \quad j = 1, \ldots, m, \tag{2.1}$$

where m is the number of reactions in the network, and the factors $S_{ij}^{(r)} \in \mathbb{N}_0$ and $S_{ij}^{(p)} \in \mathbb{N}_0$ are the stoichiometric coefficients of the reactant and product species, respectively (Higham, 2008; Klipp *et al.*, 2005). Reversible reactions can always be written in the form (2.1) by splitting the forward and reverse path into two separate irreversible reactions.

The structural information of the reaction network is usually subsumed in the stoichiometric matrix, given by

$$S = \left(S_{ij}^{(p)} - S_{ij}^{(r)} \right)_{i=1,\ldots,n,\ j=1,\ldots,m} \in \mathbb{R}^{n \times m}. \tag{2.2}$$

The state vector of the system consists of the concentrations of the involved chemical species and is denoted by

$$x = \left([X_i] \right)_{i=1,\ldots,n} \in \mathbb{R}^n,$$

where $[X_i]$ represents the concentration of species X_i.

The kinetic information for the reaction network is represented by reaction rate functions, which depend on the state $x \in \mathbb{R}^n$ and the kinetic parameters $p \in \mathbb{R}^q$. The reaction rates are given by the vector

$$v(x,p) = (v_j(x,p))_{j=1,\dots,m} \in \mathbb{R}^m,$$

where $v_j(x,p)$ is the rate of the j–th reaction in (2.1). A common model for the reaction rate functions is the law of mass action, given by

$$v_j(x,p) = k_j \prod_{i=1}^{n} x_i^{S_{ij}^{(r)}}, \tag{2.3}$$

where $k_j \geq 0$ is the reaction rate constant, which is integrated into the model as an element of the parameter vector p. In metabolic networks, reaction rates are often modelled with Michaelis-Menten expressions, which are derived from the law of mass action for an enzymatic reaction by singular perturbation (Keener and Sneyd, 2004). A Michaelis-Menten reaction rate where X_i is the substrate of the enzymatic reaction is given by

$$v_j(x,p) = \frac{k_j x_i}{1 + M_j x_i}, \tag{2.4}$$

where $k_j \geq 0$ and $M_j \geq 0$ are kinetic parameters.

Independently of the chosen reaction rate mechanisms, a model for the dynamics of the reaction network is obtained by mass balancing. The dynamics are described by an ordinary differential equation given as

$$\dot{x} = Sv(x,p). \tag{2.5}$$

2.1.2 Elimination of conservation relations

Biochemical reaction networks are subject to the law of mass conservation. Specifically, the amount of entities which are neither added to nor removed from the system will not change with time. Mathematically, conservation relations in a biochemical reaction network are described by a vector $\theta \in \mathbb{R}^n$ such that

$$\theta^{\mathrm{T}} \dot{x} = \theta^{\mathrm{T}} S v(x,p) = 0. \tag{2.6}$$

For a conservation relation, (2.6) is required to hold true for all possible reaction rate vectors $v(x,p)$. The space spanned by all conservation relations is thus given by $\ker S^{\mathrm{T}}$ (Heinrich and Schuster, 1996).

If the biochemical reaction network (2.5) satisfies a conservation relation, the dimension of the state space can be reduced by introducing the initial concentration of the concerned species as an additional parameter $p_\theta = \theta^{\mathrm{T}} x(0)$. We shortly outline the procedure to achieve this reduction (see Heinrich and Schuster, 1996, for more details). Without loss of generality, assume that $\theta_1 \neq 0$. Denote $\theta_R = (\theta_2, \dots, \theta_n)^{\mathrm{T}}$ and $x_R = (x_2, \dots, x_n)^{\mathrm{T}}$. From (2.6) and the definition of p_θ, we obtain

$$x_1(t) = \frac{1}{\theta_1}(p_\theta - \theta_R^{\mathrm{T}} x_R(t)).$$

Thus, a reduced model of the biochemical reaction network (2.5) is given by

$$\dot{x}_R = Sv(\frac{1}{\theta_1}(p_\theta - \theta_R^{\mathrm{T}} x_R(t)), x_R, p) = Sv_R(x_R, p, p_\theta). \tag{2.7}$$

A conservation relation has an important effect on the dynamical properties of equilibrium points of (2.5): it leads to a zero eigenvalue of the Jacobian $S\frac{\partial v}{\partial x}(x_0, p)$ at an equilibrium point x_0. The zero eigenvalue emerges directly from the structure of the system, and it is independent of the state and parameter values x_0 and p. However, the zero eigenvalue does not have an effect on the dynamical properties of equilibrium points. In fact, the state space of the original system is stratified into invariant hyperplanes by the conservation relation, and the system evolves on these hyperplanes according to the reduced equation (2.7).

Yet, if not taken into account explicitly, the existence of conservation relations may complicate the analysis of dynamical properties of the model (2.5), where the eigenvalues of the Jacobian at an equilibrium point are considered. To remove the problem with the zero eigenvalue, it will be assumed tacitly in Chapters 4 to 6 that conservation relations are not present in the model under study, which can always be achieved by the procedure sketched above.

Example 2.1. As a very simple example, consider the reaction network $X_1 \underset{v_2}{\overset{v_1}{\rightleftharpoons}} X_2$. Using mass action kinetics, the network can be modelled by the ODE

$$\begin{aligned}\dot{x}_1 &= -k_1 x_1 + k_2 x_2\\ \dot{x}_2 &= k_1 x_1 - k_2 x_2.\end{aligned}$$

The network satisfies the conservation relation $\dot{x}_1 + \dot{x}_2 = 0$. We introduce the additional parameter $x_{tot} = x_1(0) + x_2(0)$, and obtain the reduced order model

$$\dot{x}_1 = -k_1 x_2 + k_2(x_{tot} - x_1).$$

2.2 Local sensitivity analysis

A first approach to evaluate the effect of parameter variations on the characteristics of a biochemical reaction network is a local sensitivity analysis of the steady state. A huge amount of literature on sensitivity analysis of biochemical reaction networks is available, see e.g. (Heinrich and Schuster, 1996; Ingalls, 2004; Kahn and Westerhoff, 1991; Rabitz *et al.*, 1983) and references therein. Sensitivity analysis is restricted to small (strictly speaking infinitesimal) perturbations of parameters from their nominal values, and aims to characterise the resulting small perturbations of steady states. It is based on a first order approximation of the steady state equation (Rabitz *et al.*, 1983). Local sensitivity analysis is also the main tool within the framework of metabolic control analysis to study the regulation of biochemical reaction networks (Heinrich and Schuster, 1996).

For the analysis, one considers a pair (x_0, p_0) of a nominal steady state $x_0 \in \mathbb{R}^n$ and $p_0 \in \mathbb{R}^q$ satisfying the steady state equation

$$Sv(x_0, p_0) = 0. \tag{2.8}$$

Thereby, it is assumed that the steady state is non-degenerate, i.e.

$$\det(S\frac{\partial v}{\partial x}(x_0, p_0)) \neq 0.$$

As discussed before, this requires that conservation relations are removed from the system by an appropriate order reduction. Then, by the implicit function theorem, there exists locally around (x_0, p_0) a function

$$x_s : \mathbb{R}^q \to \mathbb{R}^n : p \mapsto x_s(p) \tag{2.9}$$

which satisfies $x_0 = x_s(p_0)$ and $Sv(x_s(p), p) = 0$.

The local sensitivity $\bar{\Sigma}$ of the steady state x_0 with respect to parameter variations is defined as

$$\bar{\Sigma} = \frac{\partial x_s}{\partial p}(p_0). \tag{2.10}$$

In biochemical networks, individual state variables or parameters frequently differ by several orders of magnitudes. It is therefore common to use the scaled sensitivity (Klipp *et al.*, 2005)

$$\Sigma = \operatorname{diag}(x_0)^{-1}\frac{\partial x_s}{\partial p}(p_0)\operatorname{diag}(p_0), \tag{2.11}$$

which gives the relative variations in the steady state if parameters are varied, and is often a better measure for the effects of small parameter variations on the steady state than the unscaled sensitivity $\bar{\Sigma}$.

2.3 Classical models in systems biology

In this section, we present two biochemical signal transduction pathways, the MAPK cascade and the NF-κB pathway, for which extensive modelling efforts have been made in the past. We shortly discuss some of the models which have been developed for these systems. These models have found widespread attention in systems biology and provide benchmark problems for the development of new methods in model analysis. The models discussed here are also used in this thesis to illustrate the application of the newly developed analysis methods.

2.3.1 The MAPK cascade

A central element of signal transduction in eukaryotic cells is the mitogen activated protein kinase (MAPK) cascade. The MAPK cascade is a conserved structure of three kinases in a sequential pathway, where one kinase phosphorylates the next kinase in the pathway. The basic scheme is shown in Figure 2.1. This structure appears in many eukaryotic organisms, from *Dictyostelium discoideum* to mammals (Widmann *et al.*, 1999). Even within the same organism, MAPK cascades appear in several signalling pathways, and different kinases are involved in the different variants, but always following the same structure. Signalling pathways with MAPK cascades are involved in a number of important cellular events, such as cell proliferation, differentiation, and response to external stress signals (Pearson *et al.*, 2001; Widmann *et al.*, 1999).

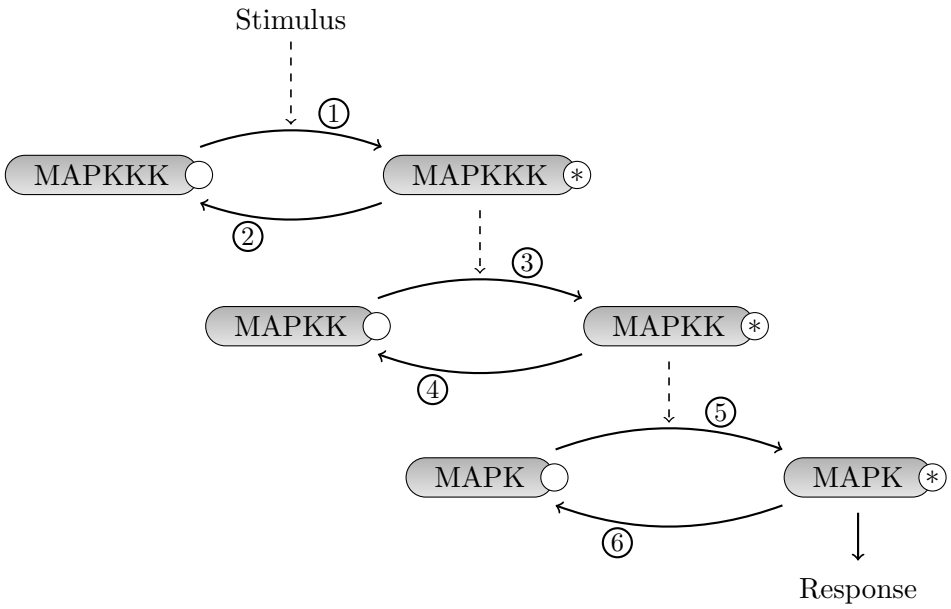

Figure 2.1: Schematic model for the MAPK cascade. The input stimulus S typically represents the activity of a specific receptor complex. The molecular species in the cascade are called (from last to first step): mitogen activated protein kinase (MAPK), MAPK kinase (MAPKK), and MAPKK kinase (MAPKKK). Activated, i.e. fully phosphorylated forms of the individual species are marked with an asterisk.

Due to its relevance in intracellular signalling pathways, the MAPK cascade has become a representative object of study in the field of systems biology during the past decade. Several dynamical models have been proposed for MAPK cascades, either directly including all possible complexes and using mass action kinetics (Huang and Ferrell, 1996), or based on a Michaelis-Menten approximation for the enzymatic reactions (Kholodenko, 2000). Other models do not only consider the MAPK cascade in isolation, but include the Raf/MEK/ERK cascade as part of a model for the EGF receptor signalling pathway[1] (Asthagiri and Lauffenburger, 2001; Brightman and Fell, 2000; Schoeberl *et al.*, 2002).

In the scope of this work, the MAPK cascade is of interest, because it is one of the first signalling pathways where bistability, a common dynamical behaviour in biological systems, has been discussed. The initial experimental observations of switch–like behaviour in the MAPK cascade (Huang and Ferrell, 1996) have stimulated the analysis of different MAPK cascade models with respect to bistability (Ferrell and Machleder, 1998; Ferrell and Xiong, 2001; Markevich *et al.*, 2004; Qiao *et al.*, 2007).

For some MAPK cascades, feedback interconnections are known and may have a profound effect on the cascade's dynamics. For the Raf/MEK/ERK cascade, active ERK phosphorylates and thereby inhibits SOS (son of sevenless homologue), which is required in the activation of Raf (Brightman and Fell, 2000). This interaction constitutes a negative feedback loop around the cascade (see Figure 2.2), and has been proposed as a

[1] MEK – MAP/ERK kinase (more recently also called MAP2K), ERK – extracellular signal regulated kinase, EGF – epidermal growth factor

Table 2.1: Simplistic reaction model for the MAPK cascade. Molecular species: S – stimulus, KKK – MAPKK kinase, KK – MAPK kinase, K – MAPK. The asterisk denotes the activated forms of the kinases.

Reaction	Rate	Parameter values
$\mathrm{KKK} + \mathrm{S} \to \mathrm{KKK}^* + \mathrm{S}$	$v_1 = k_{11}[\mathrm{KKK}][\mathrm{S}]$	$k_{11} = 0.1\,\frac{1}{\mathrm{min\,nM}}$, $[\mathrm{S}] = 5\,\mathrm{nM}$
$\mathrm{KKK}^* \to \mathrm{KKK}$	$v_2 = k_{12}[\mathrm{KKK}^*]$	$k_{12} = 0.2\,\frac{1}{\mathrm{min}}$
$\mathrm{KK} + \mathrm{KKK}^* \to \mathrm{KK}^* + \mathrm{KKK}^*$	$v_3 = k_{21}[\mathrm{KK}][\mathrm{KKK}^*]$	$k_{21} = 0.1\,\frac{1}{\mathrm{min\,nM}}$
$\mathrm{KK}^* \to \mathrm{KK}$	$v_4 = k_{22}[\mathrm{KK}^*]$	$k_{22} = 0.2\,\frac{1}{\mathrm{min}}$
$\mathrm{K} + \mathrm{KK}^* \to \mathrm{K}^* + \mathrm{KK}^*$	$v_5 = k_{31}[\mathrm{K}][\mathrm{KK}^*]$	$k_{31} = 0.1\,\frac{1}{\mathrm{min\,nM}}$
$\mathrm{K}^* \to \mathrm{K}$	$v_6 = k_{32}[\mathrm{K}^*]$	$k_{32} = 0.2\,\frac{1}{\mathrm{min}}$

possible mechanism for sustained oscillations (Kholodenko, 2000). The possibility of sustained oscillations in the MAPK cascade has further been investigated by computational studies (Chickarmane *et al.*, 2007; Qiao *et al.*, 2007). More recently, sustained oscillations have been observed experimentally in a MAPK cascade, albeit for another type of MAPK cascade, involved in the pheromone response of yeast cells (Hilioti *et al.*, 2008).

A simplistic MAPK model

First, let us introduce a simplistic model of the MAPK cascade. Despite its simplicity, it possesses some of the relevant features which are observed in experiments, such as ultrasensitivity of the cascade and amplification of the stimulus from one step to the next. The model is obtained by directly translating the basic scheme from Figure 2.1 into a biochemical reaction network with mass action kinetics. The reactions and corresponding rates describing the model are given in Table 2.1.

Synthesis and decay of the kinases are neglected, and thus the system contains three conservation relations, one for each of the kinases. The conservation relations are given by

$$\begin{aligned} [\mathrm{KKK}] + [\mathrm{KKK}^*] &= \mathrm{KKK}_{tot} = 100\,\mathrm{nM} \\ [\mathrm{KK}] + [\mathrm{KK}^*] &= \mathrm{KK}_{tot} = 300\,\mathrm{nM} \\ [\mathrm{K}] + [\mathrm{K}^*] &= \mathrm{K}_{tot} = 300\,\mathrm{nM}, \end{aligned} \tag{2.12}$$

introducing the parameters KKK_{tot}, KK_{tot} and K_{tot} for the total concentrations of MAPKKK, MAPKK, and MAPK, respectively. The values are taken from the model proposed by Kholodenko (2000), and they are based on direct experimental measurements of the kinase concentrations.

Denoting $u = [\mathrm{S}]$, $x_1 = [\mathrm{KKK}^*]$, $x_2 = [\mathrm{KK}^*]$, and $x_3 = [\mathrm{K}^*]$, and taking advantage of the conservation relations (2.12), the reaction dynamics are described by the ODEs

$$\begin{aligned} \dot{x}_1 &= k_{11}(\mathrm{KKK}_{tot} - x_1)u - k_{12}x_1 \\ \dot{x}_2 &= k_{21}(\mathrm{KK}_{tot} - x_2)x_1 - k_{22}x_2 \\ \dot{x}_3 &= k_{31}(\mathrm{K}_{tot} - x_3)x_2 - k_{32}x_3. \end{aligned} \tag{2.13}$$

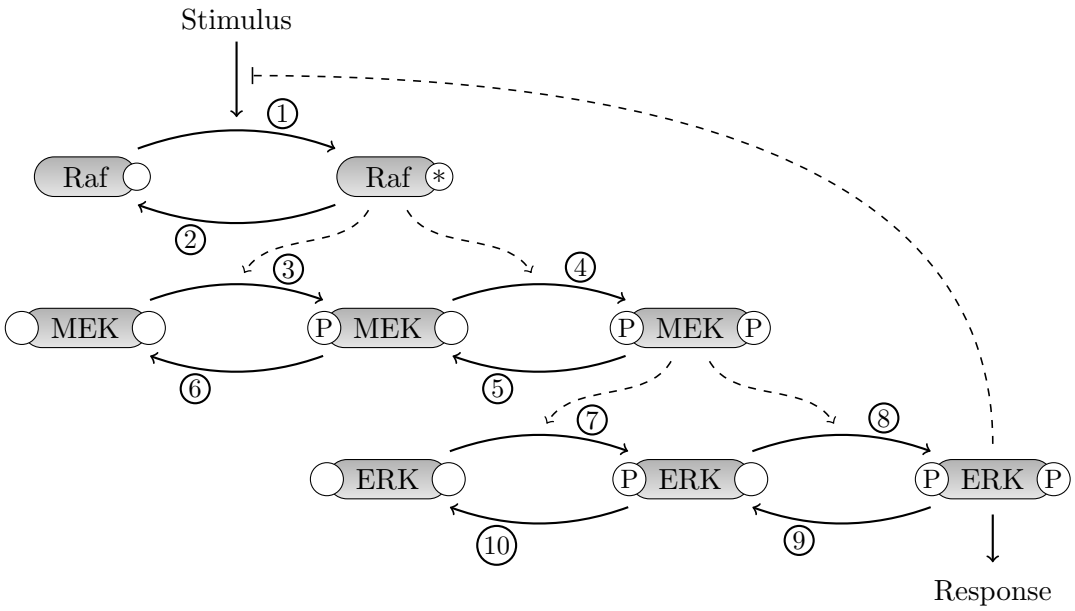

Figure 2.2: Illustration of the Raf/MEK/ERK cascade model in the EGF receptor pathway according to Kholodenko (2000). The numbers on the reaction arrows correspond to the reaction rate numbering in Table 2.2.

A more detailed MAPK model

Next, we specifically consider the MAPK cascade as it appears in the EGF receptor pathway (Brightman and Fell, 2000) with a negative feedback circuit around the cascade due to inhibition of SOS by phosphorylated ERK. Here, we use a model as suggested by Kholodenko (2000), which is a subsystem of the EGF pathway as modelled by Brightman and Fell (2000). A schematic diagram of the biochemical reactions in the model is shown in Figure 2.2.

In the equations, the concentrations of phosphorylated kinases are denoted as $x_{11} =$ [Raf*], $x_{21} =$ [MEK-P], $x_{22} =$ [MEK-PP], $x_{31} =$ [ERK-P], and $x_{32} =$ [ERK-PP]. The concentrations of unphosphorylated, inactive kinases Raf, MEK, and ERK need not to be included as state variables, as they can be computed via the conservation relations

$$\begin{aligned} [\text{Raf}] + x_{11} &= \text{KKK}_{tot} \\ [\text{MEK}] + x_{21} + x_{22} &= \text{KK}_{tot} \\ [\text{ERK}] + x_{31} + x_{32} &= \text{K}_{tot}. \end{aligned}$$

As in the previous model (2.13), KKK_{tot}, KK_{tot} and K_{tot} are parameters for the total concentrations of kinases, which are constant. Table 2.2 gives the mathematical expressions for the reaction rates. Nominal parameter values are shown in Table 2.3.

Using the reaction rates from Table 2.2, the model can be written as a system of five

Table 2.2: Reaction rates in the MAPK cascade model according to Kholodenko (2000). Reaction rate numbers are according to the labels in Figure 2.2.

Reaction	Rate	Reaction	Rate
v_1	$\frac{V_1(\mathrm{KKK}_{tot}-x_{11})}{(1+(x_{32}/K_i)^n)(K_{m1}+\mathrm{KKK}_{tot}-x_{11})}$	v_2	$\frac{V_2 x_{11}}{K_{m2}+x_{11}}$
v_3	$\frac{k_3 x_{11}(\mathrm{KK}_{tot}-x_{21}-x_{22})}{K_{m3}+\mathrm{KK}_{tot}-x_{21}-x_{22}}$	v_4	$\frac{k_4 x_{11} x_{21}}{K_{m4}+x_{21}}$
v_5	$\frac{V_5 x_{22}}{K_{m5}+x_{22}}$	v_6	$\frac{V_6 x_{21}}{K_{m6}+x_{21}}$
v_7	$\frac{k_7 x_{22}(\mathrm{K}_{tot}-x_{31}-x_{32})}{K_{m7}+\mathrm{K}_{tot}-x_{31}-x_{32}}$	v_8	$\frac{k_8 x_{22} x_{31}}{K_{m8}+x_{31}}$
v_9	$\frac{V_9 x_{32}}{K_{m9}+x_{32}}$	v_{10}	$\frac{V_{10} x_{31}}{K_{m10}+x_{31}}$

Table 2.3: Two sets of nominal parameter values (A and B) for the MAPK cascade model in the EGF receptor pathway (Kholodenko, 2000).

Parameter	Value A	Value B	Parameter	Value A	Value B
V_1	2.5 nM s^{-1}	2.5 nM s^{-1}	K_i	9 nM	18 nM
K_{m1}	10 nM	50 nM	V_2	0.25 nM s^{-1}	0.25 nM s^{-1}
K_{m2}	8 nM	40 nM	k_3	0.025 s^{-1}	0.025 s^{-1}
K_{m3}	15 nM	100 nM	k_4	0.025 s^{-1}	0.025 s^{-1}
K_{m4}	15 nM	100 nM	V_5	0.75 nM s^{-1}	0.75 nM s^{-1}
K_{m5}	15 nM	100 nM	V_6	0.75 nM s^{-1}	0.75 nM s^{-1}
K_{m6}	15 nM	100 nM	k_7	0.025 s^{-1}	0.025 s^{-1}
K_{m7}	15 nM	100 nM	k_8	0.025 s^{-1}	0.025 s^{-1}
K_{m8}	15 nM	100 nM	V_9	0.5 nM s^{-1}	1.25 nM s^{-1}
K_{m9}	15 nM	100 nM	V_{10}	0.5 nM s^{-1}	1.25 nM s^{-1}
K_{m10}	15 nM	100 nM	n	1	2
KKK_{tot}	100 nM	100 nM	KK_{tot}	300 nM	300 nM
K_{tot}	300 nM	300 nM			

Table 2.4: Reaction rates in the Krishna NF-κB pathway model (2.16). The reaction rates are numbered according to the labels in Figure 2.3.

Reaction	Rate	Reaction	Rate
v_1	$k_f x_4 x_1$	v_2	$k_b x_5$
v_3	αx_5	v_4	$k_{N,in} x_4$
v_5	$k_{I,in} x_1$	v_6	$k_{I,out} x_3$
v_7	$k_f x_3 x_6$	v_8	$k_b(N_{tot} - x_4 - x_5 - x_6)$
v_9	$k_{NI,out}(N_{tot} - x_4 - x_5 - x_6)$	v_{10}	$k_t x_6^2$
v_{11}	$\gamma_m x_2$	v_{12}	$k_{tl} x_2$

ODEs with 20 parameters:

$$\begin{aligned} \dot{x}_{11} &= v_1 - v_2 \\ \dot{x}_{21} &= v_3 + v_5 - v_4 - v_6 \\ \dot{x}_{22} &= v_4 - v_5 \\ \dot{x}_{31} &= v_7 + v_9 - v_8 - v_{10} \\ \dot{x}_{32} &= v_8 - v_9. \end{aligned} \tag{2.14}$$

2.3.2 The NF-κB pathway

Recently, the TNF induced NF-κB signalling pathway has attracted much attention in systems biology. This is due to the fact that NF-κB is a central transcription factor involved in the inflammatory response of mammalian cells and directly interacting with the apoptotic pathway by upregulation of anti-apoptotic proteins (Li and Verma, 2002). Therefore, the NF-κB pathway is highly relevant for understanding cancer or autoimmune diseases. Several ODE based models have been suggested for the NF-κB pathway (Hoffmann *et al.*, 2002; Krishna *et al.*, 2006; Lipniacki *et al.*, 2004).

Here, we consider the model suggested by Krishna *et al.* (2006), which reproduces experimentally observed oscillations. This model is therefore of particular interest with respect to this thesis. Krishna *et al.* (2006) already describe several variants of the model, which have been derived with a quasi-stationarity assumption from a basic biochemical reaction network. In this thesis, we consider both the original model without any quasi-stationarity assumptions, as well as a reduced order model.

The original model consists of seven chemical species and a total of twelve reactions. Due to a conservation relation for the amount of NF-κB, only six state variables are needed. A scheme of the model is depicted in Figure 2.3. The reaction rates are given in Table 2.4. Parameter values are listed in Table 2.5. The state variables are species concentrations according to the following list: x_1 – cytosolic I-κBα, x_2 – I-κBα mRNA, x_3 – nuclear I-κBα, x_4 – cytosolic NF-κB, x_5 – cytosolic complex of NF-κB and I-κBα, x_6 – nuclear NF-κB. The concentration of the nuclear complex of NF-κB and I-κBα follows

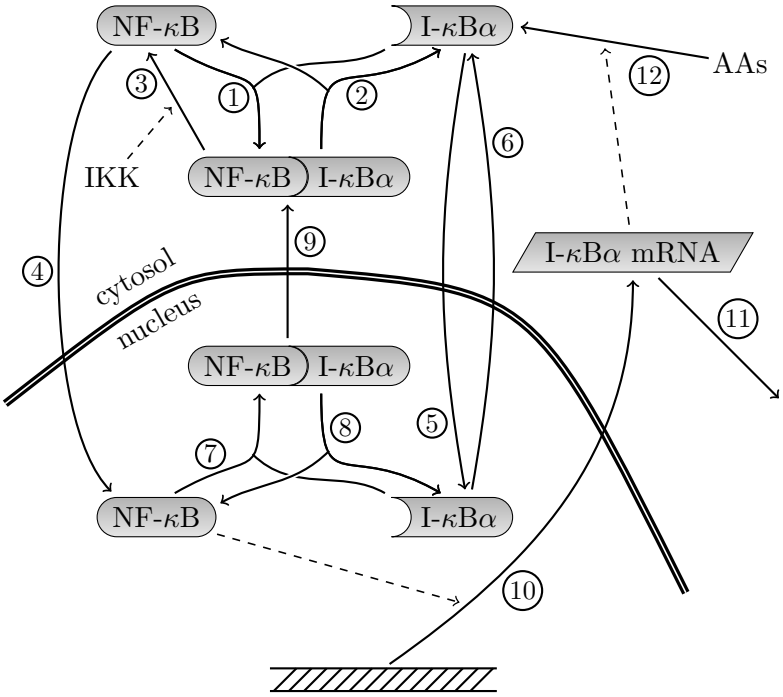

Figure 2.3: Reaction scheme for the NF-κB pathway model according to Krishna *et al.* (2006). The numbers on the reaction arrows correspond to the reaction rate numbering in the dynamical model (2.16) and Table 2.4.

Table 2.5: Nominal parameter sets for the NF-κB models (2.16) and (2.17), for two different operating conditions. The parameters p_1 (Krishna *et al.*, 2006) give sustained oscillations, and the parameters p_2 lead to damped oscillations of the nuclear NF-κB concentration.

Parameters	p_1	p_2	Unit
$k_{N,in}$	5.4	5.4	min^{-1}
$k_{I,in}$	0.018	0.018	min^{-1}
$k_{I,out}$	0.012	0.012	min^{-1}
$k_{NI,out}$	0.83	0.83	min^{-1}
k_f	30	30	$(\mu\mathrm{M}\,\mathrm{min})^{-1}$
k_b	0.03	0.03	min^{-1}
k_t	1.03	0.1	$(\mu\mathrm{M}\,\mathrm{min})^{-1}$
k_{tl}	0.24	0.2	min^{-1}
α	0.525	0.525	min^{-1}
γ_m	0.017	0.017	min^{-1}
N_{tot}	1	1	$\mu\mathrm{M}$

from a conservation relation of total NF-κB as

$$[\text{NF-}\kappa\text{Bn/I-}\kappa\text{B}\alpha\text{n}] = N_{tot} - x_4 - x_5 - x_6, \tag{2.15}$$

where the parameter N_{tot} denotes the total NF-κB concentration. The resulting ODE model is given by

$$\begin{aligned}
\dot{x}_1 &= -v_1 + v_2 - v_5 + v_6 + v_{12} \\
\dot{x}_2 &= v_{10} - v_{11} \\
\dot{x}_3 &= v_5 - v_6 - v_7 + v_8 \\
\dot{x}_4 &= -v_1 + v_2 + v_3 - v_4 \\
\dot{x}_5 &= v_1 - v_2 - v_3 + v_9 \\
\dot{x}_6 &= v_4 - v_7 + v_8.
\end{aligned} \tag{2.16}$$

The original parameter values proposed by Krishna *et al.* (2006) result in sustained oscillations of the active NF-κB amount in the nucleus for a constant stimulus. In this thesis, we will also consider a second set of parameter values, where the transcription and translation rates for I-κBα have been reduced from the original values. This corresponds to a situation where the cell has a reduced gene expression, such as in certain cell cycle phases or under specific environmental conditions. Notably, the model does not show sustained oscillations for the modified parameters, but rather damped oscillations towards an asymptotically stable equilibrium point.

A reduced order model is obtained from a fast equilibrium assumption for the association and dissociation of the NF-κB/I-κB complex. The reduced order model contains four state variables according to the following list: x_1 – cytosolic I-κBα, x_2 – I-κBα mRNA, x_3 – total nuclear I-κBα, x_4 – total nuclear NF-κB. The parameter values are the same as given in Table 2.5. As a short-hand notation, the additional dependent parameters

$$\begin{aligned}
K_I &= \frac{k_b + \alpha}{k_f} \\
K_N &= \frac{k_b + k_{NI,out}}{k_f}
\end{aligned}$$

are introduced.

The equations for the reduced order model are then given by

$$\begin{aligned}
\dot{x}_1 &= k_{tl} x_2 - \frac{\alpha(N_{tot} - x_4)x_1}{K_I + x_1} - k_{I,in} x_1 + \frac{k_{I,out} K_N x_3}{K_N + x_4} \\
\dot{x}_2 &= k_t x_4^2 - \gamma_m x_2 \\
\dot{x}_3 &= k_{I,in} x_1 - \frac{k_{I,out} K_N x_3}{K_N + x_4} - \frac{k_{NI,out} x_3 x_4}{K_N + x_4} \\
\dot{x}_4 &= \frac{k_{N,in} K_I (N_{tot} - x_4)}{K_I + x_1} - \frac{k_{NI,out} x_3 x_4}{K_N + x_4}.
\end{aligned} \tag{2.17}$$

Since complex formation is fast, i.e. k_f is large compared to the time-scale of the system's dynamics, the reduced order model (2.17) has a similar behaviour as the original model (2.16).

Chapter 3

Uncertainty and robustness analysis of steady states

In this chapter, we consider the problem of how uncertainty in the parameters affects the steady states of the network. Section 3.1 contains an introduction to the problem, and a formal definition of steady state uncertainty and robustness analysis in terms of set-based uncertainty descriptions. In Section 3.2, we suggest the computation of infeasibility certificates for the uncertain steady state equation by semidefinite programming. Using this approach, a solution to the uncertainty analysis problem is proposed in Section 3.3, and a solution to the robustness analysis problem is developed in Section 3.4. Parts of this chapter are based on Waldherr *et al.* (2008c).

3.1 Introduction and problem statement

One of the most relevant properties of biochemical reaction networks is the location of steady states. Steady states in biochemical networks correspond to operating points in metabolic networks, cell differentiation states in gene regulatory networks (Thomas and Kaufman, 2001), or the signalling state reached after adaptation in biochemical signal transduction (Alon *et al.*, 1999). In a dynamical model of a biochemical reaction network, the steady states will vary with parameter changes. As outlined in Section 2.2, sensitivity analysis is an efficient method to study the effects of small parameter variations. However, the assumption of variations being small does often not hold for biological systems. In particular, gene mutations, variations in the environment and experimental techniques such as gene knockout, gene knockdown or overexpression of a protein all correspond to rather large parameter variations. In contrast to sensitivity analysis, which is restricted to local considerations, the goal of uncertainty analysis generally is to estimate the range of feasible model predictions under a specific uncertainty in the independent variables or parameters (Cacuci, 2003). Thus we will refer to the analysis of the effect of large parameter variations on steady states as *steady state uncertainty analysis*.

In this chapter, we deal with two problems in the analysis of steady states of biochemical reaction networks: the steady state uncertainty analysis and the steady state robustness analysis. Both problems consider the steady state equation

$$0 = Sv(x, p) \tag{3.1}$$

of the biochemical reaction network (2.5). Throughout this chapter, it is assumed that

reaction rates are modelled using the law of mass action, where v takes the form

$$v_j(x,p) = k_j \prod_{i=1}^{n} x_i^{S_{ij}^{(r)}}, \quad j = 1,\ldots,m. \tag{3.2}$$

However, the method can easily be extended to rational reaction rate expressions (Hasenauer, 2008), thereby allowing to consider also Michaelis-Menten reaction rates. For the sake of clarity, we restrict the description of the results to the polynomial case.

Since the stoichiometric coefficients $S_{ij}^{(r)}$ are derived from the structure of the network, they are considered to be constant, and the parameter vector is built from the reaction rate constants, $p = (k_1,\ldots,k_m)^{\mathrm{T}}$. Thus, if the state space dimension is not reduced via conservation relations, the number of parameters is in general equal to the number of reactions, and $p \in \mathbb{R}^m$.

In this chapter, the state of the system (2.5) will generally be restricted to the set $\mathcal{X}_0 \subset \mathbb{R}^n$, which is assumed to contain all states which are physically plausible without considering parameter values. With state variables being concentrations or molecular amounts, we have $\mathcal{X}_0 \subset \mathbb{R}^n_+$. Often, there are additional upper bounds on state variables, derived from conservation relations which are not subject to parametric uncertainty.

3.1.1 The uncertainty analysis problem

The goal of steady state uncertainty analysis is to compute the set of possible steady state values, given a set of allowable parameter values. Formally, the steady state uncertainty analysis problem is posed as follows. Given a set $\mathcal{P} \subset \mathbb{R}^m$ in parameter space, compute the set of all states satisfying the steady state equation (3.1),

$$\mathcal{X}^* = \{x \in \mathcal{X}_0 \mid \exists p \in \mathcal{P} : Sv(x,p) = 0\}. \tag{3.3}$$

For models of typical complexity, computing $\mathcal{X}^*$ is often very difficult or even impossible. $\mathcal{X}^*$ may show different complex features, such as non-connectedness, or a non-smooth or self-intersecting boundary. Instead of trying to compute $\mathcal{X}^*$ explicitly, the goal pursued in this work is to compute outer bounds on possible steady state values, in the form of another set $\mathcal{X}_s \subset \mathbb{R}^n_+$ such that

$$\mathcal{X}_s \supset \mathcal{X}^*. \tag{3.4}$$

Then it can be guaranteed that all feasible steady states are located within $\mathcal{X}_s$, and the set $\mathcal{X}_s$ can be interpreted as an outer bound on feasible steady state values. Clearly, the goal in the computation of $\mathcal{X}_s$ is to make the bounds as tight as possible.

3.1.2 The robustness analysis problem

The robustness analysis problem is the inverse to uncertainty analysis. Thereby, a set $\mathcal{X} \subset \mathcal{X}_0$ of tolerable steady states is given, corresponding to a certain biological function of the considered network. The problem is to find the set of parameter values which ensures that all steady states are located within $\mathcal{X}$. We denote this parameter set by

$$\mathcal{P}^* = \{p \in \mathbb{R}^m \mid \forall x \in \mathcal{X}_0 : Sv(x,p) = 0 \Rightarrow x \in \mathcal{X}\}. \tag{3.5}$$

The set $\mathcal{P}^*$ typically cannot be computed explicitly. Our approach will rather be to compute inner bounds in the form of a set $\mathcal{P}_r \subset \mathbb{R}^m$ which satisfies

$$\mathcal{P}_r \subset \mathcal{P}^*. \tag{3.6}$$

Then one can guarantee that for any parameter $p \in \mathcal{P}_r$, the steady states of the system will be located within the allowable set $\mathcal{X}$. The set $\mathcal{P}_r$ can therefore be used to evaluate the robustness of steady states with respect to parameter variations.

3.1.3 Established solution approaches

If the model has the S-system structure (Savageau, 1976), a transformation to logarithmic coordinates makes the steady state depend linearly on parameters. In this case, the uncertainty and robustness problems can be solved efficiently (Chen *et al.*, 2005).

However, most biochemical reaction networks do not have this special structure. Then, a classical approach to study both the uncertainty and the robustness problem is to extrapolate the local sensitivity of the steady state with respect to parameter variations. For nominal parameter values p_0 and a corresponding steady state x_0, the local sensitivity $\bar{\Sigma}$ can be computed easily, as discussed in Section 2.2. The idea is then to approximate the steady state by the equation

$$x_s(p) \approx x_0 + \bar{\Sigma}(p - p_0). \tag{3.7}$$

With this approximation, estimates for both the steady state region under parametric uncertainty and the robust parameter region for an allowable steady state set can be computed. For a non-linear relation between parameters and the steady state, and for a parameter variation which is not small, this method has severe drawbacks: the quality of the estimates is not known, nor is there any guarantee that the estimated regions either underapproximate or overapproximate the exact result. Notice that for biochemical reaction networks, a non-linear relation between parameters and the steady state is very common[1]. In addition, as argued above, parameter variations for biochemical reaction networks are not small in typical applications. As a conclusion, steady state uncertainty and robustness analysis based on local sensitivity is usually insufficient. Therefore, other ways to approach the two problems have been proposed in the literature.

One approach to broaden the validity of results from local sensitivity analysis is to include higher order approximations at the nominal point (Streif *et al.*, 2007). Although such an approach may extend the validity of the approximation, it still gives results which are generally only valid for small parameter variations, and no bounds on the approximation error for large variations are available.

The study of uncertain trajectories of dynamical systems by set based methods is commonly called reachability analysis, and results for this problem are mainly available for linear systems (e.g. Girard, 2005). Although methods for reachability analysis of non-linear systems have been suggested, these remain often restricted to special system classes (Ramdani *et al.*, 2008), or do not consider the problem of uncertainty in the system's dynamics (Asarin *et al.*, 2003).

[1] Even if the model is affine in the states and parameters, the steady state may be non-linear in the parameters. Consider e.g. the system $\dot{x} = -p_1 x + p_2$, with the steady state $x_s = \frac{p_2}{p_1}$.

Due to the difficulties involved in obtaining an analytic solution, non-deterministic approaches are frequently applied. A common tool are Monte Carlo methods (Robert and Casella, 2004), which are routinely used in the analysis of uncertain biochemical reaction networks (Alves and Savageau, 2000; Feng *et al.*, 2004). However, Monte Carlo methods do not give reliable results, because it is possible to miss important solutions. This is particularly problematic for highly non-linear dependencies of the steady state on parameters. Also, Monte Carlo methods require that all of the possibly multiple steady states for specific parameter values can be computed explicitly, which is often a difficult task in itself. Despite these drawbacks, Monte Carlo methods present a suitable way to obtain an estimate of the conservatism involved in the methods developed in this chapter. By computing points in the steady state set $\mathcal{X}^*$ explicitly, these methods provide a lower bound on the possible steady state variation for the uncertain parameter set $\mathcal{P}$.

Global optimisation methods employing branch and bound techniques or interval arithmetics would in principle be suited to compute steady state regions (Maranas and Floudas, 1995; Neumaier, 1990). However, it seems that the corresponding computational cost has obstructed their application to the analysis of biochemical reaction networks so far.

3.1.4 Solution approach with infeasibility certificates

In this thesis, solutions to the uncertainty and robustness analysis problems which overcome the drawbacks of established approaches are proposed. To this end, we directly consider the system of constraints

$$\begin{aligned} Sv(x,p) &= 0 \\ x \in \widehat{\mathcal{X}},\, p &\in \widehat{\mathcal{P}}, \end{aligned} \tag{3.8}$$

where $\widehat{\mathcal{X}} \subset \mathbb{R}^n$ and $\widehat{\mathcal{P}} \subset \mathbb{R}^m$ are test regions which will be chosen iteratively in the algorithms for uncertainty and robustness analysis, respectively. As we show in Section 3.2, for suitable test regions $\widehat{\mathcal{X}}$ and $\widehat{\mathcal{P}}$, it is possible to obtain a computational proof that (3.8) does not have a solution. We refer to such proofs as *infeasibility certificates*. The computation is based on semidefinite programming and can therefore be implemented with good numerical efficiency.

To solve the uncertainty and robustness analysis problems, the test regions $\widehat{\mathcal{X}}$ and $\widehat{\mathcal{P}}$ are constructed in an appropriate manner. This construction is done iteratively, and in each iteration, we try to obtain an infeasibility certificate for (3.8). In the steady state uncertainty analysis, the parameter test region $\widehat{\mathcal{P}}$ is kept fixed at $\widehat{\mathcal{P}} = \mathcal{P}$, while the state test region $\widehat{\mathcal{X}}$ is changed in iterations. Each test region $\widehat{\mathcal{X}}$ which yields an infeasibility certificate for (3.8) is excluded from the approximation $\mathcal{X}_s$ of the steady state uncertainty set. In the steady state robustness analysis, the state test region $\widehat{\mathcal{X}}$ is fixed (see Section 3.4 for more details), while the parameter test region $\widehat{\mathcal{P}}$ is varied in iterations. The largest test region $\widehat{\mathcal{P}}$ yielding an infeasibility certificate for (3.8) is taken as the approximation $\mathcal{P}_r$ of the robust parameter set.

3.2 Steady state infeasibility certificates via semidefinite programming

Notation. $\mathcal{S}^k$ denotes the space of real symmetric $k \times k$ matrices. $W \succeq 0$ means that the symmetric matrix W is positive semidefinite. By $M \geq 0$, we denote that the matrix M is elementwise non-negative.

3.2.1 Construction of the feasibility problem

In the following, we restrict the class of regions in state and parameter space to hyperrectangles. This restriction is mainly introduced for ease of notation. In general, the methods can directly be applied for any convex polytopes. However, in applications it may not be obvious how to choose the polytopes, and the generalisation does not necessarily offer an advantage. Using hyperrectangles, the test regions $\widehat{\mathcal{X}}$ and $\widehat{\mathcal{P}}$ are described by

$$\begin{aligned} \widehat{\mathcal{X}} &= \{x \in \mathbb{R}^n \mid x_{i,min} \leq x_i \leq x_{i,max},\ i = 1, \ldots, n\} \\ \widehat{\mathcal{P}} &= \{p \in \mathbb{R}^m \mid p_{j,min} \leq p_j \leq p_{j,max},\ j = 1, \ldots, m\}. \end{aligned} \tag{3.9}$$

Then, the constraints (3.8) are described by the feasibility problem

$$(P): \begin{cases} \text{find} & x \in \mathbb{R}^n,\, p \in \mathbb{R}^m \\ \text{s.t.} & Sv(x,p) = 0 \\ & x_{i,min} \leq x_i \leq x_{i,max} \quad i = 1, \ldots, n \\ & p_{j,min} \leq p_j \leq p_{j,max} \quad j = 1, \ldots, m. \end{cases} \tag{3.10}$$

In general, this is a non-convex problem and hard to solve. Such a problem is also considered in the context of parameter identification in a recent paper (Kuepfer *et al.*, 2007). We will show in the next section that the Lagrangian dual to a suitably relaxed feasibility problem allows to obtain (possibly conservative) infeasibility certificates for problem (3.10).

3.2.2 Relaxation to a semidefinite program

A relaxation of the feasibility problem (3.10) to a semidefinite program (Vandenberghe and Boyd, 1996) makes the problem amenable to an efficient computational solution. The applied relaxation is based on a quadratic representation of a multivariate polynomial of arbitrary degree (Parrilo, 2003). In the first step, we construct a vector ξ containing monomials which occur in the reaction flux vector $v(x,p)$. In the special case where no single reaction has more than two reactants, a starting point for the construction of ξ is

$$\xi^{\mathrm{T}} = (1, p_1, \ldots, p_m, x_1, \ldots, x_n, p_1x_1, \ldots, p_jx_i, \ldots, p_mx_n),$$

which usually can be reduced by eliminating components which are not required for representing the reaction fluxes. Define k such that $\xi \in \mathbb{R}^k$. Note that this approach is not limited to second order reaction networks. In more general cases, one has to extend the vector ξ by monomials which are products of several state variables.

Using the vector ξ, the elements of the flux vector $v(x,p)$ can be expressed as

$$v_j(x,p) = \xi^{\mathrm{T}} \Upsilon_j \xi, \quad j = 1, \ldots, m, \tag{3.11}$$

where $\Upsilon_j \in \mathcal{S}^k$ is a constant symmetric matrix. The choice of Υ_j is generally not unique: for example, an expression of the form $p_j x_i x_l$ can be decomposed as either $(p_j x_i)(x_l)$ or $(p_j x_l)(x_i)$.

Using (3.11), the system's ODE (2.5) can be written as

$$\dot{x}_i = \xi^{\mathrm{T}} U_i \xi, \quad i = 1, \ldots, n, \tag{3.12}$$

where

$$U_i = \sum_{j=1}^{m} S_{ij} \Upsilon_j \in \mathcal{S}^k, \quad i = 1, \ldots, n.$$

By the non-uniqueness of the decomposition for terms of order three or higher, we have additional equality constraints of the form

$$\xi^{\mathrm{T}} U_i \xi = 0, \quad i = n+1, \ldots, n+l \tag{3.13}$$

with $U_i \in \mathcal{S}^k$, and l the number of additional equality constraints.

The original feasibility problem (3.10) is thus equivalent to the problem

$$(P') : \begin{cases} \text{find} & \xi \in \mathbb{R}^k \\ \text{s.t.} & \xi^{\mathrm{T}} U_i \xi = 0 \quad i = 1, \ldots, n+l \\ & K\xi \geq 0 \\ & \xi_1 = 1, \end{cases} \tag{3.14}$$

where the matrix $K \in \mathbb{R}^{(2k-2)\times k}$ is constructed to cover the inequality constraints in (3.10), e.g. the constraint $p_{1,min} \leq p_1 \leq p_{1,max}$ is represented as

$$\begin{pmatrix} -p_{1,min} & 1 & 0 & \ldots & 0 \\ p_{1,max} & -1 & 0 & \ldots & 0 \end{pmatrix} \xi \geq 0.$$

The constraints on x and p in the feasibility problem (P) also yield constraints on the higher order monomials in ξ, given by

$$p_{j,min} x_{i,min} \leq p_j x_i \leq p_{j,max} x_{i,max}, \quad i = 1, \ldots, n, \ j = 1, \ldots, m.$$

These constraints are also included in the matrix K to reduce the conservatism of the subsequent relaxation.

A relaxation to a semidefinite program is found by introducing the matrix $W = \xi\xi^{\mathrm{T}}$. The problem is then first transformed to the equivalent feasibility problem

$$(P'') : \begin{cases} \text{find} & W \in \mathcal{S}^k \\ \text{s.t.} & \operatorname{tr}(U_i W) = 0 \qquad i = 1, \ldots, n+l \\ & \operatorname{tr}(e_1 e_1^{\mathrm{T}} W) = 1 \\ & KWe_1 \geq 0 \\ & W \succcurlyeq 0 \\ & \operatorname{rank} W = 1, \end{cases} \tag{3.15}$$

where $e_1 = (1, 0, \ldots, 0)^{\mathrm{T}} \in \mathbb{R}^k$. The two last constraints assure the existence of a decomposition of W as $W = \xi\xi^{\mathrm{T}}$. In the second step, the problem is relaxed by omitting the non-convex constraint $\operatorname{rank} W = 1$. The relaxed version of the original feasibility problem (3.10) is thus obtained as

$$(RP): \begin{cases} \text{find} & W \in \mathcal{S}^k \\ \text{s.t.} & \operatorname{tr}(U_i W) = 0 \qquad i = 1, \ldots, n+l \\ & \operatorname{tr}(e_1 e_1^{\mathrm{T}} W) = 1 \\ & KWe_1 \geq 0 \\ & KWK^{\mathrm{T}} \geq 0 \\ & W \succcurlyeq 0, \end{cases} \tag{3.16}$$

which is a semidefinite program.

Note that the constraint $KWK^{\mathrm{T}} \geq 0$ would be redundant in the non-relaxed problem (3.15), because it is automatically satisfied if W can be decomposed as $W = \xi\xi^{\mathrm{T}}$. However, when the decomposition constraint is relaxed, the constraint $KWK^{\mathrm{T}} \geq 0$ is not redundant and serves to reduce the conservatism of the relaxation.

By removing the non-convex rank constraint, the feasible set of the problem has been enlarged. Thus, the basic relationship between the original problem (3.10) and the relaxed problem (3.16) is that feasibility of the original problem implies feasibility of the relaxed problem. In the next step, the Lagrange dual problem is used to check infeasibility of the relaxed problem, which then also allows to certify the original problem as infeasible.

Although the derivation of (RP) as outlined above is restricted to polynomial reaction rates, the approach can easily be extended to rational reaction rates. This can either be achieved by multiplying the equations with the denominators, thus arriving at polynomial equations, or by introducing additional variables for rational terms (Hasenauer, 2008). Whether the first or the second approach is more efficient in dealing with rational terms depends on the individual model.

3.2.3 Infeasibility certificates from the dual problem

The Lagrange dual problem can be used to certify infeasibility of the primal problem. First, the Lagrangian function L (Boyd and Vandenberghe, 2004) is constructed for the primal problem (3.16). By the standard construction of L in convex optimisation (Boyd and Vandenberghe, 2004), we obtain

$$\begin{aligned} L(W, \lambda_1, \lambda_2, \lambda_3, \nu) = &-\lambda_1^{\mathrm{T}} KWe_1 - \operatorname{tr}(\lambda_2^{\mathrm{T}} KWK^{\mathrm{T}}) \\ &- \operatorname{tr}(\lambda_3^{\mathrm{T}} W) - \nu_1(\operatorname{tr}(e_1 e_1^{\mathrm{T}} W) - 1) - \sum_{i=1}^{n+l} \nu_{i+1} \operatorname{tr}(U_i W), \end{aligned} \tag{3.17}$$

where $\lambda_1 \in \mathbb{R}^{2k-2}$, $\lambda_2 \in \mathcal{S}^{2k-2}$, $\lambda_3 \in \mathcal{S}^k$ and $\nu \in \mathbb{R}^{n+l+1}$. Using the cyclic property of the trace operator, i.e. $\operatorname{tr}(ABC) = \operatorname{tr}(BCA) = \operatorname{tr}(CAB)$, we rewrite

$$\operatorname{tr}(\lambda_2^{\mathrm{T}} KWK^{\mathrm{T}}) = \operatorname{tr}(K^{\mathrm{T}} \lambda_2^{\mathrm{T}} KW)$$

and

$$\begin{aligned}\lambda_1^{\mathrm{T}} K W e_1 &= \operatorname{tr}(e_1 \frac{\lambda_1^{\mathrm{T}}}{2} K W) + \operatorname{tr}(e_1^{\mathrm{T}} \frac{\lambda_1}{2} K^{\mathrm{T}} W) \\ &= \operatorname{tr}((e_1 \frac{\lambda_1^{\mathrm{T}}}{2} K + e_1^{\mathrm{T}} \frac{\lambda_1}{2} K^{\mathrm{T}}) W).\end{aligned}$$

Based on the Lagrangian L, the dual problem is obtained as

$$\begin{aligned}&\max_{\lambda_1,\lambda_2,\lambda_3,\nu} \ \inf_{W \in \mathcal{S}^k} L(W, \lambda_1, \lambda_2, \lambda_3, \nu) \\ &\text{s.t.} \quad \lambda_1 \succeq 0, \ \lambda_2 \succeq 0, \ \lambda_3 \succcurlyeq 0.\end{aligned} \tag{3.18}$$

Observe that L as given in (3.17) is affine in W and thus the infimum in (3.18) yields an equality constraint to zero for the term multiplying W. With this constraint, the Lagrangian becomes $L(0, \lambda_1, \lambda_2, \lambda_3, \nu) = \nu_1$. Thus, (3.18) is equivalent to the semidefinite program

$$(D): \begin{cases} \max\limits_{\lambda_1,\lambda_2,\lambda_3,\nu} \quad \nu_1 \\ \text{s.t.} \quad K^{\mathrm{T}} \lambda_2 K + \frac{1}{2}\big(e_1 \lambda_1^{\mathrm{T}} K + K^{\mathrm{T}} \lambda_1 e_1^{\mathrm{T}}\big) + \lambda_3 + \nu_1 e_1 e_1^{\mathrm{T}} + \sum\limits_{i=1}^{n+l} \nu_{i+1} U_i = 0 \\ \qquad\qquad \lambda_1 \succeq 0, \ \lambda_2 \succeq 0, \ \lambda_3 \succcurlyeq 0. \end{cases} \tag{3.19}$$

It is a standard procedure in convex optimisation to use the dual problem in order to find a certificate which guarantees infeasibility of the primal problem (Boyd and Vandenberghe, 2004). For the problem at hand, this principle is formulated in the following theorem.

Theorem 3.1. *If the dual problem* (3.19) *has a feasible solution with* $\nu_1 > 0$*, then the primal problem* (3.10) *is infeasible.*

Proof. Note that the constraints of the dual problem (3.19) are homogenous in the free variables: if $(\lambda_1, \lambda_2, \lambda_3, \nu)$ is feasible, then also $(\alpha\lambda_1, \alpha\lambda_2, \alpha\lambda_3, \alpha\nu)$ with any $\alpha \geq 0$ is feasible. Choosing all free variables to be zero is always a feasible solution of the dual problem (3.19).

Let μ_D be the optimal value of the dual problem (3.19). By the previous argument, it is clear that either $\mu_D = 0$ or $\mu_D = \infty$. Under the assumption made in the theorem, we have $\mu_D = \infty$.

To the primal feasibility problem (3.16), we can associate a minimization problem with zero objective function and the same constraints as in (3.16). Let μ_P be the optimal value of this minimization problem. We have $\mu_P = 0$, if the primal problem (3.16) is feasible, and $\mu_P = \infty$ otherwise. Weak duality of semidefinite programs (Vandenberghe and Boyd, 1996) assures that $\mu_D \leq \mu_P$. In particular, $\mu_D = \infty$ implies $\mu_P = \infty$, and the primal problem (3.16) as well as the original feasibility problem (3.10) are both infeasible. □

Theorem 3.1 provides an infeasibility certificate for problem (3.10), since any feasible solution for the dual relaxed problem (3.19) with a positive objective function value is a certificate for the infeasibility of problem (3.10). In the uncertainty and robustness analysis algorithms which are developed in the following sections, infeasibility certificates will be computed for suitable, iteratively chosen test regions $\widehat{\mathcal{X}}$ and $\widehat{\mathcal{P}}$ in order to compute uncertainty regions $\mathcal{X}_s$ and robustness regions $\mathcal{P}_r$ for the given problems.

3.3 Uncertainty analysis for steady states

3.3.1 Bounding feasible steady states

In this section, we present an approach to find bounds on the steady state region $\mathcal{X}_s$, based on the results obtained in the previous section. As a basic additional requirement, we assume that the *a priori* state set $\mathcal{X}_0$ is bounded. For ease of notation, we restrict the discussion to hyperrectangles. Then $\mathcal{X}_0$ can be written as

$$\mathcal{X}_0 = \{x \in \mathbb{R}^n \mid x_{i,lower} \leq x_i \leq x_{i,upper},\ i = 1, \ldots, n\}. \tag{3.20}$$

In biochemical reaction networks, such bounds can often be obtained from mass conservation relations, as in the example in Section 3.3.2. Also, it is often possible to show positive invariance of a sufficiently large compact set in state space for the system (2.5), as we will do for the NF-κB model (2.17) in Proposition 4.5. These bounds may be very loose though, and the main objective of the proposed method is to tighten them as far as possible.

To this end, we use a bisection algorithm (Jaulin *et al.*, 2001) which computes the maximum ranges $[x_{j,lower}, x_{j,min}]$ and $[x_{j,max}, x_{j,upper}]$ for which an infeasibility certificate can be obtained via Theorem 3.1. The algorithm iterates over $j = 1, \ldots, n$, while the steady state values x_i for $i \neq j$ are assumed to be located within the intervals defined by the set $\mathcal{X}_0$.

The algorithm for computing the lower bound $x_{1,min}$ is given in Figure 3.1. The computation of the upper bound $x_{1,max}$ is implemented in essentially the same way, with some small modifications, primarily in the construction of the steady state test set $\widehat{\mathcal{X}}$.

Solvers for semidefinite programs are quite efficient, and for the bisection method used here, the number of solver calls is only $\mathcal{O}(\log_2 \frac{1}{tol})$, where *tol* is the remaining gap between the lower and upper estimate in the bisection algorithm (see Figure 3.1). Therefore, the uncertainty analysis algorithm can be executed efficiently on standard desktop computers, as we will see in the example discussed in the following subsection.

In our analysis method, the algorithm shown in Figure 3.1 is executed for all state variables, and as both maximization of the lower bound and minimization of the upper bound of the steady state values. Its output is the hyperrectangle

$$\mathcal{X}_s = \{x \in \mathbb{R}^n \mid x_{i,min} \leq x_i \leq x_{i,max},\ i = 1, \ldots, n\}, \tag{3.21}$$

which contains all possible steady states for parameters in the uncertainty set $\mathcal{P}$. In this way, $\mathcal{X}_s$ quantifies the uncertainty about the steady states of the model.

Note that the proposed algorithm is independent of the number of steady states for any fixed parameter and may directly be applied to models where multiple steady states are possible. In such a case, the obtained uncertainty set $\mathcal{X}_s$ will be an outer bound on the convex hull of the possibly disconnected steady state set $\mathcal{X}^*$. Thus, while multiple steady states do not affect the application of the algorithm, it is also not possible to detect this situation. If such a detection is desired, it may be more appropriate to use a multi-dimensional bisection algorithm with the same infeasibility certificates as applied here (Hasenauer *et al.*, 2009a). However, a multi-dimensional bisection algorithm generally requires a significantly higher computational effort compared to the approach suggested here, becoming quickly prohibitive for a high-dimensional parameter space.

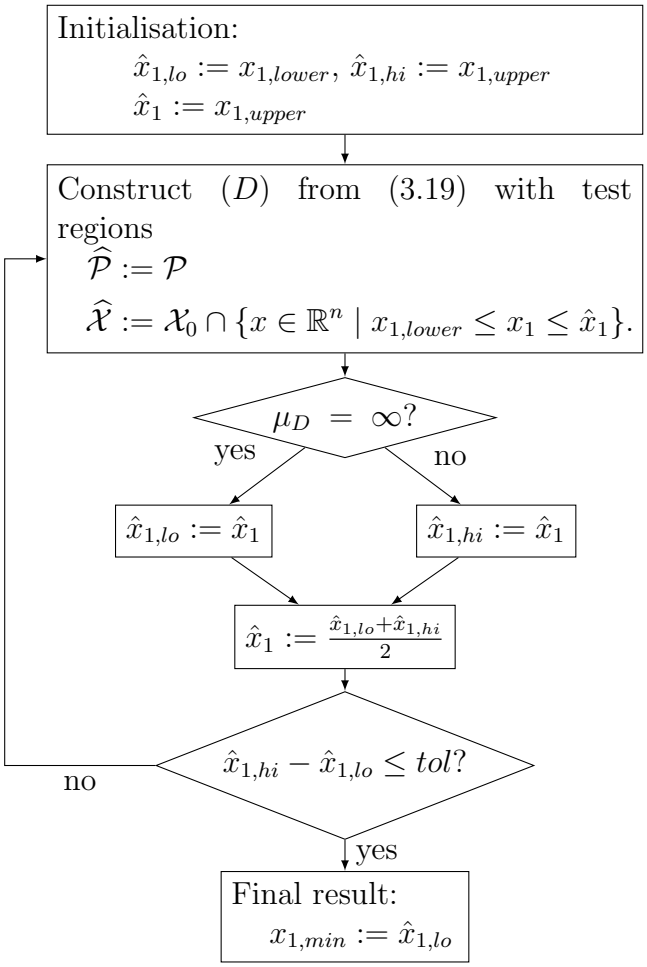

Figure 3.1: Flowchart for the steady state uncertainty analysis algorithm based on semidefinite programming. The algorithm takes an initial bounding set $\mathcal{X}_0$ and the uncertain parameter set $\mathcal{P}$ from the problem data. As a numerical parameter, the stopping tolerance tol needs to be supplied.

3.3.2 Example: Uncertainty analysis of an enzymatic cycle

As an example for the uncertainty analysis, we consider an enzymatic cycle. These cycles appear very frequently in cellular reaction networks, in particular in the form of phosphorylation and dephosphorylation cycles (Shacter *et al.*, 1984). In this example, we consider a cycle as suggested by Goldbeter and Koshland (1981) for a hypothetical protein A. The reaction network is given by

$$\begin{aligned} E + A &\underset{k_2}{\overset{k_1}{\rightleftarrows}} C_1 \\ C_1 &\xrightarrow{k_3} E + A^* \\ P + A^* &\underset{k_5}{\overset{k_4}{\rightleftarrows}} C_2 \\ C_2 &\xrightarrow{k_6} P + A. \end{aligned} \tag{3.22}$$

The network is subject to the three conservation relations

$$\begin{aligned}[A] + [A^*] + [C_1] + [C_2] &= A_0\\ [E] + [C_1] &= E_0\\ [P] + [C_2] &= P_0.\end{aligned}$$

Denoting $a = [A^*]$, $c_1 = [C_1]$ and $c_2 = [C_2]$, and using the law of mass action, the reaction flux vector is given by

$$v = \begin{pmatrix} k_1(A_0 - a - c_1 - c_2)(E_0 - c_1)\\ k_2 c_1\\ k_3 c_1\\ k_4(P_0 - c_2)a\\ k_5 c_2\\ k_6 c_2 \end{pmatrix}.$$

Due to the conservation relations, we only need to use three differential equations in the model, which is given by

$$\frac{d}{dt}\begin{pmatrix} a\\ c_1\\ c_2\end{pmatrix} = \begin{pmatrix} 0 & 0 & 1 & -1 & 1 & 0\\ 1 & -1 & -1 & 0 & 0 & 0\\ 0 & 0 & 0 & 1 & -1 & -1\end{pmatrix} v. \tag{3.23}$$

For the uncertainty analysis, the parameters k_1 and k_4 as well as the total concentrations A_0, E_0 and P_0 are assumed to be fixed at $k_1 = 10^5 \frac{1}{\mu\mathrm{M}\,\mathrm{min}}$, $k_4 = 5 \cdot 10^4 \frac{1}{\mu\mathrm{M}\,\mathrm{min}}$, $A_0 = 1\mu\mathrm{M}$ and $E_0 = P_0 = 0.01\mu\mathrm{M}$. The other parameters are assumed to be uncertain parameters, with variations around their nominal values $k_{2,nom} = k_{5,nom} = 1\frac{1}{\mathrm{min}}$ and $k_{3,nom} = k_{6,nom} = 10^3\frac{1}{\mathrm{min}}$.

From the conservation relations and invariance of the positive orthant we have the steady state bounds

$$0 \le a \le A_0, \quad 0 \le c_1 \le E_0, \quad 0 \le c_2 \le P_0,$$

which are valid for any parameter values.

We apply the analysis method proposed in this section to find tighter bounds on possible steady state values, comparing three different regions in which parameters of the enzymatic cycle are allowed to vary. The three different regions are given by $\mathcal{P}_1$, $\mathcal{P}_2$ and $\mathcal{P}_3$, where $\mathcal{P}_1, \mathcal{P}_2, \mathcal{P}_3 \subset \mathbb{R}^4$ and

- $(k_2, k_3, k_5, k_6) \in \mathcal{P}_1 \Leftrightarrow 0.98\, k_{i,nom} \le k_i \le 1.02\, k_{i,nom}$, corresponding to parameter variations of up to 2%,
- $(k_2, k_3, k_5, k_6) \in \mathcal{P}_2 \Leftrightarrow 0.9\, k_{i,nom} \le k_i \le 1.1\, k_{i,nom}$, corresponding to parameter variations of up to 10%, and
- $(k_2, k_3, k_5, k_6) \in \mathcal{P}_3 \Leftrightarrow 0.5\, k_{i,nom} \le k_i \le 2\, k_{i,nom}$, corresponding to parameter variations of up to a factor of 2,

with $i = 2, 3, 5, 6$ in all three cases.

The dual problem (D) is constructed by using $\xi^{\mathrm{T}} = (1,\ k_2,\ k_3,\ k_5,\ k_6,\ a,\ c_1,\ c_2)$ and deriving appropriate matrices U_i, K, for the steady state equations and the constraints, respectively. The uncertainty analysis algorithm (Figure 3.1) was then used to compute bounds on the steady state concentrations. We compare these results to an estimate for the region of steady state concentrations obtained by Monte Carlo tests. The results are shown in Figure 3.2. The average computation time to obtain the feasible intervals for all three state variables and one parameter region was about 25 seconds. The Monte Carlo tests conducted to produce the figures consistently took about 20 % more computation time, using 1000 parameter points for each test. However, for a reliable evaluation by Monte Carlo methods, much more points should be used, which would increase computation time significantly.

As can be seen from the figure, our approach is able to find tight intervals for the steady state values of the individual concentrations. However, the results also highlight the limitations of using hyperrectangles if different state variables are highly correlated in steady state under the considered parameter uncertainty. A potential extension to deal with this problem is to use the infeasibility certificates within a multi-dimensional bisection algorithm, as suggested by Hasenauer *et al.* (2009a).

As illustrated with this example, the result of the uncertainty analysis indicates the range of possible variation in the steady states, for a given level of parametric uncertainty. From a biological perspective, this result needs to be interpreted with respect to a biological function. For the present example, such an interpretation is given by the property of ultrasensitivity in the enzymatic cycle (Goldbeter and Koshland, 1981). For a further discussion of this point, we refer to Waldherr *et al.* (2008c).

3.4 Robustness analysis for steady states

3.4.1 Robustness analysis method

In this section, the infeasibility certificates proposed in Section 3.2 are used to compute an approximation to the robust parameter set defined in Section 3.1.2. The robustness analysis is more challenging than the uncertainty analysis. In the uncertainty analysis, for a physically plausible model, the steady state set $\mathcal{X}^*$ to be approximated should be compact for a compact set $\mathcal{P}$ of physically plausible parameters. Thus there is a reasonable definition of the "optimal" approximation $\mathcal{X}_s$ to $\mathcal{X}^*$ as the smallest hyperrectangle which contains $\mathcal{X}^*$, and the so defined $\mathcal{X}_s$ is unique. Although the method presented in the previous section may not compute the optimal approximation exactly due to the conservatism in the computation of infeasibility certificates, the examples show that the result can come quite close to the optimum. In the robustness analysis, the goal is to find inner bounds $\mathcal{P}_r \subset \mathcal{P}^*$. Note that $\mathcal{P}^*$ is typically non-compact, and a good, i.e. large, inner bounding set cannot be defined uniquely in a reasonable way. To overcome this problem, we resort to the consideration of nominal parameter values p_0, and ask for the robustness of the steady state values with respect to (possibly large) parameter variations around p_0. We then compute a robust parameter region $\mathcal{P}_r$ by looking at hypercubes of

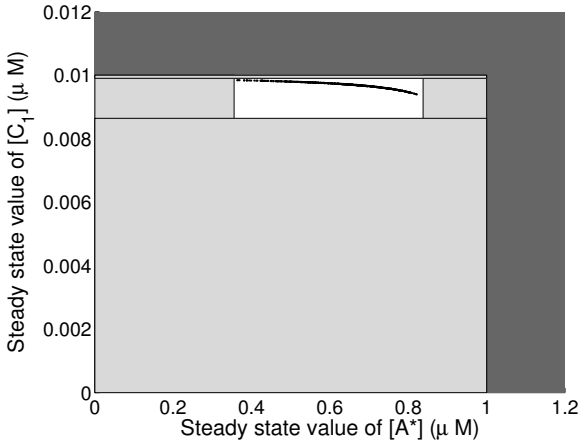

(a) Parameter uncertainty region $\mathcal{P}_1$ (2% variation)

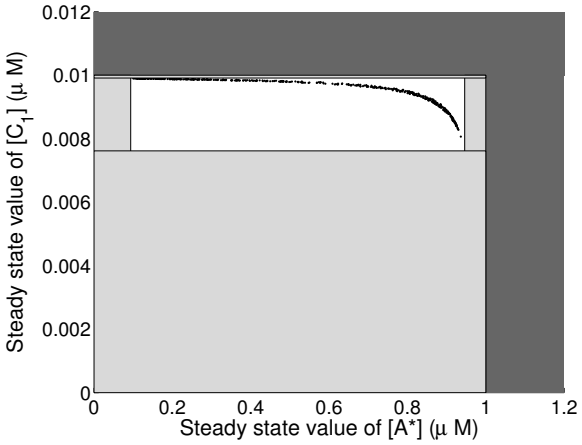

(b) Parameter uncertainty region $\mathcal{P}_2$ (10% variation)

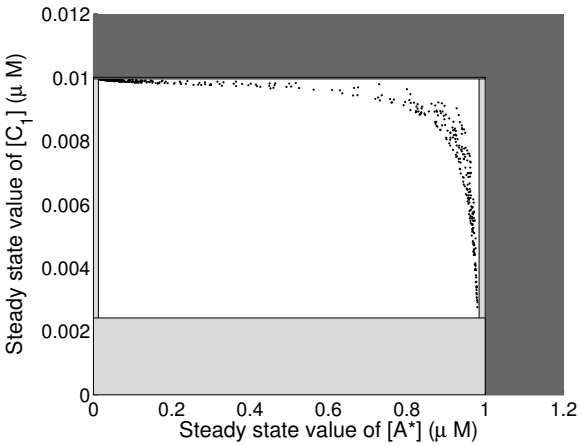

(c) Parameter uncertainty region $\mathcal{P}_3$ (2–fold variation)

Figure 3.2: Feasible steady states for the enzymatic cycle with three different parameter regions, comparison of reliable bounds obtained by the uncertainty analysis algorithm and Monte Carlo estimates. All steady states are guaranteed to be located inside the white regions. Light gray regions have been certified infeasible by Theorem 3.1. Black dots are steady state values obtained from Monte Carlo tests. The darkest gray regions, where $[\mathrm{A}^*] > 1$ or $[\mathrm{C}_1] > 0.01$, are known to be infeasible from conservation relations.

the form

$$\mathcal{P}_r(\varrho, p_0) = \left\{ p \in \mathbb{R}^m \mid \frac{1}{\varrho} \leq \frac{p_j}{p_{0,j}} \leq \varrho,\ j = 1, \ldots, m \right\}, \tag{3.24}$$

where $\varrho \in \mathbb{R}$ is a measure for the size of the hypercube $\mathcal{P}_r(\varrho, p_0)$. ϱ can also be interpreted as the logarithmic radius of $\mathcal{P}_r(\varrho, p_0)$. In this framework, the optimal approximation to $\mathcal{P}^*$ is defined as $\mathcal{P}_r(\varrho^*, p_0)$, where ϱ^* is computed according to the following definition.

Definition 3.2. *The* steady state robustness radius $\varrho^* \in [1, \infty)$ *is given by*

$$\begin{aligned} \varrho^* = \quad & \sup \varrho \\ & \text{s.t. } \mathcal{P}_r(\varrho, p_0) \subset \mathcal{P}^*. \end{aligned} \tag{3.25}$$

In this way, we arrive at a unique definition of an optimal set $\mathcal{P}_r$ and can devise an algorithm to approximate it.

Recall that the allowable steady state values are given by the set $\mathcal{X}$. As in Section 3.3, we assume that a set $\mathcal{X}_0$ containing all steady states is known *a priori*. Then by definition $\mathcal{X}_0 \setminus \mathcal{X}$ should not contain steady states for any parameter $p \in \mathcal{P}_r$. Let $\mathcal{X}$ be such that we can decompose $\mathcal{X}_0 \setminus \mathcal{X}$ into hyperrectangles $\mathcal{X}_i$, $i = 1, \ldots, l$:

$$\mathcal{X}_0 \setminus \mathcal{X} = \bigcup_{i=1}^{l} \mathcal{X}_i. \tag{3.26}$$

In analogy to the uncertainty analysis, we propose a robustness analysis algorithm which combines a bisection on the radius ϱ of the parameter hypercube $\mathcal{P}_r(\varrho, p_0)$ with suitable semidefinite programs. These programs are constructed to compute infeasibility certificates for the steady state feasibility problems obtained with the test regions $\mathcal{P}_r(\varrho, p_0)$ in parameter space and the $\mathcal{X}_i$ in state space. The algorithm is illustrated in Figure 3.3. As a result, the algorithm returns a lower bound $\widehat{\varrho}^* \leq \varrho^*$ of the steady state robustness radius ϱ^*. Note that due to the conservatism involved in the computation of the infeasibility certificates, it may be that the lower bound is not tight.

All steady states are guaranteed to be located within the set $\mathcal{X}$, for any parameter taken from $\mathcal{P}_r(\widehat{\varrho}^*, p_0)$. As for the uncertainty analysis, a sampling based approach can be used to estimate the conservatism of the computed robust parameter set. To this end, we have to find steady state–parameter pairs (x, p) with $x \in \mathcal{X}_0 \setminus \mathcal{X}$ and $p \notin \mathcal{P}_r(\widehat{\varrho}^*, p_0)$. The gap between $\widehat{\varrho}^*$ and the multiplicative variation between such parameters p and the nominal parameters p_0 is an indication of how conservative the approximation $\mathcal{P}_r(\widehat{\varrho}^*, p_0)$ to $\mathcal{P}_r(\varrho^*, p_0)$ is.

3.4.2 Steady state robustness of the MAPK cascade

The steady state robustness analysis method has been applied to the simplistic model (2.13) of the MAPK cascade presented in Section 2.3.1. From conservation relations, we have the *a priori* set of physically plausible steady states

$$\mathcal{X}_0 = \{x \in \mathbb{R}^3 \mid 0 \leq x_1 \leq \mathrm{K}_{tot},\ 0 \leq x_2 \leq \mathrm{KK}_{tot},\ 0 \leq x_3 \leq \mathrm{KKK}_{tot}\}.$$

Throughout this example, the allowed steady state region is given by

$$\mathcal{X} = \{x \in \mathcal{X}_0 \mid 0.8\mathrm{K}_{tot} \leq x_3 \leq \mathrm{K}_{tot}\}, \tag{3.27}$$

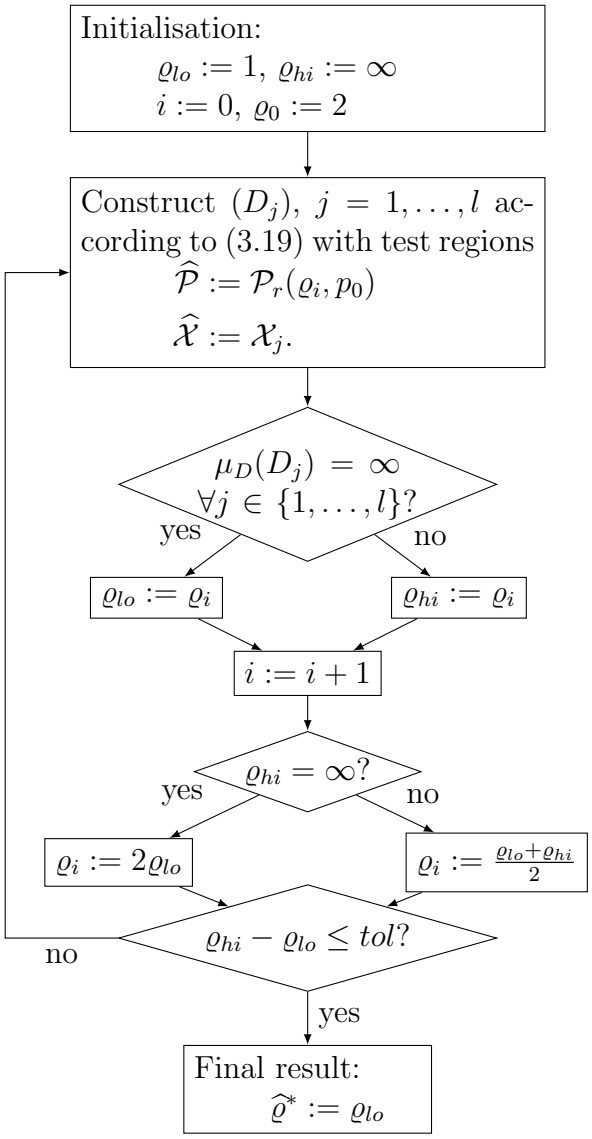

Figure 3.3: Flowchart for the steady state robustness analysis algorithm based on semidefinite programming. The algorithm takes nominal parameters p_0 and the hyperrectangles $\mathcal{X}_i$ from the problem data. As a numerical parameter, the stopping tolerance tol needs to be supplied.

Table 3.1: Robustness radii for steady state robustness of the MAPK cascade. The uncertain parameters are k_{11} and k_{12}. Divisions of the hyperrectangular test region $\mathcal{X}_0 \setminus \mathcal{X}$ in l subsets as defined in (3.26) are compared according to the resulting approximation of the robustness radius and the corresponding computation time.

	$l = 1$	$l = 4$	$l = 8$
Robustness radius $\widehat{\varrho}^* \leq \varrho^*$	9.5	48.3	48.3
Comp. time (sec)	3.1	11.0	19.4

i.e. the output of the cascade should reach at least 80 % of its maximum activity level. The robustness radius $\widehat{\varrho}^*$ is computed for parameter variations around the nominal values given in Table 2.1.

For the model according to the ODE (2.13), the equilibrium point can be computed analytically. This example therefore serves as a test case of the proposed robustness analysis algorithm. From the analytical solution for the steady state, we can infer that the parameters satisfy the robustness condition whenever

$$0.8 \leq \frac{k_{11}k_{21}k_{31}\mathrm{KKK}_{tot}\mathrm{KK}_{tot}u}{k_{11}k_{21}k_{31}\mathrm{KKK}_{tot}\mathrm{KK}_{tot}u + k_{32}(k_{11}k_{21}\mathrm{KKK}_{tot}u + k_{22}(k_{11}u + k_{12}))}. \tag{3.28}$$

In the following, we consider different uncertainty cases, and compare the results of the proposed algorithm to the optimal robustness radius obtained from the analytical condition, in order to evaluate the performance of the algorithm. We will also see that the results of the robustness analysis lead to interesting conclusions about the properties of the MAPK cascade.

Uncertainty in two kinetic parameters

Let us first consider two cases where only two of the kinetic parameters are assumed to be uncertain. We compare uncertainty on the first level of the cascade, i.e. in k_{11} and k_{12}, to uncertainty on the third level of the cascade, i.e. in k_{31} and k_{32}. With nominal parameters as given in Table 2.1, the analytical robustness radius for the allowed steady state set as given in (3.27) is computed as $\varrho^* = 67.5$ for uncertainty on the first cascade level, and $\varrho^* = 6.04$ for uncertainty on the third cascade level. The results from the proposed algorithm are given in Table 3.1 for uncertainty on the first cascade level and in Table 3.2 for uncertainty on the third level. The corresponding robust parameter regions for the first case are also illustrated in Figure 3.4.

As can be seen from the results, the proposed algorithm for robustness analysis is well able to approximate the steady state robustness radius according to Definition 3.2. The examples show that conservatism of the results can be traded for computation time by partitioning the test region $\mathcal{X}_0 \setminus \mathcal{X}$ into more subsets. For large robustness radii, conservatism may also be reduced by partitioning the parameter test region $\widehat{\mathcal{P}}$ into subsets, and solving one optimisation problem per subset in each iteration of the bisection algorithm. Such an extension might for example reduce the conservatism in the analysis regarding the first level of the MAPK cascade, where a further partitioning of the state space does

Table 3.2: Robustness radii for steady state robustness of the MAPK cascade. The uncertain parameters are k_{31} and k_{32}. Divisions of the test region $\mathcal{X}_0 \setminus \mathcal{X}$ in l subsets as defined in (3.26) are compared according to the resulting approximation of the robustness radius and the corresponding computation time.

	$l = 1$	$l = 4$	$l = 8$
Robustness radius $\widehat{\varrho}^* \leq \varrho^*$	5.1	6.0	6.0
Comp. time (sec)	3.3	8.0	15.6

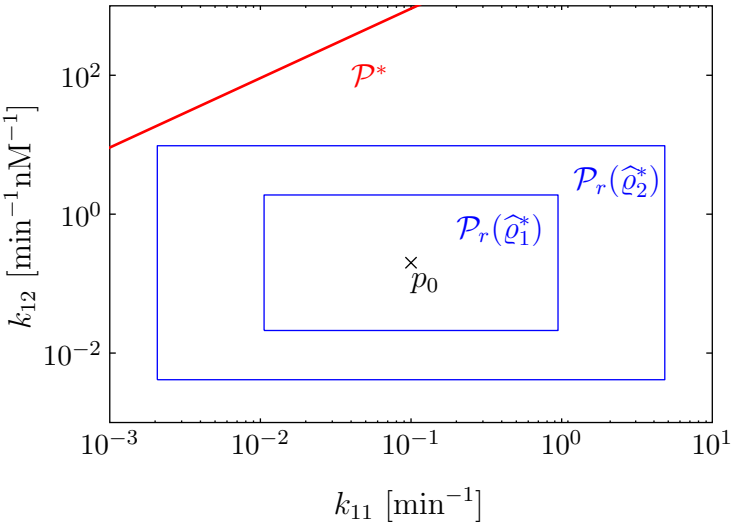

Figure 3.4: Robust parameter regions of the MAPK cascade for different divisions of the test region. The uncertain parameters are k_{11} and k_{12}. The robust parameter regions $\mathcal{P}_r(\widehat{\varrho}_1^*, p_0)$ and $\mathcal{P}_r(\widehat{\varrho}_2^*, p_0)$, where $\widehat{\varrho}_1^*$ is from $l = 1$ and $\widehat{\varrho}_2^*$ from $l = 8$ in Table 3.1, are shown as rectangles. In this example, the region $\mathcal{P}^*$, below the inclined line, is known to be robust from an analytical analysis.

not seem to help (Table 3.1). The estimated robustness radius for uncertainty on the third level of the MAPK cascade is already very close to the analytical optimal value.

Comparing the robustness analysis results for uncertainty on the first and third level of the MAPK cascade leads to a striking observation. On the first level, the system can tolerate a level of uncertainty which is about a factor of ten larger than the one it can tolerate on the third level. A possible explanation for this effect is that the downstream levels typically operate in a more saturated regime, and as a consequence variations on upstream levels are not propagated downstream strongly. In any case, this result highlights the compelling ability of biochemical signal transduction networks to tolerate perturbations or uncertainty in the upstream part of a pathway.

Uncertainty in all kinetic parameters

To show that the proposed algorithm also works efficiently in higher dimensional parameter spaces, we next turn to the case where all six kinetic parameters in the model (2.13) of

Table 3.3: Robustness radii for steady state robustness of the MAPK cascade. All reaction parameters are assumed to be uncertain. Divisions of the test region $\mathcal{X}_0 \setminus \mathcal{X}$ in l subsets as defined in (3.26) are compared according to the resulting approximation of the robustness radius and the corresponding computation time.

	$l = 1$	$l = 4$	$l = 8$
Robustness radius $\widehat{\varrho}^* \leq \varrho^*$	1.9	3.5	3.5
Comp. time (sec)	4.1	16.7	31.4

Table 3.4: Upper bounds on the robustness radius in the MAPK cascade obtained from Monte Carlo tests.

Number of sample points	10^4	10^6	10^8
Robustness radius $\varrho_{mc} \geq \varrho^*$	6.2	4.9	4.1
Comp. time (sec)	0.4	40	3705

the MAPK cascade are assumed to be uncertain. The results are given in Table 3.3. The results should be compared to the optimal robustness radius $\varrho^* = 3.69$ obtained via condition (3.28). Although some conservatism remains, the robustness radius computed via the proposed algorithm comes quite close to the analytical result. Clearly, the robustness radius is reduced compared to the case where only two parameters are uncertain.

As discussed previously, Monte Carlo tests are a general approach to obtain an estimate for the conservatism of the computed lower bound on the robustness radius. It is illustrative to apply this approach to the considered example, even though an analytical solution is available. The Monte Carlo tests are performed by randomly generating a number of sample points within the set of non-desirable steady states $\mathcal{X}_0 \setminus \mathcal{X}$, and computing corresponding parameter values such that the steady state equation (3.1) is satisfied. For each sample point, the maximum deviation of a parameter value from the corresponding nominal parameter value is an upper bound on the robustness radius. The upper bound resulting from the test is taken as the minimum upper bound over all sample points. This test has been applied to the estimation of the robustness radius in the considered example. The resulting upper bounds for different choices of the number of sample points are shown in Table 3.4.

A comparison of the proposed algorithm with the Monte Carlo estimates yields two observations. First, the computation time required for the Monte Carlo test in order to obtain a reasonable upper bound on the robustness radius, i.e., for a large number of sample points, is significantly higher than the computation time required by the proposed robustness analysis algorithm in this example. Second, the gap between the conservative lower bound and the analytical robustness radius is comparable in magnitude to the gap between the upper bound and the analytical robustness radius for the highest number of sampling points used in this example. Although these conclusions apply only to the example considered here, they indicate that the proposed algorithm provides an efficient

complement to existing methods of steady state robustness analysis.

3.5 Summary and discussion of the steady state analysis

We have studied the problems of steady state uncertainty and robustness analysis with respect to parameter variations in biochemical reaction networks. This is an important problem in systems biology, where parameter values are frequently uncertain up to several orders of magnitude. Due to this large uncertainty, classical approaches based on local steady state sensitivity are often inappropriate.

Our approach is based on formulating a feasibility problem for suitable test regions in state and parameter space in order to check whether there are solutions to the steady state equation (3.1) within the test regions or not. This feasibility problem is relaxed to a semidefinite program, and the Lagrangian dual may provide infeasibility certificates for the considered test regions.

The first application of the infeasibility certificates is the steady state uncertainty analysis. In Section 3.3, we develop an algorithm which computes an outer bound on the region of possible steady states for a given set of parameter values. The proposed uncertainty analysis method is illustrated with a simple example network. To evaluate the obtained approximation, we compare the bounds obtained from our algorithm to steady state values obtained through Monte Carlo tests. In this example, our approach was computationally more efficient than Monte Carlo tests. Also, it gives guaranteed bounds on the steady state values, which cannot be achieved by sampling based methods such as Monte Carlo tests. Based on the premise that we are working with hyperrectangles only, the obtained bounds are fairly tight, and the conservatism in the infeasibility certificates did not have a significant impact in this example. In summary, the uncertainty analysis method proposed in this thesis is a reliable and computationally efficient method to estimate the range of possible steady state variations due to multiple simultaneous parameter variations in biochemical reaction networks, and thus provides a valuable tool for global uncertainty analysis.

The second application of the infeasibility certificates is the steady state robustness analysis with respect to uncertain parameters. The algorithm proposed in Section 3.4 can be used to compute a lower bound on the maximal parameter variation maintaining the steady state within a predefined region. In general, lower bounds are more important in robustness analysis, because they give guarantees on the allowable parameter variation. Upper bounds can not achieve this. The proposed robustness analysis method is applied to different models of the MAPK cascade. The results are compared to upper bounds on the robustness radius obtained via a Monte Carlo approach. In the examples considered in Section 3.4, the proposed algorithm based on semidefinite programming is computationally much more efficient than Monte Carlo tests, if a reasonably large number of sample points is used. Although there is some conservatism in the lower bounds, it is shown that the conservatism can be reduced at the expense of additional computation time by subdividing the test regions into more subsets.

Chapter 4

Robustness analysis of qualitative dynamical behaviour

This chapter deals with the robustness of dynamical behaviour with respect to parameter variations. An introduction to the problem and a formal problem statement is given in Section 4.1. We propose two new methods for robustness analysis. The first one, described in Section 4.2, directly builds on the results of Chapter 3 by computing the uncertainty in the Jacobian at steady states. The second method, given in Section 4.3, uses the newly introduced concept of feedback loop breaking, and in contrast to the first method also allows to evaluate the robustness of nominally unstable systems. The feedback loop breaking approach was first introduced in Waldherr and Allgöwer (2007).

4.1 Introduction and problem statement

The previous chapter was concerned with the location of steady states for uncertain parameters. However, the characteristics of non-constant trajectories were not considered. In this chapter, we turn to the qualitative dynamical behaviour around equilibrium points in the system, considering the characteristics of trajectories in a neighbourhood of the equilibrium points. In biochemical reaction networks, the dynamical behaviour around equilibrium points is frequently also the most distinct aspect of the global dynamical properties. Since the qualitative dynamical behaviour is usually classified into very few types (e.g. stability, instability with a single positive eigenvalue, instability with two complex conjugated eigenvalues, ...), the uncertainty analysis problem is not as relevant in this respect as in the previous chapter. Therefore, we focus exlusively on the robustness analysis problem.

Under parametric uncertainty, changes in the qualitative dynamical behaviour around equilibrium points are always related to the occurence of local bifurcations of equilibrium points. Bifurcation analysis is therefore frequently applied to biochemical reaction networks (Angeli *et al.*, 2004; Conradi *et al.*, 2007a,b; Eissing *et al.*, 2007b). In particular, local bifurcations typically correspond to emergence or loss of complex dynamical behaviour such as sustained oscillations or bistability. These types of dynamical behaviour have been studied in a large number of cell-biological systems, including metabolic networks, signal transduction systems like the MAPK cascade or apoptosis, and gene regulation systems like the circadian clock and the cell cycle (Eissing *et al.*, 2004; Ferrell and Machleder, 1998; Leloup and Goldbeter, 2003; Madsen *et al.*, 2005; Novak and Tyson, 1993; Pomerening *et al.*, 2003).

In this framework, the robustness analysis problem is to estimate the deviations from nominal parameter values that the system may tolerate without any local bifurcations

occuring. Such a robustness concept has been utilized in several previous studies. Bifurcation analysis can in fact be applied easily if only one or two parameters are assumed uncertain (Ma and Iglesias, 2002; Morohashi *et al.*, 2002). Yet, a major difficulty is that the bifurcation surface can usually not be computed explicitly in a high-dimensional parameter space. To deal with multiparametric uncertainty, it was suggested to use the structured singular value as analysis tool (Kim *et al.*, 2006; Ma and Iglesias, 2002). However, the uncertainty in the steady state upon parameter variations cannot be taken into account directly with this approach.

Although robustness analysis is a classical topic in control engineering, it remains surprisingly challenging to apply established methods to the analysis of biological networks. As discussed in Chapter 1, the difficulties of applying classical control methods to the analysis of biochemical reaction networks may be caused by the challenges of non-linearity and dependence of the steady state on uncertain parameters. In addition, the typical question in control engineering is the robustness of stability, whereas in biochemical networks also the robustness of complex dynamical behaviour, such as bistability or sustained oscillations, is highly relevant.

The approach developed in this thesis overcomes the outlined problems and is directly applicable to typical models for biochemical reaction networks. Two methods for robustness analysis are presented, both making use of convex optimisation to obtain robustness certificates for a given parametric uncertainty in a computationally efficient way. In our approach, a robustness measure is defined based on an uncertainty of parameters around a nominal parameter value p_0 which does not affect the qualitative dynamical behaviour of the system. Such a definition clearly implies that the robustness of a given system depends on the nominal parameter values. The basic idea of the proposed robustness definition is that dynamical properties of steady states should not be affected by parameter variations. A change in the dynamical properties of steady states is characterised by the condition that the system's Jacobian, evaluated at a steady state, has an eigenvalue on the imaginary axis. We assume throughout that all steady states are hyperbolic for nominal parameters p_0, i.e. none of the nominal steady states yields eigenvalues of the system's Jacobian on the imaginary axis.

The proposed concept for robustness of dynamical properties is formalised in the following definitions. As in the previous chapter, we consider an *a priori* known set $\mathcal{X}_0 \subset \mathbb{R}^n$ in which all physically relevant steady states are contained. We denote by $\mathrm{Path}(p, p_0)$ the set of all paths in $\mathbb{R}^q$ connecting two points $p, p_0 \in \mathbb{R}^q$. The spectrum of a square matrix A is denoted by $\mathrm{spect}(A)$.

Definition 4.1. *The set*

$$\begin{aligned}\mathcal{P}^*(p_0) = \Big\{ p \in \mathbb{R}^q \mid \exists\, \Gamma \in \mathrm{Path}(p, p_0) \forall \tilde{p} \in \Gamma\, \forall x \in \mathcal{X}_0 : \\ Sv(x, \tilde{p}) = 0 \Rightarrow \mathrm{spect}\big(S\frac{\partial v}{\partial x}(x, \tilde{p})\big) \cap j\mathbb{R} = \emptyset \Big\}\end{aligned} \tag{4.1}$$

is called the robust parameter set *for the system* (2.5) *with nominal parameter values* p_0.

In words, the robust parameter set is the set of all $p \in \mathbb{R}^q$ for which there is a path to p_0 on which the system's Jacobian evaluated at a steady state does not have eigenvalues

on the imaginary axis. From this definition, it is guaranteed that no local bifurcations occur in $\mathcal{P}^*(p_0)$.

In most cases, it will not be possible to compute the robust parameter set $\mathcal{P}^*$ explicitly. Also, in many cases the exact global shape of $\mathcal{P}^*$ is not even relevant for robustness analysis. This is related to the observation that e.g. a large volume of the robust parameter set does not imply large robustness, if $\mathcal{P}^*$ is very "thin" around the nominal parameter values, and may easily be left by only slight variations in the parameter values (Chaves *et al.*, 2009; Morohashi *et al.*, 2002). For robustness issues, it is more informative how large a compact region of regular shape (like a hyperrectangle or -ellipsoid) around the nominal parameters can be, while still being contained in $\mathcal{P}^*$. Therefore, the following definition is a natural way to define a robustness measure.

Definition 4.2. *The* dynamical robustness radius $\psi^* \in [1, \infty)$ *is given by*

$$\begin{aligned} \psi^* = \quad & \sup \psi \\ & \text{s.t. } \mathcal{P}_r(\psi, p_0) \subset \mathcal{P}^*(p_0), \end{aligned} \tag{4.2}$$

where $\mathcal{P}_r(\psi, p_0) = \left\{ p \in \mathbb{R}^q \mid \frac{1}{\psi} \leq \frac{p_j}{p_{0,j}} \leq \psi,\ j = 1, \ldots, q \right\}$.

The set $\mathcal{P}_r(\psi, p_0)$ is a hyperrectangle of all parameter values within a factor variation of at most ψ from p_0. The dynamical robustness radius is defined by the supremum of the logarithmic radius ψ of all such hyperrectangles inside the robust parameter set $\mathcal{P}^*(p_0)$. Thus, if the dynamical robustness radius is finite, it is equal to the minimal factor by which parameter values have to be varied from p_0 in order to leave the robust parameter set.

In the following sections, the goal will be to compute a lower bound $\widehat{\psi}^* \leq \psi^*$ on the dynamical robustness radius. By definition 4.2, $\mathcal{P}_r(\widehat{\psi}^*, p_0) \subset \mathcal{P}^*(p_0)$. Thus, knowledge of a lower bound allows to guarantee that the system does not undergo local bifurcations of steady states for parameter variations up to a factor of $\widehat{\psi}^*$.

As for the steady state analysis, we propose a bisection approach to solve problem (4.2). The first result is a computational test to decide whether it can be guaranteed that a test region $\widehat{\mathcal{P}}(\psi, p_0)$ is a subset of the robust parameter region $\mathcal{P}_r(\psi^*, p_0)$. This step is applied iteratively for different values of ψ, by doing a bisection on ψ depending on the results of the robustness test in each step. The estimate $\widehat{\psi}^*$ returned by the algorithm is the largest ψ for which robustness can still be guaranteed by the applied computational test.

4.2 Robustness analysis based on Jacobian uncertainty

4.2.1 Introduction

The first method for robustness analysis of dynamical properties proposed in this thesis focuses on the uncertain Jacobian at an uncertain steady state. The robustness test for a given parameter uncertainty is thereby based on Lyapunov techniques. This implies that only systems where all steady states in the considered region are nominally stable can be analysed. For ease of notation, all sets in state and parameter space are assumed to be hyperrectangles. In general, the approach is directly applicable to any convex polytopes.

In the method developed in this section, we need the concept of a linear differential inclusion (LDI), defined as follows (Boyd *et al.*, 1994).

Definition 4.3. *A* polytopic linear differential inclusion (PLDI) *is given by*

$$\dot{x} \in \{Ax \mid A \in \Omega\} \tag{4.3}$$

with $\Omega = \mathbf{Co}\{A_1, \ldots, A_N\} \subset \mathbb{R}^{n\times n}$*, where* $\mathbf{Co}\,\mathcal{A}$ *denotes the convex hull of the set* $\mathcal{A}$*.*

The goal of the robustness test developed in this section is to certify, if possible, robust stability for all equilibrium points within a region $\mathcal{X}_0$ of the state space, for uncertain parameters from a test region $\widehat{\mathcal{P}}$. The approach proposed in this section is to transfer the problem of robust stability in the non-linear model with uncertain steady states to the problem of robust stability of a related PLDI. We show in the sequel that the steady state bounds proposed in Chapter 3 provide the means to achieve such a transfer.

4.2.2 Robustness analysis algorithm

As a first step in the robustness test, we compute an outer bound $\mathcal{X}$ on feasible equilibrium points contained within the region $\mathcal{X}_0$ for parameters in $\widehat{\mathcal{P}}$. Using the global uncertainty analysis developed in Section 3.3, it is possible to compute a set $\mathcal{X}$ satisfying

$$\mathcal{X} \supset \{x \in \mathcal{X}_0 \mid \exists p \in \widehat{\mathcal{P}} : Sv(x,p) = 0\}. \tag{4.4}$$

In the second step, let us consider the Jacobian of the system (2.5), evaluated at a point $x \in \mathcal{X}$ and parameter $p \in \widehat{\mathcal{P}}$. The Jacobian is given by

$$A(x,p) = S\frac{\partial v}{\partial x}(x,p), \tag{4.5}$$

where $\frac{\partial v}{\partial x}(x,p)$ depends polynomially on x and p. Using the bounds $x \in \mathcal{X}$ and $p \in \widehat{\mathcal{P}}$ obtained in the previous step, the goal is to compute a polytope Ω containing all feasible Jacobians $A(x,p)$ for any $x \in \mathcal{X}$ and $p \in \widehat{\mathcal{P}}$.

To this end, let us write the Jacobian as a sum of constant base matrices $A^{(i)}$, $i = 0, \ldots, M$, multiplied with uncertain scalar terms γ_j, $j = 1, \ldots, M$:

$$A(x,p) = A^{(0)} + \gamma_1(x,p)A^{(1)} + \cdots + \gamma_M(x,p)A^{(M)} \tag{4.6}$$

with $\gamma_j(x,p) \in \mathbb{R}$ and $A^{(i)} \in \mathbb{R}^{n\times n}$. This is often useful to exploit the specific structure of biochemical reaction networks, where some terms appear in several elements of the Jacobian. The decomposition (4.6) may then help to reduce the number of vertices in the polytope Ω. Using the uncertainty analysis as described in Section 3.3, one can then compute bounds on the $\gamma_j(x,p)$ as

$$x \in \mathcal{X}, p \in \widehat{\mathcal{P}} \Rightarrow \gamma_{j,min} \leq \gamma_j(x,p) \leq \gamma_{j,max}, \quad j = 1, \ldots, M. \tag{4.7}$$

The number M depends on the specific network under study. As an example, consider a biochemical reaction network with m reactions, modelled with mass action kinetics, where

each reaction is assumed to involve two reactants. Then, there are generally $2m$ distinct terms in the reaction rate Jacobian $\frac{\partial v}{\partial x}$, and therefore $M = 2m$.

The set Ω for the PLDI is then obtained as $\Omega = \mathbf{Co}\{A_1, \ldots, A_N\}$, where the vertex matrices are computed as

$$\begin{aligned} A_1 &= A^{(0)} + \gamma_{1,min}A^{(1)} + \gamma_{2,min}A^{(2)} + \cdots + \gamma_{M,min}A^{(M)} \\ A_2 &= A^{(0)} + \gamma_{1,max}A^{(1)} + \gamma_{2,min}A^{(2)} + \cdots + \gamma_{M,min}A^{(M)} \\ &\vdots \\ A_N &= A^{(0)} + \gamma_{1,max}A^{(1)} + \gamma_{2,max}A^{(2)} + \cdots + \gamma_{M,max}A^{(M)} \end{aligned} \tag{4.8}$$

with $N = 2^M$. Thus, the number of vertices is exponential in the number of reactions. This makes the computation NP-hard, which may pose a problem to the computational implementation for medium- to large-scale systems. However, the optimisation problem may be simplified by further relaxations (Chesi, 2003; Schwenk and Tibken, 2008), leading to a reduced number of vertices in the stability test. In this way, the computational effort may be reduced.

In the third step, the remaining task is to check robust stability of the PLDI (4.3), with vertex matrices as in (4.8). This is a standard problem in robust control theory, and is conveniently achieved via the use of Lyapunov techniques and linear matrix inequalities. In this exposition, we only use the most basic result for this problem, namely the quadratic stability theorem (Boyd *et al.*, 1994). The robustness test is thereby based on finding a common Lyapunov function for all systems described by the PLDI (4.3), and is formulated as follows.

Theorem 4.4. *If there exists a matrix $P \in \mathcal{S}^n$ such that $P \succ 0$ and $A_i^{\mathrm{T}}P + PA_i \prec 0$, $i = 1, \ldots, N$, then all feasible steady states $x_s \in \{x \in \mathcal{X}_0 \mid \exists p \in \widehat{\mathcal{P}} : Sv(x,p) = 0\}$ are asymptotically stable.*

Proof. A sufficient condition for asymptotic stability of all feasible steady states is that the Jacobian $A(x,p)$ is Hurwitz for any $x \in \mathcal{X}_0$ and $p \in \widehat{\mathcal{P}}$ with $Sv(x,p) = 0$. Using the bounds from the uncertainty analysis, it can be established that $A(x,p) \in \Omega$ for all x and p which need to be considered. It remains to show that all matrices in Ω are Hurwitz. By standard Lyapunov stability arguments, a sufficient condition for this is that there exists $P \in \mathcal{S}^n$ with $P \succ 0$ and $A^{\mathrm{T}}P + PA \prec 0$ for all $A \in \Omega$. From the conditions in the theorem, this can be established by convex combination of the terms $A_i^{\mathrm{T}}P + PA_i$ (see Boyd *et al.*, 1994, for more details). □

Since a positive result of the robustness test requires that the same Lyapunov matrix P can be used for any uncertain matrix $A \in \Omega$, the robustness test is conservative. In the recent literature, more elaborated results than the basic quadratic stability theorem have been obtained, significantly reducing the conservatism of the robust stability test. The main idea behind the suggested extensions is to use a parameter-dependent Lyapunov function. It has been shown that, for any robustly stable PLDI, there exists a Lyapunov function which depends polynomially on the uncertain parameters used in the convex combination representing $A \in \Omega$. Moreover, it is possible to compute this Lyapunov function by solving LMIs (Bliman, 2004). The provided conditions are thus sufficient and

asymptotically necessary for robust stability, where necessity is achieved in the limit of an unbounded degree of the polynomial. However, the robust stability test based on these conditions may involve a huge computational effort. Several other approaches for the considered problem have been proposed, e.g. (Chesi, 2005; Henrion *et al.*, 2004; Oliveira and Peres, 2006). Each of these methods could be used to design a robust stability test, but for ease of exposition we restrict ourselves to the use of the quadratic stability condition as proposed in Theorem 4.4.

Based on Theorem 4.4, an algorithm for computing a lower bound on the dynamical robustness radius ψ^* is devised. The algorithm takes the nominal parameter values p_0 and the decomposition of the uncertain Jacobian $A(x,p)$ as given in (4.6), with base matrices $A^{(i)}$, $i = 0,\ldots,M$ and value functions $\gamma_j(x,p)$, $j = 1,\ldots,M$, as input. The output of the algorithm is a certified lower bound $\widehat{\psi^*}$ on the dynamical robustness radius ψ^*. A flowchart illustration of the proposed algorithm is shown in Figure 4.1.

Upper bounds on the dynamical robustness radius can be obtained from testing parameter samples for stability of the corresponding equilibrium points. For each sample, the largest variation in each parameter compared to its nominal value is an upper bound on the dynamical robustness radius ψ^*. The overall upper bound from such a sampling test is then given by the minimal upper bound across all samples.

4.2.3 Application to the NF-κB pathway model

As an example application, the algorithm developed in this section is used to analyse the model (2.16) of the NF-κB pathway described in Section 2.3.2. Nominal parameter values are taken from vector p_2 in Table 2.5, where the model shows damped oscillations towards an asymptotically stable equilibrium point.

The uncertain parameters were chosen as k_t, k_{tl}, γ_m, and α. These parameters are a lumped representation of complex processes within the cell, and are therefore expected to be subject to some variability, depending on internal and external conditions. Other parameters describe only simple processes or direct biochemical interactions and are expected to be much less variable.

In order to apply the algorithm developed in Section 4.2.2, an *a priori* set $\mathcal{X}_0$ containing all steady states has to be constructed. For the NF-κB pathway model (2.16), determination of the *a priori* set deserves special attention, since for this model, such a set is not obvious from conservation relations. The set $\mathcal{X}_0$ is constructed by considering the reduced order model (2.17). Since the reduction is based on a quasi steady state assumption, and the parameters k_f and k_b involved in complex formation are not assumed to be uncertain, the reduced order model (2.17) and the original model (2.16) are equivalent with respect to steady states. Boundedness of steady states reachable from relevant initial conditions in the NF-κB pathway model (2.17) is established by the following result.

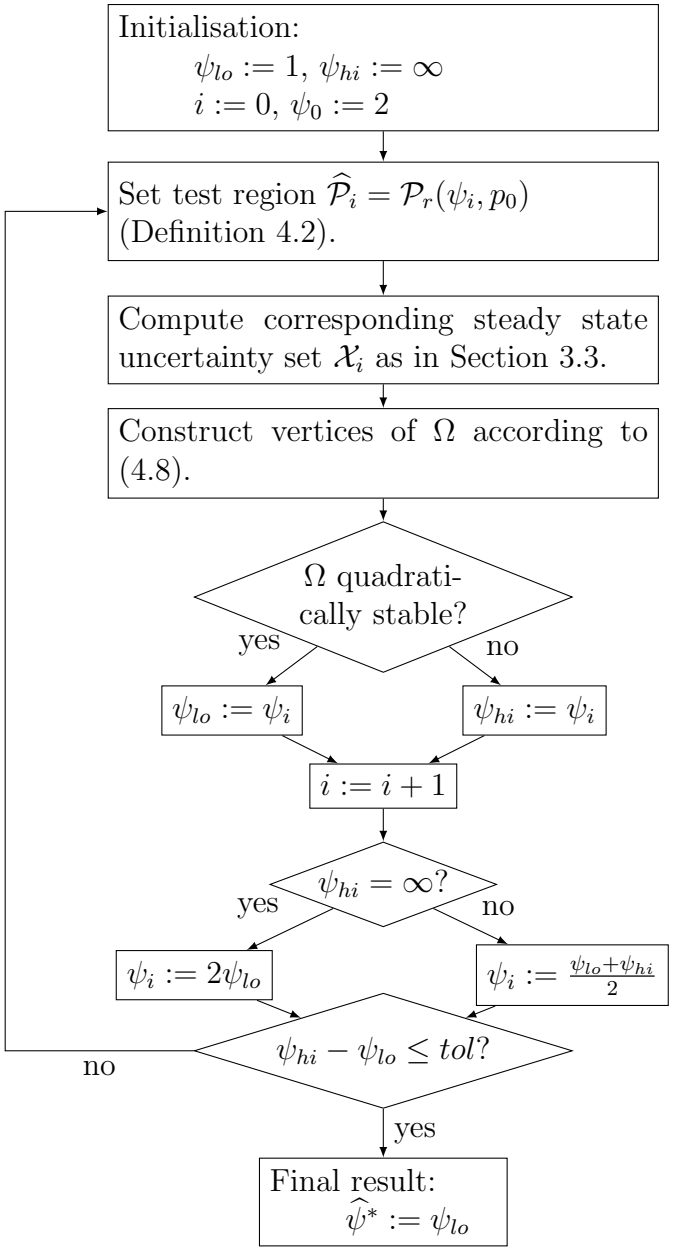

Figure 4.1: Flowchart for the robust stability analysis algorithm based on Jacobian uncertainty, using semidefinite programming for the uncertainty analysis and the quadratic stability theorem for the robustness test. As numerical parameter, a stopping tolerance tol needs to be supplied.

Proposition 4.5. *The set defined by the constraints*

$$0 \leq x_i, \qquad i = 1, \ldots, 4 \tag{4.9a}$$

$$x_2 \leq \frac{k_t N_{tot}^2}{\gamma_m} \tag{4.9b}$$

$$x_4 \leq N_{tot} \tag{4.9c}$$

$$k_{I,out} K_N x_3 \leq (K_N + N_{tot})(k_{I,in} x_1 + \alpha N_{tot}) \tag{4.9d}$$

$$K_N k_{I,in} x_1 - K_N \frac{k_t k_{tl} N_{tot}^2}{\gamma_m} \leq (k_{I,out} K_N + k_{NI,out} N_{tot}) x_3 \tag{4.9e}$$

$$\frac{k_{tl}}{\gamma_m} x_2 + x_1 + x_3 \leq L, \tag{4.9f}$$

is positively invariant with respect to the system (2.17)*, where* $L > 0$ *is such that* $x_2 \geq \frac{k_t k_{tl} N_{tot}(K_N + N_{tot})}{\gamma_m k_{NI,out}}$ *for any* x *satisfying the constraints* (4.9a)–(4.9e) *and* $\frac{k_{tl}}{\gamma_m} x_2 + x_1 + x_3 = L$.

Proof. By Nagumo's theorem (Blanchini, 1999), it is sufficient to show that the vector field for the model (2.17) is contained in the tangent cone to the set defined by the constraints (4.9). In this case, we need to show that, for each of the affine constraints in (4.9), the vector field is contained in the half-space satisfying the corresponding constraint.

The constraints (4.9a)–(4.9c) result directly from the differential equations for the individual state variables in the inequalities.

Let us next consider the constraint (4.9d). If (4.9d) is satisfied with equality, then $\dot{x}_1 = k_{tl} x_2 + \alpha N_{tot} - \frac{\alpha(N_{tot} - x_4) x_1}{K_I + x_1} \geq 0$ and $\dot{x}_3 = -\alpha N_{tot} - k_{NI,out} \frac{x_3 x_4}{K_N + x_4} \leq 0$. Thus the vector field is contained in the half-space corresponding to (4.9d). Using a similar argument for (4.9e), we find that $\dot{x}_1 \leq 0$ and $\dot{x}_3 \geq 0$, if (4.9e) is satisfied with equality, and thus again the vector field is contained in the corresponding half-space.

Considering finally the constraint (4.9f), we find that $\frac{d}{dt}(\frac{k_{tl}}{\gamma_m} x_2 + x_1 + x_3) \leq 0$ for any $x_2 \geq \frac{k_t k_{tl} N_{tot}(K_N + N_{tot})}{\gamma_m k_{NI,out}}$. Thus, if the constraints (4.9a)–(4.9e) are satisfied, the vector field is contained in the half-space corresponding to (4.9f) whenever $\frac{k_{tl}}{\gamma_m} x_2 + x_1 + x_3 = L$. □

For any given parameter set $\mathcal{P}$, a set $\mathcal{X}_0$ containing all steady states of the model (2.16) is constructed by Proposition 4.5. To obtain a lower bound on the dynamical robustness radius, we apply the robustness analysis algorithm developed in this section (Figure 4.1). For the example considered here, we have $M = 8$ base matrices in the Jacobian decomposition (4.6), and the resulting size of the PLDI (256 vertices) is handled well by current numerical SDP solvers. The result from the algorithm is a lower bound on the robustness radius of $\widehat{\psi}^* = 1.54 \leq \psi^*$. The computation takes about six minutes on a standard desktop computer. Upper bounds have been computed using simple Monte Carlo tests, and are shown in Table 4.1. The best bound is $1.83 \geq \psi^*$, found with 10^6 samples after a computation time of about 37 hours. Probably this bound is still not tight, but as the computation time is proportional to the number of samples, the sample number cannot be increased much further while maintaining a reasonable computational cost.

From the results of the robustness analysis, we conclude that the steady state in the NF-κB pathway model (2.16) with nominal parameters p_2 from Table 2.5 will remain

Table 4.1: Upper bounds on the dynamical robustness radius in the NF-κB pathway model obtained from Monte Carlo tests.

Number of sample points	10^4	$5 \cdot 10^5$	10^6
Robustness radius $\psi_{mc} \geq \psi^*$	1.93	1.86	1.83
Computation time (hours)	0.35	18	37

stable for parameter variations of up to a factor 1.54. In particular, a Hopf bifurcation with a corresponding onset of oscillations is excluded up to this level of uncertainty. Biologically, this means that small to medium perturbations in the processes described by the uncertain parameters seem not to affect the qualitative dynamics of the NF-κB pathway in the configuration considered here.

On the methodological side, we observe that the proposed algorithm quite efficiently provides a reasonably good lower bound on the robustness radius for relevant small to medium scale problems. Such a lower bound is a valuable complement to the upper bounds available from common "robustness tests" via Monte Carlo sampling.

4.3 Robustness analysis via Positivstellensatz infeasibility certificates

The approach developed in the previous section is limited to considering robustness of stability. This may be well suited for control engineering applications, but it is often insufficient for analysing dynamical behaviour in biochemical reaction networks. In fact, biological function based on complex dynamical behaviour like sustained oscillations or bistability is typically directly related to instability of an equilibrium point (Eissing *et al.*, 2007b; Schmidt and Jacobsen, 2004). This observation motivates the study of robust instability for models of biochemical reaction networks. Although converse Lyapunov theorems provide sufficient conditions for instability (Khalil, 2002), they are not as useful for dynamical robustness analysis, because the admissible functions to be used are not as convenient as in the stability analysis case. The approach proposed in this section avoids this drawback by building on frequency domain methods, specifically the generalised Nyquist criterion. We propose conditions for robustness of instability as well as a computational algorithm to compute a lower bound on the dynamical robustness radius for a model with a nominally unstable equilibrium point.

To simplify the notation, let us rewrite the right hand side of the system (2.5) as $Sv(x,p) = F(x,p)$. Thus, the system to be considered is given by

$$\dot{x} = F(x,p), \tag{4.10}$$

with $x \in \mathbb{R}^n$, $p \in \mathcal{P} \subset \mathbb{R}^q$ and $F : \mathbb{R}^n \times \mathbb{R}^q \to \mathbb{R}^n$ being a smooth vector field.

To deal with steady states for uncertain parameter values, we introduce the notation of a state–parameter pair χ as

$$\chi = (x,p) \in \mathbb{R}^n \times \mathbb{R}^q. \tag{4.11}$$

We call χ a *steady state–parameter pair* if the corresponding x and p satisfy the equation

$$F(x, p) = 0. \tag{4.12}$$

Let $\mathcal{M} \subset \mathbb{R}^n \times \mathcal{P}$ be a q-dimensional manifold of steady state–parameter pairs in $\mathbb{R}^n \times \mathcal{P}$, i.e.

$$\forall (x, p) \in \mathcal{M} : F(x, p) = 0. \tag{4.13}$$

In the simplest case, there is a unique steady state for each $p \in \mathcal{P}$, and one could use a function $x_s(p)$ to characterise the manifold of steady state–parameter pairs more easily. However, such a function is usually difficult to compute explicitly. In addition, the approach taken here is more general and also allows to consider e.g. saddle-node bifurcations, where uniqueness of an equilibrium point for each $p \in \mathcal{P}$ is not satisfied. For most applications, $\mathcal{M}$ can just be defined by the equilibrium point equation $F(x, p) = 0$. In some cases, it may however be beneficial to reduce the steady state equation by analytical means. To account for this, we introduce the function $\Phi : \mathbb{R}^{n+q} \to \mathbb{R}^n$ which characterises the manifold $\mathcal{M}$ via

$$\mathcal{M} = \{\chi \in \mathbb{R}^{n+q} \mid \Phi(\chi) = 0\}. \tag{4.14}$$

In most cases, we can choose $\Phi = F$. Yet, the definition of $\mathcal{M}$ used here is more general and e.g. allows to remove steady state branches which should not be considered in the analysis from the problem.

4.3.1 Characterisation of critical points via the loop transfer function

The major structural feature in biochemical reaction networks contributing to changes in the local dynamical behaviour are feedback circuits (see e.g. Waldherr *et al.* (2008a) and references therein). Mathematically, the system (4.10) is said to contain a feedback loop if the influence graph of its Jacobian $\frac{\partial F}{\partial x}$ contains a nontrivial loop (Cinquin and Demongeot, 2002). The sign of the feedback loop is defined as the product of the weights on the edges, taken from the corresponding entries in the Jacobian. Concerning the dynamical behaviour, it can be shown that a positive feedback circuit in the system is required for multistationarity (Kaufman *et al.*, 2007), whereas a negative circuit is required for limit cycle oscillations (Snoussi, 1998). As a consequence, it seems quite intuitive to characterise the occurence of local bifurcations by considering the feedback circuits of a dynamical system.

In the remainder of this section, we will assume that (4.10) contains a feedback loop. If this assumption is not satisfied, the problem is simplified significantly. Without a feedback loop, the analytical expressions for the eigenvalues in terms of parameters and the state variables can directly be taken from the diagonal of the Jacobian $\frac{\partial F}{\partial x}$. In this case, it is usually easy to find parameter values for a change in stability properties of the equilibrium points, if such values exist. Based on these considerations, the robustness analysis method proposed in this section is built upon a *feedback loop breaking* approach, where properties of the original system are characterised by studying an appropriately constructed input–output system. The original system is then interpreted as the closed loop description of the constructed input–output system. Formally, we define a feedback loop breaking as follows.

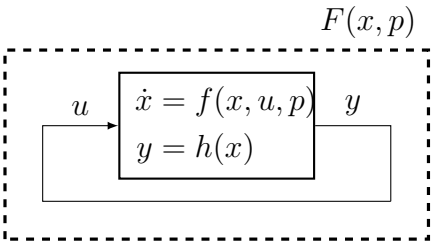

Figure 4.2: Illustration of feedback loop breaking

Definition 4.6. *A* feedback loop breaking *for the system* (4.10) *is a tuple* (f, h)*, where* $f : \mathbb{R}^n \times \mathbb{R} \times \mathbb{R}^q \to \mathbb{R}^n$ *is a smooth vector field and* $h : \mathbb{R}^n \to \mathbb{R}$ *is a smooth function, such that*

$$F(x, p) = f(x, h(x), p). \tag{4.15}$$

The corresponding open loop system is then given by the equation

$$\begin{aligned} \dot{x} &= f(x, u, p) \\ y &= h(x), \end{aligned} \tag{4.16}$$

and the closed loop system (4.10) is recovered by setting $u = y$. This situation is illustrated in Figure 4.2. Note that there is a direct relation between steady states in the closed and the open loop system: for a steady state–parameter pair (x_0, p) of the closed loop system (4.10), setting the input $u = h(x_0)$ in the open loop system (4.16) leads to (x_0, p) being a steady state–parameter pair of the open loop system (4.16). We denote $u_0 = h(x_0)$.

To deal with the question whether different steady state–parameter pairs in $\mathcal{M}$ can have different stability properties, it is reasonable to consider the linear approximation of the system (4.10) close to some $\chi \in \mathcal{M}$. Only the pairs χ where the Jacobian $\frac{\partial F}{\partial x}(\chi)$ has eigenvalues on the imaginary axis are candidate points for local bifurcations. Any such pair is called a *critical point*, and is denoted as χ_c.

The linear approximation for the open loop system (4.16) in the neighbourhood of the steady state–parameter pair $\chi \in \mathcal{M}$ is given by

$$\begin{aligned} \frac{d}{dt}\Delta x &= A_o(\chi)\Delta x + B_o(\chi)\Delta u \\ \Delta y &= C_o(\chi)\Delta x, \end{aligned} \tag{4.17}$$

where $\Delta x = x - x_0$, $\Delta y = y - u_0$, $\Delta u = u - u_0$, $A_o(\chi) = \frac{\partial f}{\partial x}(x_0, u_0, p)$, $B_o(\chi) = \frac{\partial f}{\partial u}(x_0, u_0, p)$, $C_o(\chi) = \frac{\partial h}{\partial x}(x_0)$.

Denote the Jacobian of the closed loop system (4.10) as

$$A(\chi) = \frac{\partial F}{\partial x}(\chi). \tag{4.18}$$

As a relation between $A(\chi)$ and the linearised open loop system (4.17), we have the following result.

Proposition 4.7. *The closed loop Jacobian $A(\chi)$ satisfies*

$$A(\chi) = A_o(\chi) + B_o(\chi)C_o(\chi). \tag{4.19}$$

Proof. This follows directly from the loop breaking definition (4.15) and the chain rule. □

The linearised open loop system (4.17) can also be described by its transfer function, which is defined as

$$G(\chi, s) = C_o(\chi)\left(sI_n - A_o(\chi)\right)^{-1} B_o(\chi) = \frac{\det\begin{pmatrix} sI_n - A_o(\chi) & -B_o(\chi) \\ C_o(\chi) & 0 \end{pmatrix}}{\det(sI_n - A_o(\chi))} \tag{4.20}$$

with the complex variable $s \in \mathbb{C}$.

The following lemma is a tool to characterise eigenvalues of the closed loop Jacobian $A(\chi)$ by analysing the linearised open loop system (4.17).

Lemma 4.8. *$s_0 \in \mathbb{C}$ is an eigenvalue of $A(\chi)$, if and only if either of the following conditions holds:*

(i) s_0 is not an eigenvalue of $A_o(\chi)$ and $G(\chi, s_0) = 1$;

(ii) s_0 is an eigenvalue of $A_o(\chi)$ and $\det\begin{pmatrix} s_0 I_n - A_o(\chi) & -B_o(\chi) \\ C_o(\chi) & 0 \end{pmatrix} = 0.$

The proof is provided in the appendix, Section A.1. In the following, Lemma 4.8 is used with s_0 on the imaginary axis to characterise critical points χ_c with the condition $G(\chi_c, s_0) = 1$. To this end, the transfer function G is represented as a complex rational function with real coefficients

$$G(\chi, s) = \frac{Q(\chi, s)}{R(\chi, s)}, \tag{4.21}$$

where $Q(\chi, s)$, $R(\chi, s)$ are polynomials in s with real scalar functions of χ as coefficients.

The following result then characterises critical steady state–parameter pairs.

Theorem 4.9. *Assume that the open loop Jacobian $A_o(\chi)$ does not have an eigenvalue on the imaginary axis for any $\chi \in \mathcal{M} \cap \mathcal{X}_0 \times \mathcal{P}$. Also assume that the degrees of $Q(\chi, s)$ and $R(\chi, s)$ in s are constant with respect to $\chi \in \mathcal{M} \cap \mathcal{X}_0 \times \mathcal{P}$. Then the following two conditions are equivalent.*

(i) There exists a critical point $\chi_c \in \mathcal{M} \cap \mathcal{X}_0 \times \mathcal{P}$.

(ii) The system of equations

$$\begin{aligned} Q(\chi, j\omega) &= R(\chi, j\omega) \\ \Phi(\chi) &= 0 \end{aligned} \tag{4.22}$$

in the variables $\chi \in \mathbb{R}^{n+q}$ and $\omega \in \mathbb{R}$ has a solution with $\chi \in \mathcal{X}_0 \times \mathcal{P}$.

Proof. By assumption, there does not exist $\omega \in \mathbb{R}$ such that $j\omega$ is an eigenvalue of $A_o(\chi)$.

(i) ⇒ (ii): Let $j\omega_c$ be an imaginary eigenvalue of $A(\chi_c)$. By Lemma 4.8, χ_c and ω_c solve (4.22).

(ii) ⇒ (i): Let χ and ω be a solution of (4.22). In particular, by (4.14), we have $\chi \in \mathcal{M} \cap \mathcal{X}_0 \times \mathcal{P}$. By Lemma 4.8, χ is a critical point, with $j\omega$ being an eigenvalue of $A(\chi)$. □

The assumption that $A_o(\chi)$ does not have an eigenvalue on the imaginary axis for any $\chi \in \mathcal{M} \cap \mathcal{X}_0 \times \mathcal{P}$ is made since we are interested in case *(i)* of Lemma 4.8. From a control engineering perspective, this assumption assures that no pole–zero cancellations of eigenvalues on the imaginary axis occur in the transfer function $G(\chi, s)$. The assumption on $A_o(\chi)$ can often be satisfied by structural properties. For instance, if the open loop system does not have a feedback circuit, the eigenvalues can directly be read from the Jacobian. In this case, it is typically easy to check whether imaginary eigenvalues are possible for $p \in \mathcal{P}$ and $x \in \mathcal{X}_0$. Otherwise, one may use the following result.

Proposition 4.10. *Assume that no pole–zero cancellations occur in the transfer function $G(\chi, s)$. If the system of equations*

$$\begin{aligned} R(\chi, j\omega) &= 0 \\ \Phi(\chi) &= 0 \end{aligned} \tag{4.23}$$

does not have a solution with $\chi \in \mathcal{X}_0 \times \mathcal{P}$ and $\omega \in \mathbb{R}$, then $A_o(\chi)$ does not have eigenvalues on the imaginary axis for any $\chi \in \mathcal{M} \cap \mathcal{X}_0 \times \mathcal{P}$.

Proof. Under the assumption that no pole–zero cancellations occur, we have $R(\chi, j\omega) = \det(j\omega I_n - A_o(\chi))$. The proof is by negation: if there exist $\chi \in \mathcal{M} \cap \mathcal{X}_0 \times \mathcal{P}$ and $\omega \in \mathbb{R}$ such that $j\omega$ is an eigenvalue of $A_o(\chi)$, then χ and ω satisfy (4.23). □

4.3.2 Robustness certificates from the Positivstellensatz

In this section, we develop an approach to test whether the dynamical behaviour of the system (2.5) is robust with respect to uncertain parameters inside a given region $\mathcal{P} \subset \mathbb{R}^q$ and a given region of equilibrium points $\mathcal{X}_0 \subset \mathbb{R}^n$. From Theorem 4.9, this is equivalent to checking infeasibility of (4.22). Observe that, for reaction rates $v(x, p)$ which are rational in state variables and parameters, (4.22) is a system of polynomial equations. In the next step, we use results from real algebraic geometry and convex optimisation to obtain robustness certificates.

As usual, let us denote the ring of polynomials in the vector variable χ over the field of real numbers as $\mathbb{R}[\chi]$ (Cox *et al.*, 1995). The following definition states two prerequisites for the further discussion in this section.

Definition 4.11. *The ideal generated by a set of polynomials $\mathcal{Y} = \{Y_1, \ldots, Y_N\} \subset \mathbb{R}[\chi]$ is defined as*

$$\mathcal{I}(Y_1, \ldots, Y_N) = \Big\{ \sum_{i=1}^{N} T_i Y_i \mid T_i \in \mathbb{R}[\chi] \Big\}. \tag{4.24}$$

The cone generated by $\mathcal{Y}$ is denoted by $\mathcal{C}(Y_1, \ldots, Y_N)$ and defined by the properties

(i) $T \in \mathbb{R}[\chi] \Rightarrow T^2 \in \mathcal{C}(Y_1, \ldots, Y_N)$,

(ii) $Y \in \mathcal{C}(Y_1, \ldots, Y_N),\ \bar{Y} \in \mathcal{C}(Y_1, \ldots, Y_N) \Rightarrow Y + \bar{Y} \in \mathcal{C}(Y_1, \ldots, Y_N)$,

(iii) $Y \in \mathcal{C}(Y_1, \ldots, Y_N),\ \bar{Y} \in \mathcal{C}(Y_1, \ldots, Y_N) \Rightarrow Y\bar{Y} \in \mathcal{C}(Y_1, \ldots, Y_N)$.

The basic result from real algebraic geometry required in our approach is the Positivstellensatz, cited from Bochnak *et al.* (1998).

Theorem 4.12 (Positivstellensatz). *Consider a system of polynomial (in-)equalities given by*

$$\begin{aligned} Y_i(\chi) &= 0, \quad i = 1, \ldots, N \\ Z_j(\chi) &\geq 0, \quad j = 1, \ldots, M, \end{aligned} \tag{4.25}$$

with $\chi \in \mathbb{R}^{n+q}$. System (4.25) does not have a solution in $\mathbb{R}^{n+q}$, if and only if there exist $Y \in \mathcal{I}(Y_1, \ldots, Y_N)$ and $Z \in \mathcal{C}(Z_1, \ldots, Z_M)$ such that

$$Y + Z + 1 = 0. \tag{4.26}$$

In the recent literature, the Positivstellensatz has been combined with sum of squares relaxations (Parrilo, 2003) to obtain computationally efficient proofs for the infeasibility of inequality systems of the form (4.25). In particular, positive semidefiniteness constraints on multiplier polynomials in the parametrisation of the cone $\mathcal{C}(Z_1, \ldots, Z_M)$ can be formulated as a positive semidefiniteness constraint on a suitably constructed matrix. Thus, the problem of existence of Y and Z satisfying (4.26) can be relaxed to a semidefinite program. However, the sum of squares relaxation typically leads to very large semidefinite programs, which may pose computational problems even for the efficient solvers which are available. In addition, numerical studies of this approach suggest that the resulting semidefinite programs may be intrinsically degenerate and thus impracticable for typical numerical solvers (Monniaux, 2009).

To avoid these difficulties, the problem under consideration is further transformed, such that it reduces to the solution of a linear program, for which solvers are more efficient than for semidefinite programs. The basic tool for this further transformation is the Handelman representation theorem (Handelman, 1988). This theorem makes use of so-called Handelman monomials H_d. These are constructed from the inequality constraints Z as

$$H_d(\chi) = \prod_{j=1}^{M} Z_j(\chi)^{d_j}, \tag{4.27}$$

where $d \in \mathbb{N}_0^M$ is the vectorial degree of the Handelman monomial H_d. The Handelman representation theorem is given in the following statement.

Theorem 4.13 (Handelman, 1988). *Let $\mathcal{K} \subset \mathbb{R}^{n+q}$ be a compact polytope defined by the equations*

$$Z_j(\chi) \geq 0, \quad j = 1, \ldots, M, \tag{4.28}$$

with $\chi \in \mathbb{R}^{n+q}$ and $Z_j : \mathbb{R}^{n+q} \to \mathbb{R}$ affine functions. The polynomial $Y : \mathbb{R}^{n+q} \to \mathbb{R}$ is non-negative on $\mathcal{K}$, if and only if Y can be represented as

$$Y = \sum_{d \in \mathbb{N}_0^M} c_{H,d} H_d, \tag{4.29}$$

with non-negative coefficients $c_{H,d}$.

Example 4.14. Consider the polynomial $Y(x) = -2x^2 + 7x - 5$ in the variable $x \in \mathbb{R}$. The polynomial is non-negative on the domain $1 \leq x \leq 2$. This domain is represented by the constraints $Z_1(x) = x - 1 \geq 0$ and $Z_2(x) = 2 - x \geq 0$. Using the two Handelman monomials $H_{(1,0)}(x) = x - 1$ and $H_{(1,1)}(x) = (x-1)(2-x)$, a Handelman representation for the polynomial Y is given by

$$Y(x) = -2x^2 + 7x - 5 = 1 \cdot (x-1) + 2 \cdot (x-1)(2-x).$$

The original result by Handelman (1988) gives a necessary and sufficient condition for positivity of a single polynomial Y on a compact polytope. Compared to the Positivstellensatz, the assumption that the inequalities (4.28) describe a compact polytope is more restrictive, since the Positivstellensatz makes no specific assumption on the Z_j. Yet this restriction is not an obstacle for the application pursued in this section, as we are generally working with polytopic sets anyway. Another restriction is that the result concerns positivity of a single polynomial only. However, in the present problem, it is necessary to guarantee non-existance of solutions for a set of polynomial equations within a polytope. The following result combines the Positivstellensatz with the Handelman representation theorem to achieve a statement suitable for this purpose.

Theorem 4.15. *Let $\mathcal{K} \subset \mathbb{R}^{n+q}$ be a compact polytope defined as in Theorem 4.13. Then the following two conditions are equivalent.*

(i) The system of equations

$$Y_i(\chi) = 0, \quad i = 1, \ldots, N \tag{4.30}$$

with $\chi \in \mathbb{R}^{n+q}$ and polynomials $Y_i \in \mathbb{R}[\chi]$ does not have a solution in $\mathcal{K}$.

(ii) There exist polynomials $T_i \in \mathbb{R}[\chi]$, $i = 1, \ldots, N$ such that the polynomial

$$Y = \sum_{i=1}^{N} T_i Y_i - 1 \tag{4.31}$$

can be represented as

$$Y = \sum_{d \in \mathbb{N}_0^M} c_{H,d} H_d, \tag{4.32}$$

with non-negative coefficients $c_{H,d}$.

Proof. (i) $\Rightarrow$ (ii). By the Positivstellensatz, there exist polynomials $\tilde{Y} \in \mathcal{I}(Y_1, \ldots, Y_N)$ and $Z \in \mathcal{C}(Z_1, \ldots, Z_M)$ such that $\tilde{Y} + Z + 1 = 0$. By $Z \geq 0$ on $\mathcal{K}$, we have that $-\tilde{Y} - 1 \geq 0$ on $\mathcal{K}$. Since $\tilde{Y} \in \mathcal{I}(Y_1, \ldots, Y_N)$, it can be represented as $\tilde{Y} = -\sum_{i=1}^{N} T_i Y_i$ with $T_i \in \mathbb{R}[\chi]$. Thus, there exist T_i, $i = 1, \ldots, N$ such that the polynomial Y as defined in (4.31) is non-negative on $\mathcal{K}$. The result then follows from Theorem 4.13.

(ii) $\Rightarrow$ (i). By Theorem 4.13, Y is non-negative on $\mathcal{K}$. Since any $Z \in \mathcal{C}(Z_1, \ldots, Z_M)$ is also non-negative on $\mathcal{K}$, there does not exist such Z satisfying $Y + Z + 1 = 0$, and, from the Positivstellensatz, (4.30) does not have a solution on $\mathcal{K}$. □

Example 4.16. Consider the system of equations

$$\begin{aligned} 7 + 3x_1 - 4x_2 &= 0 \\ x_2 - x_1 - 1 &= 0. \end{aligned} \tag{4.33}$$

Using Theorem 4.15, we want to establish that (4.33) does not have a solution in the set $\mathcal{X} = \{x \in \mathbb{R}^2 \mid 0 \leq x_i \leq 2,\ i = 1, 2\}$. To this end, consider the polynomial

$$Y = 7 + 3x_1 - 4x_2 + x_2(x_2 - x_1 - 1) - 1,$$

constructed with the multipliers $T_1 = 1$ and $T_2 = x_2$ according to (4.31). By algebraic manipulation, we find the Handelman representation

$$Y = x_1 + x_1(2 - x_2) + (2 - x_2) + (2 - x_2)^2, \tag{4.34}$$

which shows that (4.33) does not have a solution in $\mathcal{X}$.

A relaxed result for which only the conclusion *(ii)* $\Rightarrow$ *(i)* in Theorem 4.15 is valid can be obtained by restricting the degree of the multipliers T_i. With this relaxation, a finite parametrisation of the problem is achieved, where the coefficients of the polynomials T_i are free parameters. The procedure to compute an infeasibility certificate, i.e. specific multipliers T_i such that condition *(ii)* is satisfied, then reduces to the solution of a linear program and is outlined as follows.

1. Construct the multiplier polynomials T_i, $i = 1, \ldots, N$, according to

$$T_i = \sum_{d \in \mathcal{D}_i} c_{T,d}^{(i)} \chi^d, \tag{4.35}$$

   where $\mathcal{D}_i \subset \mathbb{N}_0^{n+q}$ contains all vectorial degrees to be used in the multipliers, $c_{T,d}^{(i)} \in \mathbb{R}$ are free parameters to be chosen later, and $\chi^d = \prod_{i=1}^{n+q} \chi_i^{d_i}$. From (4.31), the coefficients of the polynomial Y are then given as affine functions of the multiplier coefficients $c_{T,\mathcal{D}_i}^{(i)}$.

2. Construct all Handelman monomials $H_d(\chi)$ of the form (4.27), for all $d \in \mathbb{N}_0^M$ such that the vectorial degrees of H_d do not exceed the vectorial degree of Y.

3. Construct the Handelman polynomial

$$Y_H = \sum_{d \leq d_{max}} c_{H,d} H_d, \tag{4.36}$$

   where $d_{max} \in \mathbb{N}_0^M$ is the maximal vectorial degree of Y_H, and the $c_{H,d} \in \mathbb{R}$ are non-negatively constrained parameters to be determined in the next step.

4. Check whether the linear program

$$\begin{aligned} \text{find} \quad & c_{T,d}^{(i)} && i = 1, \ldots, N,\ d \in \mathcal{D}_i \\ & c_{H,d} \geq 0 && d \leq d_{max} \\ \text{s.t.} \quad & \operatorname{coeff}_\chi(Y) = \operatorname{coeff}_\chi(Y_H) \end{aligned} \tag{4.37}$$

   is feasible or not, where $\operatorname{coeff}_\chi(Y)$ denotes the coefficient vector of Y with respect to monomials in χ.

The conclusion obtained from the above procedure is given in the following result.

Corollary 4.17. *If the linear feasibility problem* (4.37)*, constructed for the equations* (4.22) *with affine constraints* $\chi \in \mathcal{X}_0 \times \mathcal{P}$*, is solvable, then there does not exist a critical point* $\chi_c \in \mathcal{M} \cap \mathcal{X}_0 \times \mathcal{P}$*.*

Corollary 4.17 provides a Positivstellensatz robustness certificate for the considered system under the parameteric uncertainty $p \in \mathcal{P}$, in the sense that any feasible solution to the corresponding linear program proves robustness of the system's qualitative dynamical behaviour.

Similarly to the algorithm proposed in Section 4.2.2, a lower bound $\widehat{\psi}^*$ on the robustness radius ψ^* is computed by a bisection on the logarithmic radius ψ of the parameter uncertainty region $\mathcal{P}(\psi, p_0)$, using the Positivstellensatz robustness certificates according to Corollary 4.17 in each step.

4.3.3 Application to the NF-κB pathway model

The robustness analysis method developed in the previous section is applied to the reduced order NF-κB pathway model (2.17), with parameter values given by p_1 in Table 2.5. For nominal parameter values, there is an unstable equilibrium point and a stable limit cycle, giving rise to periodic oscillations.

For the purpose of this example, let us assume that translation and transcription rates for I-κBα are uncertain. The question to be addressed is how much the two corresponding parameters k_t and k_{tl} may be varied while maintaining the oscillatory behaviour. The algorithm computes a lower bound on the robustness radius for instability of the equilibrium point by bisection on the parametric uncertainty factor ψ. In each bisection step, the algorithm tries to obtain an infeasibility certificate for the critical point condition (4.22), with $\mathcal{P}(\psi, k_t, k_{tl}) = [\frac{1}{\psi}k_t, \psi k_t] \times [\frac{1}{\psi}k_{tl}, \psi k_{tl}] \subset \mathbb{R}^2$, where k_t and k_{tl} are taken from the nominal parameter vector p_1 in Table 2.5. As loop breaking point, the influence of nuclear NF-κB on the transcription of the I-κBα gene is used (Reaction 10 in Figure 2.3). This influence is part of the negative feedback circuit responsible for oscillations in the NF-κB pathway model, and therefore is a reasonable choice for the loop breaking point.

In the computation of the robustness radius for the NF-κB pathway model, it is crucial to get good bounds on the set $\mathcal{X}_0$ of possible steady states to be considered for any given parameter uncertainty. Here, we use bounds obtained from the steady state uncertainty analysis method developed in Chapter 3. Thereby, the positively invariant set derived in Proposition 4.5 was used as *a priori* set $\mathcal{X}_0$.

Another critical factor is the number of variables which need to be considered in the polynomial equations (4.22), as the computational effort grows significantly with the number of variables. For the NF-κB pathway model, a good way to reduce the number of variables is to solve partially for the equilibrium point of (2.17). In steady state, it holds that

$$x_2 = k_t \frac{x_4^2}{\gamma_m}$$
$$x_3 = \frac{k_{I,in} x_1 (K_N + x_4)}{k_{I,out} K_N + k_{NI,out} x_4}.$$

Exploiting this relation, the critical point conditions (4.22) involve only the five variables x_1, x_4, k_t, k_{tl}, and the frequency ω.

The maximum degree of the critical point conditions (4.22) for the NF-κB pathway model is four. In the analysis, the degree sets $\mathcal{D}_i$ for the multipliers T_i are chosen such that all terms T_iY_i in the construction of Y have degree five with respect to any individual variable. To this end, a total of 635 unknown coefficients $c_{T,d}^{(i)}$ for the multipliers T_i has to be used. With a lower and upper bound on each individual variable, we have $M = 10$ inequality constraints. Constructing the Handelman polynomial Y_H according to (4.36) up to the required degree results in 168282 Handelman monomials of the form (4.27). Expanding the Handelman polynomial $Y_{H,d}$ in monomials based on the original five variables gives 2162 terms, with coefficients depending affinely on the 168282 unknown parameters $c_{H,d}$ in the Handelman representation. On a standard desktop computer, constructing these coefficients takes about 2.3 hours. However, this step is only carried out once in the analysis, since the resulting coefficients can be reused in all iterations of the bisection algorithm.

In each iteration of the bisection algorithm, a linear program with 635 free parameters, 168282 non-negatively constrained parameters and 2162 equality constraints from the comparison of coefficients has to be solved. To solve the linear program, we use the Matlab toolbox SeDuMi (Sturm, 1999), which deals well with the sparsity of the equality constraints and the large number of non-negatively constrained parameters. One call to the linear program solver requires about 13 minutes of computation time on a standard desktop computer for this example.

The lower bound on the dynamical robustness radius obtained for the NF-κB pathway model is $\widehat{\psi}^* = 2.25 \leq \psi^*$, up to a tolerance of $tol = 0.1$ used as termination criterion for the bisection. To find an upper bound, we compute a Hopf bifurcation locus by numerical continuation methods (Kuznetsov, 1995). In this way, a Hopf bifurcation is discovered at $(k_t, k_{tl})^* = (0.45, 0.10)$, corresponding to an upper bound of $2.31 \geq \psi^*$. Notice that the lower bound computed with our method is exact within the chosen tolerance. The results are also depicted in Figure 4.3. In conclusion, the NF-κB pathway as modelled by Krishna *et al.* (2006) can tolerate an uncertainty in gene expression parameters of more than a factor 2 without experiencing a loss of sustained oscillations. The pathway is therefore expected to maintain the biological function related to the oscillations for a considerable amount of uncertainty in gene expression parameters.

4.4 Summary and discussion of dynamical analysis

In this chapter, we study the robustness of qualitative dynamical properties in biochemical reaction networks, in particular the question whether equilibria of the system maintain their dynamical properties under parametric uncertainty or not. Note that most approaches to robustness analysis in control engineering assume that the steady state does not vary with parameters. This assumption can typically not be sustained when considering biochemical reaction networks, where most parameters influence both the position of a steady state and the dynamical behaviour of the system in its neighbourhood. For this reason, classical robustness analysis tools from control theory need to be extended to deal with biochemical reaction networks.

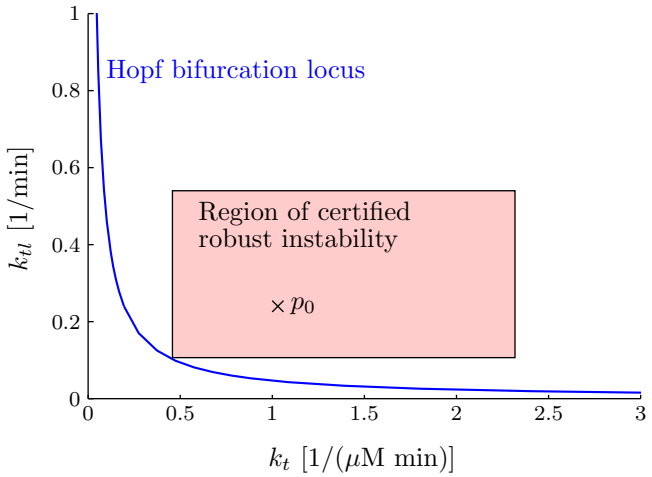

Figure 4.3: Region of guaranteed robustness and Hopf bifurcation locus for the NF-κB pathway model (2.17) in the k_t–k_{tl} plane. The Hopf bifurcation locus is computed with the bifurcation analysis software `auto` (Doedel *et al.*, 2006), while the region with certified non-existence of bifurcations is computed by the algorithm developed in this section.

We propose two different robustness analysis methods which are well suited for the analysis of biochemical reaction networks. The first approach relies directly on the results of Chapter 3. From the bounds on steady state values obtained via global uncertainty analysis, we can directly compute bounds on the Jacobian of the system at steady state. Using classical conditions for robust stability of a linear differential inclusion, robustness of stability can be checked. The drawbacks of this approach are that it may be conservative, and that only robustness of stability, but not instability, can be checked.

The motivation for the second approach is to check robustness of instability, which is of high relevance in the analysis of complex dynamical behaviour such as sustained oscillations or bistability. We propose a feedback loop breaking approach to obtain conditions for non-existence of local bifurcations for uncertain parameters. The conditions are checked computationally by constructing a Handelman representation for a Positivstellensatz robustness certificate. This construction is efficiently accomplished with linear programming. Although theoretically such a certificate does always exist, if the equations are infeasible, in practice the method is conservative due to limitations on the polynomial degree. Yet, the approach is quite efficient, and is, to the best of our knowledge, presently the only method to check robust instability of non-linear systems with respect to generic parametric uncertainty.

Both methods have been applied to models of the NF-κB signalling pathway. The application shows that the proposed methods are suitable for the analysis of small to medium size biochemical reaction networks.

Chapter 5

Locating bifurcation points in high-dimensional parameter spaces

Based on the feedback loop breaking approach developed in Chapter 4, an algorithm to search bifurcation points in a high-dimensional parameter space is developed in this chapter. In Section 5.2, criteria for topological equivalence of equilibria are developed for use within the feedback loop breaking approach. Section 5.3 describes the bifurcation search algorithm, and also contains a discussion where the approach is set into relation with classical bifurcation analysis methods. Applications to oscillations in biochemical signal transduction are given in Section 5.4. The bifurcation search algorithm is based on work published in Waldherr and Allgöwer (2009).

5.1 Introduction

The methods developed in Chapter 4 can be used to compute a parameter region for which dynamical robustness, i.e. non-existence of local bifurcations, can be guaranteed. However, the methods are conservative in the sense that the resulting region usually constitutes a lower bound only, and it may be the case that a fragile parameter point is actually further away than the results suggest. To estimate the degree of conservatism, one has to compute upper bounds on the allowable parameter variations, usually in the form of actual parameter values for which a change in dynamical behaviour occurs. In Chapter 4, such points were searched for by simple Monte Carlo tests. In this chapter, we develop a more sophisticated approach, which is based on classical concepts from control engineering.

As discussed in Section 4.3.1, the characteristics of feedback circuits are the main factor for occurence of local bifurcations in biochemical reaction networks, and are typically related to emergence or loss of complex dynamical behaviour (Schmidt and Jacobsen, 2004; Waldherr *et al.*, 2007). In this chapter, we develop a method to search for local bifurcations of equilibrium points, based on the feedback loop breaking concept introduced in Section 4.3.1. Such bifurcations typically hint to underlying mechanisms for the emergence of complex dynamical behaviour. Standard cases of complex dynamical behaviour are multistability, i.e. the existence of several stable steady states, limit cycle oscillations, and non-periodic oscillations.

Bifurcation analysis is a classical tool for analysing the influence of parameter values on the location and stability of equilibrium points. However, the common numerical continuation methods are only suited for bifurcation search along a pre-specified one-dimensional search direction in parameter space (Kuznetsov, 1995). Methods for numerical bifurcation analysis with several uncertain parameters are now being developed (Henderson,

2007; Stiefs *et al.*, 2008), but due to practical considerations, they remain limited to two or three adjustable bifurcation parameters.

The challenge to find parameter values for bifurcations in a high-dimensional parameter space is of particular relevance in the area of biological systems. This is due to the fact that biochemical systems contain a high number of model parameters, usually even more parameters than state variables. Due to the limited knowledge of the system, it is usually required to assume that most of these parameters are allowed to vary simultaneously over a wide range of values. In order to apply classical continuation methods in a multi-dimensional parameter space, it is necessary to pre-define a line in parameter space along which parameter values are varied during the continuation. A good choice of this line is essential for obtaining meaningful results. Yet, this choice is often made by intuitive understanding of the system in the better case or iterative trials in the worse. Often only a single parameter is varied at a time, but then again the choice of the varying parameter is not trivial and needs to be taken e.g. via sensitivity considerations.

In this chapter, we develop a new method to locate points in a possibly high-dimensional parameter space where a change in the stability properties of equilibrium points occurs. Such points may then be used as an upper bound on the robustness measures derived in Chapter 4. To this end, we extend the results from Section 4.3.1 by further characterising the relationship between local bifurcations and the properties of the open loop transfer function $G(\chi, s)$ as defined in (4.20). With the obtained conditions, a numerical method for searching parameter values leading to a change in stability properties is developed. In theory, the method can be applied for parameter spaces of arbitrary dimension, as neither the conditions nor the algorithm we use depend on the dimension of the parameter space. We consider only codimension one bifurcations, as they are the case usually encountered for generic parameter variations in non-linear systems.

The use of frequency domain methods for bifurcation analysis has already been introduced by Allwright (1977) (see also Mees and Chua, 1979), and relevant results have also been presented by Moiola and coworkers over the last decade (Moiola *et al.*, 1991, 1997). Several authors have also studied the problem of finding bifurcations in systems with many parameters using geometric tools. Based on a description of vectors normal to a bifurcation manifold (Mönnigmann and Marquardt, 2002), a method to search for locally closest bifurcations from a given reference point has been developed by Dobson (2003). These approaches can be seen as complementary to our results. A recent application of the geometric concept to biological systems has been discussed by Lu *et al.* (2006).

5.2 Loop breaking and steady state stability properties

5.2.1 Feedback loop breaking and critical frequencies

In this section, we directly build on the feedback loop breaking (Definition 4.6), linear approximation and transformation to the frequency domain as outlined in Section 4.3. From these results, specifically Lemma 4.8, we see that the main object to be studied is the open loop transfer function $G(\chi, s)$. Let us recall the representation of G as a complex

rational function with real coefficients from (4.21):

$$G(\chi, s) = \frac{Q(\chi, s)}{R(\chi, s)}, \tag{5.1}$$

where $Q(\chi, s)$, $R(\chi, s)$ are polynomials in s with real scalar functions of χ as coefficients. A key result obtained in Section 4.3 to be reused in this chapter is Lemma 4.8, which allows to characterise imaginary eigenvalues $j\omega$ of the Jacobian $A(\chi)$ by the condition $G(\chi, j\omega) = 1$.

The following technical assumption is required for the next steps.

Assumption (A1): For any $\chi \in \mathcal{M}$, the Jacobian $A_o(\chi)$ of the open loop system (4.17) does not have an eigenvalue on the imaginary axis, and the transfer function $G(\chi, s)$ does not have zeros on the imaginary axis, i.e.

$$\forall \chi \in \mathcal{M}\ \forall \omega \in \mathbb{R} : Q(\chi, j\omega) \neq 0 \text{ and } \det(j\omega I_n - A_o(\chi)) \neq 0. \tag{5.2}$$

In addition, the degrees of $Q(\chi, s)$ and $R(\chi, s)$ in s are assumed to be constant with respect to $\chi \in \mathcal{M}$.

Starting from the premise that we are interested in stability changes produced by changing the characteristics of the feedback loop broken in Definition 4.6, this assumption is usually satisfied.

The notion of a critical frequency which is introduced in the next definition will be useful to compute possible eigenvalues of the closed loop Jacobian $A(\chi)$, as given by (4.19), on the imaginary axis.

Definition 5.1. *$\omega_c \in \mathbb{R}$ is said to be a* critical frequency *for the transfer function $G(\chi, s)$, if*

$$G(\chi, j\omega_c) \in \mathbb{R}. \tag{5.3}$$

Obviously, different values of χ will result in different critical frequencies. For a specific χ, all critical frequencies are given by the solutions of the equation

$$\mathrm{Im}(Q(\chi, j\omega_c)R(\chi, -j\omega_c)) = 0, \tag{5.4}$$

which is a scalar polynomial equation in ω_c, with coefficients which are real scalar functions of χ.

We define the set of all critical frequencies for a specific χ as

$$\mathcal{R}(\chi) = \{\omega \in \mathbb{R} \mid \mathrm{Im}(Q(\chi, j\omega)R(\chi, -j\omega)) = 0\}. \tag{5.5}$$

In classical control theory, $\mathcal{R}$ is also called the realness locus of $G(\chi, j\omega)$ (Hinrichsen and Pritchard, 2005). Since only the imaginary part is considered, the polynomial in (5.4) is odd. The following properties of the set $\mathcal{R}(\chi)$ can then be shown easily.

Proposition 5.2. *For any $\chi \in \mathcal{M}$, the set $\mathcal{R}(\chi)$ satisfies the conditions*

(i) $0 \in \mathcal{R}(\chi)$;

(ii) $\omega_c \in \mathcal{R}(\chi)$ *implies that* $-\omega_c \in \mathcal{R}(\chi)$*;*

(iii) either $\mathcal{R}(\chi) = \mathbb{R}$ *or* $\mathcal{R}(\chi)$ *has finitely many elements.*

Note that $\mathcal{R}(\chi) = \mathbb{R}$ whenever $\mathrm{Im}(Q(\chi, j\omega)R(\chi, -j\omega))$ is the zero polynomial, which in turn is the case whenever only the even powers of s in the polynomials $Q(\chi, s)$ and $R(\chi, s)$ have non-zero coefficients. This case is highly non-generic and usually does not occur in the applications we are interested in. Consequently, this case is not considered specifically.

The concept of critical frequencies can be understood intuitively when considering the Nyquist curve of the transfer function $G(\chi, s)$. A critical frequency is any value ω_c at which the Nyquist curve crosses the real axis. This is obviously a necessary condition for having $G(\chi, j\omega_c) = 1$, which corresponds to the existence of an eigenvalue on the imaginary axis as shown in Lemma 4.8. Our concept is thus closely related to the idea of the gain margin for robustness analysis of linear control systems (Skogestad and Postlethwaite, 1996). An illustration of critical frequencies in the Nyquist plot is shown in Figure 5.1 on page 64.

Since a variation of the steady state–parameter pair χ influences the polynomial equation (5.4), the set of critical frequencies $\mathcal{R}(\chi)$ may change significantly with χ. In particular, the number of elements in $\mathcal{R}(\chi)$ generally does not have to be constant with respect to χ, which complicates the analysis. However, one can show that there is a minimal number of critical frequencies of the transfer function $G(\chi, s)$. As we will show below, this minimal number depends on the number of open loop poles and zeros and whether they are located in the right or the left half complex plane. To this end, define the number

$$\tilde{\beta} = |n_{p+} - n_{p-} + n_{z-} - n_{z+}|, \tag{5.6}$$

where n_{p+} (n_{p-}) is the number of poles of $G(\chi, s)$, and n_{z+} (n_{z-}) is the number of zeros of $G(\chi, s)$ in the right (left) half complex plane. Under Assumption (A1), $\tilde{\beta}$ is constant with respect to $\chi \in \mathcal{M}$. The number of elements in the set of critical frequencies can now be characterised by $\tilde{\beta}$.

Proposition 5.3. *Let* $\tilde{\beta}$ *be defined by* (5.6) *and assume that (A1) is satisfied. Then, for any* $\chi \in \mathcal{M}$, $\mathcal{R}(\chi)$ *has at least* $\tilde{\beta}$ *distinct elements, if* $\tilde{\beta}$ *is odd, and at least* $\tilde{\beta} - 1$ *distinct elements, if* $\tilde{\beta}$ *is even.*

The proof is presented in the appendix, Section A.2. Proposition 5.3 is used to formulate the property of minimality for the set of critical frequencies.

Definition 5.4. *Under Assumption (A1), the set of critical frequencies* $\mathcal{R}(\chi)$ *is called* minimal*, if it contains exactly* β *elements, where*

$$\beta = \begin{cases} \tilde{\beta}, & \text{if } \tilde{\beta} \text{ is odd} \\ \tilde{\beta} - 1, & \text{if } \tilde{\beta} \text{ is even.} \end{cases} \tag{5.7}$$

The concept of minimality is applied in the second assumption made to derive the main results.

Assumption (A2): The set of critical frequencies $\mathcal{R}(\chi)$ is minimal for any $\chi \in \mathcal{M}$.

Given a transfer function $G(\chi, s)$ and a corresponding set of critical frequencies $\mathcal{R}(\chi)$, Proposition 5.3 can be used to easily check the minimality of $\mathcal{R}(\chi)$. Graphically, a sufficient condition for minimality of $\mathcal{R}(\chi)$ is that the Nyquist curve $G(\chi, j\omega)$ encircles the origin monotonically as ω varies from $-\infty$ to ∞. This is e.g. satisfied for stable transfer functions without zero dynamics, or with an anti-stable zero dynamics. In practice, minimality of $\mathcal{R}(\chi)$ is satisfied by many stable transfer functions.

If Assumption (A2) holds, we can label the roots of the polynomial equation (5.4) in a consistent manner, writing

$$\mathcal{R}(\chi) = \left\{\omega_c^1(\chi), \omega_c^2(\chi), \ldots, \omega_c^\beta(\chi)\right\}, \tag{5.8}$$

where the ω_c^i are continuous functions of the steady state–parameter pair χ and can be identified with different solution branches of the polynomial equation (5.4).

5.2.2 Topological equivalence of equilibria

Changes in stability properties of equilibrium points are most easily studied using the concept of topological equivalence. Here, we consider topological equivalence of hyperbolic equilibrium points only, for which by definition the Jacobian does not have eigenvalues on the imaginary axis (Kuznetsov, 1995).

Definition 5.5. *Let $\chi_1, \chi_2 \in \mathcal{M}$ be two hyperbolic steady state–parameter pairs of the system* (4.10)*. χ_1 and χ_2 are said to be* topologically equivalent*, if the Jacobians $\frac{\partial F}{\partial x}(\chi_1)$ and $\frac{\partial F}{\partial x}(\chi_2)$ have the same number of eigenvalues in the left and right half complex plane, respectively.*

It is a well known result from dynamical systems theory that the topological equivalence of all equilibria in two systems is a necessary condition for topological equivalence of the flows (Kuznetsov, 1995). Let us consider two variants of the system (4.10), one with parameter values p_1 and the other with parameter values p_2. In the simple case when there is only one steady state in each variant of the system, corresponding to the pairs χ_1 and χ_2, topological equivalence of χ_1 and χ_2 is a necessary condition for topological equivalence of the flows. In applications, we often aim at finding parameter values p_2 such that the system (4.10) changes its dynamical behaviour when parameters are varied from initial values p_1 to p_2. For this problem, it is sufficient to find pairs χ_1 and χ_2 which are not topologically equivalent. Due to the continuous dependence of eigenvalues on parameters, this can only happen when the Jacobian $\frac{\partial F}{\partial x}(\chi_c)$ has eigenvalues on the imaginary axis for some critical point $\chi_c \in \mathcal{M}$. At this point, we can make use of the methodology developed in the previous subsection.

To this end, consider the set of critical frequencies $\mathcal{R}(\chi)$ for a specific value of the steady state–parameter pair χ. Define the number $\beta^*(\chi)$ to be the number of elements ω in $\mathcal{R}(\chi)$ such that $G(\chi, j\omega) > 1$, i.e.

$$\beta^*(\chi) = \operatorname{card}\left\{\omega \in \mathcal{R}(\chi) \mid G(\chi, j\omega) > 1\right\}, \tag{5.9}$$

where $\operatorname{card}\mathcal{A}$ denotes the number of elements in the set $\mathcal{A}$.

Geometrically, if $\mathcal{R}(\chi)$ is minimal, $\beta^*(\chi)$ gives the winding number of the graph of $G(\chi, j\omega)$ around the point 1 in the complex plane (see Lemma A.3 on page 116). The

Argument Principle (Whittaker and Watson, 1965) can then be used to characterise topologically equivalent steady state–parameter pairs of the system (4.10) via the number $\beta^*(\chi)$. This characterisation is given in the following result.

Theorem 5.6. *Assume that (A1) is satisfied. Let $\chi_1, \chi_2 \in \mathcal{M}$ be two hyperbolic steady state–parameter pairs of* (4.10) *such that $\mathcal{R}(\chi_1)$ and $\mathcal{R}(\chi_2)$ are minimal. Then χ_1 and χ_2 are topologically equivalent, if and only if*

$$\beta^*(\chi_1) = \beta^*(\chi_2).$$

The proof is given in the appendix, Section A.3. It makes use of several intermediate statements which are given as lemmas in Section A.3. There are two main steps in the proof. First, we observe that minimality of the set of critical frequencies implies that the graph of $G(\chi, j\omega)$ cuts the positive and negative parts of the real axis in an alternating manner. The second step is to show that $\beta^*(\chi)$ is equal to the winding number of the graph of $G(\chi, j\omega)$ around the point 1.

5.2.3 Existence of marginally stable equilibria

Let us now turn to the problem of how to find parameter values for which a change in stability properties of equilibria can occur. This is equivalent to searching for critical points χ_c at which the Jacobian $\frac{\partial F}{\partial x}(\chi_c)$ has an eigenvalue on the imaginary axis. This typically means that χ_c is part of a submanifold of $\mathcal{M}$ which separates regions of topological equivalence. In view of Theorem 5.6, there are typically steady state–parameter pairs χ_1 and χ_2 close to χ_c such that $\beta^*(\chi_1) \neq \beta^*(\chi_2)$. Equivalently, for a specific critical frequency branch ω_c^i, the transfer function value $G(\chi, j\omega_c^i(\chi))$ on that branch has to cross the value 1 when χ is varied continuously along a path from χ_1 to χ_2. These observations are formalised in the following theorem.

Theorem 5.7. *Assume that Assumptions (A1) and (A2) are satisfied, and that $\mathcal{M}$ is connected. There exists a critical point $\chi_c \in \mathcal{M}$ such that $\frac{\partial F}{\partial x}(\chi_c)$ has an eigenvalue on the imaginary axis, if and only if there exist $\chi_1, \chi_2 \in \mathcal{M}$ such that, for some $i \in \{1, 2, \ldots, \beta\}$,*

$$G(\chi_1, j\omega_c^i(\chi_1)) \leq 1 \leq G(\chi_2, j\omega_c^i(\chi_2)), \tag{5.10}$$

where $\omega_c^i(\chi) \in \mathcal{R}(\chi)$. In that case, $\pm j\omega_c^i(\chi_c)$ is an eigenvalue of $\frac{\partial F}{\partial x}(\chi_c)$.

Proof. With Lemma 4.8, Assumption (A1) assures that a point χ_c is critical if and only if $G(\chi_c, j\omega_c^i(\chi_c)) = 1$.

Necessity. Under the condition $G(\chi_c, j\omega_c) = 1$, take $\chi_1 = \chi_2 = \chi_c$ and (5.10) follows trivially.

Sufficiency. Let χ_1 and χ_2 be such that (5.10) holds. Connectivity of $\mathcal{M}$ implies that there is a path from χ_1 to χ_2 in $\mathcal{M}$. Continuity of the critical frequency $\omega_c^i(\chi)$ and the transfer function coefficients result in continuity of $G(\chi, j\omega_c^i(\chi))$ with respect to χ. This implies existence of χ_c such that $G(\chi_c, j\omega_c^i(\chi_c)) = 1$ along any path from χ_1 to χ_2. □

A graphical illustration of Theorem 5.7 is given in Figure 5.1. The figure also illustrates the relation to the classical Nyquist stability criterion.

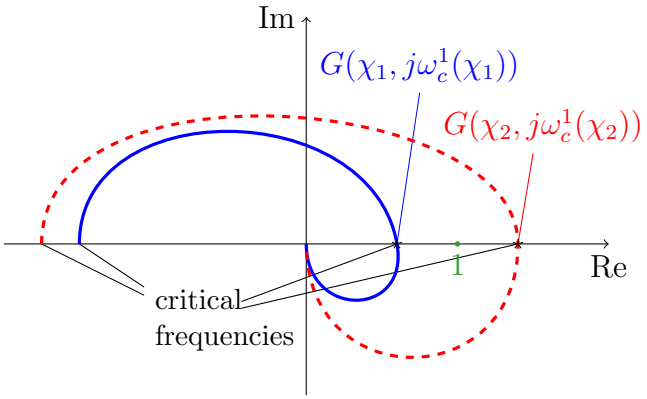

Figure 5.1: Illustration of Theorem 5.7 in the Nyquist plot. Full line: $G(\chi_1, j\omega)$, dashed line: $G(\chi_2, j\omega)$, both drawn only for $\omega \geq 0$. The theorem asserts existence of a critical point χ_c on any path between χ_1 and χ_2 in $\mathcal{M}$.

The proof shows that the critical point χ_c is usually far from unique. It may be unique if $\mathcal{M}$ is of dimension one, i.e. there is only one free parameter to vary. In general, one will expect that there is a submanifold of critical points in $\mathcal{M}$ separating regions which represent different topological equivalence classes, where χ_1 is an element of one such class, and χ_2 is an element of the other class. On this submanifold, the bifurcations which can be encountered generically are codimension one bifurcations. Therefore, the bifurcation condition provided by Theorem 5.7 is mainly useful in the search for codimension one bifurcations, although condition (5.10) also holds for bifurcations of higher codimension.

Using Theorem 5.7, it is easily possible to distinguish dynamical bifurcations from static bifurcations. In fact, if i is chosen such that the critical frequency $\omega_c^i(\chi) = 0$ is considered, $A(\chi_c)$ has a zero eigenvalue, which generically corresponds to a saddle-node bifurcation. If a critical frequency $\omega_c^i(\chi) \neq 0$ is considered, $A(\chi_c)$ has conjugated imaginary eigenvalues, and generically a Hopf bifurcation will occur.

To conclude this section, we give an illustrative example for the application of the loop breaking approach to a small biochemical network. In this example, all the computations can be done analytically.

Example 5.8. Consider a biochemical reaction network described by the ODE

$$\begin{aligned} \dot{x}_1 &= \frac{1}{1 + x_3^\delta} - x_1 \\ \dot{x}_2 &= x_1 - \frac{1}{2} x_2 \\ \dot{x}_3 &= x_2 - x_3, \end{aligned} \tag{5.11}$$

with one uncertain parameter $\delta > 0$ (Griffith, 1968a). It is easily verified that $x_0 = (\frac{1}{2}, 1, 1)^{\mathrm{T}}$ is a steady state for any value of δ. We apply a loop breaking such that the

open loop system is given by

$$\begin{aligned} \dot{x}_1 &= \frac{1}{1+u^\delta} - x_1 \qquad y = x_3 \\ \dot{x}_2 &= x_1 - \frac{1}{2}x_2 \\ \dot{x}_3 &= x_2 - x_3. \end{aligned} \tag{5.12}$$

The linear approximation of the open loop system (5.12) around the steady state x_0 is described by the matrices

$$A_o = \begin{pmatrix} -1 & 0 & 0 \\ 1 & -\frac{1}{2} & 0 \\ 0 & 1 & -1 \end{pmatrix} \qquad B_o = \begin{pmatrix} -\frac{\delta}{4} \\ 0 \\ 0 \end{pmatrix} \qquad C_o = \begin{pmatrix} 0 & 0 & 1 \end{pmatrix}.$$

The resulting transfer function is

$$G(\delta, s) = -\frac{\delta}{4(s+1)^2(s+\frac{1}{2})}, \tag{5.13}$$

and Assumption (A1) holds true for any value of $\delta > 0$. The set of critical frequencies is given by

$$\mathcal{R} = \{0, \pm\sqrt{2}\}, \tag{5.14}$$

independently of δ. By Proposition 5.3, $\mathcal{R}$ is minimal.

Considering the critical frequency $\omega_c^3 = \sqrt{2}$, we obtain $G(\delta, j\sqrt{2}) = \frac{\delta}{18}$. Thus, by Theorem 5.7, there exists a critical parameter value δ_c in any interval $[\delta_1, \delta_2]$, where $\delta_1 \leq 18$ and $\delta_2 \geq 18$. In this example, we see that the critical parameter value is unique and given by $\delta_c = 18$. For this value, the Jacobian of system (5.11) around x_0 has eigenvalues at $\pm j\sqrt{2}$, and we conclude to the occurrence of a Hopf bifurcation.

For systems with a structure as in (5.11), the secant condition provides a necessary condition for instability (Arcak and Sontag, 2006; Thron, 1991; Tyson and Othmer, 1978). For this example, it implies that $\delta \geq 16$ is necessary for instability. However, the secant condition is not sufficient for instability, and clearly underestimates the actual critical parameter value $\delta_c = 18$ in this example.

5.3 Bifurcation search via feedback loop breaking

5.3.1 Bifurcation search algorithm

In this section, we develop an algorithm to search for parameter values which lead to a change in stability properties of an equilibrium point. This algorithm has first been proposed in Waldherr and Allgöwer (2009). We assume that a preliminary parameter vector p_1 and a corresponding steady state x_1 are known, which we combine in the pair $\chi_1 = (x_1, p_1) \in \mathcal{M}$. It is reasonable to assume that the pair χ_1 is not critical, otherwise it is usually straightforward to find parameter values yielding equilibrium points with different stability properties. The aim of the algorithm is to find a steady state–parameter pair $\chi_2 \in \mathcal{M}$ such that χ_2 is not topologically equivalent to χ_1. The main theoretical basis of

the algorithm is the result of Theorem 5.7. Thus it is also possible to search specifically for either static or dynamic bifurcations on a path from χ_1 to χ_2 by choosing an appropriate critical frequency.

In order to put the problem in the previously developed framework, a loop breaking for the system (4.10) has to be defined. Then, by looking at the resulting transfer function $G(\chi_1, s)$, possible changes in stability properties can be determined. In particular, one has to decide whether to search for a static or for a dynamic bifurcation. This leads to the choice of a critical frequency ω_c^i which is to be considered in the algorithm.

Denote the transfer function value for the critical frequency branch ω_c^i at a point χ as $g^i(\chi)$. At the starting point χ_1, this value can be computed as

$$g^i(\chi_1) = G(\chi_1, j\omega_c^i(\chi_1)). \tag{5.15}$$

Now two cases have to be distinguished:

1. If $g^i(\chi_1) < 1$, the algorithm searches a pair $\chi_2 \in \mathcal{M}$ such that $g^i(\chi_2) > 1$.
2. If $g^i(\chi_1) > 1$, the algorithm searches $\chi_2 \in \mathcal{M}$ such that $g^i(\chi_2) < 1$.

The algorithm proposed here is best described by the term *gradient-directed continuation method*. Continuation methods (Richter and DeCarlo, 1983) are popular in numerical bifurcation analysis, where they are used to trace the equilibrium curve in the combined state-parameter space. In our algorithm, continuation is used to stay on the manifold $\mathcal{M}$. However, a continuation method alone is not sufficient, as $\mathcal{M}$ is q-dimensional with typically $q > 1$. Thus, the continuation is complemented by a gradient ascent or descent approach to achieve the desired value for $g^i(\chi_2)$.

Since the algorithm is based on Theorem 5.7, Assumptions (A1) and (A2) need to be checked. Depending on the system under consideration, this may be a difficult problem globally over the steady state–parameter manifold $\mathcal{M}$. However, for the validity of the algorithm's results it is sufficient that (A1) and (A2) are satisfied locally along the path used for the continuation. These checks can directly be included into the algorithm. If the assumptions are violated at any point, the algorithm issues a warning message. The results may still be valid, but need to be checked separately in this case.

In detail, the algorithm works as follows. For the sake of conciseness, we are discussing case 1 only. Small extensions are required for dealing with both cases.

1. **Initialisation.** Set $\chi^{(0)} = \chi_1$. Choose numerical parameters: Δg for the minimal required change in $g^i(\chi)$ per iteration, $\delta^{(0)}$ as the initial step size and δ_{min} (δ_{max}) as minimal (maximal) step size.

2. **Checking assumptions.** (A1) is checked locally by computing the poles and zeros of $G(\chi^{(j)}, s)$. (A2) is checked locally by computing the critical frequencies $\mathcal{R}(\chi^{(j)})$ and applying Proposition 5.3. If the assumptions are not satisfied, issue a warning message.

3. **Prediction step.** This step assures the desired increase in $g^i(\chi)$.

   a) Compute the gradient $\nabla g^i\left(\chi^{(j)}\right)$.

b) Compute the subspace which is tangent to $\mathcal{M}$ in the point $\chi^{(j)}$ (Appendix A in Isidori, 1995):

$$T_{\chi^{(j)}}\mathcal{M} = \operatorname{null} \frac{\partial \Phi}{\partial \chi}\left(\chi^{(j)}\right), \tag{5.16}$$

where $\operatorname{null} A$ denotes the null-space of the matrix A.

c) Project $\nabla g^i\left(\chi^{(j)}\right)$ on $T_{\chi^{(j)}}\mathcal{M}$:

$$\vartheta^{(j)} = \operatorname{Proj}\left(\nabla g^i\big(\chi^{(j)}\big), T_{\chi^{(j)}}\mathcal{M}\right). \tag{5.17}$$

d) Set the predicted point

$$\chi_{pre}^{(j+1)} = \chi^{(j)} + \delta^{(j)}\vartheta^{(j)}. \tag{5.18}$$

Step size control is used in the sense that $\delta^{(j)}$ is varied to assure that

$$g^i\big(\chi_{pre}^{(j+1)}\big) - g^i\big(\chi^{(j)}\big) \geq \Delta g, \tag{5.19}$$

while keeping $\delta_{min} \leq \delta^{(j)} \leq \delta_{max}$.

4. **Correction step.** Generally, $\chi_{pre}^{(j+1)} \notin \mathcal{M}$, and a correction step is required to achieve $\chi^{(j+1)} \in \mathcal{M}$. To this end, the Gauss-Newton method is used to solve the non-linear equation

$$\begin{aligned} \Phi(\chi^{(j+1)}) &= 0 \\ g^i\big(\chi^{(j+1)}\big) &= g^i\big(\chi_{pre}^{(j+1)}\big) \end{aligned} \tag{5.20}$$

for $\chi^{(j+1)}$, where $\chi_{pre}^{(j+1)}$ is used as starting point for the Gauss-Newton algorithm. If the Gauss-Newton algorithm converges, take the solution as value for $\chi^{(j+1)}$ and proceed to the next step. Otherwise, reduce the step size $\delta^{(j)}$ and go back to 3d).

5. **Finishing criterion.** Compute $g^i\big(\chi^{(j+1)}\big)$. If $g^i\big(\chi^{(j+1)}\big) > 1$, finish successfully, otherwise iterate to step 2.

If the algorithm finishes successfully, it does so in a finite number of steps with a previously known upper bound due to step size control via inequality (5.19).

However, in the same way as classical continuation methods, the algorithm may fail if the Gauss-Newton algorithm in step 4 does not converge, and the step size $\delta^{(j)}$ may not be reduced further due to the constraint $\delta_{min} \leq \delta^{(j)}$ at the same time. This problem may appear if the system is numerically ill-conditioned, but can typically be avoided by choosing a smaller value for either Δg or for δ_{min}, with the drawback of increased computational effort. Also, it can generally not be excluded that the function $g^i(\chi)$ has local extrema, which may pose problems to the algorithm. Such problems may be detected numerically from the vector $\vartheta^{(j)}$ taking very small values.

The algorithm as described above does not consider constraints on the parameters p. Such constraints can typically be included by slight modifications of the system equations, e.g. by a diffeomorphic transformation which maps a constrained parameter set onto the full parameter space $\mathbb{R}^q$.

5.3.2 Discussion of the feedback loop breaking approach

Two key steps in the approach taken in this section are (i) the transformation of the problem to the frequency domain and (ii) the consideration of the critical frequencies. This is quite different from established methods in numerical bifurcation analysis, and shall be discussed from the perspective of more classical approaches. In classical bifurcation analysis, so-called bifurcation test functions are used to check whether a bifurcation may occur when changing a parameter value (Kuznetsov, 1995). The test function Ψ is defined such that $\Psi(\chi_c) = 0$ if the bifurcation being tested for occurs at χ_c. For example, a test function for the saddle–node bifurcation, which requires a zero eigenvalue in the Jacobian, is given by the determinant of the system's Jacobian, $\Psi(\chi) = \det\left(\frac{\partial F}{\partial x}(\chi)\right)$. Bifurcations are detected by the test function $\Psi(\chi)$ changing sign when the parameter is varied, i.e. if a bifurcation occurs between χ_1 and χ_2, then $\Psi(\chi_1)\Psi(\chi_2) < 0$. For bifurcations of codimension one, suitable test functions are known and are routinely used in numerical continuation algorithms. Note that in the frequency domain approach, the expression $G(\chi, j\omega_c^i(\chi)) - 1$ is a test function for a generic saddle-node bifurcation, if we consider $\omega_c^i = 0$, and it is a test function for a generic Hopf bifurcation when considering $\omega_c^i \neq 0$. Computing classical test functions for a given point χ requires a similar or slightly less computational effort as computing the transfer function values at the critical frequency. So we need to justify why we do not use classical test functions for bifurcation search in a high-dimensional parameter space.

Since classical continuation methods cannot be used in a high-dimensional parameter space, one has to search for different approaches. A naive approach to find parameters for a bifurcation would be trying directly to solve the equations

$$\begin{aligned} \Psi(\chi) &= 0 \\ \Phi(\chi) &= 0. \end{aligned} \tag{5.21}$$

However, in most cases this will be numerically infeasible with classical test functions, even if the combined parameter/state space is of very low dimension. A more sophisticated approach could basically use the algorithm we have presented in Section 5.3, the gradient-directed continuation method, and just use the gradient of a classical bifurcation test function instead of the gradient of the transfer function $G(\chi, j\omega_c(\chi))$. We have also implemented this approach for several examples, but run into numerical problems for any system of medium complexity. In particular, the example presented in Section 5.4.1 could not be handled in this way with a classical bifurcation test function for a Hopf bifurcation due to numerical problems. A potential explanation for these problems is that the value of the classical bifurcation test function seems to be numerically much less well behaved with respect to parameter variations than the transfer function value at critical frequencies. Using the transfer function value $g^i(\chi)$ as bifurcation test function in fact also allows to apply generic optimisation methods to locate bifurcations in high-dimensional parameter spaces (Waldherr and Allgöwer, 2007).

5.4 Application to biochemical signal transduction

5.4.1 Oscillations in a MAPK cascade model

The model of the MAPK cascade as given in (2.14), Section 2.3.1, shows sustained oscillations for the parameter values given in Table 2.3 (Kholodenko, 2000). The analysis in this section is based on the parameter value set A in Table 2.3. Compared to the actual reaction mechanism of the MAPK cascade as proposed by Huang and Ferrell (1996), Kholodenko's model contains a considerable simplification by using the Michaelis-Menten mechanism for the individual phosphorylation and dephosphorylation reactions.

Using Michaelis-Menten reaction rates is a good approximation of the underlying reaction mechanism, if the concentration of the enzyme is significantly smaller than the concentration of the substrate (Keener and Sneyd, 2004). In other cases, the Michaelis-Menten rate law is typically not a good approximation of the actual reaction flux. In Kholodenko's model of the MAPK cascade, the different kinases are present at comparable concentrations, which would usually prohibit the use of Michaelis-Menten reaction rates for the phosphorylation reactions catalysed by MAPKKK and MAPKK.

To obtain a more faithful description of the underlying reaction mechanisms, we extend the original model of the MAPK cascade as given in (2.14) by explicitly introducing the complexes of the kinases with their substrates, and adding appropriate reactions to the network. This procedure is actually a reversal of the quasi steady state assumption underlying the Michaelis-Menten reaction rate, and has been referred to as *unpacking* of the reaction network by Sabouri-Ghomi *et al.* (2007). For example, the reaction 3 in the original model is replaced by the corresponding association, dissociation, and catalytic reactions, yielding

$$\begin{aligned} v_{3a}: &\quad \mathrm{Raf}^* + \mathrm{MEK} \rightleftharpoons \mathrm{CKK1} \\ v_{3b}: &\quad \mathrm{CKK1} \rightarrow \mathrm{Raf}^* + \mathrm{MEK\text{–}P}, \end{aligned} \tag{5.22}$$

where CKK1 is the intermediate complex for reaction 3. The corresponding reaction rates are constructed from the law of mass action as

$$\begin{aligned} v_{3a} &= k_{3f}[\mathrm{Raf}^*][\mathrm{MEK}] - k_{3r}[\mathrm{CKK1}] \\ v_{3b} &= k_3[\mathrm{CKK1}], \end{aligned} \tag{5.23}$$

where the additional parameters k_{3f} and k_{3b} are introduced. From the construction of the Michaelis-Menten rate, these parameters have to satisfy

$$K_{m3} = \frac{k_{3r} + k_3}{k_{3f}}. \tag{5.24}$$

k_3 and K_{m3} are parameters of the original model as given in Table 2.3. For typical enzyme–substrate kinetics, k_{3r} is expected to be fast compared to k_3 (Sabouri-Ghomi *et al.*, 2007). In this example, we choose $k_{3r} = 2k_3$. The value for k_{3f} then follows from (5.24). In the same way, the other phosphorylation reactions 4, 7 and 8 are replaced by pairs of reactions v_{ia} and v_{ib}, $i \in \{4, 7, 8\}$, introducing new parameters k_{if} and k_{ir} as above. The parameter values for the unpacked MAPK cascade model are given in Table 5.1 as parameter vector p_1.

Table 5.1: Reference parameters p_1 and parameters for instability p_2 in the unpacked MAPK cascade model.

Param.	p_1	p_2	Unit	rel. change
V_1	2.5	3.03	nM/s	1.21
K_i	9	10.2	nM	1.13
K_{m1}	10	9.1	nM	1.10^{-1}
V_2	0.25	0.31	nM/s	1.22
K_{m2}	8	4.9	nM	1.64^{-1}
k_3	0.025	0.030	1/s	1.19
k_{3r}	0.05	0.052	1/s	1.05
k_{3f}	0.005	$4.6 \cdot 10^{-3}$	1/(s nM)	1.08^{-1}
k_4	0.025	0.0254	1/s	1.01
k_{4r}	0.05	0.054	1/s	1.08
k_{4f}	0.005	$4.3 \cdot 10^{-3}$	1/(s nM)	1.15^{-1}
V_5	0.75	0.50	nM/s	1.5^{-1}
K_{m5}	15	5.5	nM	2.72^{-1}
V_6	0.75	0.95	nM/s	1.26
K_{m6}	15	14.6	nM	1.03^{-1}
k_7	0.025	0.023	1/s	1.08^{-1}
k_{7r}	0.05	0.091	1/s	1.83
k_{7f}	0.005	$1.8 \cdot 10^{-3}$	1/(s nM)	2.76^{-1}
k_8	0.025	0.022	1/s	1.16^{-1}
k_{8r}	0.05	0.05	1/s	1.00
k_{8f}	0.005	$4.8 \cdot 10^{-3}$	1/(s nM)	1.03^{-1}
V_9	0.5	0.44	nM/s	1.15^{-1}
K_{m9}	15	14.7	nM	1.02^{-1}
V_{10}	0.5	0.69	nM/s	1.39
K_{m10}	15	17.3	nM	1.15
KKK_{tot}	100	130	nM	1.30
KK_{tot}	300	323	nM	1.08
K_{tot}	300	297	nM	1.01^{-1}

It has been observed that such unpacking of a reaction network can drastically alter the dynamical behaviour of the network, if the assumptions for the Michaelis-Menten approximation are not satisfied. In particular, Sabouri-Ghomi *et al.* (2007) consider an example where the original network shows hysteresis with respect to a particular stimulus, while the unpacked network is not hysteretic. In the example considered here, the unpacking has a similarly drastic effect: the oscillations occuring in the original model vanish in the unpacked model. Instead, trajectories in the unpacked model converge towards an asymptotically stable steady state, as shown in Figure 5.2. Whereas Sabouri-Ghomi *et al.* (2007) discuss various additional mechanisms for their example to restore hysteresis in the unpacked model, we follow a different route here. Using the method developed in this chapter, our goal is to find parameter values in the unpacked model of the MAPK cascade for which sustained oscillations are restored.

The first step in our analysis is to choose a suitable loop breaking. For the considered model, an intuitive approach is to break the loop at the feedback inhibition of reaction v_1 by ERK-PP (cf. Figure 2.2). This is achieved by choosing $h(x) = x_{32}$ and replacing x_{32} by the input u in the reaction rate v_1. A linearisation of the resulting open loop system around the equilibrium point and a Laplace transformation give the transfer function $G(\chi, s)$, whose graph is shown in Figure 5.3. The problem is now to find parameters p_2 with a corresponding unstable steady state x_2. To reach this goal, the numerical algorithm presented in Section 5.3 is applied.

The set of critical frequencies is minimal with $\beta = 5$. Note that in Figure 5.3, two of the critical frequencies cannot be observed from crossings of the Nyquist curve with the real axis, since the corresponding transfer function values are very small compared to the scale of the figure. The critical frequency with the largest positive transfer function value is $\omega_c^4(\chi_1) = 0.006\,\mathrm{s}^{-1}$. We will consider only ω_c^4 in the search for destabilising parameters, because our goal is to find a Hopf bifurcation. The corresponding transfer function value is $G(\chi_1, j\omega_c^4(\chi_1)) = g^4(\chi_1) = 0.065$, corresponding to the steady state x_1 being stable in the closed loop system.

The goal for the parameter search algorithm is to find a steady state–parameter pair χ_2 such that $g^4(\chi_2) > 1$. The corresponding steady state x_2 will then not be topologically equivalent to the nominal steady state x_1, and we can expect a Hopf bifurcation when varying parameters from the nominal value p_1 to the new value p_2. To ensure that the algorithm does not stop at the bifurcation point, but continues to vary parameters until the oscillations have reached a considerable amplitude, we aim for $g^4(\chi_2) \geq 1.3$ in the implementation used here.

With these settings, the algorithm returns the parameters p_2 and a steady state x_2 with the transfer function value $G(\chi_2, j\omega_c^4(\chi_2)) = 1.3$ and the critical frequency $\omega_c^4(\chi_2) = 0.003\,\mathrm{s}^{-1}$, where $\chi_2 = (x_2, p_2)$. The parameter values in p_2 are shown in Table 5.1.

The graph of $G(\chi_2, j\omega)$ is shown in Figure 5.3. For the new parameters p_2, the graph now encircles the point 1. By Theorem 5.6, we see that the equilibria x_1 and x_2 are not topologically equivalent. Indeed, x_2 is unstable, and the trajectories converge to a limit cycle for parameters p_2. The time course of these oscillations is plotted in Figure 5.2.

In conclusion, our method is able to compute parameters which render the corresponding steady state unstable and thus lead to the emergence of sustained oscillations in the treated example. As a biochemical interpretation, we conclude that occurrence of sustained oscillations in the MAPK cascade is not in conflict with the unpacked description

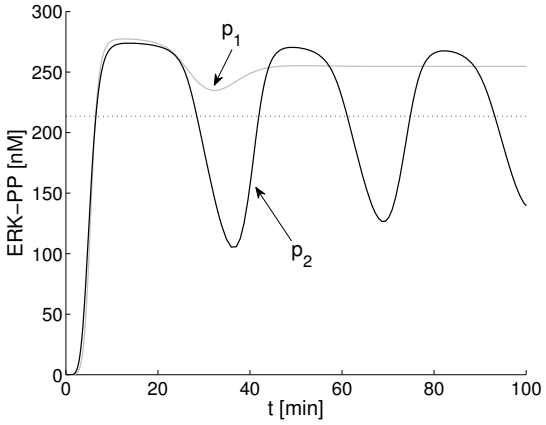

Figure 5.2: Dynamical behaviour in the unpacked MAPK cascade model: convergence to steady state for nominal parameters p_1 (grey line) and sustained oscillations for parameters p_2 (black line). The oscillations coexist with the unstable steady state x_2 (dotted line).

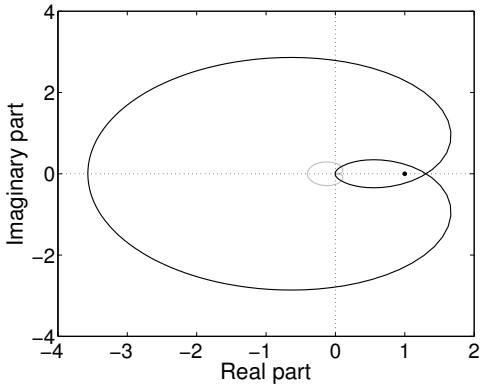

Figure 5.3: Nyquist plots of open loop unpacked MAPK cascade model for parameters p_1 (grey line) and p_2 (black line).

of enzymatic reactions. In fact, oscillations can be recovered in the unpacked model by appropriate parameter changes. In contrast to the approach taken by Sabouri-Ghomi *et al.* (2007), it is not necessary to introduce additional mechanisms into the network to recover the dynamical behaviour of the original model in this example.

5.4.2 Oscillations in the NF-κB pathway

The second example is an application to the NF-κB pathway as presented in Section 2.3.2. The results obtained in Section 4.2.3 show that the equilibrium point in the model with low transcription and translation rates is robustly stable, with damped oscillations, for parameter variations up to a factor of $\widehat{\psi}^* = 1.54$. However, this value is a possibly conservative lower bound. From computationally expensive Monte Carlo simulations, we have an upper bound on the allowable variation of 1.83.

The aim in this example is to find a Hopf bifurcation in the NF-κB pathway, specifically

Table 5.2: Reference parameters p_1 (damped oscillations) and parameters p_2 for instability (sustained oscillations) in the NF-κB pathway model (2.16).

Param.	p_1	p_2	Unit	rel. change
k_t	0.1	0.136	$(\mu\mathrm{M}\,\mathrm{min})^{-1}$	1.36
k_{tl}	0.2	0.256	min^{-1}	1.28
γ_m	0.525	0.309	min^{-1}	1.70^{-1}
α	0.017	0.02	min^{-1}	1.18

the model given in (2.16), via the feedback loop breaking approach. To be consistent with the analysis in Section 4.2.3, only variations in the parameters k_t, k_{tl}, γ_m, and α are considered. The nominal values for this parameters are denoted as $p_1 \in \mathbb{R}^4$ and indicated in Table 5.2.

To apply the feedback loop breaking approach to the NF-κB pathway, we first have to choose an appropriate loop breaking. The NF-κB pathway features several feedback circuits. From biological intuition, we presume that the feedback circuit which underlies the oscillations most likely involves the NF-κB regulated expression of the inhibitor I-κBα (Reaction 10 in Figure 2.3). Thus the loop breaking is defined by choosing nuclear NF-κB as an output: $h(x) = x_6$. Correspondingly, the input acts on the transcription rate of I-κBα, i.e. we change the corresponding reaction rate to $v_{10} = k_t u^2$. The reference parameters are the same as in Section 4.2.3 and given in Table 5.2. The resulting open loop model is linearised around the (unique) equilibrium point. By transformation to the frequency domain, we obtain the loop transfer function $G(\chi_1, s)$, where χ_1 is the steady state–parameter pair for nominal parameters p_1. The Nyquist plot of the transfer function is depicted in Figure 5.4. There are three critical frequencies, with one of them being positive, $\omega_c^3(\chi_1) = 0.14\,\frac{1}{\mathrm{min}}$, and yielding the transfer function value $g^3(\chi_1) = G(\chi_1, j\omega_c^3(\chi_1)) = 0.43$. Thus, we expect that a Hopf bifurcation may be reached with a suitable parameter variation.

The algorithm developed in Section 5.3 is applied to the model, with the goal of finding a steady state–parameter pair χ_2 such that the transfer function value satisfies $g(\chi_2) > 1$. From Section 4.2.3, we already know that the steady state looses stability for parameter variations by a factor of 1.83. Therefore, we restrict the allowable parameter variations in the gradient-directed continuation algorithm to less than a factor of 2 by an appropriate parameter space transformation. After 324 iterations, the algorithm returns the parameter vector p_2, which is given in Table 5.2. The Nyquist plot of the corresponding transfer function is shown in Figure 5.4. The Nyquist graph of the transfer function now encircles the critical point 1. By Theorem 5.6, we conclude that the steady state is unstable for the parameter values p_2. By inspection of the critical frequency, we also see that a Hopf bifurcation occurs for this parameter change. The emerging sustained oscillations in the nuclear NF-κB concentration are shown in Figure 5.5.

The parameter values which have been found by the gradient-directed continuation method in this example are of particular significance when comparing them to the results

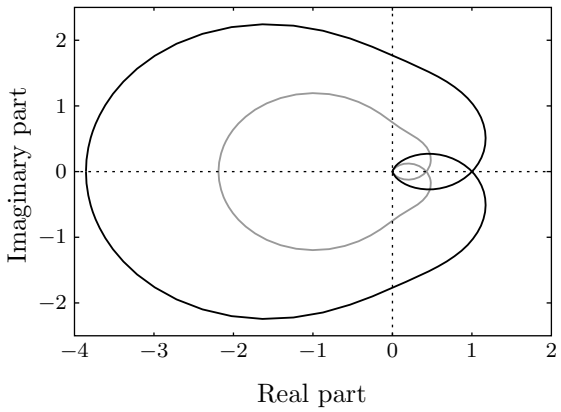

Figure 5.4: Nyquist plot of the open loop transfer function for the NF-κB pathway. Grey line from nominal parameters p_1, black line from p_2.

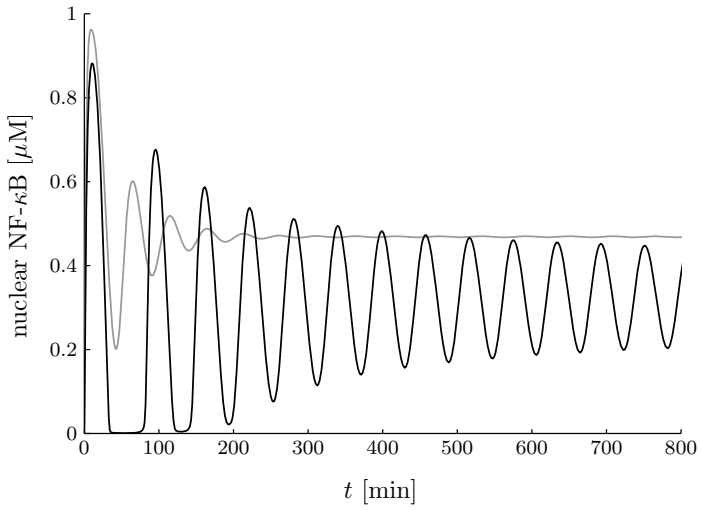

Figure 5.5: Time courses of the nuclear NF-κB concentration. Damped oscillations for nominal parameters p_1 and sustained oscillations for perturbed parameters p_2.

in Section 4.2.3. Using extensive Monte Carlo sampling, an upper bound of $1.83 \geq \psi^*$ on the dynamical robustness radius has been obtained. In the results obtained here, parameters are maximally varied by a factor of 1.7. This factor is a new upper bound of $1.7 \geq \psi^*$ on the dynamical robustness radius for this example, which is significantly better than the bound obtained by Monte Carlo sampling. It should be pointed out that single parameter bifurcation analyses leads to much higher variations in this example before a bifurcation is detected. Therefore, such a low upper bound on the robustness radius would not have been encountered by classical continuation analysis in a single parameter.

5.5 Summary and discussion of the bifurcation search method

Based on the loop breaking introduced in Chapter 4, we present results on topological equivalence of equilibria in systems with high-dimensional parameter spaces and on the existence of critical parameters, for which stability properties of equilibria may change. In addition, an algorithm is given to systematically search for critical parameters. Using an ODE model for a MAPK cascade, we show that the algorithm can be used to efficiently search for parameter values leading to limit cycle oscillations in the system. As another example, we consider the NF-κB pathway model as already studied in Section 4.2.3. From the application of the proposed algorithm, a new upper bound on the dynamical robustness radius is obtained in this example which is significantly better than the one obtained from simple Monte Carlo tests.

Non-uniqueness of critical parameter values is a problem inherent to this kind of analysis. If the dimension of the parameter space is higher than the codimension of the bifurcation, then there will be a submanifold of bifurcation points in the parameter space. Our algorithm computes one of these points. Starting from a critical point thus found, one can then use continuation methods to further explore the structure of the set of critical points.

Another possibility for further studies would be to search for a bifurcation which is locally closest to some reference parameter values. A method for this has been presented by Dobson (2003). The method requires a bifurcation point where the search is started, and we expect our algorithm to give a starting point which is better suited for the method discussed in (Dobson, 2003) than a bifurcation search along a random line in parameter space.

The biological examples we study in Section 5.4 are simple in that they contain only one biologically meaningful feedback loop. For systems with a single feedback loop, the results of the proposed analysis method are independent of how the loop breaking point is chosen (Reinschke, 1988). Of course, many biological systems contain several intertwined feedback loops. Then, the choice of the loop breaking point needs more attention, because the results in general depend on this choice. In our experience, it is often beneficial to choose a loop breaking point where several feedback loops are affected simultaneously. Furthermore, a comparison of different loop breaking points is usually helpful and could give hints to the role played by individual loops in the dynamical behaviour of the system. The differential roles of individual feedback loops for the dynamical behaviour of a biochemical network are in fact of great interest in systems biology, but are so far mainly studied by a combination of simulation and biological insight (Kim *et al.*, 2007; Waldherr *et al.*, 2008b).

Chapter 6

Kinetic perturbations for robustness analysis and sensitivity modification

In this chapter, we introduce kinetic perturbations as a special uncertainty class for biochemical reaction networks. Section 6.2 formalises the concept and discusses the applicability of kinetic perturbations to various network types. Two applications of this concept to the analysis of biochemical reaction networks are proposed in this chapter. In Section 6.3, we show how robustness analysis with respect to kinetic perturbations can be used to find fragilities in the model. In Section 6.4, we propose a method to shape the steady state response of a network to an adjustable parameter by kinetic perturbations. The concept of kinetic perturbations and the robustness analysis are based on Waldherr *et al.* (2009a).

6.1 Introduction

In the previous chapters, the effects of generic parametric variations on the properties of a given model have been analysed. From a systems analysis viewpoint, generic parametric variations have the disadvantage of affecting the steady states of the system, which in turn generically leads to variations in all parts of the system. This makes modular approaches to model analysis impossible and obscures structural insight into the effects of perturbations. In this chapter, we consider a more specialised perturbation class, which is less general than arbitrary parameter variations, but well motivated from a biochemical perspective. It also allows to obtain more stringent results than with generic perturbations. In addition, the considered perturbation class is related to the type of structural uncertainties which have been considered previously, e.g. arising from unmodelled dynamics in the system (Jacobsen and Cedersund, 2008; Trané and Jacobsen, 2008).

The novel concept proposed here is an intermediate between parametric and structural uncertainty. The basic idea is to consider variations in the reaction rate expressions which leave the steady state reaction rates unaffected, but lead to changes in the reaction rate slopes. We define such perturbations as *kinetic perturbations*. We show that kinetic perturbations are directly related to specific parameter variations in important network classes. Kinetic perturbations may e.g. be used to study the possible effect of unmodelled additional interactions in a network. A systematic approach to analyse the robustness of the qualitative dynamical behaviour with respect to kinetic perturbations is proposed. In fact, the problem can directly be transformed to the framework of the structured singular values, which are studied extensively in robust control theory, and it admits explicit solutions in relevant simple cases. In addition, the concept of kinetic perturbations is

used to change the local sensitivity of a nominal steady state with respect to an adjustable parameter (e.g. an external stimulus) in a specified way.

6.2 Theory of kinetic perturbations

6.2.1 Definition of a kinetic perturbation

First, let us define the perturbation class considered in this chapter. For the moment, let us neglect the dependence of the model (2.5) on parameters, and consider a model given by

$$\dot{x} = Sv(x). \tag{6.1}$$

The approach is local in the sense that it aims at properties of the network (6.1) around an equilibrium point x_0, where $Sv(x_0, p) = 0$. The corresponding steady state reaction fluxes are denoted as $v_0 = v(x_0)$. For ease of notation, we will denote $V = \frac{\partial v}{\partial x}$. Locally around x_0, the dynamical behaviour is characterised by the Jacobian of the system (6.1) evaluated at x_0, which we denote by

$$A = SV(x_0). \tag{6.2}$$

From a biochemical perspective, the stoichiometric matrix S contains the structural mass flow interactions, while the reaction flux vector $v(x)$ describes the dependence of reaction rates on the substrate concentrations, and also captures the structural regulatory interactions.

Perturbations to the system which leave the mass flow structure unaffected can therefore be characterised by a change in the reaction flux vector, yielding the perturbed system

$$\dot{x} = S\tilde{v}(x), \tag{6.3}$$

where $\tilde{v}(x)$ is the perturbed reaction flux vector.

As can be seen from (6.2), the Jacobian A depends on the stoichiometry S as well as the local kinetic slopes V, i.e., the rate derivatives with respect to reactants at the steady state. In general, a perturbation of reaction parameters will have two separate effects on the local kinetic slopes. First, the perturbation will directly modify the slope of the corresponding reaction. Second, the perturbation will in general also affect the reaction rates and thereby the steady state of the complete network. This secondary effect implies that the local slopes of most reaction rates will change from the perturbation of a single parameter because of their dependence on x. This complicates the robustness analysis and, more importantly, obscures structural insight.

Here, we introduce *kinetic perturbations*, which affect the steady state Jacobian $V(x_0)$ of the reaction fluxes, but leave the stationary fluxes v_0, and as a consequence also the steady state concentrations x_0, unchanged.

Definition 6.1. *The system* (6.3) *is said to be subject to a* kinetic perturbation*, if*

$$\tilde{v}(x_0) = v_0. \tag{6.4}$$

From condition (6.4), we directly obtain $S\tilde{v}(x_0) = Sv_0 = 0$ and conclude that x_0 is also a steady state of the perturbed system.

Perturbations are often related to parameter variations in a parameter dependent reaction flux vector $v(x, p)$, where $p \in \mathbb{R}^q$ is the vector of reaction parameters. The nominal reaction flux vector is then given by $v(x) = v(x, p)$, and the perturbed reaction rate vector is

$$\tilde{v}(x) = v(x, \tilde{p}), \tag{6.5}$$

with perturbed parameters $\tilde{p}$. Parameter variations corresponding to kinetic perturbations can be characterised by the perturbation set $\mathcal{P} = \{p \in \mathbb{R}^q \mid v(x_0, p) = v_0\}$.

Kinetic perturbations of parametrised reaction rate expressions can also be related to structural perturbations by introducing implicit parameters. With the term "implicit parameters", we denote any parameters which do not appear in the nominal parametrised model (2.5), but are introduced as free parameters only during the model analysis. Typical examples are parameters which are supposed to be fixed at trivial constant values through choice of the model class (as in mass action networks), or which are related to interactions within the system which have been neglected in formulating the nominal model. Still, perturbations which affect implicit parameters may be relevant to the system and thus should be considered in robustness analysis.

While the steady state reaction rates are not affected by a kinetic perturbation, the reaction rate Jacobian V at the steady state will generally change. Similar to the nominal case, we denote $\tilde{V} = \frac{\partial \tilde{v}}{\partial x}$. The change in the reaction rate Jacobian at the steady state is denoted by

$$\bar{\Delta} = \tilde{V}(x_0) - V(x_0). \tag{6.6}$$

The perturbed Jacobian of the system at the steady state x_0 is denoted by $\tilde{A} \in \mathbb{R}^{n \times n}$ and is given by

$$\tilde{A} = S\tilde{V}(x_0) = A + S\bar{\Delta}. \tag{6.7}$$

We conclude that with respect to the dynamical behaviour in the neighbourhood of the steady state x_0, any kinetic perturbation is completely characterised by the perturbation matrix $\bar{\Delta}$.

For kinetic perturbations introduced by parameter variations, it is important that for any given perturbation matrix $\bar{\Delta}$, the corresponding parameter change is determined uniquely. This will for example allow to relate a specific $\bar{\Delta}$, computed e.g. as a fragile perturbation in the robustness analysis, to the system by appropriate parameter variations. In the following sections, we show that the parameter change corresponding to a given $\bar{\Delta}$ can be computed analytically for the common modelling frameworks of generalised mass action networks, Michaelis-Menten kinetics and metabolic networks where enzymes are subject to allosteric regulation.

6.2.2 Kinetic perturbations in generalised mass action networks

Kinetic perturbations have an illustrative physical interpretation for generalised mass action (GMA) networks. In a GMA network, reaction rates are given by the expression

$$v_i(x) = k_i \prod_{j=1}^{n} x_j^{\alpha_{ij}}, \quad i = 1, \ldots, m, \tag{6.8}$$

where $k_i > 0$ is the nominal reaction rate constant, and $\alpha_{ij} \in \mathbb{R}$ is the nominal kinetic order of the j-th species. Note that in contrast to classical mass action networks, non-integer kinetic orders α_{ij} are allowed in GMA networks. Non-integer kinetic orders are supported by simulation studies of reaction systems under diffusion constraints (Kopelman, 1988; Macheras and Ilidias, 2006; Savageau, 1995), or may represent the aggregation of mechanistic detail in a single reaction step (Vera *et al.*, 2007). For a GMA network with reaction rates as given in (6.8), a parameter vector p is introduced which contains the rate constants k_i as well as the kinetic orders α_{ij}, $i = 1, \ldots, m$, $j = 1, \ldots, n$.

If the nominal model is a classical mass action network, the α_{ij} can be considered as implicit parameters, fixed to the values given by the stoichiometry of the reaction. Furthermore, a value of $\alpha_{ij} = 0$ means that the j-th species does not affect the i-th reaction. Changing this value then corresponds to a structural perturbation of the nominal model.

In the following, we derive explicit expressions for parameter variations in a GMA network subject to a kinetic perturbation. From (6.4), a kinetic perturbation is characterised by the condition

$$\tilde{k}_i \prod_{j=1}^{n} x_{0,j}^{\tilde{\alpha}_{ij}} = k_i \prod_{j=1}^{n} x_{0,j}^{\alpha_{ij}}$$

or equivalently

$$\tilde{k}_i = k_i \prod_{j=1}^{n} x_{0,j}^{\alpha_{ij} - \tilde{\alpha}_{ij}}.$$

Considering the elements of the reaction rate Jacobian V, we obtain

$$V_{ij}(x) = \alpha_{ij} x_j^{-1} v_i(x),$$

and a kinetic perturbation where the reaction rate Jacobian V is changed additively by $\bar{\Delta}$ is given by

$$\tilde{\alpha}_{ij} x_{0,j}^{-1} v_{0,i} = \alpha_{ij} x_{0,j}^{-1} v_{0,i} + \bar{\Delta}_{ij},$$

or equivalently

$$\tilde{\alpha}_{ij} - \alpha_{ij} = \frac{x_{0,j}}{v_{0,i}} \bar{\Delta}_{ij}.$$

For the further analysis, let us introduce a suitable scaling of the perturbation $\bar{\Delta}$ as

$$\Delta = (\operatorname{diag} v_0)^{-1} \bar{\Delta} \operatorname{diag} x_0, \tag{6.9}$$

where $\Delta \in \mathbb{R}^{m \times n}$ is the scaled perturbation matrix. The same scaling is commonly used in linear sensitivity analysis of biochemical reaction networks (Heinrich and Schuster, 1996). With this scaling, kinetic perturbations by parameter variations in a GMA network are characterised by

$$\tilde{\alpha}_{ij} = \alpha_{ij} + \Delta_{ij} \tag{6.10}$$

and

$$\tilde{k}_i = k_i \prod_{j=1}^{n} x_{0,j}^{-\Delta_{ij}}. \tag{6.11}$$

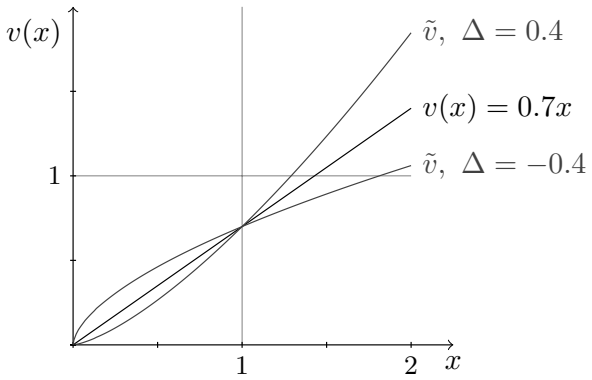

Figure 6.1: Illustration of kinetic perturbations to the nominal reaction rate $v(x) = 0.7x$. The nominal state at which the perturbation is applied is $x_0 = 1$.

In conclusion, we see that kinetic perturbations of a GMA network change the kinetic order of species in reactions, while at the same time adjusting the reaction rate constants to keep steady state reaction rates and steady state concentration values unperturbed. The scaling suggested in (6.9) thus directly relates the kinetic perturbations to an established property of the reaction rates. An illustration of the variation in a reaction rate for a kinetic perturbation is shown in Figure 6.1.

Remark The outlined approach is not applicable if $x_{0,j} = 0$ for some j. However, a kinetic perturbation in the reaction v_i can still be found if $\alpha_{ij} = 1$. Then,

$$V_{ij}(x_0, p) = k_i \prod_{l \neq j} x_{0,l}^{\alpha_{il}} \tag{6.12}$$

and the kinetic perturbation $\tilde{V}_{ij}(x_0, p) = V_{ij}(x_0, p_0) + \bar{\Delta}_{ij}$ can be realised by perturbing

$$\tilde{k}_i = k_i + \frac{\bar{\Delta}_{ij}}{\prod_{l \neq j} x_{0,l}^{\alpha_{il}}}. \tag{6.13}$$

6.2.3 Kinetic perturbations in metabolic networks

Metabolic networks describe conversions among metabolites which are catalysed by enzymes, where the metabolite concentrations are used as state variables, and the enzyme concentrations are usually considered as constant parameters. Classically, such reactions are modelled by the Michaelis-Menten law, with reaction rate expressions given as

$$v_i(x) = \frac{k_i x_j}{1 + M_i x_j}, \tag{6.14}$$

where x_j is the substrate concentration and k_i, M_i are parameters. For the derivative, we have

$$\frac{\partial v_i}{\partial x_j}(x) = \frac{k_i}{(1 + M_i x_j)^2}. \tag{6.15}$$

As we will show in the sequel, a kinetic perturbation can be constructed by using a perturbed reaction rate of the form

$$\tilde{v}_i(x) = \frac{\tilde{k}_i x_j}{1 + \tilde{M}_i x_j}. \tag{6.16}$$

We distinguish two cases for the computation of the parameters $\tilde{k}_i$ and $\tilde{M}_i$ such that they correspond to a kinetic perturbation.

Case 1: $x_{0,j} = 0$. Then, a kinetic perturbation is characterised by

$$\tilde{k}_i = k_i + \bar{\Delta}_{ij}, \tag{6.17}$$

and $\tilde{M}_i > 0$ is arbitrary, as it affects neither the steady state flux nor the Jacobian.

Case 2: $x_{0,j} \neq 0$. From (6.4) and (6.6), we have

$$\begin{aligned} \frac{\tilde{k}_i x_{0,j}}{1 + \tilde{M}_i x_{0,j}} &= \frac{k_i x_{0,j}}{1 + M_i x_{0,j}} \\ \frac{\tilde{k}_i}{(1 + \tilde{M}_i x_{0,j})^2} &= \frac{k_i}{(1 + M_i x_{0,j})^2} + \bar{\Delta}_{ij}. \end{aligned}$$

Solving for $\tilde{k}_i$ and $\tilde{M}_i$ yields

$$\begin{aligned} \tilde{k}_i &= \frac{k_i}{1 + \eta_{ij}\Delta_{ij}} \\ \tilde{M}_i &= \frac{1}{x_{0,j}}\left(\frac{\eta_{ij}}{1 + \eta_{ij}\Delta_{ij}} - 1\right), \end{aligned} \tag{6.18}$$

where $\eta_{ij} = 1 + M_i x_{0,j}$. Note that we obtain the fundamental limit

$$-\frac{1}{\eta_{ij}} < \Delta_{ij} < 1 - \frac{1}{\eta_{ij}} \tag{6.19}$$

on the scaled perturbation, which is related to the fact that the slope of the Michaelis-Menten curve is always positive and achieves its maximum at the origin. The variable η_{ij} can also be interpreted biochemically as the extent to which the reaction is saturated: In the linear regime, we have $M_j x_j \ll 1$ and $1 < \eta \ll 2$, whereas $\eta = 2$ means that the reaction flux is half the maximum flux, and for $\eta \gg 2$ the reaction operates in the saturated regime. We also see from (6.18) that the parameter change required to achieve a given change in the reaction rate slope increases with the saturation measure η_{ij}.

A more interesting network structure than with simple Michaelis-Menten reactions is obtained when considering regulatory influences of metabolites on enzyme activities. We use a reaction rate expression which is standard for modelling allosteric inhibition, given by

$$v_i(x, p) = k_i x_j \prod_{r=1}^{n} (1 + M_{ir} x_r)^{\alpha_{ir}}. \tag{6.20}$$

For a standard Michaelis-Menten reaction, $\alpha_{ij} = -1$ and $\alpha_{ir} = 0$ for $r \neq j$. A common description of an inhibitory regulation is obtained by setting $\alpha_{ir} = -1$ for some $r \neq j$.

To describe a positive regulatory influence, we may also use $\alpha_{ir} > 0$. Also, perturbations in the interaction structure may be formulated by considering α_{ir} as implicit parameter with nominal value $\alpha_{ir} = 0$. Regulatory interactions of a similar form, with $\alpha_{ir} = \pm 1$, are also considered by Wolf *et al.* (2005).

The derivatives of the reaction rate expression (6.20) are given by

$$\begin{aligned} \frac{\partial v_i}{\partial x_j} &= \frac{v_i}{x_j}\left(1 + \frac{\alpha_{ij} x_j M_{ij}}{1 + M_{ij} x_j}\right) \\ \frac{\partial v_i}{\partial x_s} &= v_i \frac{\alpha_{is} M_{is}}{1 + M_{is} x_s} \qquad \text{for } s \neq j. \end{aligned} \tag{6.21}$$

In the reaction rate expression (6.20), we have two parameters for each state variable, plus the variable k_i to adjust the steady state reaction flux. In the same way as above, we seek for a kinetic perturbation of the reaction rate by a parameter variation, where the perturbed reaction rate takes the form

$$\tilde{v}_i(x, p) = \tilde{k}_i x_j \prod_{r=1}^{n} (1 + \tilde{M}_{ir} x_r)^{\tilde{\alpha}_{ir}}. \tag{6.22}$$

To account for kinetic perturbations, we just need one adjustable parameter per state variable, so we can e.g. fix beforehand

$$\begin{aligned} \tilde{\alpha}_{ij} &= \alpha_{ij} \\ \tilde{M}_{is} &= M_{is} \quad \text{for } s \neq j. \end{aligned} \tag{6.23}$$

Solving the equations defining the kinetic perturbations for $\tilde{M}_{ij}$ and $\tilde{\alpha}_{is}$, $s \neq j$ then yields

$$\tilde{M}_{ij} = \frac{1}{x_{0,j}}\left(\frac{\eta_{ij}}{1 - \alpha_{ij}^{-1} \eta_{ij} \Delta_{ij}} - 1\right), \tag{6.24}$$

with $\eta_{ij} = 1 + M_{ij} x_{0,j}$ and

$$\tilde{\alpha}_{is} = \begin{cases} \alpha_{is} + \frac{\eta_{is}}{\eta_{is} - 1} \Delta_{is}, & x_{0,s} \neq 0 \\ \alpha_{is} + \frac{M_{is}}{v_{0,s}} \bar{\Delta}_{is}, & x_{0,s} = 0, \end{cases} \tag{6.25}$$

where we use again the scaled uncertainty

$$\Delta_{ij} = \frac{x_{0,j}}{v_{0,i}} \bar{\Delta}_{ij}. \tag{6.26}$$

As in the simple Michaelis-Menten case, we require $0 < \tilde{M}_{ij} < \infty$, which translates into the bounds

$$\frac{1}{\eta_{ij}} - 1 < \frac{\Delta_{ij}}{\alpha_{ij}} < \frac{1}{\eta_{ij}}. \tag{6.27}$$

Perturbations not satisfying these bounds can only be realised by perturbing the kinetic order α_{ij} in addition.

To keep the steady state reaction flux unaffected by the perturbation, we finally set

$$\tilde{k}_i = k_i \prod_{r \neq j} \eta_{ir}^{-\frac{\eta_{ir}}{\eta_{ir} - 1} \Delta_{ir}} (1 - \alpha_{ij}^{-1} \eta_{ij} \Delta_{ij})^{\alpha_{ij}}. \tag{6.28}$$

6.2.4 Kinetic perturbations of generic reaction rates

In this section, we construct a kinetic perturbation for a generic reaction rate. This is of relevance for networks which do not use the GMA or Michaelis-Menten type reaction kinetics. It is shown that kinetic perturbations can still be applied by directly introducing the perturbation Δ_{ij} as an implicit parameter into the reaction rate. Consider a modification to the reaction rate $v_i(x)$ given by

$$\tilde{v}_i(x) = v_i(x) x_j^{\Delta_{ij}} x_{0,j}^{-\Delta_{ij}}. \tag{6.29}$$

This is clearly a kinetic perturbation which changes only the slope $\frac{\partial v_i}{\partial x_j}$, as we have

$$\begin{aligned} \tilde{v}_i(x_0) &= v_i(x_0) \\ \frac{\partial \tilde{v}_i}{\partial x_j}(x_0) &= \frac{\partial v_i}{\partial x_j}(x_0) + v_i(x_0)\Delta_{ij} x_{0,j}^{-1} \\ \frac{\partial \tilde{v}_i}{\partial x_s}(x_0) &= \frac{\partial v_i}{\partial x_s}(x_0), \quad s \neq j. \end{aligned} \tag{6.30}$$

However, in some cases it may be biologically more relevant to implement kinetic perturbations by varying other parameters in the reaction rate $v_i(x)$. In these cases, a separate analysis has to be done, such as for the Michaelis-Menten reaction rate in Section 6.2.3.

6.3 Robustness analysis with kinetic perturbations

6.3.1 Problem statement

The problem of local robustness analysis is to evaluate the effects of perturbations on the signature of the system's Jacobian A. Since steady state concentration values and reaction fluxes are often well characterised for biochemical reaction networks, we are specifically considering perturbations which do not affect these values, i.e. kinetic perturbations.

Using kinetic perturbations with a scaled uncertainty matrix Δ as given by (6.9), according to (6.7) the perturbed Jacobian becomes

$$\tilde{A}(\Delta) = A + S(\operatorname{diag} v_0)\Delta(\operatorname{diag} x_0)^{-1}. \tag{6.31}$$

In general, the robustness problem for kinetic perturbations through parameter variations can be formulated as follows. First, one needs to introduce a measure for the perturbation strength. Usually, an operator norm $\|\Delta\|$ is chosen as perturbation measure. Next, define the robustness radius of the system (6.1) at the equilibrium x_0 as

$$\psi = \inf\{\|\Delta\| \mid \operatorname{in}(\tilde{A}(\Delta)) \neq \operatorname{in}(A)\}, \tag{6.32}$$

where $\operatorname{in}(A)$ denotes the inertia of the square matrix A. In local robustness analysis, two goals are usually pursued. The first goal is to compute the robustness radius ψ, or at least lower and upper bounds. The second goal is to construct a minimum-size non-robust perturbation Δ^* such that $\|\Delta^*\| = \psi$ and $\operatorname{in}(\tilde{A}(\Delta^*)) \neq \operatorname{in}(A)$. Depending on the specific network class, a corresponding non-robust parameter vector $\tilde{p}^*$ can be obtained through the expressions derived in Section 6.2.

Due to the proposed reformulation (6.31), the robustness problem with respect to kinetic perturbations can be solved by using the concept of the structured singular value (or μ–value) developed in the 1980s (Doyle, 1982). Since we are considering static perturbations to the reaction rate slopes only, the problem translates into a real μ problem (Qiu *et al.*, 1995). The real μ–value is defined as (Hinrichsen and Pritchard, 2005)

$$\mu_\Delta(G(j\omega)) = \Big(\inf\big\{\|\Delta\| \mid \Delta \in \mathbb{R}^{m\times n},\ \det(I_m - \Delta G(j\omega)) = 0\big\}\Big)^{-1}.$$

To compute the robustness radius ψ for the perturbed Jacobian $\tilde{A}(\Delta)$ in (6.31), the transfer function $G : \mathbb{C} \to \mathbb{C}^{n\times m}$ which needs to be considered in the μ–value is given by

$$G(j\omega) = (\operatorname{diag} x_0)^{-1}(j\omega I_n - A)^{-1} S \operatorname{diag} v_0. \tag{6.33}$$

Computation of the robustness radius from the μ–value is then a standard problem in robust control theory (Hinrichsen and Pritchard, 2005), with the solution

$$\psi = \Big(\sup_\omega \mu_\Delta(G(j\omega))\Big)^{-1}. \tag{6.34}$$

Usually, the robustness analysis will result in a symmetric interval around the nominal value $\Delta_0 = 0$. However, in some cases it may be more reasonable to consider asymmetric intervals, e.g. if a perturbation in one direction is much more likely than in another one. The analysis can be extended to such cases by defining a new interval center $\Delta_0 \neq 0$. Thus, we substitute the nominal Jacobian A by

$$A(\Delta_0) = A + S(\operatorname{diag} v_0)\Delta_0(\operatorname{diag} x_0)^{-1},$$

and the robustness radius is computed by considering the perturbed Jacobian $\tilde{A}(\Delta) = A(\Delta_0) + S(\operatorname{diag} v_0)\Delta(\operatorname{diag} x_0)^{-1}$.

In general, computation of the μ–value for real uncertainties is a difficult problem (Hinrichsen and Pritchard, 2005). For general matrix perturbations, usually only lower and upper bounds can be obtained. Fortunately, in the analysis of biochemical reaction networks, already scalar and vector perturbations give a useful insight into robustness properties of a system. For these perturbation cases, it is possible to compute the robustness radius ψ and a corresponding non-robust perturbation Δ^* explicitly. The scalar case is discussed in the following section, whereas the case of vector perturbations is described in Waldherr *et al.* (2009a). Scalar perturbations are relevant for the analysis of biochemical reaction networks, in order to detect single fragile interactions, where a perturbation can change the dynamical properties of the network.

6.3.2 Scalar perturbations

If we restrict all elements of Δ apart from one to zero, we have a scalar perturbation. For a biochemical reaction network, this corresponds to the case where only the influence of a single species on a single reaction rate is subject to a perturbation. In the analysis of biochemical networks, this approach will be useful for the detection of single fragile interactions. In terms of the robust control approach outlined in Section 6.3.1, such a

perturbation translates into a scalar uncertainty problem, for which the robustness radius and a non-robust perturbation are easily computed.

Assume that the derivative V_{ij} of reaction i with respect to the species j is subject to perturbations. Then, we have

$$\Delta = e_i^m \Delta_{ij} e_j^{n\mathrm{T}}, \tag{6.35}$$

with the uncertainty $\Delta_{ij} \in \mathbb{R}$, where $e_i^m \in \mathbb{R}^m$ ($e_j^n \in \mathbb{R}^n$) is the unit vector in the i–th (j–th) coordinate direction. The perturbed Jacobian is then given by

$$\tilde{A}(\Delta) = A + S(\operatorname{diag} v_0) e_i^m \Delta_{ij} e_j^{n\mathrm{T}} (\operatorname{diag} x_0)^{-1}. \tag{6.36}$$

Denote $B = S(\operatorname{diag} v_0) e_i^m$ and $C = e_j^{n\mathrm{T}} (\operatorname{diag} x_0)^{-1}$. Define the transfer function

$$G(j\omega) = C(j\omega I_n - A)^{-1} B. \tag{6.37}$$

For the robustness radius we obtain (Hinrichsen and Pritchard, 2005)

$$\psi = \Big(\sup_{\omega} \mu_\Delta(G(j\omega)) \Big)^{-1} = \Big(\max_{\omega \in \mathcal{R}} |G(j\omega)| \Big)^{-1}, \tag{6.38}$$

where

$$\mathcal{R} = \big\{ \omega \in \mathbb{R} \mid \operatorname{Im}(G(j\omega)) = -\omega C(\omega^2 I + A^2)^{-1} B = 0 \big\}$$

is the realness locus of $G(j\omega)$.

The remaining task is now to construct a minimum–norm non-robust perturbation Δ_{ij}^*, for which the Jacobian $\tilde{A}(e_i^m \Delta_{ij}^* e_j^{n\mathrm{T}})$ has an eigenvalue on the imaginary axis. Such a perturbation exists, if and only if $\mu_\Delta(G(j\omega)) > 0$ for some $\omega \in \mathbb{R}$. To construct a non-robust perturbation, let $\omega^* = \arg\max_{\omega \in \mathcal{R}} |G(j\omega)|$. The non-robust scalar perturbation is then given by

$$\Delta_{ij}^* = \frac{1}{G(j\omega^*)}. \tag{6.39}$$

In the scalar case, it is also possible to compute non-symmetric robustness radii: Define

$$\mu_- = \sup\Big(\big\{ |G(j\omega)| \mid \omega \in \mathcal{R}, G(j\omega) < 0 \big\} \cup \{0\} \Big)$$
$$\mu_+ = \sup\Big(\big\{ |G(j\omega)| \mid \omega \in \mathcal{R}, G(j\omega) > 0 \big\} \cup \{0\} \Big).$$

Then we have $\operatorname{in}(\tilde{A}(\Delta)) = \operatorname{in}(A)$ for

$$-\mu_-^{-1} < \Delta_{ij} < \mu_+^{-1}. \tag{6.40}$$

Example 6.2. Before considering networks of typical complexity, let us first illustrate the use of kinetic perturbations for robustness analysis with a very simple example, comprising only one species X and two reactions v_1 and v_2. The ODE model is given by

$$\dot{x} = Sv(x) = \begin{pmatrix} 1 & -1 \end{pmatrix} \begin{pmatrix} \frac{kx^2}{1+Mx^2} \\ x \end{pmatrix}, \tag{6.41}$$

where the nominal values for the two parameters in v_1 are $k = 3$ and $M = 2$. Let us consider the steady state $x_0 = 1$, yielding the stationary reaction rates $v_0 = (1, 1)^{\mathrm{T}}$

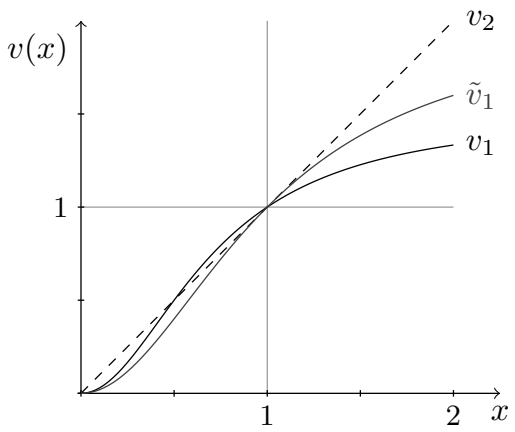

Figure 6.2: Illustration of kinetic perturbations for the simple system in Example 6.2.

and $V(x_0) = (\frac{2}{3}, 1)^{\mathrm{T}}$. According to (6.2), the nominal Jacobian is given by $A = -\frac{1}{3}$, corresponding to the steady state x_0 being stable. For a scalar kinetic perturbation $\Delta_{11} \in \mathbb{R}$, i.e. the slope of reaction v_1 is uncertain, we obtain the perturbed Jacobian

$$A(\Delta) = A + S \begin{pmatrix} 1 \\ 0 \end{pmatrix} \Delta_{11} = -\frac{1}{3} + \Delta_{11}. \tag{6.42}$$

A minimal non-robust perturbation is readily constructed as $\Delta_{11}^* = \frac{1}{3}$, with the critical frequency $\omega^* = 0$.

In the next step, we seek for perturbed parameters $\tilde{k}$ and $\tilde{M}$ corresponding to the perturbed system with $\Delta_{11} = \Delta_{11}^*$. From the conditions (6.4) and (6.6), we have

$$\begin{aligned} \tilde{v}_1(x_0) = v_1(x_0) \qquad &\Leftrightarrow \qquad \frac{\tilde{k}}{1+\tilde{M}} = 1 \\ \frac{\partial \tilde{v}_1}{\partial x}(x_0) = \frac{\partial v_1}{\partial x}(x_0) + \Delta_{11}^* \qquad &\Leftrightarrow \qquad \frac{2\tilde{k}}{(1+\tilde{M})^2} = 1, \end{aligned} \tag{6.43}$$

and the perturbed parameters are given by

$$\begin{aligned} \tilde{k} &= 2 \\ \tilde{M} &= 1. \end{aligned} \tag{6.44}$$

The nominal and perturbed reaction rates are shown in Figure 6.2. From the figure, we see that the system undergoes a saddle–node bifurcation at $x_0 = 1$ for the perturbed parameter values $\tilde{k}$ and $\tilde{M}$. For a kinetic perturbation $\Delta_{11} > \frac{1}{3}$, the steady state x_0 will turn unstable.

6.3.3 Application to the MAPK cascade

The robustness analysis with kinetic perturbations is illustrated by applying it to the model of the MAPK cascade (2.14) described in Section 2.3.1. For nominal parameter

Table 6.1: Fragile interactions in the MAPK model (2.14). The table is structured, such that all lines grouped in one field correspond to the same change in the Jacobian. This is due to the structure (non-empty kernel) of the stoichiometric matrix.

Nr.	Reaction i	Species j	Δ_{ij}^*	ω^* [s^{-1}]
1a	v_1	x_{11}	-0.21	$0.55 \cdot 10^{-2}$
1b	v_2	x_{11}	0.21	$0.55 \cdot 10^{-2}$
2a	v_1	x_{32}	0.47	$0.5 \cdot 10^{-2}$
2b	v_2	x_{32}	-0.47	$0.5 \cdot 10^{-2}$
3a	v_3	x_{11}	-0.42	$0.55 \cdot 10^{-2}$
3b	v_6	x_{11}	0.42	$0.55 \cdot 10^{-2}$
4a	v_4	x_{21}	-0.46	$0.56 \cdot 10^{-2}$
4b	v_5	x_{21}	0.46	$0.56 \cdot 10^{-2}$
5a	v_4	x_{22}	-0.21	$0.55 \cdot 10^{-2}$
5b	v_5	x_{22}	0.21	$0.55 \cdot 10^{-2}$
6a	v_4	x_{32}	-0.26	$0.58 \cdot 10^{-2}$
6b	v_5	x_{32}	0.26	$0.58 \cdot 10^{-2}$
7a	v_7	x_{22}	-0.44	$0.54 \cdot 10^{-2}$
7b	v_{10}	x_{22}	0.44	$0.54 \cdot 10^{-2}$
8a	v_7	x_{32}	-0.43	$0.57 \cdot 10^{-2}$
8b	v_{10}	x_{32}	0.43	$0.57 \cdot 10^{-2}$
9a	v_8	x_{11}	0.18	$0.58 \cdot 10^{-2}$
9b	v_9	x_{11}	-0.18	$0.58 \cdot 10^{-2}$
10a	v_8	x_{32}	-0.18	$0.55 \cdot 10^{-2}$
10b	v_9	x_{32}	0.18	$0.55 \cdot 10^{-2}$

values, the model shows limit-cycle oscillations around an unstable equilibrium point. The analysis in this section is based on the parameter value set B in Table 2.3. The Jacobian evaluated at the equilibrium point has two complex conjugated eigenvalues with positive real parts. The goal of the robustness analysis is to determine kinetic perturbations which could lead to a loss of sustained oscillations.

We consider only kinetic perturbations where the influence of each species on each reaction is perturbed individually, i.e. the scalar uncertainty case. Table 6.1 shows the interactions where a scaled kinetic perturbation smaller than 0.5 is sufficient to induce eigenvalues of the Jacobian on the imaginary axis.

The following perturbation cases are of particular biological relevance:

1a/b Change of the substrate order in the first cascade element;

2a Modification of the characteristics of the feedback interaction (Kholodenko, 2000);

3a, 7a Reduction of the efficiency of the first phosphorylation step in each cascade level;

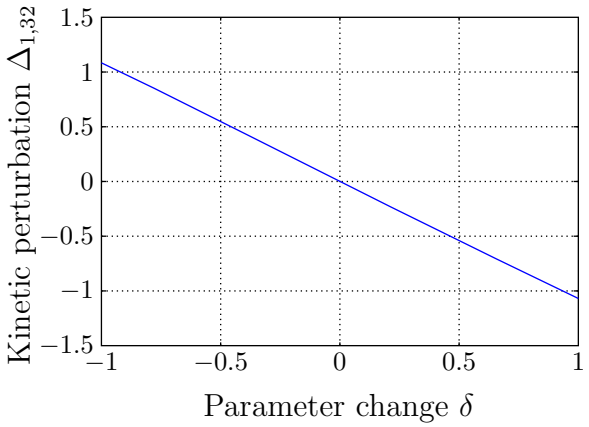

Figure 6.3: Relation between kinetic perturbation $\Delta_{1,32}$ and corresponding parameter change δ in the interaction $x_{32} \to v_1$ of the MAPK cascade model.

8b, 10b Induction of the MAPK-phosphatase MKP-1 by active MAPK-PP (Bhalla and Iyengar, 2001; Bhalla *et al.*, 2002);

9a Direct feed-through in kinase phosphorylation (impaired specificity of MAPKKK*).

From these results, we see that there are several interactions where oscillations are fragile with respect to kinetic perturbations. For some of these interactions, biochemical mechanisms that may affect them have already been suggested in the literature (Bhalla and Iyengar, 2001; Bhalla *et al.*, 2002; Kholodenko, 2000).

The perturbation case 2a is now investigated further by constructing explicit model perturbations and a bifurcation analysis, in which the model is changed gradually from the nominal to the fully perturbed case. The linear analysis of this perturbation indicates that a Hopf bifurcation is induced, where the unstable eigenvalues are moved to the imaginary axis. Thus, we expect that the perturbed model will no longer show sustained oscillations.

The perturbation 2a can be implemented by changing the exponent of x_{31} in the reaction rate v_1, which is related to the cooperativity of MAPK-PP in the feedback inhibition. We construct the perturbed reaction rate as

$$\tilde{v}_1 = k(\delta) V_1 \frac{x_{1t} - x_{11}}{(1 + (x_{32}/K_i)^{2+\delta})(K_{m1} + x_{1t} - x_{11})}, \tag{6.45}$$

where $\delta \in \mathbb{R}$ is an implicit parameter used to modify the characteristics of the feedback inhibition of reaction 1 by MAPK-PP. The multiplicative change to the reaction rate

$$k(\delta) = \frac{1 + (x_{0,32}/K_i)^{2+\delta}}{1 + (x_{0,32}/K_i)^2} \tag{6.46}$$

is constructed to maintain the same stationary reaction rate in the perturbed and nominal models. In this case, the value of δ corresponding to a specific kinetic perturbation $\Delta_{1,32}$ cannot be computed analytically. However, a numerical computation is possible, and the results are shown in Figure 6.3. The relation seems to be linear, with a slope close to -1. Thus increasing the exponent of x_{32} in v_1, while maintaining the stationary reaction

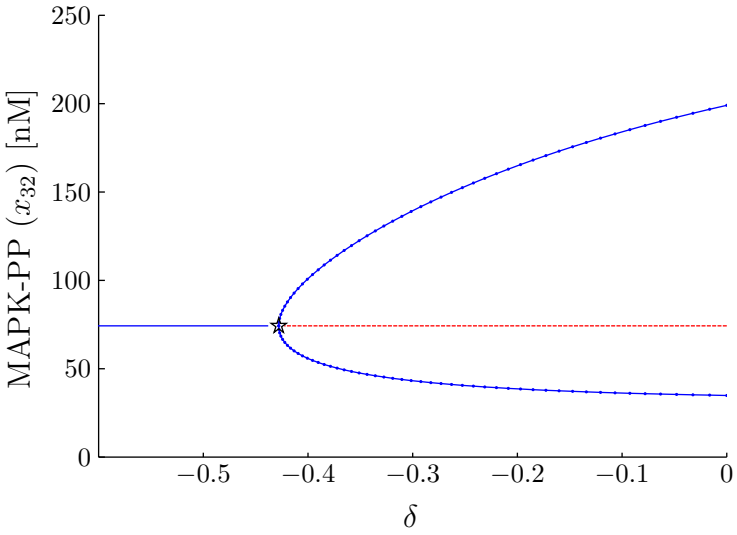

Figure 6.4: Bifurcation diagram for the kinetic perturbation $x_{32} \to v_1$ in the MAPK cascade model. The Hopf bifurcation is marked by a star.

rate, corresponds to a proportional (almost equal) decrease in the slope $\frac{\partial v_1}{\partial x_{32}}$. Another interpretation is that increasing the cooperativity in the feedback inhibition (which is achieved by a positive δ) corresponds to a reduction in the feedback strength, as measured by the corresponding Jacobian element. The non-robust kinetic perturbation $\Delta^* = 0.47$ obtained in Table 6.1 corresponds to a parameter change of $\delta^* \approx -0.42$. Typically, it is expected that an increase in feedback strengths tends to support sustained oscillations. However, in this example, we observe that a decrease in the exponent, corresponding to an increase in the strength of the feedback inhibition, actually is more efficient to stop oscillations than a decrease in the feedback strength.

The bifurcation diagram for varying the parameter δ is shown in Figure 6.4. Since this is a kinetic perturbation, the steady state value is not affected by δ. However, stability does depend on the value of δ, and, as predicted by the robustness analysis, there is a Hopf bifurcation correlating with loss of oscillations at $\delta^* \approx -0.42$.

6.4 Local sensitivity modifications via kinetic perturbations

6.4.1 Problem setup

As a second application of kinetic perturbations in biochemical networks, we study their effect on the local sensitivity of the steady state with respect to a generic parameter variation, as defined in Section 2.2. For simplicity of presentation, we only discuss the special case of sensitivity with respect to an adjustable, scalar parameter denoted by $\varphi \in \mathbb{R}$. The parameter φ may e.g. represent a stimulus which is expected to vary around a nominal value. It is assumed that φ is not affected by kinetic perturbations, but is subject to additional uncertainty.

Let us consider a parameter dependent ODE model of the network given by

$$\dot{x} = Sv(x, \varphi). \tag{6.47}$$

In this section, we will generally assume that, locally around a nominal parameter value φ_0, the steady state can be written as a smooth function $x_s(\varphi) \in \mathbb{R}^n$ of the parameter φ, i.e. we have

$$Sv(x_s(\varphi), \varphi) = 0 \tag{6.48}$$

for φ in a neighbourhood of φ_0. Denote the nominal steady state by $x_0 = x_s(\varphi_0)$.

As discussed in Section 2.2, the sensitivity $\bar{\Sigma}$ of the steady state with respect to the parameter φ at the nominal steady state is defined as

$$\bar{\Sigma} = \frac{\partial x_s}{\partial \varphi}(\varphi_0),$$

which is usually computed from the sensitivity equation

$$SV_0\bar{\Sigma} + S\frac{\partial v}{\partial \varphi}(x_0, \varphi_0) = 0, \tag{6.49}$$

where

$$V_0 = \frac{\partial v}{\partial x}(x_0, \varphi_0). \tag{6.50}$$

In the application of kinetic perturbations discussed here, we will study the problem how a specific change in the sensitivity $\bar{\Sigma}$ is related to a kinetic perturbation of the system (6.47). Kinetic perturbations are particularly relevant for this problem, because they allow changing the sensitivity, while keeping the nominal steady state value x_0 fixed. Let the requested change in $\bar{\Sigma}$ be given by

$$\bar{\sigma} = \widetilde{\bar{\Sigma}} - \bar{\Sigma}, \tag{6.51}$$

where $\widetilde{\bar{\Sigma}} \in \mathbb{R}^n$ is the sensitivity of the steady state with respect to the parameter φ in the modified system. We seek to achieve this sensitivity change by a kinetic perturbation, where the modified system is given by

$$\dot{x} = S\tilde{v}(x, \varphi), \tag{6.52}$$

and $\tilde{v}$ is the reaction rate vector subject to a kinetic perturbation as defined in Section 6.2.

As in the robustness analysis problem, we denote the change in the reaction rate slopes V_0 with respect to the state variables by

$$\bar{\Delta} = \tilde{V}_0 - V_0.$$

In addition, the change in the reaction rate slopes with respect to φ is denoted by

$$\bar{\Delta}_\varphi = \frac{\partial \tilde{v}}{\partial \varphi}(x_0, \varphi_0) - \frac{\partial v}{\partial \varphi}(x_0, \varphi_0).$$

Using (6.49), the sensitivity change $\bar{\sigma}$ has to satisfy the equation

$$SV_0\bar{\sigma} + S\bar{\Delta}(\bar{\Sigma} + \bar{\sigma}) + S\bar{\Delta}_\varphi = 0. \tag{6.53}$$

In the next section, we will address the problem of computing perturbations $\bar{\Delta}$ and $\bar{\Delta}_\varphi$ satisfying (6.53) for a specific sensitivity change $\bar{\sigma}$.

6.4.2 Kinetic perturbations for a specific sensitivity change

For a given sensitivity change $\bar{\sigma}$, (6.53) is a system of n linear equations in the unknowns $\bar{\Delta} \in \mathbb{R}^{m\times n}$ and $\bar{\Delta}_\varphi \in \mathbb{R}^n$, amounting to $nm + n$ free variables. Thus, the solution of (6.53) is generally not unique. We consider two approaches in order to obtain specific perturbations $\bar{\Delta}$ and $\bar{\Delta}_\varphi$ satisfying (6.53). In the first approach, the degrees of freedom are used to construct an explicit solution with some sparsity properties. In the second approach, we use linear programming to compute minimal-norm perturbations.

For a specific solution of the equation (6.53), we set

$$\bar{\Delta}_\varphi = 0$$

and denote

$$\begin{aligned}\bar{\Sigma} &= (\bar{\Sigma}_1, \dots, \bar{\Sigma}_n)^{\mathrm{T}}\\ \bar{\sigma} &= (\bar{\sigma}_1, \dots, \bar{\sigma}_n)^{\mathrm{T}}\\ V_0 &= (V_{0,1}, \dots, V_{0,n})\\ \bar{\Delta} &= (\bar{\Delta}_{\bullet 1}, \dots, \bar{\Delta}_{\bullet n}),\end{aligned}$$

where $\bar{\Sigma}_i, \bar{\sigma}_i \in \mathbb{R}$ and $V_{0,i}, \bar{\Delta}_{\bullet i} \in \mathbb{R}^m$.

We then rewrite (6.53) with $\bar{\Delta}_\varphi = 0$ as

$$S\sum_{i=1}^{n}(V_{0,i}\bar{\sigma}_i + \bar{\Delta}_i(\bar{\Sigma}_i + \bar{\sigma}_i)) = 0, \tag{6.54}$$

and a specific solution is constructed as

$$\bar{\Delta}_{\bullet i} = -V_{0,i}\frac{\bar{\sigma}_i}{\bar{\Sigma}_i + \bar{\sigma}_i}. \tag{6.55}$$

As discussed in Section 6.2, $\bar{\Delta}$ can always be realised by explicitly computable parameter variations for certain network classes. Note that zero elements of V_0 are not affected by the perturbation, and the interaction structure of the original system is maintained.

In applications, it is usually desirable to find a kinetic perturbation which modifies the network as little as possible, while still leading to a specific sensitivity change. This is achieved by searching for a solution $\bar{\Delta}$ of (6.53) of minimal norm. For a given sensitivity change $\bar{\sigma}$, a perturbation $\bar{\Delta}$ of minimal norm can be obtained by solving the optimisation problem

$$\begin{aligned}&\min_{\bar{\Delta},\bar{\Delta}_\varphi} \ \|\bar{\Delta}\| + \|\bar{\Delta}_\varphi\|\\ &\text{s.t. } SV_0\bar{\sigma} + S\bar{\Delta}(\bar{\Sigma} + \bar{\sigma}) + S\bar{\Delta}_\varphi = 0.\end{aligned} \tag{6.56}$$

For biochemical reaction networks, relevant norms to use in this problem are the 1– and the ∞–norm. The 1–norm is a reasonable choice if individual perturbations are independent, and their magnitudes add up to the overall perturbation magnitude. On the contrary, the ∞–norm is appropriate if perturbations are likely to occur in parallel, e.g. a change in kinase activity affecting all corresponding phosphorylation reactions simultanously. Then, the optimisation problem can be reformulated as a linear program and admits an efficient computational solution. In addition, it is possible to include structural constraints in the

optimisation problem, e.g. that certain elements of $\bar{\Delta}$ or $\bar{\Delta}_\varphi$ are equal to zero. Also upper and lower bounds on individual elements of $\bar{\Delta}_\varphi$ can be added to the constraints.

For an example of the sensitivity modification, we refer to Section 7.4. There, it is shown that this approach provides an efficient method for modifying the stationary stimulus–response behaviour of a biochemical reaction network with respect to an adjustable stimulus.

6.5 Summary and discussion of the kinetic perturbation approach

This chapter introduces kinetic perturbations as a new uncertainty class for biochemical reaction networks. It is shown that these perturbations are directly related to variations in the reaction order for general mass action networks and thereby admit an illustrative physical interpretation. We also construct parametric changes for kinetic perturbations in enzymatic networks, and show how to apply a kinetic perturbation to a generic reaction rate.

The advantage of considering kinetic perturbations for robustness analysis is that we can use the well developed theory of linear robust control, and even obtain exact solutions for the robustness radius in the scalar and vector uncertainty cases. The example considered in this chapter shows that a robustness analysis with this approach easily allows to detect possible fragile points in the network's interactions, and to transform the non-robust perturbations to physical variations in the biochemical network. In addition, the analysis method can also be used to consider variations in the network's interaction structure itself, by introducing implicit parameters.

Another application for kinetic perturbations is the variation of a network's steady state sensitivity, while maintaining the original steady state unperturbed. A minimum–norm kinetic perturbation leading to a specified sensitivity change can be computed by solving a linear program. An exemplary application of this method is given in Chapter 7.

The use of kinetic perturbations is motivated by the fact that steady state concentration values and reaction fluxes are often well characterised in biochemical networks, whereas the exact reaction kinetics are much less well known. In this respect, an important application of robustness analysis with kinetic perturbations will be model validation.

It should also be pointed out that the proposed approach does not require an explicit model of the network, apart from the problem of relating kinetic perturbations to parameter variations. It is in fact sufficient to know the steady state concentrations, reaction fluxes, and Jacobian elements for the robustness analysis, which can be inferred more easily from experiments than explicit rate expressions (Kholodenko *et al.*, 2002).

Chapter 7

Construction and analysis of a TNF signal transduction model

This chapter describes the construction and analysis of a dynamical model for a TNF signal transduction network, serving as a comprehensive application example for the methods developed in the two previous chapters. After a brief introduction to TNF signal transduction, the system to be modelled and the model construction are described in Section 7.2. Section 7.3 contains an analysis of oscillations in the model by the methods developed in Chapters 5 and 6. In Section 7.4, we use the concepts developed in Chapter 6 to study the effect of perturbations to the network on the steady state response of TRAF2, a specific target of TNF signalling. In addition to the biological contribution, this chapter thereby also serves as a case study, where the methods developed in the two previous chapters are applied within a larger and more realistic context. An uncertainty analysis with the methods described in Chapter 3 has been performed by Hasenauer (2008) for a previous version of the model presented here. Due to the complexity of the model, the analysis methods developed in Chapter 4 are not applicable in this case.

7.1 Introduction to TNF signal transduction

The tumor necrosis factor (TNF) is a cytokine which coordinates the mammalian immune response. TNF activates several intracellular pathways, notably apoptotis via the caspase cascade and the NF-κB, JNK, and MAPK pathways (Wajant *et al.*, 2003). A misregulation of TNF and the associated pathways is involved in various high-impact diseases, such as cancer or autoimmune diseases (Feldmann and Maini, 2003; Hanahan and Weinberg, 2000; Rae *et al.*, 2007). The interplay between the apoptotic and anti-apoptotic pathways activated by TNF also makes these networks worth studying from a more theoretical perspective.

TNF signalling is mediated by membrane receptors of the TNF receptor family, comprising about a dozen different receptors, of which the two receptors TNF receptor 1 (TNFR1) and TNF receptor 2 (TNFR2) are the main binding partners for the TNF-α ligand (Grell *et al.*, 1998). The TNFR1 plays a major role in apoptosis induction by signal transduction to the caspase cascade (Eissing *et al.*, 2007a; Wajant *et al.*, 2003), but it also activates anti-apoptotic pathways. The TNFR2 does not directly signal to the caspase cascade, but may have a strong influence on the results of TNFR1 signalling by crosstalk effects (Fotin-Mleczek *et al.*, 2002) and induction of TNF expression, leading to autocrine signalling. The anti-apoptotic effects of TNF signalling are mainly mediated via the transcription factor NF-κB, which is a known inducer of several anti-apoptotic

proteins like the inhibitor-of-apoptosis proteins (IAP) (Stehlik *et al.*, 1998; Wang *et al.*, 1998).

In this chapter, we develop a model for the NF-κB related part of the anti-apoptotic TNF signalling network, with a special focus on crosstalk between the two receptor types through recruitment of the same adaptor proteins. The model contains the formation of TNF receptor complexes, crosstalk effects between TNFR1 and TNFR2, as well as the TNF induced NF-κB pathway. The model is then analysed with methods developed in this thesis to gain further insights into the mechanisms of TNF induced anti-apoptotic signalling.

7.2 Development of a model for the anti-apoptotic TNF network

7.2.1 Structure of the model

The model proposed in this chapter aims at describing the response in nuclear NF-κB activity to the separate or combined stimulation of the TNF receptors 1 and 2. The model is specifically developed for the Kym-1 cell type, which is a human rhabdomyosarcoma cell line grown in cell culture. Kym-1 cells express both TNF receptor 1 and 2, and thus constitute an ideal experimental system for the study of TNF receptor crosstalk effects.

The structure of the model has been derived from basic knowledge of relevant proteins which are involved in the signalling network, and from literature data on their interactions. For the NF-κB pathway downstream of the receptor complexes, we rely mainly on previous modelling efforts. The structure of this part of the model is adapted from Lipniacki *et al.* (2004). Other sources are the models described in Hoffmann *et al.* (2002), Lipniacki *et al.* (2007), and Ashall *et al.* (2009). For the receptor complex formation, the construction of mathematical models is not as advanced as for the NF-κB pathway. The TNFR1 complex formation has been modelled by Schliemann *et al.* (2007), although focusing on different adaptor proteins than considered here. For the formation of the TNFR2 complex and its signalling, no previous mathematical models are known to the author.

The structure of the model developed in this chapter is coarsely depicted in Figure 7.1. The model is organised into four modules: the TNF receptor complex formation, the activation of the I-κB kinase (IKK), the activation and nuclear translocation of NF-κB, and the NF-κB induced gene expression.

Upon ligand binding, the TNF receptors start to recruit adaptor proteins to form the relevant signalling complexes. The TNF receptor 1 first recruits TRADD (Ermolaeva *et al.*, 2008; Micheau and Tschopp, 2003; Pobezinskaya *et al.*, 2008), but for simplicity, this step is not explicitly included in the model. Rather, TRADD is assumed to bind instantly, or to be already associated to the TNFR1. In the next step, the TNFR1 recruits the adaptor proteins RIP1 and TRAF2. From available biological data, it is not clear whether these adaptor proteins can only bind sequentially, and, if so, what the sequence is, or whether RIP1 and TRAF2 can independently bind to the TNFR1 under *in vivo* conditions. In our model, we use the hypothesis that TRAF2 is recruited to the receptor complex only after RIP1, as proposed by Festjens *et al.* (2007). Concerning signal transduction from this complex, there is experimental evidence that signalling from TNF

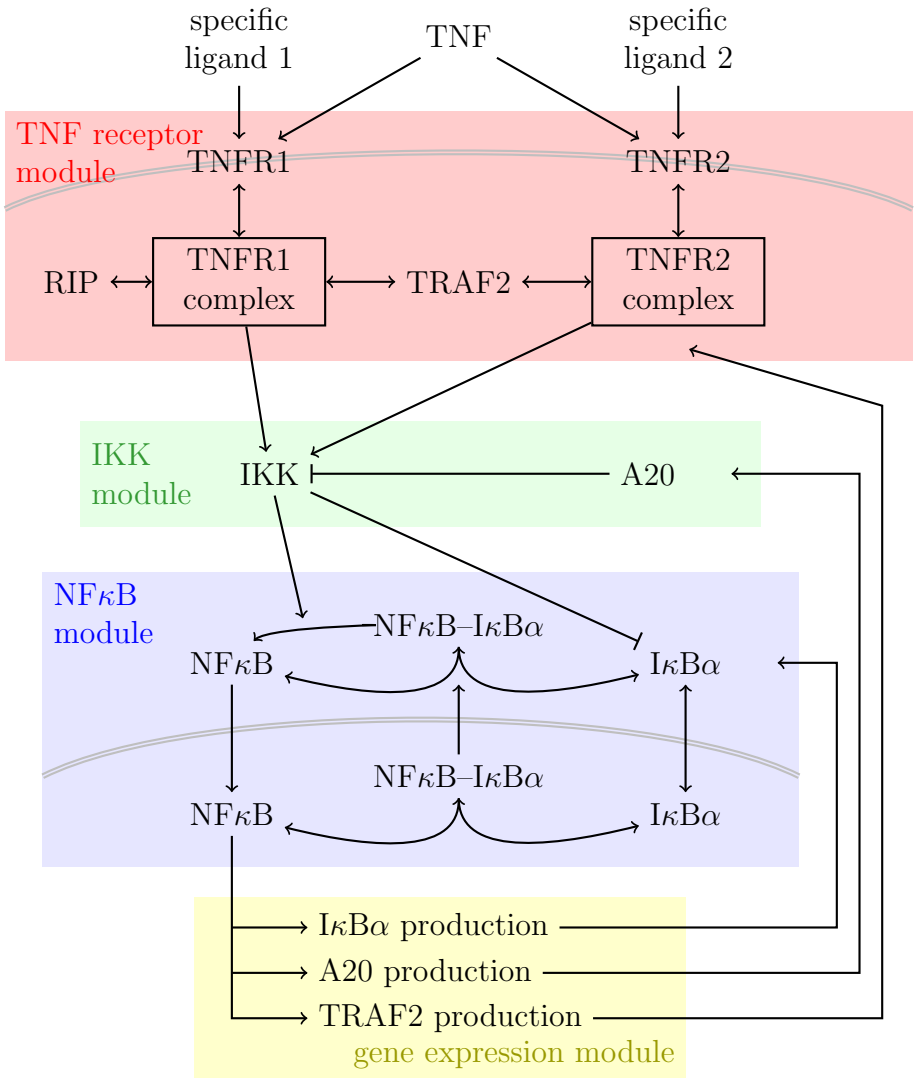

Figure 7.1: Coarse model structure of the TNF induced NF-κB pathway.

receptor 1 towards the NF-κB pathway requires both RIP1 and TRAF2 (or TRAF5 as a substitute) to be in the receptor complex (Micheau and Tschopp, 2003; Pobezinskaya *et al.*, 2008; Wertz *et al.*, 2004).

The situation is much more simple for the TNF receptor 2: the receptor directly recruits TRAF2, and the thus formed complex transmits the signal towards the NF-κB pathway (Bryde, 2004; Ye and Wu, 2000). A relevant additional effect is the ubiquitination and subsequent proteasomal degradation of TRAF2 at the TNF receptor 2 complex (Li *et al.*, 2002; Wu *et al.*, 2005). Such observations have not been made for TRAF2 when recruited to the TNF receptor 1 complex. The fact that both receptor complexes require TRAF2 for efficient signal transduction constitutes a crosstalk between the two receptor complexes, with potentially important effects on TNF signal transduction (Bryde, 2004).

The crucial mediator between the TNF receptor complexes and the NF-κB pathway is the I-κB kinase complex (IKK) which is activated at the TNF receptor complexes by TRAF2. Active IKK then phosphorylates I-κBα, which is subsequently degraded, thus liberating NF-κB to move to the nucleus (see Hayden and Ghosh, 2008, for a recent review). For the NF-κB, IKK and part of the gene expression modules, the species and reactions to be included in the model are adapted from the previous model developed by Lipniacki *et al.* (2004). Modifications are made in the transcription rates, where we assume a saturated rate expression, and in the activation of IKK, where we use the structure proposed more recently by Ashall *et al.* (2009). Whereas Lipniacki *et al.* (2004) explicitly consider intermediate complexes of IKK and its substrates, we use a quasi-steady state assumption for these complexes to arrive at a Michaelis-Menten type rate law for IKK mediated I-κBα degradation (Krishna *et al.*, 2006). An important additional inhibitor of NF-κB is the protein A20, for which we consider an inhibition of the NF-κB pathway acting directly on the level of IKK (Mauro *et al.*, 2006).

The complete lists of species, reactions and reaction rate expressions which are used in the model are given in the appendix, Sections B.1 and B.2.

7.2.2 Setting parameter values

After defining the species and reactions involved in the model, it remains to determine the model parameters, such as reaction rate constants or total concentrations of proteins subject to a conservation law. The complete list of nominal parameter values for the proposed TNF signal transduction model is given in the appendix, Section B.3, for reference. For each parameter, we also indicate how the value was obtained.

A substantial part of the parameter values could be taken from literature data, mainly from previously published models of the NF-κB signalling pathway (Ashall *et al.*, 2009; Hoffmann *et al.*, 2002; Lipniacki *et al.*, 2004, 2007), or from models of the TNFR1 complex formation and signal transduction (Schliemann, 2006; Schliemann *et al.*, 2007). Several parameters involved in the formation of the TNF receptor signalling complexes have been measured directly by Peter Scheurich and coworkers (Eissing, 2002; Grell *et al.*, 1998; Schliemann, 2006).

In support of the model construction described in this chapter, the degradation kinetics of TNFR2 and TRAF2 have been measured, and the corresponding parameters have directly been computed from the measurements under the assumption of a first order decay rate (Doszczak and Scheurich, unpublished data).

Yet, a significant number of parameters remain, for which neither previously determined values are available in the literature, nor values could be determined directly from experimental measurements. Part of these parameters do not have a significant effect on the model's trajectories (Sinini, 2008). For such parameters, we fix arbitrary values within a biologically reasonable order of magnitude. This is indicated by the comment "assumed" in the list of parameter values (Section B.3).

The values for the remaining part of the parameters need to be determined by identification from dynamical measurements. To this end, experiments have been conducted by the group of Peter Scheurich at the Institute of Cell Biology and Immunology (University of Stuttgart). In these experiments, Kym-1 cells in culture were subjected to specific stimulation of either the TNFR1 or the TNFR2, and the resulting dynamics in protein concentrations were measured by Western blotting (Doszczak and Scheurich, unpublished data). In total, 14 parameter values for the model have to be determined from these measurements by parameter estimation methods.

Over the last decade, large efforts have been made in parameter estimation for biochemical reaction networks from dynamical measurements (Balsa-Canto *et al.*, 2008; Chou *et al.*, 2006; Feng and Rabitz, 2004; Polisetty *et al.*, 2006; Raffard *et al.*, 2008; Voss *et al.*, 2004). Yet significant challenges remain, which are typically due to non-linearity of the models, non-convexity and even non-continuity of the employed performance functions (Ljung, 2008; Radde, 2009). Constraints from the experimental side such as large measurement uncertainties, limited measurement frequency and the difficulty to measure absolute concentration values on a cellular scale complicate matters further. Typical restrictions for parameter estimation algorithms are that they only find local optima (Balsa-Canto *et al.*, 2008; Raffard *et al.*, 2008; Voss *et al.*, 2004), are tailored to specific classes of models (Chou *et al.*, 2006; Polisetty *et al.*, 2006), or have a high computational cost (Feng and Rabitz, 2004). For the purpose of this thesis, the choice of nominal parameter values is not critical. In fact, we found it sufficient to adjust parameter values manually while comparing simulation results to measurement data visually. The relation between simulation results and measurement data which has been achieved with manual parameter tuning is shown in the next section.

7.2.3 Simulation results

The comparison between model simulation results and the experimental measurements is shown in Figure 7.2. Since the experiments provide only relative, not absolute, concentration data, the values are scaled to fit with the simulation results or, in the case of TRAF2, the experimentally determined initial condition. The comparison indicates a good qualitative fit of the model results to the available experimental data. There is a significant difference between experimental data and simulation results for TNFR1 stimulation after about 70 minutes. However, this might be explained by the fact that Kym-1 cells quickly activate the apoptotic pathway after TNFR1 stimulation, which has not been included in our model.

For the TNFR2 stimulation, most of the data points are fitted very well. The export of NF-κB from the nucleus between 50 and 70 minutes after stimulation seems to be slower in the model than observed in experiments. However, the timing of this export corresponds to the rise of the cytosolic I-κBα amount, and the fit for the NF-κB data cannot be

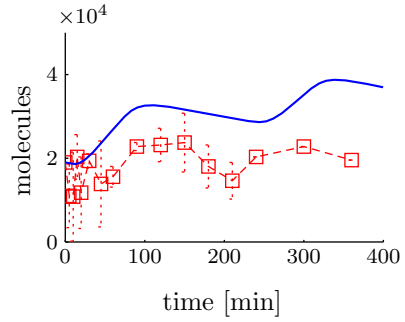

(a) TRAF2 amount (TNFR1 stimulation)

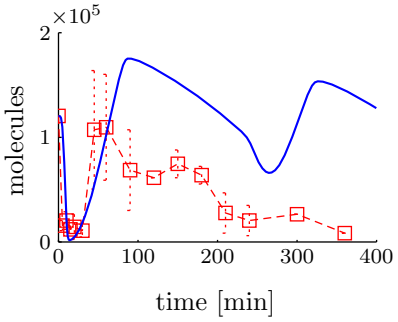

(b) cytosolic I-κBα amount (TNFR1 stimulation)

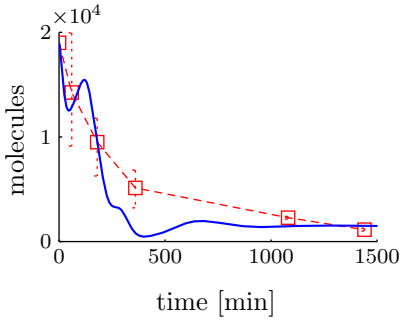

(c) TRAF2 amount (TNFR2 stimulation)

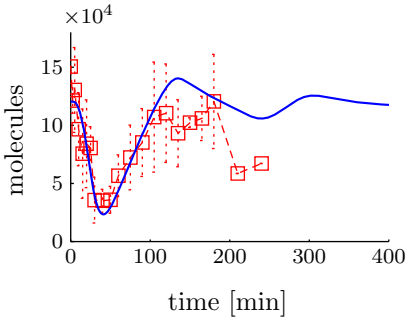

(d) cytosolic I-κBα amount (TNFR2 stimulation)

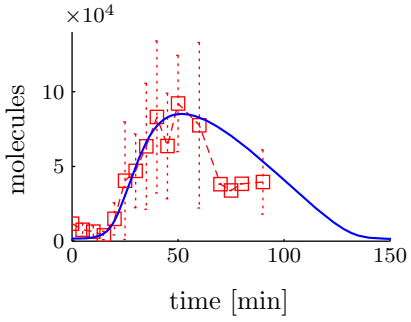

(e) nuclear NF-κB amount (TNFR2 stimulation)

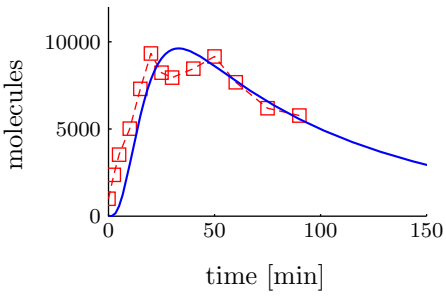

(f) active IKK amount (TNFR2 stimulation)

Figure 7.2: Simulation results for the TNF network model and comparison to experimental data. Lines: simulation results; squares: experimental data points. Errorbars on squares indicate standard deviation of experimental data. For all data points, cell cultures have been stimulated with 10 $\frac{\text{ng}}{\text{ml}}$ TNF ligand. Experimental measures have been taken to assure specificity for either TNFR1 or TNFR2, as indicated below the individual figures.

Table 7.1: Four stimulation cases for the TNF network model. Numbers given in the table correspond to TNF ligand amount used in the individual cases.

Identifier	TNFR1 stimulation	TNFR2 stimulation
LL	$0.01\ \frac{\text{ng}}{\text{ml}}$	$0.01\ \frac{\text{ng}}{\text{ml}}$
HL	$10\ \frac{\text{ng}}{\text{ml}}$	$0.01\ \frac{\text{ng}}{\text{ml}}$
LH	$0.01\ \frac{\text{ng}}{\text{ml}}$	$10\ \frac{\text{ng}}{\text{ml}}$
HH	$10\ \frac{\text{ng}}{\text{ml}}$	$10\ \frac{\text{ng}}{\text{ml}}$

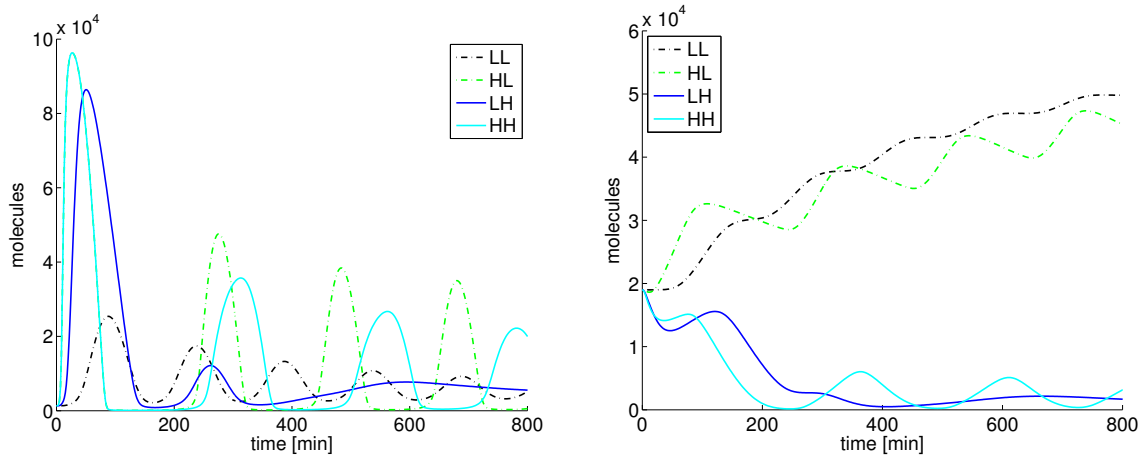

(a) Nuclear NF-κB activity

(b) Amount of TRAF2

Figure 7.3: Model simulation results with four different mixed stimulations. See Table 7.1 for the definition of the stimulation strengths.

improved without compromising the fit of the I-κBα data. One possible experimental reason for this discrepancy is that NF-κB might be precluded from the measurement while being exported from the nucleus.

In a second step, we use the model in a predictive way to study different scenarios for co-stimulation of the two TNF receptor types. Each of the receptor types is either stimulated weakly or strongly, resulting in a total of four scenarios simulated with the TNF network model. The resulting trajectories for nuclear NF-κB activity and TRAF2 amount are shown in Figure 7.3.

7.3 Analysis of oscillatory behaviour

The simulations described in the previous section result in oscillatory trajectories for some of the stimulation cases. In fact, oscillations in nuclear NF-κB activity have attracted significant attention over the past years (Ashall *et al.*, 2009; Krishna *et al.*, 2006; Nelson

et al., 2004). The idea now emerges that genes under the control of NF-κB respond differentially not only to the amount of NF-κB, but also to the temporal characteristics of its activity (Ashall *et al.*, 2009). In this section, we use analysis methods developed in this thesis to further understand the mechanisms involved in oscillatory NF-κB activity. The bifurcation search method developed in Chapter 5 and the robustness analysis method developed in Chapter 6 are used to study the influence of parameter values and specific interactions on the existence and properties of sustained oscillations.

7.3.1 Searching a Hopf bifurcation

The bifurcation search method developed in Chapter 5 is used to find Hopf bifurcation points in the TNF network model, i.e. parameter values where limit cycles emerge or vanish. We consider again the four scenarios of TNF receptor stimulation defined in Table 7.1 and compare them to each other. The simulations shown in Figure 7.3 already indicate that the stimulation type has a significant effect on the existence and properties of oscillations. The analysis in this section aims at understanding whether oscillations are affected by similar parameters in all stimulation cases or not.

In all four stimulation cases, the bifurcation search algorithm is able to locate a Hopf bifurcation within physiologically reasonable parameter variations. The suggested parameter variations are summarized in Table 7.2. Note that the stimulation where the TNFR1 is strongly and the TNFR2 weakly stimulated (HL stimulation case) yields an unstable equilibrium point and sustained oscillations for nominal parameters, while the other three cases give an asymptotically stable equilibrium point. Consequently, converse parameter changes are suggested to achieve a Hopf bifurcation for the HL stimulation case, compared to the other three. In general, the suggested parameter variations for a Hopf bifurcation are significantly smaller for the HH stimulation case than for the other cases. This indicates that oscillations are less robust, or more dependent on internal cellular conditions, under TNF receptor co-stimulation than if only one of the receptor types is being stimulated.

Apart from the case where both receptor types are only weakly stimulated, the most significant parameter changes are consistently suggested on the level of the IKK activity regulation. As second most relevant part of the system, we can identify the expression of the I-κBα gene. The implications of these results are discussed in Section 7.3.3, together with the results from the kinetic perturbation analysis obtained in Section 7.3.2.

7.3.2 Robustness of oscillations with respect to kinetic perturbations

As an alternative approach to estimate the model variations which perturb the system from non-oscillating to oscillating or vice-versa, we apply the dynamical robustness analysis method for kinetic perturbations from Section 6.3. Again, we consider the four different stimulation cases defined in Table 7.1. For the analysis with kinetic perturbations, reversible reactions are split up into two elementary reactions, one for the forward and the other for the reverse path.

For the analysis, we consider only perturbations where existing interactions are perturbed, i.e. the interaction structure of the system is not modified. The resulting non-robust kinetic perturbations are shown in Tables 7.3–7.6 for the four stimulation cases.

Table 7.2: Parameter variations leading to a Hopf bifurcation in the TNF network model for different stimulation cases. See Table 7.1 for a definition of the four stimulation cases. Parameter variations for a Hopf bifurcation are indicated through a percent change compared to the nominal values.

Param.	LL	HL*	LH	HH
k_{A8}	-0.5%	+3.3%	-39.9%	-5.7%
k_{A10c}	0.0%	+0.1%	-8.7%	0.0%
k_{A12}	0.0%	0.0%	+60.0%	+1.4%
k_{A13}	0.0%	0.1%	-25.3%	-0.4%
k_{B1a}	+13.8%	-35.6%	+83.7%	+10.8%
k_{B1b}	+0.2%	0.0%	-28.2%	+1.5%
k_{B3a}	+14.0%	-70.9%	+125.2%	+4.0%
A20s	+0.2%	-60.7%	-34.3%	-0.2%
k_{C4}	-8.3%	+51.7%	-40.8%	-1.6%
k_{C6}	0.0%	+0.8%	+0.9%	0.0%
k_{D1a}	+77.7%	-42.3%	+89.0%	+3.3%
k_{D1b}	+69.3%	-16.6%	+29.9%	-1.4%
k_{D3b}	+0.4%	-12.3%	+47.6%	+2.8%
k_{D5b}	+0.4%	+4.9%	+61.0%	-1.0%

*The equilibrium point is nominally unstable for the HL stimulation case.

Only perturbations below a certain threshold (depending on the stimulation case) are shown in the tables. For the LL stimulation case, the most fragile reaction is the degradation of I-κB transcript. This confirms the relevance of the properties of the I-κB gene expression for oscillations. However, from the bifurcation search in the previous section, the specific fragility at the transcript degradation has not been observed. This may be due to the fact that a saturation cannot be introduced in this reaction by parameter variations alone.

The two cases where only one receptor type is stimulated (LH and HL) appear to be quite robust with respect to kinetic perturbations. We find only few fragile interactions, and none of them show a strong fragility. In contrast, the HH case, where both receptor types are stimulated, is quite close to a Hopf bifurcation under kinetic perturbations, and there are many fragile interactions. This confirms the finding from the bifurcation search in the previous section, that the system is less robust with respect to existence of oscillations in the co-stimulation case than if only one receptor type is stimulated.

Based on the results of the previous investigation, let us consider the kinetic perturbations for two of the previously found fragile interactions more closely.

First, a fragile interaction with respect to kinetic perturbations in the HH stimulation case is the influence of A20 on reaction v_{B3}. This reaction corresponds to the A20-inhibited recycling of IKK to the neutral form. As indicated in Table 7.6, an increase in

Table 7.3: Fragile kinetic perturbations in the TNF network model for the LL stimulation case. Only perturbations where $\Delta_{ij}^* \leq 0.8$ are shown.

Reaction	Species	Δ_{ij}^*	ω^*
v_{C3}	NI	-0.68	$6.8 \cdot 10^{-4}\ \frac{1}{\mathrm{s}}$
v_{C4}	NFkB	-0.46	$6.8 \cdot 10^{-4}\ \frac{1}{\mathrm{s}}$
v_{C5} (forward)	NFkBn	-0.33	$7.3 \cdot 10^{-4}\ \frac{1}{\mathrm{s}}$
v_{C5} (forward)	IkBn	0.68	$7.5 \cdot 10^{-4}\ \frac{1}{\mathrm{s}}$
v_{D2}	IkBt	-0.12	$7.0 \cdot 10^{-4}\ \frac{1}{\mathrm{s}}$

Table 7.4: Fragile kinetic perturbations in the TNF network model for the HL stimulation case. Only perturbations where $\Delta_{ij}^* \leq 0.8$ are shown.

Reaction	Species	Δ_{ij}^*	ω^*
v_{C3}	IKKa	-0.79	$7.3 \cdot 10^{-4}\ \frac{1}{\mathrm{s}}$
v_{C5} (forward)	IkBn	-0.75	$5.9 \cdot 10^{-4}\ \frac{1}{\mathrm{s}}$
v_{D2}	IkBt	0.67	$6.9 \cdot 10^{-4}\ \frac{1}{\mathrm{s}}$
v_{D3}	NFkBn	-0.64	$7.3 \cdot 10^{-4}\ \frac{1}{\mathrm{s}}$

Table 7.5: Fragile kinetic perturbations in the TNF network model for the LH stimulation case. Only perturbations where $\Delta_{ij}^* \leq 0.8$ are shown.

Reaction	Species	Δ_{ij}^*	ω^*
v_{A13}	TNFR2C1	-0.52	$1.6 \cdot 10^{-4}\ \frac{1}{\mathrm{s}}$
v_{B2}	IKKa	-0.31	$1.9 \cdot 10^{-4}\ \frac{1}{\mathrm{s}}$
v_{C2} (reverse)	IkBt	-0.30	$1.9 \cdot 10^{-4}\ \frac{1}{\mathrm{s}}$
v_{D1}	NFkBn	-0.27	$1.9 \cdot 10^{-4}\ \frac{1}{\mathrm{s}}$
v_{D2}	IkBt	-0.77	$5.9 \cdot 10^{-4}\ \frac{1}{\mathrm{s}}$
v_{D4}	A20t	-0.79	$2.2 \cdot 10^{-4}\ \frac{1}{\mathrm{s}}$
v_{D6}	TRAFt	-0.35	$1.7 \cdot 10^{-4}\ \frac{1}{\mathrm{s}}$

Table 7.6: Fragile kinetic perturbations in the TNF network model for the HH stimulation case. Only perturbations where $\Delta_{ij}^* \leq 0.4$ are shown.

Reaction	Species	Δ_{ij}^*	ω^*
v_{A3} (reverse)	TRAFt	-0.32	$6.5 \cdot 10^{-4}\ \frac{1}{\mathrm{s}}$
v_{A6}	TRAF	-0.34	$6.5 \cdot 10^{-4}\ \frac{1}{\mathrm{s}}$
v_{A8}	TNFR1C1	0.39	$6.3 \cdot 10^{-4}\ \frac{1}{\mathrm{s}}$
v_{B1}	IKKi	0.21	$6.4 \cdot 10^{-4}\ \frac{1}{\mathrm{s}}$
v_{B1}	TNFR1C1	-0.30	$6.5 \cdot 10^{-4}\ \frac{1}{\mathrm{s}}$
v_{B2}	IKKa	-0.34	$5.6 \cdot 10^{-4}\ \frac{1}{\mathrm{s}}$
v_{B3}	A20	-0.21	$6.2 \cdot 10^{-4}\ \frac{1}{\mathrm{s}}$
v_{B4} (reverse)	A20t	0.22	$6.2 \cdot 10^{-4}\ \frac{1}{\mathrm{s}}$
v_{C2} (reverse)	IkBt	-0.26	$5.1 \cdot 10^{-4}\ \frac{1}{\mathrm{s}}$
v_{C7} (forward)	IkB	-0.36	$5.9 \cdot 10^{-4}\ \frac{1}{\mathrm{s}}$
v_{D1}	NFkBn	-0.23	$5.1 \cdot 10^{-4}\ \frac{1}{\mathrm{s}}$
v_{D2}	IkBt	-0.12	$6.4 \cdot 10^{-4}\ \frac{1}{\mathrm{s}}$
v_{D3}	NFkBn	0.17	$6.2 \cdot 10^{-4}\ \frac{1}{\mathrm{s}}$
v_{D4}	A20t	-0.32	$6.0 \cdot 10^{-4}\ \frac{1}{\mathrm{s}}$
v_{D5}	NFkBn	-0.26	$6.5 \cdot 10^{-4}\ \frac{1}{\mathrm{s}}$
v_{D6}	TRAFt	0.33	$6.4 \cdot 10^{-4}\ \frac{1}{\mathrm{s}}$

the inhibition strength (corresponding to a negative $\Delta_{B3,\mathrm{A20}}^*$) induces a Hopf bifurcation in the system. The effect of the kinetic perturbation on oscillations in nuclear NF-κB activity is shown in Figure 7.4(a). Clearly, a perturbation of this interaction has a profound effect on the existence and amplitude of oscillations, even for rather small perturbations.

A second fragile point with biological significance is the slope of the reaction rate v_{A13}. The reaction A13 describes the degradation of TRAF2 at the TNFR2 complex, with respect to the reactant species TNFR2C1. As indicated in Table 7.5, in the LH stimulation case, a decrease in this slope leads to a Hopf bifurcation. From a biochemical perspective, such a decrease in the slope may be the result of a saturation in the reaction rate. Therefore, in this specific case, we consider a kinetic perturbation which is induced by gradually increasing the saturation with the Michaelis-Menten type perturbed reaction rate

$$\tilde{v}_{A13} = \frac{\tilde{k}_{A13}[\mathrm{TNFR1C1}]}{1 + M_{A13}[\mathrm{TNFR1C1}]}, \tag{7.1}$$

where M_{A13} is an implicit parameter with nominal value $M_{A13} = 0$. For a given kinetic perturbation $\Delta_{A13,TNFR2C1}$, the perturbed value of M_{A13} is computed from (6.18) with

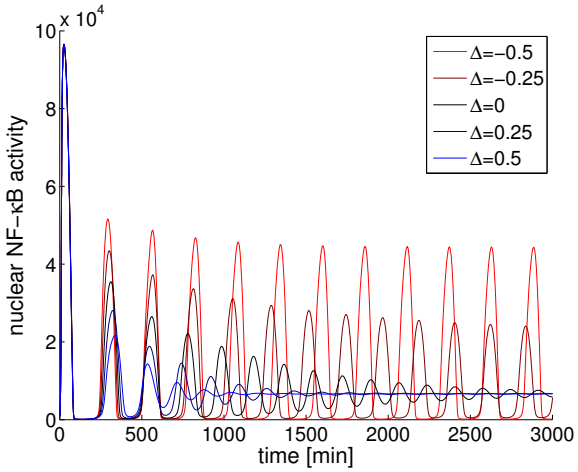

(a) Perturbation of the interaction A20 → v_{B3} in the stimulation case HH. Sustained oscillations with a period of about 200 min occur for $\Delta_{B3,\mathrm{A20}} = -0.5$ and $\Delta_{B3,\mathrm{A20}} = -0.25$.

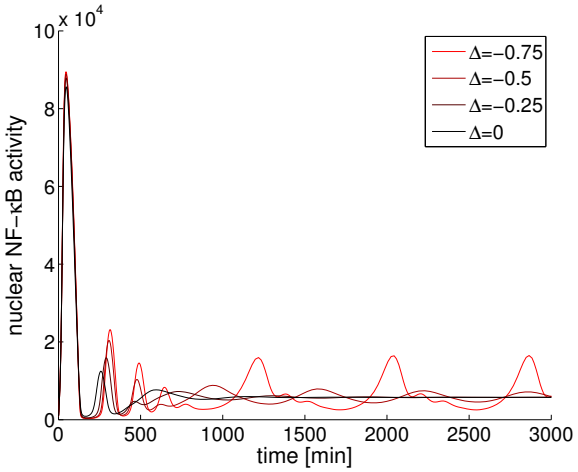

(b) Perturbation of the saturation of TNFR2C1 in v_{A13} in the stimulation case LH. Sustained oscillations with a period of about 800 min occur for $\Delta_{A13,TNFR2C1} = -0.75$.

Figure 7.4: Variation of oscillatory behaviour through kinetic perturbations in the TNF network model

$\eta_{ij} = 1$ as

$$M_{A13} = -\frac{1}{[\mathrm{TNFR1C1}]_0} \frac{\Delta_{A13,TNFR2C1}}{1 + \Delta_{A13,TNFR2C1}}. \tag{7.2}$$

The value for $\tilde{k}_{A13}$ is chosen such that $\tilde{v}_{A13}(x_0) = v_{A13}(x_0)$, where x_0 is the considered steady state. Varying the saturation beyond the critical value $\Delta^*_{A13,TNFR2C1} = -0.52$ leads to a Hopf bifurcation and results in sustained oscillation in the system as illustrated by the simulation results shown in Figure 7.4(b).

The different critical frequencies computed for the two kinetic perturbation cases considered above already indicate that the occuring periodic oscillations are significantly different with respect to their frequency. Indeed, in the first case, the observed oscillation period is about 200 min (predicted at Hopf bifurcation: 170 min), while in the second case, the period is about 800 min (predicted at Hopf bifurcation: 650 min). The difference in predicted and observed frequency may be explained by a change in frequency as the perturbation goes beyond the critical value where the Hopf bifurcation occurs. These observations indicate a variety of oscillatory behaviour in the TNF regulated NF-κB pathway which has not been observed in previous studies. The fact that the two different ranges for critical frequencies occur in several perturbation cases indicates that different oscillatory modes are not just relevant for one specific interaction, but are an inherent property of the system. Note however that the low frequency oscillations only appear in cases where the TNFR2 is stimulated, while the higher frequency appears in all four cases. The implications of these different oscillatory modes are discussed in Section 7.3.3.

7.3.3 Discussion of the results on oscillations

Let us now discuss the implications of the previous results for the oscillatory behaviour in TNF induced NF-κB signalling. From simulations, for example Figure 7.3, we observe that the existence and properties of oscillations depend on the type of stimulation. This indicates that the oscillations are at least partially controlled by factors outside of the core NF-κB/I-κB signalling module. However, the main influential factors cannot be deduced from simulations.

The results of the multiparametric bifurcation search method, given in Section 7.3.1, indicate parameters which seem to be most relevant for the existence of sustained oscillations. In all four stimulation cases, we find that parameters related to I-κB gene expression are relevant in this respect. In the cases where a high TNF stimulus is applied, we observe that also parameters involved in the regulation of IKK activity play a significant role. In summary, the results of the bifurcation search can be interpreted in the way that, for a given stimulus, existence of sustained oscillations is mainly controlled by parameters intrinsic to the IKK/NF-κB pathway.

The analysis based on kinetic perturbations gives additional insight into the properties of oscillations in NF-κB activity. First, we are able to confirm the finding from the bifurcation search, that I-κB gene expression characteristics are of high relevance for oscillations. Also, the relevance of the IKK regulation mechanism is confirmed for the cases where a high TNF stimulus is applied. These findings are in agreement with previous studies, which have already indicated the relevance of IKK activity regulation for existence of sustained oscillations in NF-κB activity (Hayot and Jayaprakash, 2006; Park *et al.*, 2006).

Both the bifurcation search and the robustness analysis with kinetic perturbations indicate that the oscillations in the network are fragile towards variations in internal conditions for the co-stimulation case. This is in contrast to the exlusive stimulation of either receptor type, where existence or non-existence of sustained oscillations is much more robust. Giving a biological interpretation for this observation remains difficult, as long as no definite results on the biological function of NF-κB oscillations in relation to the different stimuli are available. Yet, regardless of what the function may be, our observation indicates that this function is more affected by additional influences, if both receptor types are stimulated, compared to the case where only one receptor type is stimulated.

From robustness analysis with respect to kinetic perturbations, we discover in addition that a high stimulation of TNFR2 together with a weak stimulation of TNFR1 may give rise to oscillations with significantly higher period, about 800 minutes, compared to the period of about 200 minutes which is typically encountered in the other stimulation cases. To our knowledge, this is the first indication of different oscillatory modes in the TNF induced NF-κB network within a single model. At the moment, there is no experimental evidence of different oscillatory modes. However, recent findings suggest that the temporal characteristics of NF-κB activity play a major role for the induced gene expression (Ashall *et al.*, 2009; Nelson *et al.*, 2004; Tian *et al.*, 2005). This effect is mainly ascribed to a clustering of the genes under NF-κB control into an "early", "middle" and "late" group, among which the exact mechanisms of transcription initiation in response to NF-κB seem to be different (Tian *et al.*, 2005). Our observation of different oscillatory modes fits well

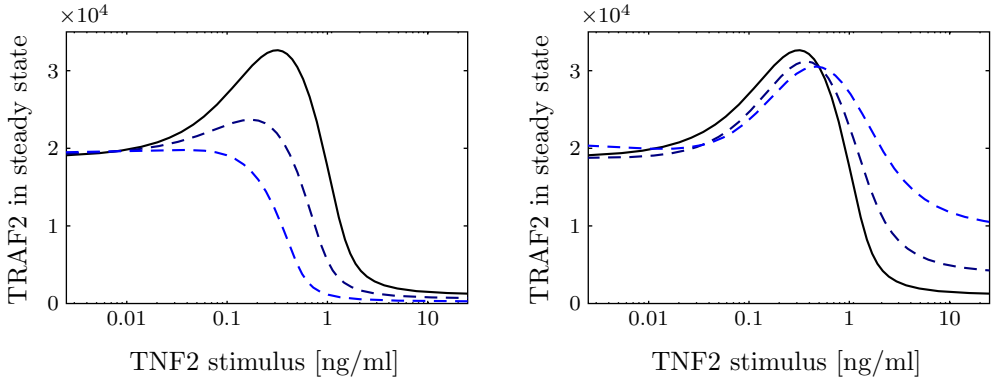

(a) Variation from nominal point with TNF2 $= 7.5 \cdot 10^{-3} \frac{\text{ng}}{\text{ml}}$. Sensitivity at the nominal point is reduced to weaken the increase in TRAF2 amount for an intermediate stimulus.

(b) Variation from nominal point with TNF2 $= 0.5 \frac{\text{ng}}{\text{ml}}$. Sensitivity at the nominal point is increased to weaken the reduction in TRAF2 amount for a high stimulus.

Figure 7.5: Sensitivity modification for the TNF network model. The goal is to vary the characteristics of the stationary TRAF2 curve with respect to a TNF2 stimulus. Full line: nominal response curve. Dashed lines: response curves with sensitivity modification achieved by kinetic perturbations.

to these results. In fact, such modes could provide a mechanism by which different stimuli can activate different NF-κB induced gene expression programs.

7.4 Sensitivity modification by kinetic perturbations

A stimulation of the TNFR2 has two conflicting effects on the long-term TRAF2 amount in the cell. First, Li *et al.* (2002) and Wu *et al.* (2005) have discovered that recruitment of TRAF2 to the receptor complex targets TRAF2 to proteasomal degradation. This effect is accounted for in the model by reaction A13. Second, the signal transduction from the TNFR2/TRAF2 complex activates NF-κB, which in turn upregulates the production of TRAF2. Using the mathematical model for the TNF signalling network developed in this chapter, we can make predictions about the net effect of a sustained TNFR2 stimulation on the resulting steady state, specifically the long-term TRAF2 concentration. As shown in Figure 7.5, up to a TNF stimulus of about $1 \frac{\text{ng}}{\text{ml}}$, the model predicts that the activating effect will dominate, while for higher stimuli it predicts a significant decrease of the steady state TRAF2 amount.

Using the sensitivity modification method proposed in Section 6.4, we investigate perturbations in the model which lead to specific variations in the dependence of the long-term TRAF2 amount with respect to a stimulation of the TNFR2.

First, we seek for a perturbation which reduces the stationary TRAF2 amount in the intermediate stimulus range of 0.1 to $1 \frac{\text{ng}}{\text{ml}}$ TNF. Therefore we construct a sensitivity modification which reduces the local sensitivity of the TRAF2 amount with respect to

Table 7.7: Suggested kinetic perturbations for a decrease of the sensitivity of TRAF2 with respect to the TNF2 stimulus by $|\bar{\sigma}|$, at a nominal stimulus of $7.5 \cdot 10^{-3}\,\frac{\text{ng}}{\text{ml}}$ and a nominal unscaled sensitivity of $9.6 \cdot 10^{4}\,\frac{\text{ml}}{\text{ng}}$.

Reaction	Species	Kinetic perturbation Δ_{ij} for a sensitivity change $\bar{\sigma}$ $[\frac{\text{ml}}{\text{ng}}]$	
		$\bar{\sigma}_{\text{TRAF}} = -4 \cdot 10^4$	$\bar{\sigma}_{\text{TRAF}} = -8 \cdot 10^4$
v_{A11}	TNFR2C0	0.016	0.074
v_{A13}	TNFR2C1	0	0.051
v_{A10b}	TNFR2L	0	0.039
v_{A3} (reverse only)	TRAFt	-0.26	-0.5

the concentration of TNFR2 ligand. The sensitivity modification is applied to the steady state reached for a stimulus of $7.5 \cdot 10^{-3}\,\frac{\text{ng}}{\text{ml}}$. The desired sensitivity change is achieved by kinetic perturbations as given in Table 7.7. Thereby, the linear programming approach as proposed in Section 6.4.2 has been used to select a kinetic perturbation of minimal 1–norm, with the constraint that no element of Δ should be less than -0.5. The kinetic perturbations shown in Table 7.7 are scaled as suggested in (6.9), and have been applied to the model as described in Section 6.2.4. Figure 7.5(a) shows the resulting changes in the global behaviour of the TRAF2 amount with respect to a varying stimulus. It illustrates that the suggested kinetic perturbations provide an effective way of reducing the peak in the TRAF2 amount for an intermediate stimulus, while not having a significant effect on the steady state TRAF2 amount for either a low or a high stimulus. From the results in Table 7.7, we conclude that the most effective way to reduce the intermediate peak in TRAF2 amount seems to be a saturation of the TRAF2 translation rate for increasing levels of the TRAF2 transcript. Such a saturation is biologically quite reasonable, and may for example be the consequence of a limitation in either ribosome activity, amino acid supply, or specific translation factors required for TRAF2 translation.

Second, we seek for a perturbation which reduces the decay of the TRAF2 amount for a strong stimulation of the TNFR2. For this problem, we choose the steady state corresponding to a TNF stimulus of $0.5\,\frac{\text{ng}}{\text{ml}}$ as nominal point. From this nominal point, we aim for a sensitivity modification by kinetic perturbations which flattens the TRAF2 curve for increasing TNF stimuli. In a first solution to this problem, the suggested perturbation implies an increase in the kinetic order of the TRAF2 translation reaction. However, since this is not biologically reasonable, a constraint has been added to the optimisation problem to prevent such a perturbation. When adhering to this constraint, we obtain the kinetic perturbations for the specified sensitivity change as shown in Table 7.8. As previously, we use the linear programming approach to minimise the 1–norm of the perturbation. Applying these perturbations to the system indeed results in an increased TRAF2 concentration for high TNF stimuli, as shown in Figure 7.5(b).

In contrast to the previous problem, the analysis with kinetic perturbations now suggests that the most effective way to achieve this effect is not a variation in TRAF2 production, but rather a saturation in the degradation of TRAF2 within the TNF receptor

Table 7.8: Suggested kinetic perturbations for an increase of the sensitivity of TRAF2 with respect to the TNF2 stimulus by $\bar{\sigma}$, at a nominal stimulus of $0.5\,\frac{\text{ng}}{\text{ml}}$ and a nominal unscaled sensitivity of $-1.96 \cdot 10^4 \frac{\text{ml}}{\text{ng}}$.

Reaction	Species	Kinetic perturbation Δ_{ij} for a sensitivity change $\bar{\sigma}$ $[\frac{\text{ml}}{\text{ng}}]$ $\bar{\sigma}_{\text{TRAF}} = 1 \cdot 10^4$	$\bar{\sigma}_{\text{TRAF}} = 1.8 \cdot 10^4$
v_{A11}	TNFR2C0	-0.28	-0.5
v_{A13}	TNFR2C1	-0.25	-0.44
v_{A10b}	TNFR2L	-0.19	-0.34
v_{A3} (forward only)	TRAF	0	0.28

complex. This is likely to occur if proteasome activity or the mechanisms tagging TRAF2 for proteasomal degradation are saturated.

In summary, the sensitivity modification approach with kinetic perturbations is able to detect efficient ways of influencing the behaviour of the TNF signalling system with respect to stimulus strength. For intermediate TNF stimuli, a reduction of the TRAF2 amount seems to be achieved most efficiently by a perturbation of the TRAF2 production, while an increase in the TRAF2 amount for high stimuli seems to be most easily reached by a variation in the degradation mechanisms.

7.5 Discussion of the TNF network model analysis

In this chapter, a dynamical model for the interaction of TNF receptor 1 and 2 via the adaptor protein TRAF2, and the TNF induced signal transduction by the NF-κB pathway is developed. The model parameters are adjusted to match experimental data, which is available for the specific stimulation of either TNFR1 or TNFR2. The model is then used to obtain new insights into the system with the help of the analysis tools developed in Chapters 5 and 6.

The model analysis conducted in this chapter pursues two goals: first, to understand the relevance of specific mechanisms in the model for occurrence of sustained oscillations, and second, to evaluate how perturbations affect the TRAF2 steady state response for a varying TNFR2 stimulation.

For the first goal, as initial step the bifurcation search method developed in Chapter 5 is applied. In accordance with previous studies, the analysis confirms the possibility of sustained oscillations for the proposed model of the TNF induced NF-κB pathway. Second, the bifurcation search indicates which parameters are most relevant for the existence of sustained oscillations. It suggests that, for all considered stimulation cases, similar mechanisms are responsible for the generation of sustained oscillations. The relevant mechanisms proposed here are in concordance with the mechanisms found to be relevant for earlier models of the NF-κB pathway.

To analyse the sustained oscillations further, we also apply the robustness analysis with respect to kinetic perturbations as developed in Chapter 6. The results of this analysis

suggest that the system exhibits modes of oscillations which are very different in frequency, mainly depending on the type of stimulation. To our knowlegde, this observation has not been made previously, and should be tested experimentally for further evidence.

Both the bifurcation search and the robustness analysis with kinetic perturbations indicate that existence or non-existence of sustained oscillations is rather robust with respect to internal perturbations, if only one receptor type is stimulated strongly. In contrast, for the co-stimulation of both receptor types, we observe that a Hopf bifurcation can be induced by small perturbations in the internal mechanisms.

In the second model analysis task, we consider the dependence of the long-term TRAF2 amount on the TNF stimulus strength, where only the TNFR2 is stimulated. This is of particular interest because of the bimodal response seen in the model, in the sense that TRAF2 is first accumulating for an increasing stimulus up to about $0.5\,\frac{\mathrm{ng}}{\mathrm{ml}}$, but then reduces to far below the original level for higher stimuli.

We have used the method of sensitivity modification by kinetic perturbations proposed in Chapter 6 to evaluate what kind of model perturbations would most efficiently achieve specific variations in the TRAF2 response to a stimulation of the TNFR2. A remarkable result from this study is that two qualitatively different modifications are suggested for the two cases being considered. Depending on the considered stimulus range, the two modifications are either targeting the production or the degradation of TRAF2 to achieve a change in the sensitivity of TRAF2 with respect to a TNFR2 stimulation. This result may be useful to guide further experimental studies, and eventually to suggest effective drug targets for a specific desired effect on the system.

Chapter 8

Conclusions

8.1 Summary and discussion

In this thesis, new methods for the analysis of parametric uncertainty in dynamical models for biochemical reaction networks are developed. The methods concern both uncertainty and robustness analysis. In particular, the challenges of non-linearity, dependence of the steady state on uncertain parameters, and the need to consider simultaneous uncertainty in several parameters are embraced throughout.

The methods introduced in this thesis depend on different techniques and concepts from the fields of convex optimisation and robust control theory. The steady state analysis relies mainly on semidefinite programming. Based on a control engineering perspective, the feedback loop breaking approach is suggested to deal with the robustness of dynamical behaviour. As another method for robustness analysis, kinetic perturbations are introduced and studied with the help of structured singular values, using well established techniques from robust control theory.

In Chapter 3, semidefinite programming is used to construct computationally efficient infeasibility certificates for the steady state equation under uncertainty. These certificates are used to construct an algorithm both for the steady state uncertainty analysis and the robustness analysis of steady states with respect to parametric uncertainty. The advantage of this approach compared to established methods is that guaranteed bounds on the steady state variations can be obtained even for large uncertainties.

The steady state uncertainty analysis also forms the basis for one of the methods developed in Chapter 4. Thereby, robust stability with respect to parametric uncertainty is studied. A solution to the robustness problem is proposed, where the steady state bounds are used to translate the problem to the question of robust stability for a linear differential inclusion. For the latter question, classical tests are used to check robust stability.

In addition, a feedback loop breaking approach is suggested in Chapter 4 for the robustness analysis of qualitative dynamical behaviour in biochemical reaction networks. This approach leads to the construction of robustness certificates via the Positivstellensatz and linear programming. Importantly, with this approach it is also possible to study the robustness of instability, which is of relevance in the analysis of complex dynamical behaviour, such as oscillations or bistability.

A limitation of the approaches developed in Chapters 3 and 4 is that the computational complexity increases significantly with the number of variables in the underlying optimisation problems. From experience, the steady state uncertainty analysis as proposed in Chapter 3 remains computationally feasible up to about thirty variables, including states,

parameters, and higher order terms. For the robust stability analysis based on the Jacobian (Section 4.2), ten reactions may already be too large. For the loop breaking based robustness analysis (Section 4.3), between five and ten variables (states and parameters) seems feasible, although the use of a partial analytical solution for the steady state, as in Section 4.3.3, may reduce the computational burden. Of course, these values are only rough estimates and may improve with advances in optimisation algorithms or computing power. Despite this limitation, the examples given in Chapters 3 and 4 illustrate that the proposed methods are a valuable tool for the analysis of small biochemical reaction networks.

The feedback loop breaking approach is also applied in Chapter 5, where it is used to characterise topological equivalence of two models by the transfer functions of appropriate open loop input–output systems. Based on this characterisation, a bifurcation search method is developed which allows to find bifurcations of specific type in a high-dimensional parameter space. The results from the search method provide efficient upper bounds for the robustness analysis suggested in Chapter 4, but may also be used independently to obtain estimates for the influence of individual parameters on the qualitative dynamical behaviour of the network.

In Chapter 6, we introduce the new uncertainty class of kinetic perturbations, which are particularly suited for the analysis of biochemical reaction networks. By definition, these perturbations affect the reaction rate slopes in steady state, but not the steady state itself. It is shown that kinetic perturbations relate in a one–to–one fashion to specific parametric perturbations in generalised mass action and enzymatic networks. Apart from parametric uncertainties, kinetic perturbations can also describe a structural uncertainty of the interactions within the network. We demonstrate that a robustness analysis with kinetic perturbations can be conducted efficiently by classical robust control methods, and that such an analysis gives valuable insight into potentially fragile interactions within the network. In addition, the concept of kinetic perturbations is used to construct system modifications which affect the local steady state sensitivity in a specific way, and thereby allow to shape a stationary stimulus–response curve in a desired way. A limitation of the kinetic perturbation concept is that only one steady state can be analysed at a time. However, in the analysis, it is sometimes desirable to consider ranges of steady states, which relates back to the methods discussed in the preceding chapters.

In addition to the methodological results, we have developed a dynamical model of TNF signal transduction, in particular TNF receptor complex formation and anti-apoptotic signalling by the NF-κB pathway. The model was fitted to experimental data, and the fitted model was analysed with methods developed in this thesis. From this analysis, we obtained several biologically significant predictions, such as the possibility of different oscillatory modes in the model. Together with the examples discussed in earlier chapters, the analysis of the TNF network model illustrates the broad applicability of the methods developed in this thesis, as well as the relevance of conclusions which can be drawn from such an analysis.

In conclusion, the methods developed in this thesis constitute significant progress towards a stringent uncertainty and robustness analysis for the dynamics of biochemical reaction networks under parametric uncertainty. As explained above, several issues remain open for further research. In the following section, we discuss possible research directions in this context.

8.2 Outlook

This thesis focuses almost exlusively on parametric uncertainty, where the structure of the network is assumed to be known. However, in a thorough uncertainty analysis, both structural and parametric uncertainty need to be considered. One aspect of structural uncertainty are dynamic perturbations (Jacobsen and Cedersund, 2008), which may e.g. result from unmodelled species in the network. In order to capture both structural and parametric uncertainty, a coupling of the methods developed in this thesis to methods of structural uncertainty analysis may be useful. Such a coupled analysis is already done in linear robust control theory (Zhou *et al.*, 1996), and the development of similar approaches for the analysis of biochemical reaction networks is desirable.

An additional point concerns the high stochasticity in intracellular processes (Rao *et al.*, 2002). Biological processes face the problem of maintaining their function despite a high amount of noise in both the environment and the individual process itself. This defines a robustness problem different to the one considered in this thesis, but also of high relevance for biological systems. While some effects of stochasticity can be linked to parametric uncertainty and thus fall within the scope of this thesis, most analyses will need to be done within a stochastic framework. To give just one example, it has been observed that, due to stochastic effects, sustained oscillations may still persist in a biochemical reaction network, although a deterministic model suggests asymptotic convergence to an equilibrium point (Lang *et al.*, 2009). A relevant question in close relation to the results of this thesis is then, how much the parameter regions in which oscillations occur can be extended due to such an effect of stochasticity.

From a more general perspective, parametric uncertainty in models for cellular processes is often related to heterogeneity among individual cells of a population. Under the precondition that this heterogeneity can be quantified efficiently (Waldherr *et al.*, 2009b), it would be interesting to set the results of this thesis in relation to cellular heterogeneity.

Let us next give an outlook on more specific ideas to build on the results obtained in this thesis. The steady state infeasibility certificates described in Chapter 3 are restricted to continuous models with polynomial or rational equations. An extension of this approach to other system classes, involving e.g. non-polynomial equations or switching behaviour, is a subject of ongoing research (Hasenauer *et al.*, 2009a). Furthermore, the applicability of the method would greatly benefit from a reduction in computational complexity. One way to achieve this might be a modularization of the system, where the uncertainty analysis can be applied iteratively to the individual modules, thereby avoiding the exponential growth of the computational cost with problem size. Such a modularization has been implemented for one example with convincing results (Hasenauer, 2008), but a general framework for this approach is still open. Using the infeasibility certificates, it is also possible to estimate parameter sets which are compatible with uncertain measurement data (Borchers *et al.*, 2009; Hasenauer *et al.*, 2009b) or to perform experimental design with little or no *a priori* information (Hasenauer *et al.*, 2009b).

Regarding the feedback loop breaking approach, two lines of further research are conceivable, particularly aiming at systems with multiple feedback circuits. First, for a system with multiple feedback circuits, the choice of the loop breaking point could be a subject of further theoretical investigations. Second, it may be possible to extend the results by using a MIMO loop breaking approach. Such investigations may also give insights into

the relevance of multiple feedback circuits in biochemical networks, which is a question of significant interest in the field (Brandman *et al.*, 2005; Kim *et al.*, 2008).

The appeal of kinetic perturbations for the analysis of biochemical reaction networks is due to the fact that they admit a natural relationship between changes in the reaction rate Jacobian and biochemically plausible variations in the network. It seems promising to explore further methodological applications of this concept, in addition to robustness analysis and sensitivity modification.

Finally, the analysis of the TNF model constructed in Chapter 7 yields several observations of biological significance, which should be tested experimentally. An experimental application of kinetic perturbations for sensitivity modification could also establish a new design approach for synthetic biology.

Appendix A

Proofs

A.1 Proof of Lemma 4.8

For simplicity of notation, we drop the dependence on χ of matrices A_o, B_o and C_o. By Schur's lemma, we have

$$\det(sI_n - A_o - B_oC_o) = \det \begin{pmatrix} sI_n - A_o & -B_o \\ -C_o & 1 \end{pmatrix}.$$

Let $(sI_n - A_o)_{-i} \in \mathbb{R}^{(n-1)\times n}$ denote the matrix $(sI_n - A_o)$ with the i-th row deleted. Then, by cofactor expansion (Lancaster and Tismenetsky, 1985),

$$\det \begin{pmatrix} sI_n - A_o & -B_o \\ -C_o & 1 \end{pmatrix} = 1 \cdot \det(sI_n - A_o) - \sum_{i=1}^{n} (-1)^{n+1+i} b_i \det \begin{pmatrix} (sI_n - A_o)_{-i} \\ -C_o \end{pmatrix},$$

where b_i is the i–th element of B_o. In the same way,

$$\det \begin{pmatrix} sI_n - A_o & -B_o \\ -C_o & 0 \end{pmatrix} = -\sum_{i=1}^{n} (-1)^{n+1+i} b_i \det \begin{pmatrix} (sI_n - A_o)_{-i} \\ -C_o \end{pmatrix}$$

and with Proposition 4.7 it follows that

$$\det(sI_n - A) = \det(sI_n - A_o) - \det \begin{pmatrix} sI_n - A_o & -B_o \\ C_o & 0 \end{pmatrix}. \tag{A.1}$$

s_0 is an eigenvalue of A if and only if $\det(s_0 I_n - A) = 0$. For condition *(i)*, we have $\det(s_0 I_n - A_o) \neq 0$, and thus, the equation

$$\frac{\det \begin{pmatrix} s_0 I_n - A_o & -B_o \\ C_o & 0 \end{pmatrix}}{\det(s_0 I_n - A_o)} = 1$$

is equivalent to s_0 being an eigenvalue of A. The claim then follows from (4.20). The other case where $\det(s_0 I - A_o) = 0$ is considered in condition *(ii)*, and (A.1) can be used directly to prove the claim.

□

A.2 Proof of Proposition 5.3

Note that $\tilde{\beta}$ is constant over $\mathcal{M}$ due to Assumption (A1). Consider the transfer function $G(\chi, s)$ for a constant $\chi \in \mathcal{M}$. For ease of notation, we drop the dependence on χ in the transfer function in the following.

It is well known from linear control theory that the argument of $G(j\omega)$ changes by $\tilde{\beta}\pi$ when varying ω from $-\infty$ to ∞ (D'Azzo and Houpis, 1975):

$$|\arg G(j\infty) - \arg G(-j\infty)| = \tilde{\beta}\pi.$$

The symmetry $G(j\omega) = \overline{G(-j\omega)}$ implies that $\arg G(j\infty) = -\arg G(-j\infty)$. From these two facts, it follows that the argument of $G(j\omega)$ spans the open interval $I_{\tilde{\beta}} = (-\frac{\tilde{\beta}\pi}{2}, \frac{\tilde{\beta}\pi}{2})$ for $\omega \in (-\infty, \infty)$. Moreover, by Definition 5.1 the condition $\omega_c \in \mathcal{R}(\chi)$ is equivalent to

$$\arg G(j\omega_c) = z\pi, \qquad z \in \mathbb{Z}.$$

If $\tilde{\beta}$ is even, the claim follows directly, since there are $\tilde{\beta} - 1$ different integers z such that $z\pi$ is inside the interval $I_{\tilde{\beta}}$. This corresponds directly to having $\tilde{\beta} - 1$ or more critical frequencies.

In the other case, if $\tilde{\beta}$ is odd, some additional reasoning is needed to prove the proposition. In this case one has

$$I_{\tilde{\beta}} = \left(-\frac{2l+1}{2}\pi, \frac{2l+1}{2}\pi\right),$$

for $l \in \mathbb{N}_0$ such that $\tilde{\beta} = 2l + 1$. Thus, the borders of the interval $I_{\tilde{\beta}}$ are not at integer multiples of π, which implies that in this case there are $\tilde{\beta}$ different integers z such that $z\pi$ is in $I_{\tilde{\beta}}$, corresponding to at least $\tilde{\beta}$ critical frequencies. □

A.3 Proof of Theorem 5.6

The proof of Theorem 5.6 uses the Argument Principle from complex analysis, which is repeated here for completeness (Whittaker and Watson, 1965).

Theorem A.1 (The Argument Principle). *Let f be a meromorphic function on the domain $D \subset \mathbb{C}$ and Γ a simply closed curve in D such that f does not have a zero or pole on Γ. The winding number $wn(f(\Gamma), 0)$ of the image of Γ under f around the origin is given by*

$$wn(f(\Gamma), 0) = z_f - p_f,$$

where z_f (p_f) is the number of zeros (poles) of f in the interior of the curve Γ, counted according to their algebraic multiplicities.

Note that the winding number is counted in the counter-clockwise direction. As typically done in linear control theory, we will generally use the imaginary axis for Γ. Then, the interior of Γ is the right half plane.

We will first proof some intermediate results, given in Lemmas A.2–A.4, before proving Theorem 5.6.

Lemma A.2. *If the set of critical frequencies $\mathcal{R}(\chi)$ is minimal, then in the ordered sequence of critical frequencies $\omega_c^1(\chi) < \omega_c^2(\chi) < \cdots < \omega_c^\beta(\chi)$, we have*

$$G(\chi, j\omega_c^i(\chi))G(\chi, j\omega_c^{i-1}(\chi)) < 0$$

where $i = 2, \ldots, \beta$.

Proof. If $\mathcal{R}(\chi)$ is minimal, then there is exactly one $\omega_c \in \mathcal{R}(\chi)$ such that $\arg G(\chi, j\omega_c) = z\pi$ for each $z \in \mathbb{Z}$ with $z\pi \in I_{\tilde{\beta}}$ (where $I_{\tilde{\beta}}$ is the interval defined in the proof of Proposition 5.3). This implies that

$$\big|\arg G(\chi, j\omega_c^i(\chi)) - \arg G(\chi, j\omega_c^{i-1}(\chi))\big| \geq \pi.$$

In addition, since the critical frequencies are ordered and the transfer function $G(\chi, j\omega)$ is continuous in ω, we have

$$\big|\arg G(\chi, j\omega_c^i(\chi)) - \arg G(\chi, j\omega_c^{i-1}(\chi))\big| \leq \pi.$$

Combining these results, we find that $G(\chi, j\omega_c^i(\chi))G(\chi, j\omega_c^{i-1}(\chi)) < 0$. □

Lemma A.3. *Under the assumptions of Theorem 5.6, the winding number of the image of the Nyquist curve Γ under the transfer function $G(\chi_i, \cdot)$, $i = 1, 2$, around the point 1 is given by*

$$|wn(G(\chi_i, \Gamma), 1)| = \beta^*(\chi_i).$$

Proof. Note that the loop breaking (4.15) assures that G has at least relative degree 1, and therefore $G(\chi, j\infty) = G(\chi, -j\infty) = 0$. Considering also Lemma A.2, it follows that every cut of $G(\chi_i, \Gamma)$ to the right of the point 1 is preceded and followed by a cut of $G(\chi_i, \Gamma)$ with the negative real axis. Thus, each cut to the right of the point 1 corresponds to one winding of $G(\chi_i, \Gamma)$ around the point 1. Moreover, Lemma A.2 assures that these windings all have the same direction and thus several windings cannot cancel each other in the total winding number. □

Lemma A.4. *Under the assumptions of Theorem 5.6, we have*

$$\big|wn(G(\chi_1, \Gamma), 1) - wn(G(\chi_2, \Gamma), 1)\big| = \big|\beta^*(\chi_1) - \beta^*(\chi_2)\big|.$$

Proof. From Assumption (A1), the transfer functions $G(\chi_1, \cdot)$ and $G(\chi_2, \cdot)$ have the same number of zeros and poles in the left and right half plane. Thus for the phase differences we have

$$\arg G(\chi_1, j\infty) - \arg G(\chi_1, -j\infty) = \arg G(\chi_2, j\infty) - \arg G(\chi_2, -j\infty).$$

This implies that the winding numbers $wn(G(\chi_1, \Gamma), 1)$ and $wn(G(\chi_2, \Gamma), 1)$ have the same sign. With Lemma A.3, we conclude

$$\begin{aligned}\big|wn(G(\chi_1, \Gamma), 1) - wn(G(\chi_2, \Gamma), 1)\big| &= \big||wn(G(\chi_1, \Gamma), 1)| - |wn(G(\chi_2, \Gamma), 1)|\big| \\ &= \big|\beta^*(\chi_1) - \beta^*(\chi_2)\big|.\end{aligned}$$

□

We are now ready to give the proof of Theorem 5.6.

Proof. (*Theorem 5.6*) By Definition 5.5, topological equivalence of χ_1 and χ_2 is equivalent to the condition that the matrices $A(\chi_1)$ and $A(\chi_2)$ have the same number of eigenvalues with positive real part. From the proof of Lemma 4.8, we know that

$$1 - G(\chi, s) = \frac{\det(sI_n - A(\chi))}{\det(sI_n - A_o(\chi))}.$$

Using the Argument Principle, it follows that

$$wn(G(\chi, \Gamma), 1) = n_c(\chi) - n_o(\chi),$$

where $n_c(\chi)$ ($n_o(\chi)$) is the number of eigenvalues of $A(\chi)$ ($A_o(\chi)$) with positive real part. By assumption, $n_o(\chi_1) = n_o(\chi_2)$ and thus χ_1 and χ_2 are topologically equivalent if and only if

$$wn(G(\chi_1, \Gamma), 1) = wn(G(\chi_2, \Gamma), 1).$$

The claim of the theorem then follows from Lemma A.4. □

Appendix B

TNF network model summary

B.1 Molecular species

The following lists specify the molecular species which are considered in the TNF receptor signalling model developed in Chapter 7.

B.1.1 Species of the receptor module

RIP TNF receptor interacting protein (RIP) 1

TRAF TNF receptor associated factor (TRAF) 2

TNFR1 TNF receptor 1 trimer

TNF1 TNFα ligand (trimer) which binds specifically to TNFR1

TNFR1L complex of TNFR1 and its ligand

TNFR1C0 complex of TNFR1, ligand, and RIP

TNFR1C1 complex of TNFR1, ligand, RIP and TRAF2

TNFR2 TNF receptor 2 trimer

TNF2 TNFα ligand (trimer) which binds specifically to TNFR2

TNFR2L complex of TNFR2 and its ligand

TNFR2C0 complex of TNFR2 and ligand, ready for adaptor protein recruitment

TNFR2C1 complex of TNFR2, ligand, and TRAF2

B.1.2 Species of the IKK module

IKKi inactive I-κB kinase (IKK), ready for activation

IKKa active (phosphorylated) IKK

IKKd deactivated IKK, not ready for activation

A20 Ubiquitin ligase A20

B.1.3 Species of the NF-κB module

NFkB NF-κB, free in cytosol

IkB inhibitor of NF-κB, I-κBα, in cytosol

NI complex of NF-κB and I-κBα, in cytosol

NFkBn NF-κB, free in nucleus

IkBn inhibitor of NF-κB, I-κBα, in nucleus

NIn complex of NF-κB and I-κBα, in nucleus

B.1.4 Species of the gene expression module

IkBt I-κBα transcript

A20t A20 transcript

TRAFt TRAF2 transcript

B.2 List of reactions

B.2.1 Reactions in the receptor module

#	Description	
	Reaction law	Reaction rate
A1	TNF receptor 1 turnover	
	$\text{TNFR1} \leftrightarrow$	$k_{A1a}\ \text{TNFR1} - k_{A1b}$
A2	RIP1 turnover	
	$\text{RIP} \leftrightarrow$	$k_{A2a}\ \text{RIP} - k_{A2b}$
A3	TRAF2 turnover	
	$\text{TRAF} \leftrightarrow$	$k_{A3a}\ \text{TRAF} - c_{D3}\text{TRAFt}$
A4	TNF1 and TNFR1 form the complex TNFR1L	
	$\text{TNFR1} + \text{TNF1} \leftrightarrow \text{TNFR1L}$	$\frac{k_{A4a}}{V_{ext}\,N_A}\ \text{TNFR1}\ \text{TNF1} - k_{A4b}\ \text{TNFR1L}$
A5	TNFR1L and RIP form the complex TNFR1C0	
	$\text{TNFR1L} + \text{RIP} \rightarrow \text{TNFR1C0}$	$\frac{k_{A5}}{V_c\,N_A}\ \text{TNFR1L}\ \text{RIP}$
A6	TNFR1C0 and TRAF form the complex TNFR1C1	
	$\text{TNFR1C0} + \text{TRAF} \rightarrow \text{TNFR1C1}$	$\frac{k_{A6}}{V_c\,N_A}\ \text{TNFR1C0}\ \text{TRAF}$
A7a	TNFR1C0 is degraded	
	$\text{TNFR1C0} \rightarrow \text{TNF1}$	$k_{A7}\ \text{TNFR1C0}$
A7b	TNFR1L is degraded	
	$\text{TNFR1L} \rightarrow \text{TNF1}$	$k_{A7}\ \text{TNFR1L}$
A8	TNFR1C1 is internalised, adaptor proteins are released	
	$\text{TNFR1C1} \rightarrow \text{TNF1} + \text{RIP} + \text{TRAF}$	$k_{A8}\ \text{TNFR1C1}$

#	Description Reaction law	 Reaction rate
A9	TNF receptor 2 turnover	
	$\text{TNFR2} \leftrightarrow$	$k_{A9a}\,\text{TNFR2} - k_{A9b}$
A10a	TNF2 and TNFR2 form the complex TNFR2L	
	$\text{TNFR2} + \text{TNF2} \leftrightarrow \text{TNFR2L}$	$\frac{k_{A10a}}{V_{ext}\,N_A}\,\text{TNFR2}\,\text{TNF2} - k_{A10b}\,\text{TNFR2L}$
A10b	TNFR2L reorganisation, e.g. clustering	
	$\text{TNFR2L} \rightarrow \text{TNFR2C0}$	$k_{A10c}\,\text{TNFR2L}$
A11	TNFR2C0 and TRAF form the complex TNFR2C1	
	$\text{TNFR2C0} + \text{TRAF} \rightarrow \text{TNFR2C1}$	$\frac{k_{A11}}{V_c\,N_A}\,\text{TNFR2C0}\,\text{TRAF}$
A12a	TNFR2C0 is degraded	
	$\text{TNFR2C0} \rightarrow \text{TNF2}$	$k_{A12}\,\text{TNFR2C0}$
A12b	TNFR2C1 is degraded	
	$\text{TNFR2C1} \rightarrow \text{TNF2}$	$k_{A12}\,\text{TNFR2C1}$
A13	TRAF is degraded when bound to the TNFR2 complex	
	$\text{TNFR2C1} \rightarrow \text{TNFR2L}$	$k_{A13}\,\text{TNFR2C1}$

B.2.2 Reactions in the IKK module

#	Description Reaction law	 Reaction rate
B1	IKK is activated at TNF receptor complexes	
	$\text{IKKi} \rightarrow \text{IKKa}$	$\frac{1}{V_c\,N_A}(k_{B1a}\,\text{TNFR1C1} + k_{B1b}\,\text{TNFR2C1})\text{IKKi}$
B2	IKK is deactivated	
	$\text{IKKa} \rightarrow \text{IKKd}$	$k_{B2}\,\text{IKKa}$
B3	IKK is recycled, inhibition by A20	
	$\text{IKKd} \rightarrow \text{IKKi}$	$\frac{k_{B3a}\,k_{B3b}\,V_c\,N_A}{k_{B3b}\,V_c\,N_A+\text{A20}}\,\text{IKKd}$
B4	A20 turnover	
	$\text{A20} \leftrightarrow$	$k_{B4}\,\text{A20} - c_{D2}\,\text{A20t}$

B.2.3 Reactions in the NF-κB module

#	Description Reaction law	 Reaction rate
C1	NFkB and IkB form a complex	
	$\text{NFkB} + \text{IkB} \leftrightarrow \text{NI}$	$\frac{k_{C1a}}{V_c N_A}\,\text{NFkB}\,\text{IkB} - k_{C1b}\,\text{NI}$
C2	IkB turnover (constitutive and IKK induced)	
	$\text{IkB} \leftrightarrow$	$(k_{C2a} + \frac{k_{C2b}\,\text{IKKa}}{k_{C2c}+\text{IkB}})\text{IkB} - c_{D1}\,\text{IkBt}$
C3	IkB is degraded when bound to NFkB	
	$\text{NI} \rightarrow \text{NFkB}$	$(k_{C3a} + \frac{k_{C3b}\,\text{IKKa}}{k_{C3c}\,V_c\,N_A+\text{NI}})\text{NI}$
C4	NFkB translocates to the nucleus	
	$\text{NFkB} \rightarrow \text{NFkBn}$	$k_{C4}\,\text{NFkB}$
C5	NFkBn and IkBn form a complex	
	$\text{NFkBn} + \text{IkBn} \leftrightarrow \text{NIn}$	$\frac{k_{C1a}}{V_n N_A}\,\text{NFkBn}\,\text{IkBn} - k_{C1b}\,\text{NIn}$

C6	NIn translocates to cytosol	
	NIn → NI	k_{C6} NIn
C7	IkB is shuttled between cytosol and nucleus	
	IkB ↔ IkBn	k_{C7a} IkB − k_{C7b} IkBn

B.2.4 Reactions in the gene expression module

#	Description	
	Reaction law	Reaction rate
D1	transcription of IkB mRNA	
	→ IkBt	$\frac{k_{D1a}\ NFkBn}{k_{D1b}+NFkBn}$
D2	degradation of IkB mRNA	
	IkBt →	k_{D2} IkBt
D3	transcription of A20 mRNA	
	→ A20t	$\frac{k_{D3a}\ NFkBn}{k_{D3b}+NFkBn}$
D4	degradation of A20 mRNA	
	A20t →	k_{D4} A20t
D5	transcription of TRAF2 mRNA	
	→ TRAFt	$\frac{k_{D5a}\ NFkBn}{k_{D5b}+NFkBn}$
D6	degradation of TRAF2 mRNA	
	TRAFt →	k_{D6}TRAFt

B.3 Nominal parameter values

Many parameter values are taken from previous models of the NF-κB pathway. A few insensitive parameters are fixed at reasonable assumed values. Other parameters have either been measured directly or are chosen to match experimental data as described in Section 7.2.2. Parameters measured recently at the Institute of Cell Biology and Immunology (Doszczak and Scheurich, unpublished data) are indicated by (MD).

B.3.1 Experimental and physical parameters

Parameter	Value	Comment/Source
N_A	$6.022 \cdot 10^{23} \frac{1}{\text{mol}}$	Avogadro's constant
V_{cell}	$3 \cdot 10^{-12}$l	cell volume (MD)
N_r	0.2	ratio nuclear to total volume (MD)
V_{ext}	$3.33 \cdot 10^{-9}$l	volume of extracellular medium (MD)

B.3.2 Parameter values for the receptor module

Parameter	Value	Comment/Source
k_{A1b}	$0.28\frac{1}{\mathrm{s}}$	Schliemann (2006)
k_{A2a}	$1.7 \cdot 10^{-4}\frac{1}{\mathrm{s}}$	Schliemann (2006)
k_{A3}	$1.4 \cdot 10^{-5}\frac{1}{\mathrm{s}}$	(MD)
k_{A4a}	$1.83 \cdot 10^{7}\frac{1}{\mathrm{M\,s}}$	Grell *et al.* (1998)
k_{A4b}	$3.5 \cdot 10^{-4}\frac{1}{\mathrm{s}}$	Grell *et al.* (1998)
k_{A5}	$1.5 \cdot 10^{5}\frac{1}{\mathrm{M\,s}}$	assumed
k_{A6}	$2 \cdot 10^{5}\frac{1}{\mathrm{M\,s}}$	assumed
k_{A7}	$1 \cdot 10^{-3}\frac{1}{\mathrm{s}}$	assumed
k_{A8}	$5 \cdot 10^{-4}\frac{1}{\mathrm{s}}$	fitted
k_{A9a}	$9.6 \cdot 10^{-5}\frac{1}{\mathrm{s}}$	(MD)
k_{A10a}	$2.5 \cdot 10^{7}\frac{1}{\mathrm{M\,s}}$	Grell *et al.* (1998)
k_{A10b}	$1.05 \cdot 10^{-2}\frac{1}{\mathrm{s}}$	Grell *et al.* (1998)
k_{A10c}	$2 \cdot 10^{-3}\frac{1}{\mathrm{s}}$	fitted
k_{A11}	$4 \cdot 10^{5}\frac{1}{\mathrm{M\,s}}$	assumed
k_{A12}	$2.5 \cdot 10^{-4}\frac{1}{\mathrm{s}}$	fitted
k_{A13}	$1 \cdot 10^{-3}\frac{1}{\mathrm{s}}$	fitted
TNFR1s	1000	stationary TNFR1 trimers, Grell *et al.* (1998)
TNFR2s	$1 \cdot 10^{4}$	stationary TNFR2 trimers, Grell *et al.* (1998)
RIPs	$1.1 \cdot 10^{5}$	stationary RIP trimers, Eissing (2002)
TRAFs	$1.9 \cdot 10^{4}$	stationary TRAF2 trimers, Eissing (2002)

B.3.3 Parameter values for the IKK module

Parameter	Value	Comment/Source
k_{B1a}	$1 \cdot 10^{7}\frac{1}{\mathrm{M\,s}}$	fitted
k_{B1b}	$1 \cdot 10^{5}\frac{1}{\mathrm{M\,s}}$	fitted, less than k_{B1a}
k_{B2}	$3 \cdot 10^{-3}\frac{1}{\mathrm{s}}$	Ashall *et al.* (2009)
k_{B3a}	$3 \cdot 10^{-4}\frac{1}{\mathrm{s}}$	fitted, Ashall *et al.* (2009) use $5 \cdot 10^{-4}\frac{1}{\mathrm{s}}$
k_{B3b}	$2 \cdot 10^{-9}\mathrm{M}$	Ashall *et al.* (2009)
k_{B4}	$2.5 \cdot 10^{-4}\frac{1}{\mathrm{s}}$	Lipniacki *et al.* (2004)
A20s	$1 \cdot 10^{4}$	fitted
IKK_{tot}	$2 \cdot 10^{5}$	total IKK amount, Lipniacki *et al.* (2004)

B.3.4 Parameter values for the NF-κB module

Parameter	Value	Comment/Source
k_{C1a}	$5 \cdot 10^5 \frac{1}{\mathrm{M\,s}}$	Hoffmann *et al.* (2002)
k_{C1b}	$5 \cdot 10^{-4} \frac{1}{\mathrm{s}}$	Hoffmann *et al.* (2002)
k_{C2a}	$1 \cdot 10^{-4} \frac{1}{\mathrm{s}}$	Hoffmann *et al.* (2002)
k_{C2b}	$4 \cdot 10^{-3} \frac{1}{\mathrm{s}}$	Hoffmann *et al.* (2002)
k_{C2c}	$0.24 \cdot 10^{-6}\mathrm{M}$	derived from Hoffmann *et al.* (2002)
k_{C3a}	$2 \cdot 10^{-5} \frac{1}{\mathrm{s}}$	Hoffmann *et al.* (2002)
k_{C3b}	$2 \cdot 10^{-2} \frac{1}{\mathrm{s}}$	Hoffmann *et al.* (2002)
k_{C3c}	$0.4 \cdot 10^{-7}\mathrm{M}$	derived from Hoffmann *et al.* (2002)
k_{C4}	$3.7 \cdot 10^{-3} \frac{1}{\mathrm{s}}$	fitted, Ashall *et al.* (2009) measured $(2.6 \pm 1.8) \cdot 10^{-3} \frac{1}{\mathrm{s}}$
k_{C6}	$3.7 \cdot 10^{-2} \frac{1}{\mathrm{s}}$	fitted, Ashall *et al.* (2009) use $0.01 \frac{1}{s}$
k_{C7a}	$7 \cdot 10^{-4} \frac{1}{\mathrm{s}}$	Ashall *et al.* (2009)
k_{C7b}	$3.5 \cdot 10^{-4} \frac{1}{\mathrm{s}}$	Ashall *et al.* (2009)
NFkB_{tot}	$1 \cdot 10^5$	Hoffmann *et al.* (2002)

B.3.5 Parameter values for the gene expression module

Parameter	Value	Comment/Source
c_{D1}	$0.5 \frac{1}{\mathrm{s}}$	Lipniacki *et al.* (2004)
k_{D1a}	$0.14 \frac{1}{\mathrm{s}}$	fitted, Lipniacki *et al.* (2004) use $0.1 \frac{1}{\mathrm{s}}$
k_{D1b}	$5 \cdot 10^4$	fitted
k_{D2}	$4 \cdot 10^{-4} \frac{1}{\mathrm{s}}$	Lipniacki *et al.* (2004)
k_{D3b}	$2 \cdot 10^4$	fitted
k_{D4}	$7.5 \cdot 10^{-4} \frac{1}{\mathrm{s}}$	Lipniacki *et al.* (2007)
k_{D5b}	$3 \cdot 10^4$	fitted
k_{D6}	$1 \cdot 10^{-3} \frac{1}{\mathrm{s}}$	assumed
A20ts	5	stationary A20 mRNA amount, assumed
TRAFts	1.5	stationary TRAF2 mRNA amount, assumed

B.3.6 Derived parameters

The following list gives dependent parameters, which are derived from other (independent) parameters. The maximal transcription rates depend on the steady state value of NF-κB in the unstimulated case, denoted by $[\mathrm{NFkBn}]_0$, which can be computed from the

independent parameters given in the previous sections.

$$V_c = (1 - N_r)V_{cell} \qquad \text{(cytosol volume)}$$
$$V_n = N_r V_{cell} \qquad \text{(nuclear volume)}$$
$$k_{A1a} = \frac{k_{A1b}}{\text{TNFR1s}} \qquad k_{A2b} = k_{A2a}\,\text{RIPs}$$
$$k_{A9b} = k_{A9a}\,\text{TNFR2s} \qquad k_{D3a} = \frac{k_{D3b} + [\text{NFkBn}]_0}{[\text{NFkBn}]_0}\,k_{D4}\,\text{A20ts}$$
$$k_{D5a} = \frac{k_{D5b} + [\text{NFkBn}]_0}{[\text{NFkBn}]_0}\,k_{D6}\,\text{TRAFts} \qquad c_{D2} = \frac{k_{B3}\,\text{A20s}}{\text{A20ts}}$$
$$c_{D3} = \frac{k_{A3}\,\text{TRAFs}}{\text{TRAFts}}$$

Bibliography

Allwright, D. J. Harmonic balance and the Hopf bifurcation theorem. *Math. Proc. Cambridge Philos. Soc.* 82:81–127, 1977.

Alon, U., M. G. Surette, N. Barkai, and S. Leibler. Robustness in bacterial chemotaxis. *Nature* 397:168–171, 1999.

Alves, R. and M. A. Savageau. Systemic properties of ensembles of metabolic networks: application of graphical and statistical methods to simple unbranched pathways. *Bioinform.* 16:534–547, 2000.

Angeli, D., J. E. Ferrell, and E. D. Sontag. Detection of multistability, bifurcations, and hysteresis in a large class of biological positive-feedback systems. *Proc. Natl. Acad. Sci.* 101:1822–27, 2004.

Arcak, M. and E. D. Sontag. Diagonal stability of a class of cyclic systems and its connection with the secant criterion. *Automatica* 42:1531–37, 2006.

Asarin, E., T. Dang, and A. Girard. Reachability analysis of nonlinear systems using conservative approximation. In: *Hybrid Systems: Computation and Control*, edited by F. Wiedijk, O. Maler, and A. Pnueli, pp. 20–35. Springer, Berlin, 2003.

Ashall, L., C. A. Horton, D. E. Nelson, P. Paszek, C. V. Harper, K. Sillitoe, S. Ryan, D. G. Spiller, J. F. Unitt, D. S. Broomhead, D. B. Kell, D. A. Rand, V. Sée, and M. R. H. White. Pulsatile stimulation determines timing and specificity of NF-kappaB-dependent transcription. *Science* 324:242–246, 2009.

Asthagiri, A. R. and D. A. Lauffenburger. A computational study of feedback effects on signal dynamics in a mitogen-activated protein kinase (MAPK) pathway model. *Biotechnol. Prog.* 17:227–239, 2001.

Balsa-Canto, E., M. Peifer, J. R. Banga, J. Timmer, and C. Fleck. Hybrid optimization method with general switching strategy for parameter estimation. *BMC Syst. Biol.* 2:26, 2008.

Barkai, N. and S. Leibler. Robustness in simple biochemical networks. *Nature* 387:913–917, 1997.

Bhalla, U. S. and R. Iyengar. Robustness of the bistable behavior of a biological signaling feedback loop. *Chaos* 11:221–226, 2001.

Bhalla, U. S., P. T. Ram, and R. Iyengar. MAP kinase phosphatase as a locus of flexibility in a mitogen-activated protein kinase signaling network. *Science* 297:1018–23, 2002.

Blanchini, F. Set invariance in control. *Automatica* 35:1747–67, 1999.

Bliman, P.-A. A convex approach to robust stability for linear systems with uncertain scalar parameters. *SIAM J. Contr. Optim.* 42:2016–42, 2004.

Bochnak, J., M. Coste, and M.-F. Roy. *Real Algebraic Geometry.* Springer, Berlin, 1998.

Borchers, S., P. Rumschinski, S. Bosio, R. Weismantel, and R. Findeisen. Model discrimi-

nation and parameter estimation via infeasibility certificates for dynamical biochemical reaction networks. In: *Proc. of the 15th IFAC Symp. Syst. Ident. (SYSID)*. 2009.

Boyd, S., L. E. Ghaoui, E. Feron, and V. Balakrishnan. *Linear Matrix Inequalities in System and Control Theory*. SIAM, Philadelphia, 1994.

Boyd, S. and L. Vandenberghe. *Convex Optimization*. Cambridge University Press, Cambridge, UK, 2004.

Brandman, O., J. E. Ferrell, R. Li, and T. Meyer. Interlinked fast and slow positive feedback loops drive reliable cell decisions. *Science* 310:496–498, 2005.

Breindl, C., S. Waldherr, A. Hausser, and F. Allgöwer. Modeling cofilin mediated regulation of cell migration as a two-input switch. In: *Proc. of the 3rd Found. Syst. Biol. Engin. (FOSBE)*. Denver, USA, 2009.

Brightman, F. A. and D. A. Fell. Differential feedback regulation of the MAPK cascade underlies the quantitative differences in EGF and NGF signalling in PC12 cells. *FEBS Lett.* 482:169–174, 2000.

Bryde, S. *Characterisation of TNF receptor-2 mediated signal initiation and transduction*. Ph.D. thesis, Universität Stuttgart, 2004.

Cacuci, D. G. *Sensitivity and Uncertainty Analysis. Volume I: Theory*. CRC Press, Boca Raton, 2003.

Carlson, J. M. and J. Doyle. Complexity and robustness. *Proc. Natl. Acad. Sci.* 99:2538–45, 2002.

Chaves, M., R. Albert, and E. D. Sontag. Robustness and fragility of Boolean models for genetic regulatory networks. *J. Theor. Biol.* 235:431–449, 2005.

Chaves, M., A. Sengupta, and E. D. Sontag. Geometry and topology of parameter space: investigating measures of robustness in regulatory networks. *J. Math. Biol.* 59:315–358, 2009.

Chen, B.-S., Y.-C. Wang, W.-S. Wu, and W.-H. Li. A new measure of the robustness of biochemical networks. *Bioinform.* 21:2698–2705, 2005.

Chesi, G. Robust analysis of linear systems affected by time-invariant hypercubic parametric uncertainty. In: *Proc. of the 42th IEEE Conf. on Dec. and Control, Maui, Hawai*, pp. 5019–24. 2003.

Chesi, G. Establishing stability and instability of matrix hypercubes. *Syst. Contr. Lett.* 54:381–388, 2005.

Chickarmane, V., B. N. Kholodenko, and H. M. Sauro. Oscillatory dynamics arising from competitive inhibition and multisite phosphorylation. *J. Theor. Biol.* 244:68–76, 2007.

Chou, I.-C., H. Martens, and E. Voit. Parameter estimation in biochemical systems models with alternating regression. *Theor. Biol. Med. Model.* 3:25, 2006.

Cimatoribus, C., T. Eißing, N. Elvassore, F. Allgöwer, and E. Bullinger. Model discrimination tools in apoptosis. In: *Proc. 1st Found. Syst. Biol. Engin. (FOSBE), Santa Barbara, USA*, pp. 197–200. 2005.

Cinquin, O. and J. Demongeot. Positive and negative feedback: striking a balance between necessary antagonists. *J. Theor. Biol.* 216:229–241, 2002.

Conradi, C., D. Flockerzi, and J. Raisch. Saddle-node bifurcations in biochemical reaction networks with mass action kinetics and application to a double-phosphorylation

mechanism. In: *Proc. of the 2007 American Contr. Conf.*, pp. 6103–09. 2007a.

Conradi, C., D. Flockerzi, J. Raisch, and J. Stelling. Subnetwork analysis reveals dynamic features of complex (bio)chemical networks. *Proc. Natl. Acad. Sci.* 104:19175–80, 2007b.

Cox, D., J. Little, and D. O'Shea. *Ideals, Varieties, and Algorithms. An Introduction to Computational Algebraic Geometry and Commutative Algebra*. Springer-Verlag, Berlin, 1995.

D'Azzo, J. J. and C. H. Houpis. *Linear Control Sytem Analysis and Design: Conventional and Modern*. McGraw-Hill, New York, 1975.

Dibrov, B. F., A. M. Zhabotinsky, and B. N. Kholodenko. Dynamic stability of steady states and static stabilization in unbranched metabolic pathways. *J. Math. Biol.* 15:51–63, 1982.

Dobson, I. Distance to bifurcation in multidimensional parameter space: Margin sensitivity and closest bifurcations. In: *Bifurcation Control, Theory and Applications*, edited by G. Chen, D. J. Hill, and X. Yu, vol. 293 of *LNCIS*, pp. 49–66. Springer-Verlag, Berlin, 2003.

Doedel, E. J., R. C. Paffenroth, A. R. Champneys, T. F. Fairgrieve, Y. A. Kuznetsov, B. E. Oldeman, B. Sandstede, and X. Wang. *AUTO 2000: continuation and bifurcation software for ordinary differential equations*. Concordia University, Montreal, Canada, 2006.

Doszczak, M. and P. Scheurich. Personal communication.

Doyle, J. Analysis of feedback systems with structured uncertainties. *IEE Proc. Contr. Theo. Appl.* 129:242–250, 1982.

Eissing, T. *Biological Advancement and Systems Analysis of a Mathematical TNF Signalling Network Model*. Diplomarbeit, Institut für Zellbiologie und Immunologie / Institut für Systemtheorie und Regelungstechnik, Universität Stuttgart, 2002.

Eissing, T., F. Allgöwer, and E. Bullinger. Robustness properties of apoptosis models with respect to parameter variations and intrinsic noise. *IEE Proc. Syst. Biol.* 152:221–228, 2005.

Eissing, T., H. Conzelmann, E. D. Gilles, F. Allgöwer, E. Bullinger, and P. Scheurich. Bistability analyses of a caspase activation model for receptor-induced apoptosis. *J. Biol. Chem.* 279:36892–97, 2004.

Eissing, T., S. Waldherr, and F. Allgöwer. Modelling and analysis of cell death signalling. In: *Biology and Control Theory: Current Challenges*, edited by I. Queinnec, S. Tarbouriech, G. Garcia, and S.-I. Niculescu, vol. 357 of *LNCIS*, pp. 161–180. Springer, Berlin, 2007a.

Eissing, T., S. Waldherr, F. Allgöwer, P. Scheurich, and E. Bullinger. Steady state and (bi-)stability evaluation of simple protease signalling networks. *BioSystems* 90:591–601, 2007b.

Ermolaeva, M. A., M.-C. Michallet, N. Papadopoulou, O. Utermöhlen, K. Kranidioti, G. Kollias, J. Tschopp, and M. Pasparakis. Function of TRADD in tumor necrosis factor receptor 1 signaling and in TRIF-dependent inflammatory responses. *Nat. Immunol.* 9:1037–46, 2008.

Eungdamrong, N. J. and R. Iyengar. Computational approaches for modeling regulatory

cellular networks. *Trends Cell Biol.* 14:661–669, 2004.

Feinberg. Chemical reaction network structure and the stability of complex isothermal reactors — II. Multiple steady states for networks of deficiency one. *Chem. Eng. Sci.* 43:1–25, 1988.

Feinberg, M. Chemical reaction network structure and the stability of complex isothermal reactors — I. The deficiency zero and deficiency one theorems. *Chem. Eng. Sci.* 42:2229–68, 1987.

Feldmann, M. and R. N. Maini. TNF defined as a therapeutic target for rheumatoid arthritis and other autoimmune diseases. *Nat. Med.* 9:1245–50, 2003.

Feng, X. and H. Rabitz. Optimal identification of biochemical reaction networks. *Biophys. J.* 86:1270–81, 2004.

Feng, X.-J., S. Hooshangi, D. Chen, G. Li, R. Weiss, and H. Rabitz. Optimizing genetic circuits by global sensitivity analysis. *Biophys. J.* 87:2195–2202, 2004.

Ferrell, J. E. and E. M. Machleder. The biochemical basis of an all-or-none cell fate switch in Xenopus oocytes. *Science* 280:895–898, 1998.

Ferrell, J. E. and W. Xiong. Bistability in cell signaling: How to make continuous processes discontinuous, and reversible processes irreversible. *Chaos* 11:227–236, 2001.

Festjens, N., T. V. Berghe, S. Cornelis, and P. Vandenabeele. RIP1, a kinase on the crossroads of a cell's decision to live or die. *Cell Death Differ.* 14:400–410, 2007.

Fotin-Mleczek, M., F. Henkler, D. Samel, M. Reichwein, A. Hausser, I. Parmryd, P. Scheurich, J. A. Schmid, and H. Wajant. Apoptotic crosstalk of TNF receptors: TNF-R2-induces depletion of TRAF2 and IAP proteins and accelerates TNF-R1-dependent activation of caspase-8. *J. Cell Sci.* 115:2757–70, 2002.

Girard, A. Reachability of uncertain linear systems using zonotopes. In: *Hybrid Systems: Computation and Control*, edited by M. Morari, L. Thiele, and F. Rossi, pp. 291–305. Springer, Berlin, 2005.

Goldbeter, A. A minimal cascade model for the mitotic oscillator involving cyclin and cdc2 kinase. *Proc. Natl. Acad. Sci.* 88:9107–11, 1991.

Goldbeter, A. and D. E. Koshland. An amplified sensitivity arising from covalent modification in biological systems. *Proc. Natl. Acad. Sci.* 78:6840–44, 1981.

Grell, M., H. Wajant, G. Zimmermann, and P. Scheurich. The type 1 receptor (CD120a) is the high-affinity receptor for soluble tumor necrosis factor. *Proc. Natl. Acad. Sci.* 95:570–575, 1998.

Griffith, J. S. Mathematics of cellular control processes. I. Negative feedback to one gene. *J. Theor. Biol.* 20:202–208, 1968a.

Griffith, J. S. Mathematics of cellular control processes. II. Positive feedback to one gene. *J. Theor. Biol.* 20:209–216, 1968b.

Hanahan, D. and R. A. Weinberg. The hallmarks of cancer. *Cell* 100:57–70, 2000.

Handelman, D. Representing polynomials by positive linear functions on compact convex polyhedra. *Pac. J. Math.* 132:35–62, 1988.

Hasenauer, J. *Globale Sensitivitätsanalyse der TNF-induzierten antiapoptotischen Signaltransduktion mit semidefiniter Programmierung.* Diplomarbeit, Institut für Systemtheorie und Regelungstechnik, Universität Stuttgart, 2008.

Hasenauer, J., P. Rumschinski, S. Waldherr, S. Borchers, F. Allgöwer, and R. Findeisen. Guaranteed steady-state bounds for uncertain chemical processes. In: *Proc. Intern. Symp. Adv. Contr. Chem. Proc. (ADCHEM)*. Istanbul, 2009a.

Hasenauer, J., S. Waldherr, K. Wagner, and F. Allgöwer. Parameter identification, experimental design and model falsification for biological network models using semidefinite programming, 2009b. IET Systems Biology. Accepted for publication.

Hayden, M. S. and S. Ghosh. Shared principles in NF-κB signaling. *Cell* 132:344–362, 2008.

Hayot, F. and C. Jayaprakash. NF-κB oscillations and cell-to-cell variability. *J. Theor. Biol.* 240:583–591, 2006.

Heinrich, R. and S. Schuster. *The Regulation of Cellular Systems*. Chapman & Hall, New York, 1996.

Henderson, M. E. Higher-dimensional continuation. In: *Numerical continuation methods for dynamical systems*, edited by B. Krauskopf, pp. 77–115. Springer, Dordrecht, 2007.

Henrion, D., D. Arzelier, D. Peaucelle, and J. Lasserre. On parameter-dependent Lyapunov functions for robust stability of linear systems. In: *Proc. of the 43th IEEE Conf. on Dec. and Control, Atlantis, Bahamas*, pp. 887–892. 2004.

Higham, D. J. Modeling and simulating chemical reactions. *SIAM Rev.* 50:347–368, 2008.

Hilioti, Z., W. Sabbagh, S. Paliwal, A. Bergmann, M. D. Goncalves, L. Bardwell, and A. Levchenko. Oscillatory phosphorylation of yeast Fus3 MAP kinase controls periodic gene expression and morphogenesis. *Curr. Biol.* 18:1700–06, 2008.

Hinrichsen, D. and A. J. Pritchard. *Mathematical Systems Theory I*. Springer-Verlag, Berlin, 2005.

Hoffmann, A., A. Levchenko, M. L. Scott, and D. Baltimore. The IkappaB-NF-kappaB signaling module: temporal control and selective gene activation. *Science* 298:1241–45, 2002.

Huang, C. Y. and J. E. Ferrell. Ultrasensitivity in the mitogen-activated protein kinase cascade. *Proc. Natl. Acad. Sci.* 93:10078–83, 1996.

Ingalls, B. A frequency domain approach to sensitivity analysis of biochemical networks. *J. Phys. Chem. B* 108:1143–52, 2004.

Isidori, A. *Nonlinear Control Systems*. Springer-Verlag, London, 3rd ed., 1995.

Jacobsen, E. W. and G. Cedersund. Structural robustness of biochemical network models—with application to the oscillatory metabolism of activated neutrophils. *IET Syst. Biol.* 2:39–47, 2008.

Jaulin, L., M. Kieffer, O. Didrit, and É.. Walter. *Applied Interval Analysis*. Springer-Verlag, London, 2001.

Kacser, H., J. A. Burns, and D. A. Fell. The control of flux. *Biochem. Soc. Trans.* 23:341–366, 1995.

Kahn, D. and H. V. Westerhoff. Control theory of regulatory cascades. *J. Theor. Biol.* 153:255–285, 1991.

Kaufman, M., C. Soule, and R. Thomas. A new necessary condition on interaction graphs for multistationarity. *J. Theor. Biol.* 248:675–685, 2007.

Keener, J. and J. Sneyd. *Mathematical Physiology*. Springer, New York, 2004.

Khalil, H. K. *Nonlinear Systems*. Prentice Hall, Upper Saddle River, New Jersey, 3rd ed., 2002.

Kholodenko, B. N. Negative feedback and ultrasensitivity can bring about oscillations in the mitogen-activated protein kinase cascades. *Eur. J. Biochem.* 267:1583–88, 2000.

Kholodenko, B. N., A. Kiyatkin, F. J. Bruggeman, E. Sontag, H. V. Westerhoff, and J. B. Hoek. Untangling the wires: A strategy to trace functional interactions in signaling and gene networks. *Proc. Natl. Acad. Sci.* 99:12841–46, 2002.

Kim, D., Y.-K. Kwon, and K.-H. Cho. Coupled positive and negative feedback circuits form an essential building block of cellular signaling pathways. *Bioessays* 29:85–90, 2007.

Kim, J., D. G. Bates, I. Postlethwaite, L. Ma, and P. A. Iglesias. Robustness analysis of biochemical network models. *IEE Proc. Syst. Biol.* 153:96–104, 2006.

Kim, J.-R., Y. Yoon, and K.-H. Cho. Coupled feedback loops form dynamic motifs of cellular networks. *Biophys. J.* 94:359–365, 2008.

Kitano, H. Biological robustness. *Nat. Rev. Genet.* 5:826–837, 2004.

Kitano, H. Towards a theory of biological robustness. *Mol. Syst. Biol.* 3:137, 2007.

Klipp, E., R. Herwig, A. Kowald, C. Wierling, and H. Lehrach. *Systems Biology in Practice. Concepts, Implementation and Application*. Wiley-VCH Verlag, Weinheim, 2005.

Kopelman, R. Fractal reaction kinetics. *Science* 241:1620–26, 1988.

Krishna, S., M. H. Jensen, and K. Sneppen. Minimal model of spiky oscillations in NF-kappaB signaling. *Proc. Natl. Acad. Sci.* 103:10840–45, 2006.

Kuepfer, L., U. Sauer, and P. Parrilo. Efficient classification of complete parameter regions based on semidefinite programming. *BMC Bioinform.* 8:12, 2007.

Kuznetsov, Y. A. *Elements of Applied Bifurcation Theory*. Springer-Verlag, New York, 1995.

Lancaster, P. and M. Tismenetsky. *The Theory of Matrices*. Academic Press, San Diego, 1985.

Lang, M., S. Waldherr, and F. Allgöwer. Amplitude distribution of stochastic oscillations in biochemical networks due to intrinsic noise, 2009. PMC Biophysics. Provisionally accepted for publication.

Leloup, J.-C. and A. Goldbeter. Toward a detailed computational model for the mammalian circadian clock. *Proc. Natl. Acad. Sci.* 100:7051–56, 2003.

Li, Q. and I. M. Verma. NF-kappaB regulation in the immune system. *Nat. Rev. Immunol.* 2:725–734, 2002.

Li, X., Y. Yang, and J. D. Ashwell. TNF-RII and c-IAP1 mediate ubiquitination and degradation of TRAF2. *Nature* 416:345–347, 2002.

Lipniacki, T., P. Paszek, A. R. Brasier, B. Luxon, and M. Kimmel. Mathematical model of NF-κB regulatory module. *J. Theor. Biol.* 228:195–215, 2004.

Lipniacki, T., K. Puszynski, P. Paszek, A. R. Brasier, and M. Kimmel. Single TNFalpha trimers mediating NF-kappaB activation: Stochastic robustness of NF-kappaB signal-

ing. *BMC Bioinform.* 8:376, 2007.

Ljung, L. Perspectives on system identification. In: *Proc. of the 17th IFAC World Congress, Seoul, Korea*, pp. 7172–84. 2008.

Lu, J., H. Engl, and P. Schuster. Inverse bifurcation analysis: Application to simple gene systems. *Algorithms Mol. Biol.* 1:11, 2006.

Ma, L. and P. A. Iglesias. Quantifying robustness of biochemical network models. *BMC Bioinform.* 3:38, 2002.

Macheras, P. and A. Ilidias. *Modeling in Biopharmaceutics, Pharmacokinetics, and Pharmacodynamics*. Springer, New York, 2006.

Madsen, M. F., S. Danø, and P. G. Sørensen. On the mechanisms of glycolytic oscillations in yeast. *FEBS J.* 272:2648–60, 2005.

Maranas, C. D. and C. A. Floudas. Finding all solutions of nonlinearly constrained systems of equations. *J. Global Optim.* 7:143–182, 1995.

Markevich, N. I., J. B. Hoek, and B. N. Kholodenko. Signaling switches and bistability arising from multisite phosphorylation in protein kinase cascades. *J. Cell Biol.* 164:353–359, 2004.

Mauro, C., F. Pacifico, A. Lavorgna, S. Mellone, A. Iannetti, R. Acquaviva, S. Formisano, P. Vito, and A. Leonardi. ABIN-1 binds to NEMO/IKKgamma and co-operates with A20 in inhibiting NF-kappaB. *J. Biol. Chem.* 281:18482–88, 2006.

Mees, A. I. and L. O. Chua. The Hopf bifurcation theorem and its applications to nonlinear oscillations in circuits and systems. *IEEE Trans. Circ. Syst.* 26:235–254, 1979.

Michaelis, L. and M. Menten. Die Kinetik der Invertinwirkung. *Biochem. Z.* 49:333–369, 1913.

Micheau, O. and J. Tschopp. Induction of TNF receptor I-mediated apoptosis via two sequential signaling complexes. *Cell* 114:181–190, 2003.

Moiola, J., A. Desages, and J. Romagnoli. Computing bifurcation points via characteristic gain loci. *IEEE Trans. Autom. Control* 36:358–362, 1991.

Moiola, J. L., M. C. Colantonio, and P. D. Donate. Analysis of static and dynamic bifurcations from a feedback systems perspective. *Dyn. Stab. Syst.* 12:293–317, 1997.

Monniaux, D. Fatal degeneracy in the semidefinite programming approach to the decision of polynomial inequalities, 2009. ArXiv:0901.4907v1 [math.NA].

Mönnigmann, M. and W. Marquardt. Normal vectors on manifolds of critical points for parametric robustness of equilibrium solutions of ODE systems. *J. of Nonlin. Sci.* 12:85–112, 2002.

Monod, J., J. Wyman, and J.-P. Changeux. On the nature of allosteric transitions: A plausible model. *J. Molec. Biol.* 12:88–118, 1965.

Morohashi, M., A. E. Winn, M. T. Borisuk, H. Bolouri, J. Doyle, and H. Kitano. Robustness as a measure of plausibility in models of biochemical networks. *J. Theor. Biol.* 216:19–30, 2002.

Müller, M. A., S. Waldherr, and F. Allgöwer. The transcritical bifurcation in absolutely stable feedback systems. In: *Proc. of the 10th Europ. Contr. Conf. (ECC)*. Budapest, Hungary, 2009.

Nelson, D. E., A. E. C. Ihekwaba, M. Elliott, J. R. Johnson, C. A. Gibney, B. E. Foreman, G. Nelson, V. See, C. A. Horton, D. G. Spiller, S. W. Edwards, H. P. McDowell, J. F. Unitt, E. Sullivan, R. Grimley, N. Benson, D. Broomhead, D. B. Kell, and M. R. H. White. Oscillations in NF-kappa B signaling control the dynamics of gene expression. *Science* 306:704–708, 2004.

Neumaier, A. *Interval Methods for Systems of Equations*. Cambridge University Press, Cambridge, UK, 1990.

Novak, B. and J. J. Tyson. Modeling the cell division cycle: M-phase trigger, oscillations, and size control. *J. Theor. Biol.* 165:101–134, 1993.

Oliveira, R. and P. Peres. LMI conditions for robust stability analysis based on polynomially parameter-dependent Lyapunov functions. *Syst. Contr. Lett.* 55:52–61, 2006.

Ozbudak, E. M., M. Thattai, H. N. Lim, B. I. Shraiman, and A. V. Oudenaarden. Multistability in the lactose utilization network of *escherichia coli*. *Nature* 427:737–740, 2004.

Park, S. G., T. Lee, H. Y. Kang, K. Park, K.-H. Cho, and G. Jung. The influence of the signal dynamics of activated form of IKK on NF-kappaB and anti-apoptotic gene expressions: a systems biology approach. *FEBS Lett.* 580:822–830, 2006.

Parrilo, P. A. Semidefinite programming relaxations for semialgebraic problems. *Math. Program.* 96:293–320, 2003.

Pearson, G., F. Robinson, T. B. Gibson, B. E. Xu, M. Karandikar, K. Berman, and M. H. Cobb. Mitogen-activated protein (MAP) kinase pathways: regulation and physiological functions. *Endocr. Rev.* 22:153–183, 2001.

Pobezinskaya, Y. L., Y.-S. Kim, S. Choksi, M. J. Morgan, T. Li, C. Liu, and Z. Liu. The function of TRADD in signaling through tumor necrosis factor receptor 1 and TRIF-dependent Toll-like receptors. *Nat. Immunol.* 9:1047–54, 2008.

Polisetty, P. K., E. O. Voit, and E. P. Gatzke. Identification of metabolic system parameters using global optimization methods. *Theor. Biol. Med. Model.* 3:4, 2006.

Pomerening, J. R., E. D. Sontag, and J. E. Ferrell. Building a cell cycle oscillator: hysteresis and bistability in the activation of Cdc2. *Nat. Cell Biol.* 5:346–351, 2003.

Prill, R. J., P. A. Iglesias, and A. Levchenko. Dynamic properties of network motifs contribute to biological network organization. *PLoS Biology* 3:1881–92, 2005.

Purnick, P. E. M. and R. Weiss. The second wave of synthetic biology: from modules to systems. *Nat. Rev. Mol. Cell Biol.* 10:410–422, 2009.

Qiao, L., R. B. Nachbar, I. G. Kevrekidis, and S. Y. Shvartsman. Bistability and oscillations in the Huang–Ferrell model of MAPK signaling. *PLoS Comp. Biol.* 3:e184, 2007.

Qiu, L., B. Bernhardsson, A. Rantzer, E. J. Davison, P. M. Young, and J. C. Doyle. A formula for computation of the real stability radius. *Automatica* 31:879–890, 1995.

Rabitz, H., M. Kramer, and D. Dacol. Sensitivity analysis in chemical kinetics. *Ann. Rev. Phys. Chem.* 34:419–461, 1983.

Radde, N. The impact of time delays on the robustness of biological oscillators and the effect of bifurcations on the inverse problem. *EURASIP J. Bioinf. Syst. Biol.* 2009:327503, 2009.

Rae, C., S. Langa, S. J. Tucker, and D. J. Macewan. Elevated NF-κB responses and FLIP levels in leukemic but not normal lymphocytes: reduction by salicylate allows TNF-induced apoptosis. *Proc. Natl. Acad. Sci.* 104:12790–95, 2007.

Raffard, R., K. Amonlirdviman, J. Axelrod, and C. Tomlin. An adjoint-based parameter identification algorithm applied to planar cell polarity signaling. *IEEE Trans. Autom. Control* 53:109–121, 2008.

Ramdani, N., N. Meslem, and Y. Candau. Reachability analysis of uncertain nonlinear systems using guaranteed set integration. In: *Proc. of the 17th IFAC World Congress, Seoul, Korea*, pp. 8972–8977. 2008.

Rao, C. V., D. M. Wolf, and A. P. Arkin. Control, exploitation and tolerance of intracellular noise. *Nature* 420:231–237, 2002.

Reder, C. Metabolic control theory: a structural approach. *J. Theor. Biol.* 135:175–201, 1988.

Reinschke, K. J. *Multivariable Control. A Graph-theoretic Approach.* No. 108 in LNCIS. Springer-Verlag, Berlin, 1988.

Richter, S. L. and R. A. DeCarlo. Continuation methods: theory and applications. *IEEE Trans. Circ. Syst.* 30:347–352, 1983.

Robert, C. P. and G. Casella. *Monte Carlo Statistical Methods.* Springer-Verlag, New York, 2004.

Sabouri-Ghomi, M., A. Ciliberto, S. Kar, B. Novak, and J. J. Tyson. Antagonism and bistability in protein interaction networks. *J. Theor. Biol.* 250:209–218, 2007.

Savageau, M. A. *Biochemical Systems Analysis. A study of Function and Design in Molecular Biology.* Addison-Wesley, Reading, Massachusetts, 1976.

Savageau, M. A. Michaelis-Menten mechanism reconsidered: implications of fractal kinetics. *J. Theor. Biol.* 176:115–124, 1995.

Schliemann, M. *Mathematische Modellierung des TNF-induzierten apoptotischen und antiapoptotischen Signaltransduktionsweges in Säugerzellen.* Diplomarbeit, Institut für Systemtheorie und Regelungstechnik, Universität Stuttgart, 2006.

Schliemann, M., T. Eissing, P. Scheurich, and E. Bullinger. Mathematical modelling of TNF-α induced apoptotic and anti-apoptotic signalling pathways in mammalian cells based on dynamic and quantitative experiments. In: *Proc. of the 2nd Found. Syst. Biol. Engin. (FOSBE)*, pp. 213–218. Stuttgart, Germany, 2007.

Schmidt, H. and E. W. Jacobsen. Linear systems approach to analysis of complex dynamic behaviours in biochemical networks. *IEE Proc. Syst. Biol.* 1:149–158, 2004.

Schoeberl, B., C. Eichler-Jonsson, E. D. Gilles, and G. Müller. Computational modeling of the dynamics of the MAP kinase cascade activated by surface and internalized EGF receptors. *Nat. Biotechnol.* 20:370–375, 2002.

Schwenk, S. and B. Tibken. Robust stability of nonlinear systems. In: *Proc. of the 17th IFAC World Congress, Seoul, Korea*, pp. 11375–78. 2008.

Shacter, E., P. B. Chock, and E. R. Stadtman. Regulation through phosphorylation/dephosphorylation cascade systems. *J. Biol. Chem.* 259:12252–59, 1984.

Shoemaker, J. E. and F. J. Doyle III. Identifying fragilities in biochemical networks: Robust performance analysis of Fas signaling-induced apoptosis. *Biophys. J.* 95:2610–

23, 2008.

Sinini, A. *Parameteridentifikation des TNF-induzierten NF-κB Signalweg-Modells*. Studienarbeit, Institut für Systemtheorie und Regelungstechnik, Universität Stuttgart, 2008.

Skogestad, S. and I. Postlethwaite. *Multivariable Feedback Control. Analysis and Design*. John Wiley & Sons, Chichester, 1996.

Snoussi, E. H. Necessary conditions for multistationarity and stable periodicity. *J. Biol. Syst.* 6:3–9, 1998.

Stehlik, C., R. de Martin, B. R. Binder, and J. Lipp. Cytokine induced expression of porcine inhibitor of apoptosis protein (iap) family member is regulated by NF-κB. *Biochem. Biophys. Res. Commun.* 243:827–832, 1998.

Stelling, J., U. Sauer, Z. Szallasi, F. J. Doyle, and J. Doyle. Robustness of cellular functions. *Cell* 118:675–685, 2004.

Stephanopoulos, G. Metabolic fluxes and metabolic engineering. *Metab. Eng.* 1:1–11, 1999.

Stiefs, D., T. Gross, R. Steuer, and U. Feudel. Computation and visualization of bifurcation surfaces. *Int. J. Bif. Chaos* 18:2191–2206, 2008.

Streif, S., R. Findeisen, and E. Bullinger. Sensitivity analysis of biochemical reaction networks by bilinear approximation. In: *Proc. of the 2nd Found. Syst. Biol. Engin. (FOSBE)*, pp. 521–526. 2007.

Streif, S., S. Waldherr, F. Allgöwer, and R. Findeisen. Steady state sensitivity analysis of biochemical reaction networks: A brief review and new methods. In: *Systems Analysis of Biological Networks*, edited by A. Jayaraman and J. Hahn, Methods in Bioengineering, pp. 129–148. Artech House, Boston, USA, 2009.

Sturm, J. F. Using SeDuMi 1.02, a Matlab toolbox for optimization over symmetric cones. *Optim. Meth. Softw.* 11:625–653, 1999.

Thomas, R. and M. Kaufman. Multistationarity, the basis of cell differentiation and memory. I. Structural conditions of multistationarity and other nontrivial behavior. *Chaos* 11:170–179, 2001.

Thron, C. D. The secant condition for instability in biochemical feedback-control. 1. The role of cooperativity and saturability. *Bull. Math. Biol.* 53:383–401, 1991.

Tian, B., D. E. Nowak, and A. R. Brasier. A TNF-induced gene expression program under oscillatory NF-kappaB control. *BMC Genom.* 6:137, 2005.

Trané, C. and E. W. Jacobsen. On robustness as the rationale behind multiple feedback loops in the circadian clock. In: *Proc. of the 2nd Found. Syst. Biol. Engin. (FOSBE), Stuttgart, Germany*, pp. 439–444. 2007.

Trané, C. and E. W. Jacobsen. Network structure and robustness of intracellular oscillators. In: *Proc. of the 17th IFAC World Congress, Seoul, Korea*, pp. 10989–94. 2008.

Turing, A. M. The chemical basis of morphogenesis. *Phil. Trans. Royal Soc. London Series B* 237:37–72, 1952.

Tyson, J. J., K. C. Chen, and B. Novak. Sniffers, buzzers, toggles and blinkers: dynamics of regulatory and signaling pathways in the cell. *Curr. Opin. Cell Biol.* 15:221–231, 2003.

Tyson, J. J., A. Csikasz-Nagy, and B. Novak. The dynamics of cell cycle regulation. *Bioessays* 24:1095–1109, 2002.

Tyson, J. J. and H. G. Othmer. The dynamics of feedback control circuits in biochemical pathways. *Progr. Theor. Biol.* 5:2–62, 1978.

Vandenberghe, L. and S. Boyd. Semidefinite programming. *SIAM Rev.* 38:49–95, 1996.

Varma, A., M. Morbidelli, and H. Wu. *Parametric Sensitivity in Chemical Systems*. Cambridge University Press, Cambridge, 1999.

Vera, J., E. Balsa-Canto, P. Wellstead, J. R. Banga, and O. Wolkenhauer. Power-law models of signal transduction pathways. *Cell. Signal.* 19:1531–41, 2007.

Voss, H. U., J. Timmer, and J. Kurths. Nonlinear dynamical system identification from uncertain and indirect measurements. *Int. J. Bif. Chaos* 14:1905–33, 2004.

Wajant, H., K. Pfizenmaier, and P. Scheurich. Tumor necrosis factor signaling. *Cell Death Differ.* 10:45–65, 2003.

Waldherr, S. and F. Allgöwer. A feedback approach to bifurcation analysis in biochemical networks with many parameters. In: *Proc. of the 2nd Found. Syst. Biol. Engin. (FOSBE)*, pp. 479–484. Stuttgart, Germany, 2007.

Waldherr, S. and F. Allgöwer. Searching bifurcations in high-dimensional parameter space via a feedback loop breaking approach. *Int. J. Syst. Sci.* 40:769–782, 2009.

Waldherr, S., F. Allgöwer, and E. W. Jacobsen. Kinetic perturbations as robustness analysis tool for biochemical reaction networks, 2009a. Proc. of the 48th IEEE Conf. on Dec. and Control, Shanghai, China, Accepted for publication.

Waldherr, S., T. Eissing, and F. Allgöwer. Analysis of feedback mechanisms in cell-biological systems. In: *Proc. of the 17th IFAC World Congress, Seoul, Korea*, pp. 15861–66. 2008a.

Waldherr, S., T. Eissing, and F. Allgöwer. Rückkopplungen im Leben und Sterben einer Zelle: Ansätze zur systemtheoretischen Analyse. *at – Automatisierungstechnik* 56:233–240, 2008b.

Waldherr, S., T. Eissing, M. Chaves, and F. Allgöwer. Bistability preserving model reduction in apoptosis. In: *Proc. of the 10th IFAC Comp. Appl. in Biotechn., Cancun, Mexico*, pp. 327–332. 2007.

Waldherr, S., R. Findeisen, and F. Allgöwer. Global sensitivity analysis of biochemical reaction networks via semidefinite programming. In: *Proc. of the 17th IFAC World Congress, Seoul, Korea*, pp. 9701–06. 2008c.

Waldherr, S., J. Hasenauer, and F. Allgöwer. Estimation of biochemical network parameter distributions in cell populations. In: *Proc. of the 15th IFAC Symp. Syst. Ident. (SYSID)*, pp. 1265–1270. Saint-Malo, France, 2009b.

Wang, C. Y., M. W. Mayo, R. G. Korneluk, D. V. Goeddel, and A. S. Baldwin. NF-kappaB antiapoptosis: induction of TRAF1 and TRAF2 and c-IAP1 and c-IAP2 to suppress caspase-8 activation. *Science* 281:1680–83, 1998.

Wertz, I. E., K. M. O'Rourke, H. Zhou, M. Eby, L. Aravind, S. Seshagiri, P. Wu, C. Wiesmann, R. Baker, D. L. Boone, A. Ma, E. V. Koonin, and V. M. Dixit. De-ubiquitination and ubiquitin ligase domains of A20 downregulate NF-kappaB signalling. *Nature* 430:694–699, 2004.

Whittaker, E. T. and G. N. Watson. *A Course of Modern Analysis*. Cambridge University Press, Cambridge, UK, 1965. Reprint of the 4th edition.

Widmann, C., S. Gibson, M. B. Jarpe, and G. L. Johnson. Mitogen-activated protein kinase: conservation of a three-kinase module from yeast to human. *Physiol. Rev.* 79:143–180, 1999.

Wolf, J., S. Becker-Weimann, and R. Heinrich. Analysing the robustness of cellular rhythms. *Syst. Biol.* 2:35–41, 2005.

Wu, C.-J., D. B. Conze, X. Li, S.-X. Ying, J. A. Hanover, and J. D. Ashwell. TNF-alpha induced c-IAP1/TRAF2 complex translocation to a Ubc6-containing compartment and TRAF2 ubiquitination. *EMBO J.* 24:1886–98, 2005.

Ye, H. and H. Wu. Thermodynamic characterization of the interaction between TRAF2 and tumor necrosis factor receptor peptides by isothermal titration calorimetry. *Proc. Natl. Acad. Sci.* 97:8961–66, 2000.

Zhou, K., J. C. Doyle, and K. Glover. *Robust and Optimal Control*. Prentice Hall, Upper Saddle River, New Jersey, 1996.